CHARACTERIZING VERTICAL MASS FLUX PROFILES IN AEOLIAN SALTATION SYSTEMS

A Dissertation

by

EUGENE JOHN FARRELL

Submitted to the Office of Graduate Studies of
Texas A&M University
in partial fulfillment of the requirements for the degree of

DOCTOR OF PHILOSOPHY

May 2012

Major Subject: Geography

Characterizing vertical mass flux profiles in aeolian saltation systems

CHARACTERIZING VERTICAL MASS FLUX PROFILES IN AEOLIAN SALTATION SYSTEMS

A Dissertation

by

EUGENE JOHN FARRELL

Submitted to the Office of Graduate Studies of
Texas A&M University
in partial fulfillment of the requirements for the degree of

DOCTOR OF PHILOSOPHY

Approved by:

Co-Chair of Committee,	Douglas J. Sherman
Co-Chair of Committee,	Chris Houser
Committee Members,	Vatche P. Tchakerian
	Dave M. Cairns
	Steve F. DiMarco
Head of Department,	Vatche P. Tchakerian

May 2012

Major Subject: Geography

ABSTRACT

Characterizing Vertical Mass Flux Profiles in Aeolian Saltation Systems. (May 2012)

Eugene John Farrell, B.Sc., University College Cork;

M.S., University of Southern California

Co-Chairs of Advisory Committee, Dr. Douglas J. Sherman
Dr. Chris Houser

This dissertation investigates characteristics of the vertical distributions of mass flux observed in field and laboratory experiments. Thirty vertical mass flux profiles were measured during a field experiment in Jericoacoara, Brazil from October to November, 2008. These data were supplemented with 621 profiles gathered from an extensive review of the aeolian literature. From the field experiment, the analysis of the grain-size statistics for the flux caught in each trap shows that a reverse in grain-size trends occurs at an inflection zone located 0.05 – 0.15 m above the bed. Below this inflection, mean grain-size decreases steeply with elevation in the near bed region dominated by reptation and saltation modes of transport. Above the inflection there is a coarsening of grain size with elevation; as saltation becomes the dominant transport mode. These results indicate that the coarsest grains are found close to and farthest from the bed.

Using a data set comprising 274 vertical flux profiles, the performance of the exponential, power and logarithmic functions were tested to see which provided the best fit to the vertical flux distributions. The exponential function performed best 88% of the time. The average r^2 value for the grouped exponential, logarithmic, and power function fits are 0.98, 0.85 and 0.91, respectively. The populations of the exponent coefficients, representing the relative rate of decrease with height above the surface, or slope of the vertical mass flux profiles, are statistically different in wind tunnels and field experiments. The slopes of the vertical flux profiles observed in wind tunnel experiments

are steeper compared to field environments, which infers that saltation is suppressed in wind tunnels. These differences are magnified in wind tunnels with small working cross section areas, and in wind tunnel experiments that use extreme environmental conditions, such as very high shear velocities.

The Rouse concentration model, widely used in water studies, was tested to see if it could replicate the observed vertical flux distributions and transport rates. A fall velocity (w_0) equation for particles falling in air was derived using a grain size (d) dependency: w_0 (in m/s) = 4.23d (in mm) + 0.1956 (r^2=0.88). The Rouse model performs poorly when the value of the β (a form of the Schmidt number in the Rouse number exponent) is assumed to be unity. The values of β were modeled using a relationship derived from a dependency of β on the w_0/u_* ratio: $\beta = 3.2778(w_0/u_*) - 0.4133$ (r^2=0.65). The values of β ranged from 6.11 – 17.83 for all the experiments. The Rouse profiles calculated using this approach predict very similar vertical distributions to the observed data and predicted 86% and 81% of the observed transport rate in field and wind tunnel experiments respectively. The Rouse approach is more physically meaningful than current approaches that use standard curve fitting functions to represent the vertical flux data but do not provide any explanatory power for the shape or magnitude of the profile.

.

DEDICATION

This work is dedicated to the memory of James (Jim) P. McDermott.

My family and friends will understand why this is dedicated to you, *mo chara* (my friend).

You were truly family, a best friend, a colleague, a partner-in-crime, and an inspiration.

It was fun starting the journey with you.

It is still very bitter sweet finishing it without you.

You are missed tremendously but your legacy lives on and runs deep in this community.

*Sláinte (*Cheers - and still raising pints in your memory)!

ACKNOWLEDGEMENTS

I would like to thank my advisor Prof. Douglas J. Sherman for his support through the years. As an advisor he frequently went above and beyond the call of duty. He has delivered on every promise he made to me when I decided to come back to academia. I did travel to many phenomenal locations around the world to conduct research experiments. I did learn how to write proposals and publish articles. I was part of a supportive, productive research team. I did get teaching experience. I did have lots of fun. I did learn (hopefully). I can only hope that I can provide the same mentoring and experiences to other students. Thank you for setting a high standard and being patient enough to allow me to get there at my own pace.

My colleagues Prof. Jean Ellis and Dr. Bailiang Li were particularly important in helping me succeed in this program. Under the guiding light of Doug, we completed many research experiments together. I hope these successful collaborations will continue for many years to come as we all define our own paths. Their support spanned the full spectrum of technological to social. It was very satisfying to draw on their work during different parts of this research.

I would like to thank my committee for their support and patience: Prof. Dave Cairns, Prof. Chris Houser, Prof. Steve DiMarco, and Prof. Vatche Tchakerian. Their comments and feedback definitely improved the quality of this work.

I would like to thank the Geography and Regional Science (GRS) Program, National Science Foundation for supporting the Brazil field experiment described in this work (Grant 0822482). The field support of this work was provided by Prof. Jean Ellis, Dr. Bailiang Li, Walter Cox, and also from the staff of LABOMAR, at University of Ceará, Prof. Luís P. Maia, Paulo H. G. O. Sousa, Robério M. Sampaio, and Eduardo C. M. de Borbaand.

I would like to thank the Department of Geography, Texas A&M University for continued support of graduate students. The Excellence in Academics and Geographical Research Awards are invaluable to support our education. I would like to thank a number of organizations within Texas A&M University for providing funding

opportunities to graduate students to support our research during our tenure at TAMU: Graduate Student Council Travel Award; Graduate Student Research and Presentation Grant Travel from the Association of Former Students and Office of Graduate Studies; the U.S. Senator Phil Gramm Doctoral Fellowship for *Excellence in scholarly research and teaching and for exemplifying the meaning of scholar/mentor in the highest sense.*

To all my friends and colleagues in Aggieland and further afield: thank you so much. Mentoring takes on many capacities and I think I have been fortunate to be surrounded by good people who continue to inspire me and challenge me in many different ways. Liam Carr in particular was a worthy comrade-in-arms during our tenures at 4324 and 1809. We finally achieve the self-anointed titles of 'Dr' in May 2012.

Most importantly, I would like to thank my parents and family. Although this dissertation is dedicated to Jim, yours is, by far, the heaviest mark on this work and the large number of unwritten chapters that have defined my story the past years. Without your support none of this would have been possible. It is difficult being away for so long but it is comforting to have the support of two of the kindest, loving, generous, most caring parents any son could wish for. Thank you so much. Whatever else happens, I am very happy that you got to see me finish the journey that started many moons ago in Earth Science in University College Cork. It is not a coincidence that this chapter of my life - the one most influenced by you than any of the previous chapters - has been the happiest. Now I realize I should have listened more to you years ago. From Cissies to Hollywood; from Texas to New Jersey; and to wherever next….. the only sure thing in all these locations was that #64 and Duagh are the only places I ever truly call home. *Garbh míle a maith agaibh* (Thank you very much).

TABLE OF CONTENTS

LIST OF FIGURES

Page

Page

Page

LIST OF TABLES

Page

I. INTRODUCTION

It is well established in aeolian sand transport studies that intense sand transport is manifested as a saltation layer whose form acts like a large “effective” surface roughness element (Owen, 1964; Sherman and Farrell, 2008). This alters the flow field immediately above the saltation layer, resulting in wind speed near the bed to decrease and the wind-speed profile to steepen (Bauer et al., 2004). This modification of the velocity profile is believed to be a fundamental response of a self-regulating saltation process in both air and water (Farrell and Sherman, 2004). So too is the development of a characteristic, or representative, vertical mass flux (sediment) profile although the nature of the vertical distribution is contested (Butterfield, 1999; Ni et al., 2002; Dong and Qian, 2007; Dong et al., 2011). It is accepted that the proportion of mass flux rapidly decays with increasing distance away from the bed and the rate of decay is dependent on characteristics of the saltation system (e.g. wind speed and grain size). Since the concept of a saltation layer was first introduced into transport models by Bagnold (1935, 1936) researchers have attempted to accommodate this important feature into the saltation transport models, especially as it represents the link between important feedback processes that drive the fluid flow - surface interactions. Initial attempts modeled the initiation, growth and equilibrium stages of the saltation layer by developing strong theoretical relationships of the feedback mechanisms between moving particles, usually moving in uniform trajectories, and the fluid flow.

The classic approaches of Bagnold (1936, 1941) and Kawamura (1951) first predicted the behavior of a single sand grain moving over a uniform, planar bed comprising both similar sized and volume particles, and iterated this single trajectory for a mass of homogenous sand moving in similar fashion over a certain time period. These studies were later expanded for heterogeneous, or mixed, grain populations. In these studies it is commonly assumed that the coarsest fraction of the grain-size population moves nearest the bed because the largest grains are least susceptible to lifting (Bagnold,

---

This dissertation follows the style of Geomorphology.

1941; Willets and Rice, 1986a; Anderson and Hallet, 1986; Shao, 2000). In natural environments, however, wind-blown sand grains may vary considerably in size and shape and have very different trajectory heights and lengths (Li et al., 2008). **Understanding how grain sizes in a saltating population vary with elevation is fundamental to physics-based modeling of the sand transport process, especially as numerical modeling relies on trajectory calculations to engineer the vertical distributions of mass that are a primary control on the saltation system.**

Researchers have since refined these one-species, homogenous saltation models (i.e., all saltation trajectories are uniform, at least statistically) and dismantled the *saltation* process into four different elements: calculations of 1) conditions for aerodynamic entrainment; 2) geometries of particle trajectories; 3) the dynamics of grain-bed collisions; and 4) the physics of particle-wind feedback (Anderson and Haff, 1986; Anderson et al., 1991; McEwan and Willetts, 1991; Namikas, 2003; Spies and McEwan, 2000; Andreotti, 2004; Kok and Renno, 2009). When combined, these four elements represent the self-limiting saltation process from entrainment to equilibrium. One of the important aspects of understanding the different components of the saltation system is that it allows investigators to model the behavior of the grains near the bed, and more importantly, to eventually accurately define the characteristics of the bulk saltation layer for different wind speeds and environmental conditions. Transport rates and/or vertical distribution profiles of windblown sand can then be then predicted from grain trajectory calculations. This implies that **a thorough understanding of the vertical distribution of mass flux is key to further refining the saltation models** (Namikas, 2003). Unfortunately, testing the models requires direct observations of both the distribution of the fluid shear stresses or wind profiles that force the transport, and the consequent distribution of the saltating grain population (the vertical flux profile) above the surface. To date, because of the **paucity of data of vertical flux profiles**, **especially from field environments**, many numerical and mathematical approaches have relied on the results of only a few laboratory experiments even though it has been demonstrated that these results, based upon observations of wind velocity and sediment flux profiles, may not be

readily applicable to prototype conditions (e.g. Owen and Gillette, 1985; McKenna Neuman and Nickling, 1994; Simiu and Scanlon, 1997; Bauer et al., 2004; Sherman and Farrell, 2008).

Most published research on vertical flux profiles assesses either the rate of decay of sediment away from the surface or the environmental controls influencing the flux characteristics. Because vertical flux distributions are closely related to the modes of sand transport it would be expected that saltation studies should find similar functions to fit the observed transport. However there have been numerous additions, revisions, and modifications of the curves to describe the vertical distributions of wind blown sand. To date **there is still no consensus on which function best parameterizes the observed mass flux distribution** (power, logarithmic, exponential or modified forms thereof). Many published field and wind tunnel results have reported flux profiles with more than one characteristic curve. In most cases the different curves represent the change from one dominant transport mode to another, usually saltation to suspension (Zobeck and Fyrear, 1986; Vories and Fryrear, 1991; Stout and Zobeck, 1996; Sterk and Raats 1996; Youssef et al., 2008) or, to account for deviations of predicted fluxes nearest the bed where a bedload transport component mixes with reptating and saltating modes of transport but does not contribute at higher elevations as saltation becomes the dominant transport mode, e.g., Weinan et al., 1996; Butterfield, 1999; and Zhang et al., 2007a. As Butterfield (1999) remarks "*that this obvious discrepancy in published work has not drawn more attention is perhaps surprising* (p.394)". However, the fact that no consensus has been reached on the contribution of the different controls to the vertical distribution of fluxes and the range of reported relationships for observed fluxes suggests **there may be other experimentally derived controls on the vertical distributions of mass flux** e.g. wind tunnel dimensions (see Li and Ni, 2002), sediment shape (Williams, 1964) and density (Gerety and Slingerland, 1983) or sampling efficiency (see Ni et al., 2002; Li and Ni, 2003; Rasmussen and Mikkelsen, 1998). Further, Mikkelsen (1989) found that similar type traps produced different mass flux profiles for wind tunnel and field experiments. He found that the laboratory flux profile had much more sediment

moving nearer the bed and suggested that "*a sand composition could explain the discrepancies, which may, however, also emanate from a real difference between flux profiles in nature and wind tunnel(s)* (p.22)". The findings of Sherman and Farrell (2008) provide evidence to explain why flux profiles measured in wind tunnels could have different distribution characteristics to those observed in nature. From their analysis of 334 velocity profiles from 32 different wind tunnel and field experiments, they proposed several sources of error (categorized as measurement errors and conceptual errors) that cause wind velocity profiles measured in wind tunnel and field results to be different. These include, but are not limited to, critical constraints on the replication of fundamental wind/sand interactions in wind tunnels and the inability of wind tunnel flow fields to reproduce large coherent structures common in prototype boundary layers. The implications of their results is that wind tunnels constrain the ability of particles to attain maximum or "*true*" trajectory paths during equilibrium saltation. **If the interpretation of their results is to be tested (*i.e.* saltation is suppressed in wind tunnels) then we would expect this anomalous behavior between the two systems to be manifested in the characteristics of mass flux profiles.** This question is an integral part of this research.

Following this logic, the first objective of this work was to collect the requisite high quality, high resolution data of vertical flux distributions in a field experiment. This data was analyzed to assess the performance of the commonly used functions to describe the vertical mass flux profile. Analysis of the sediment grain size distribution statistics at each sampling interval will explore the shape of the vertical profiles of grain sizes. In light of the fact that very few quality data sets exist, this data could also support numerical modelling as a means to deduce some of the complex relationships that control grain trajectories of different grain sizes that comprise the vertical flux profile. Establishing these relationships provides important boundary conditions for a suite of transport models (Anderson and Haff, 1991; McEwan and Willetts, 1991; Shao and Li, 1999; Doorschot and Lehning, 2002; Almeiada et al. 2006; Kok and Renno, 2009).

The second set of objectives of this research is to compile vertical flux profile data from six decades of published aeolian studies and analyze the impact, if any, of different experimental designs and methodologies on the vertical flux profiles. This is done in order to examine if it is possible to identify experimental controls on how mass flux is distributed for different environmental conditions e.g. different grain sizes or wind speeds. The results will determine if it is possible to determine *a priori* the values of the coefficients that describe the shape of the mass flux profiles for a given wind speed and grain size. The results will also appraise if it is physically correct to apply results obtained from laboratory wind tunnel experiments to field studies without including some type of scaling correction. All these results have widespread ramifications in aeolian geomorphology.

A careful review of field and laboratory flux studies examining the characteristics of the vertical flux profiles indicates that there are both methodological and theoretical problems with current approaches. The methodological issues alone, associated mainly with experimental environments, measurement data representation, and/or analytic methods, render some of the earlier data un-interpretable for reanalysis and comparison purposes (Ellis et al., 2009). The theoretical inadequacies of most of the existing research, in the context of a characteristic saltation distribution, stem from an incomplete specification of the variables controlling the development of the mass flux profile. From parallel studies of suspended sediments in water (e.g., Nielsen and Teakle, 2004) or dust in air (e.g., Sundborg, 1955), it is recognized that the so-called **Rouse profile represents a theoretically sound, first approximation of characteristic concentration gradients**. Application of the Rouse profile to a particular environment requires measurement and specification of a reference concentration at a reference height, and estimates of shear velocity and grain settling velocities. The latter two variables are combined into a dimensionless exponent commonly referred to as the Rouse number (e.g. Lee et al., 2004, or Grams et al., 2006) whose value controls the characteristic shape of the distribution, e.g., bedload dominated transport, where all the sediment moves very close to the bed, and fully suspended loads, where the sediment is

uniformly distributed with depth represent two end members of distribution. The Rouse profile is more physically meaningful than current approaches that use standard curve fitting functions to represent the vertical flux data but do not provide any explanatory power for the shape or magnitude of the profile. It is not known whether the Rouse Profile (and therefore, the Rouse number) can be widely applied to aeolian saltation vertical flux gradients - and this does not seem to have been tested empirically - although Scott et al. (1995) produced some theoretical distributions based on the Rouse concept and Udo and Mano (2011) tested a form of the Rouse profile on one set of laboratory flux data with varied success. To date, very few experiments involving aeolian saltation, especially from field environments, have the requisite high quality, high resolution data to allow an assessment of the Rouse-type representation of non-linear flux gradients. The third objective for this research will be to use the data set, collected during the field experiment to supplement the first set of objectives, to test the Rouse relationship for aeolian saltation systems.

The main research objectives are formalized in three research hypotheses:

I. The average grain size of the sediments comprising the vertical mass flux profile become smaller with distance away from the bed.

II. The observed mass flux distribution profiles observed in wind tunnel and field environments all decay exponentially away from the bed but at different rates for each environment.

III. The rate of decay changes as a function of wind speed and/or grain size parameters and can be accounted for using a form of the Rouse number.

In order to test the three hypotheses, four specific research objectives must be accomplished:

I. Collect detailed measurements of 1) mass flux profiles; 2) wind velocity profiles; and 3) grain-size characteristics from a suitable field site characterized by large, flat unobstructed sand surfaces with widely varying transport conditions.

II. Build a comprehensive and detailed repository of mass flux profiles published from wind tunnel and field experiments where saltation is the dominant mode of sediment transport and where (optimally) a wide range of environmental conditions (especially grain size and shear velocity) are reported.

III. Compare mass flux profiles in wind tunnel and field environments by assessing the fitted functions that best describe the decay rate of sand away from the surface and the controls on the vertical mass flux distributions.

IV. Test the validity of using the Rouse concentration model to predict the vertical flux of wind blown sand for a given set of environmental conditions. This will be done by examining (i) the shape of the Rouse-type mass flux profiles which depict the nature of the sediment distribution and, (ii) the magnitude of the Rouse-type mass flux profiles which predicts the volume or flux of sediment being transported for a given set of sediment and fluid conditions.

Formalizing the research hypotheses has been a logical extension of research conducted by the author and colleagues the past decade. This heuristic approach focuses on investigating some of the methodological and theoretical foundations in aeolian research, and, in particular, tries to provide scientific explanations to resolve the continued disagreement regarding the characteristics of the vertical distribution of wind blown sand. Data collected in the field experiment complements a relatively small number of commensurate field and laboratory in the discipline. This meets a critical need for the numerical modeling community. Arnold (2002, p. 818) states "*numerical model predictions of the behavior of the sand transport system have advanced further than the available physical data required for their verification*". A driving motivation for this approach is the conviction that direct application of laboratory results to prototype environments (the current practice) translates the scaling limitations of wind tunnel findings into erroneous predictions of real world conditions. If Hypothesis 1 is

confirmed then there are serious ramifications for existing protocols to calibrate any models using empirical relationships derived from wind tunnel studies of saltation. If Hypothesis 2 is confirmed, then successful application of the Rouse concentration model approach to vertical distributions of mass flux in air provides a strong theoretical foundation to expand current approaches beyond the pervading *impasse* that has failed to provide a physically meaningful, universally representative vertical flux distribution model. Further, if the Rouse model successfully predicts, within the range of acceptable error, the observed transport rates and mirrors the characteristics of the observed mass flux profiles, then serious obstacles that have challenged aeolian researchers for decades may be removed.

II. BACKGROUND

2.1 Introduction

Physically-based models of aeolian sand transport rely, implicitly or explicitly, on an understanding of the trajectories of saltating grains (e.g., Bagnold, 1936; Kawamura, 1951; or, more recently, Anderson and Hallet, 1986; Werner, 1990; Spies et al., 2000; Andreotti, 2004, or Sørensen, 2004). After grain movement has been initiated by drag (mainly) and lift forces alone (aerodynamic entrainment), the transport system typically switches to a saltation-dominated mode where grain-grain impacts become critical to maintaining transport. As aerodynamically entrained grains return to the sand surface most of them rebound away from the surface after imparting approximately half of their momentum to the surface, some of which ejects other grains (e.g., McEwan and Willetts,1991; McKenna-Neuman and Nickling, 1994). Because most wind-blown sand is moved through the impact saltation process, it is the trajectories of these latter grains that are of greatest interest for predicting transport rates and related phenomena. One of the obvious, bulk manifestations of saltation trajectories is the development of a characteristic concentration profile above the surface (e.g., Zingg, 1953; Butterfield, 1999; or Dong et al., 2006).

Quantitative representation of the concentration profile is fundamental for understanding grain behavior, sand transport rates, and abrasion potential. A number of functions have been proposed as best representing the rapid decrease in flux away from the bed, including power functions (e.g., Zingg, 1953; Scott et al., 1995; Sterk and Raats, 1996; Stout and Zobeck, 1996; Butterfield, 1999, and Dong et al., 2006; Ni et al., 2002), logarithmic functions (Iwagaki, 1952; Rasmussen and Mikkelsen, 1998), and exponential decay functions (e.g., Williams, 1964; Gerety and Slingerland, 1983; Nalpanis, 1985; Rasmussen et al., 1985; Butterfield, 1991, 1999; Shao and Raupach, 1992; White and Mounla, 1991; Weinan et al., 1996; White, 1996; Greeley et al., 1996; Zhou et al., 2002; Namikas 2003; and Dong et al., 2002, 2004a, 2006, Feng et al., 2009). The application of this technique to flux data is paramount, as the regression equations are usually the primary empirical source for calibration or verification of computer and

mathematical models (Ellis et al., 2009). More importantly, in cases where sampling occurred at some distance above the bed, extension of the fitted curves provides estimates of the near-bed flux estimates.Despite decades of examination of flux profiles, it is apparent that there remains no agreement concerning the exact nature of function that best represents the concentration gradient. Not only is there disagreement concerning the nature of the vertical distribution, there is also disagreement about the values of the coefficients that describe any particular distribution form.

2.2 Grain size-sorting characteristics

Aeolian research has established that the coarsest fraction of a grain-size population should move near the bed because the largest grains are least susceptible to lifting (Bagnold, 1941; Willets and Rice, 1986a; Anderson and Hallet, 1986; Shao, 2000). It is commonly assumed, for that reason, grain size should decrease with elevation above the bed surface. However, contradictory evidence from field experiments (Draga 1983, Van Dijk, 1990; Greeley et al., 1996; van der Wal, 2000; Arens et al., 2002; and Xing, 2007) and wind tunnel experiments (Williams, 1964 and Xing, 2007) suggests that this simple size-decay concept may not be typical. In those studies the mean grain-size first decreases from a maximum close to the surface, and then increases with increasing elevation (Table 2.1). The change in grain-size trend typically occurs within a short distance above the bed (ca. 0.20 m or less). This discrepancy between theory and observation deserves further attention because of the importance of understanding distributions of grain trajectories during saltation. Saltation theory states that the concentration of particles of a given size and height is determined by the balance of forces between gravitational and fluid forces (Kok and Renno, 2009) and by particle inertia. With a mixed-size sand population this implies that there should be a decrease in mean grain size away from the surface. For example, if a saltating grain impacts the surface and imparts a particular momentum to ejected grains that leave the bed at a given angle, then a smaller grain should be traveling faster, and therefore higher, than a larger grain. That observations of grain size distributions do not confirm this logic

indicate that this fundamental issue requires further consideration. Part of this study examines the characteristics of grain size distributions above the bed from vertical flux profiles collected in a natural coastal environment.

Table 2-1. List of sources reporting grain-size inflection[a]

Source	***Site***	***Inflection* (m)**	***d* (mm)**	**u_* (m/s)**
Arens et al. (2002)	B	0.15 - 0.20	0.171 - 0.176[1]	15.2[2]
Greeley et al. (1996)	B	0.075 - 0.15[3]	0.235 - 0.325[4]	0.312 - 0.489
Jericoacoara site				
CSFF	B	0.05 - 0.15	0.253 - 0.366	0.41 - 0.54
CSFC	B	0.05 - 0.15	0.364 - 0.408	0.49 - 0.50
Beach	B	0.05 - 0.15	0.235 - 0.263	
Williams (1964)	WT	0.055 - 0.095	0.32 - 0.34[5]	0.362 - 1.356
Xing (2007)	WT	0.05 - 0.15[6]	0.30 - 0.50[7]	7.5 - 15.3[8]

[a] In the table, *Site* describes the environment where the data were gathered (*B* = beach, *WT* = wind tunnel); *Inflection* describes the height at which a reversal in grain-size was observed; *d* is grain size in mm; u_* is the shear velocity (ms^{-1}). The Jericoacoara nomenclature is explained in Section 3.1.1. Other reports of reversals in grain-size with elevation do not provide adequate information to include in the table e.g. Sharp (1964), van Dijk (1990) and Van der Wal (2000).

[1] Approximated from their Figure 5, p.1169
[2] Wind velocity at 5 m elevation
[3] Height estimated from horizontal inflection distances of 1.05 - 2.10 m using a length-to-height ratio of 14, following Nalpanis et al., 1993
[4] Modal grain sizes reported in their Figure 15, p.51
[5] Approximated for the uniformly distributes samples from his Table I, p.263
[6] Approximated from his Figure 7, p.235
[7] Approximated from his Figure 4, p.232
[8] Free stream wind velocity

Understanding how grain sizes in a saltating population vary with elevation is fundamental to physics-based modeling of the sand transport process, especially as numerical modeling relies on trajectory calculations. Further, the mechanisms by which saltating grains leave the surface and the velocities and angles that they attain are still not fully understood (Zhang et al., 2007). Establishing these relationships can provide important boundary conditions for a suite of transport models (Anderson and Haff, 1991; McEwan and Willetts, 1991; Shao and Li, 1999; Doorschot and Lehning, 2002; Almeiada et al. 2006; Kok and Renno, 2009). An understanding of the distribution of

trajectory heights and lengths for different grain sizes should be an integral part of the new saltation models (Namikas, 2003, 2006; Rasmussen and Sørensen, 2008; Namikas et al., 2009). Indeed, it would be the ability of a numerical model to replicate the size-sorting characteristics with elevation that provides one means of evaluating that model's performance. Unfortunately, there are few examples of quality data sets gathered from field experiments (described in section 3). As stated by Mikami et al. (2005, p. 2), "*field data, which include information of the whole saltation process and can be used for verifying the (heterogeneous saltation) theory, are lacking*". Similarly, Xing (2007, p. 230) notes, "*the movement of grains in a mixed-grain-size sand bed is different to the grain movement in a uniform sand bed due to the relative difference of grain size or grain mass*". An important contribution of this work is to provide data that describe the grain size and sorting characteristics of vertical flux distributions observed during transport events with a naturally mixed-size grain population.

2.3 Controls on vertical distributions of mass flux

Numerous workers have carried out extensive wind tunnel experiments to examine sediment and wind speed controls on flux distribution (or rate of decay of sediment above the surface), both of which are commonly reported as being first order controls on the characteristic slope of the vertical flux profile. Controlled wind tunnels studies provide insight into the influence of these variables on the distribution of flux above the surface. For example, Dong et al., (2002) measured 58 vertical flux profiles for nine different grain size populations (ranging from 0.90 – 0.125 mm), transporting over a wide range of wind speeds (ranging from 8 – 22 m/s). Their data is plotted in Figure 2-1 where slope is the decay coefficient derived from fitting an exponential function to the measured flux data. The slopes of the flux profiles decrease from approximately -3.20 for the first four runs (d = 0.90 mm) to approximately -16 for the last set of eight runs (d = 0.125 mm). A physical interpretation of these slope values is given in a dimensionless simulation in Figures 2-2A and 2-2B. The lowest slope value of -20 demonstrates that the flux decays rapidly a short distance from the bed and there is

little flux measured at higher elevations. Therefore there is a rapid, or steep, steep decrease in total flux. As the slope value increases, to say -5, a greater proportion of the flux is moving at higher elevations above the bed and the slope of the profile becomes less steep.

Looking at the Dong et al., (2002) data, as the mean group grain size decreases from Run 1 (d = 0.90mm) to Run 58 (d = 0.125 mm), the slopes of the measured flux profiles become steeper. The physical interpretation of this is that flux decreases more rapidly as grain size decreases, or, stated another way, more sand is transported to higher levels as grain size increases. Conversely, looking at the slope values within each grain size group, a decrease in wind speed also causes the flux to decay more rapidly. Physically, we would expect this to occur, as the volume of sand moving at higher elevations decreases as wind speed decreases.

For example, for the grain size group d = 0.225 mm in Figure 2-1, increasing the wind speed in seven 2 m/s increments from 10 to 22 m/s results in the slope value increasing from approximately -9.5 to -6.5. Again, we would expect that more grains are moved higher above the bed as wind speed increases resulting. These types of controls are evident in many other published wind tunnel studies, e.g., Williams (1964); Shao and Raupach (1992); Hotta and Horikawa (1993); Hotta et al., (2006); Butterfield, (1999); Zou et al., (2001); Ni et al., (2002); Dong et al., (2004a), Liu and Dong (2004); Rasmussen and Sørensen (2008); and Feng et al.,(2009). For field experiments the impact of grain size and wind speed is less apparent although the same general trends are observed. The variation in the field distributions can be attributed to any number of factors such as experimental error, spatial and temporal boundary-layer development, transport intermittency or unsteadiness, or mixed grain populations. The variation in flux profile slopes between different experiments may offer important insight into model performances Recently, more efficient and less obstructive ‘trapping’ or ‘counting’ devices and mathematical models have shown that the near-bed flux distribution deviates from the standard exponential relationship. The range of relationships for observed

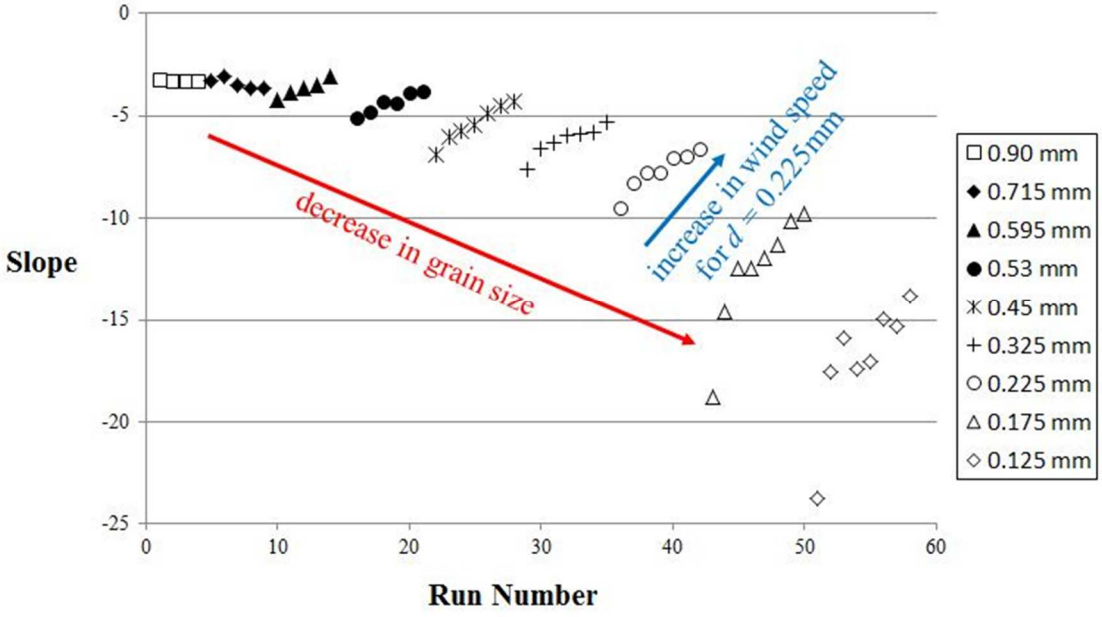

Figure 2-1. The relationship between the decay coefficient (*b)*, representing the *slope*, and *grain size* obtained from regression analyses ($q_h = \alpha exp(bz)$) using the 58 runs reported in Dong et al., (2002). Physically, *b* represents the rate of decrease of flux with height above the bed. As the value of *b* decreases, the flux rate decays much more rapidly away from the surface than for higher values (see: Figure 2-2). Two important trends are shown:
(1) the red arrow highlights how slope values decrease as grain size decreases from run 1 (d = 0.99mm) to 58 (d = 0.125mm).
(2) the blue arrow illustrates the increase in slope value as wind speed increases within each grain size group; in this case, the change in slope for the 7 runs with d = 0.225mm are highlighted.

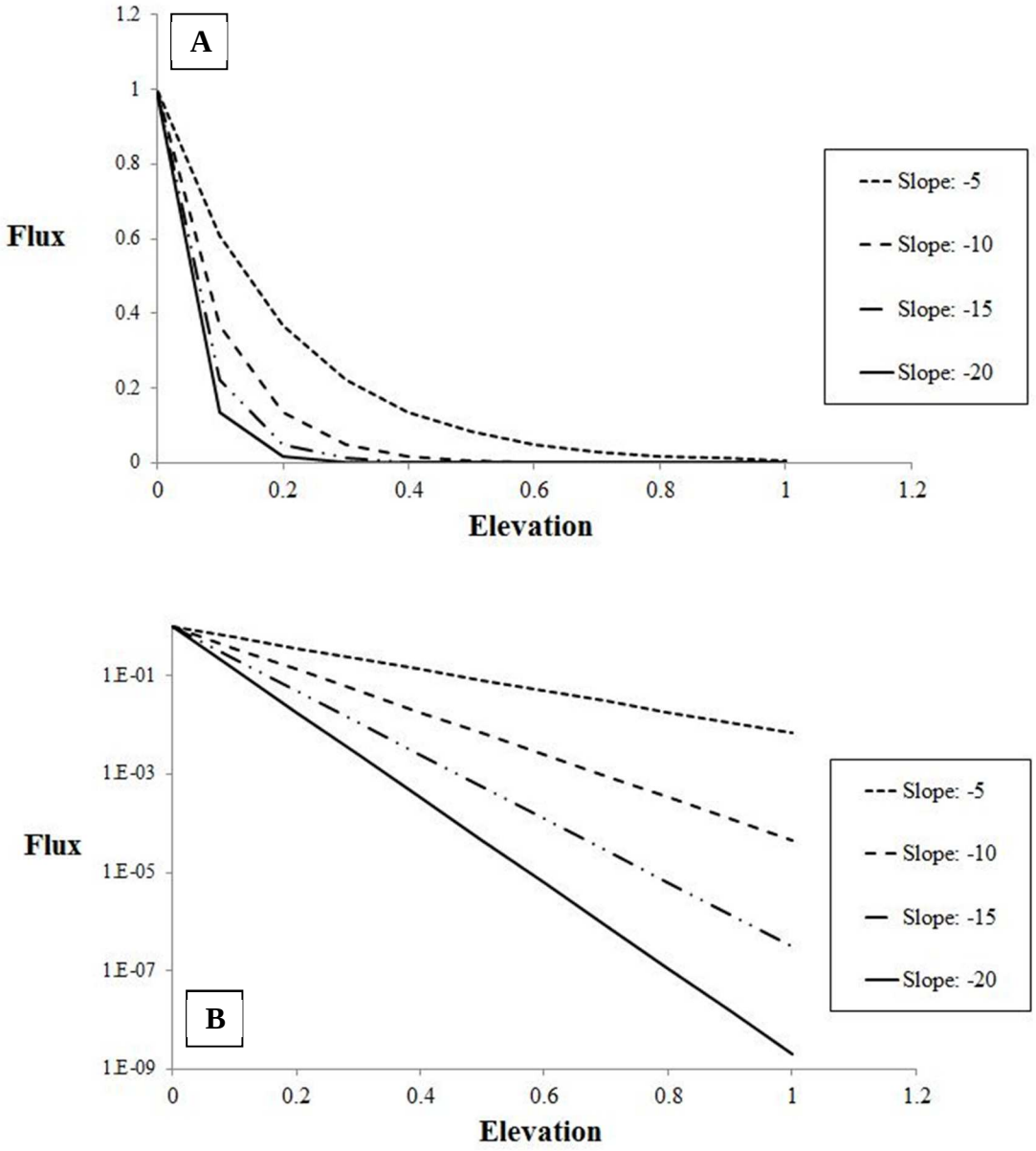

Figure 2-2. (A) Linear-linear plot of elevation (*z*) *vs.* flux (*q*) calculated using $q = exp(-bz)$ for a constant range of elevations (z = 0 – 1.0 m) and variable slopes (b = -5, -10, -15, -20) **(B).** Log-linear plot of elevation *vs.* flux. Slopes are all straight lines which make comparison of the vertical distributions easier. A slope value of '-20' is said to be *steeper* than a slope value of '-5' as the proportion of flux decreases much more rapidly with elevation away from the bed for the former slope value.

fluxes suggests there may be experimentally derived controls on sand transport (Ellis et al., 2009). Quantitative analyses comparing mass flux experiments are difficult due to the large number of potential controls. This may be one reason why many fitted functions for mass flux have been proposed. This suggests that further investigations may provide useful information for refining our understanding on the controlling factors of current saltation models and improving the predictive performance of the next series of aeolian transport models. One such method done in this research (and based on an initial pilot study) is to evaluate the data in the context of the classic Rouse concentration profile distribution.

2.4 Laboratory *vs.* field experiments

Wind tunnels have been indispensable to explore and elucidate some of the fundamental wind/surface interactions that comprise the aeolian transport system. Researchers can control some or all of the environmental variables that cause complexity in the prototype, thereby refining our understanding of some of the first and second order effects of different variables on transport characteristics. There are, however, several critical scaling constraints on the replication of physical processes in wind tunnels, and these have been discussed in detail in Gerety, (1985), Owen and Gillette (1985), McKenna-Neuman and Nickling (1994), Simiu and Scanlon (1997), Arnold (2002) and Bauer et al., (2004). Some of these scaling constraints have been addressed explicitly in the wind tunnel literature. For example, the appropriateness of using the log law to estimate shear velocity from velocity profiles has received considerable attention (Owen and Gillette, 1985; Janin and Cermark, 1988; White and Mounla, 1991; Spies et al., 1995; Butterfield, 1999; Bauer et al., 2004). Conversely, other scaling constraints - specifically, scaling of the sediments - have not received similar analytical or theoretical treatment but remain implicit in wind tunnel tests. These may provide the key to understanding some of the differences we have found in our examination of saltation characteristics in wind tunnel and field studies.

Following the findings of Sherman and Farrell (2008) and others, it is clear that the restricted length scales of wind tunnels prevent the development of the full spectrum of turbulent motions found in the atmospheric boundary layers. We would also expect that the saltation layer is not free to grow vertically in unrestricted fashion due to wind tunnel dimensions (Bauer et al., 2004). Indeed, as wind tunnel researchers continue to refine their models and adjust for scaling constraints of the boundary layer dynamics, it is surprising that no similar treatment for the moving sand grains has been forthcoming. For example, White (1996) addressed the topic of laboratory wind tunnel simulations of aeolian sand transport and, following a very comprehensive review of the complexities of boundary layer similarity criteria, stated that "*the true forte of wind tunnel applications lies in the study of saltation. In effect, there is little compromise on the physical process of saltation occurring in the wind tunnel. This is due to the fact that saltation is not scaled but simply replicated in the tunnel. Only a few basic similitude rules need to be followed to produce high-quality saltation flow in the wind tunnel* (p.211)". There is mounting evidence that this cannot, literally, hold true. In fact White, paradoxically, alludes to the scaling impact of saltating sand in the same paper. He points out that the important dimensionless similitude parameter z_o'/D (equivalent roughness height in saltation proportional to particle diameter) cannot be satisfied as the decrease in sand grain size, as required for geometric similarity, would result in grain diameters so small that cohesive forces not present in field models would occur and if introduced to the flow would go into suspension and the saltation process would not occur (Hughes, 1983). By addressing this distortion it has to be assumed that White is alluding to the fact that the effective roughness (z_o') is much higher in the full scale field models than measured in wind tunnels. This agrees with other research findings (e.g., Greeley and Sullivan, 1992; McKenna Neuman and Maljaars, 1997; Sherman and Farrell, 2008).

The Froude Number also illustrates the scaling problem that affects all saltation studies conducted in wind tunnels (Figure 2-3). Broadly, the scaling laws involve matching the non-dimensional coefficients of the equations of motion (between field and

FIELD **WIND TUNNEL**

$$F_r = \frac{u_*}{\sqrt{gl}} \qquad F_r = \frac{u_*}{\sqrt{gl}} \qquad (2\text{-}1)$$

$$F_r = \frac{\mathbf{0.14}}{\sqrt{(9.8)(0.40)(\mathbf{2.0})}} \qquad F_r = \frac{\mathbf{0.14}}{\sqrt{(9.8)(0.40)(\mathbf{0.15})}}$$

$$F_r \approx 0.05 \qquad F_r \approx 0.18$$

Figure 2-3. A simple scaling analysis using the Froude number for field and wind tunnel environments (photo on left: beach location in Brazil (2008) experiment; photo on right: Atmospheric boundary layer wind tunnel in UC Davis, Mechanical and Aeronautical Engineering from http://mae.ucdavis.edu/~wind (Feb 8, 2012)).

The Froude number (Equation 2-1) is one common non-dimensional scaling number used to assess similarity of the saltation process between prototype and scale models. For aeolian saltation, it is calculated using the shear velocity (u_*), the gravitational constant (g), and a length scale (l). Boundary layer theory suggests that using the mixing length is a reasonable length scale, where the mixing length defines the spatial and length scales of coherent turbulent structures that can occur for given boundary conditions. The mixing length, (l) = $k\delta$, where k is the von Kármán constant and δ is the height of boundary layer.

To obtain similitude in Fr (i.e. change 0.18 to 0.05) the laboratory researcher has two choices:

(1) Change the denominator by simulating a boundary layer height that is 2m high. However, as a general rule, the boundary layer height in a wind tunnel is approximately half the wind tunnel height. Therefore, the wind tunnel needs to be 4m high to obtain an equivalent boundary layer height to that observed in the field (2m).

(2) Change the numerator. However, if shear velocity is decreased, then grain size must also be decreased to reduce the critical threshold for motion and ensure that sediment is moving. The grain size cannot be reduced so small that cohesive forces become important or that sediment moves in suspension, rather than saltation, both of which can occur in silts and clays.

From this scaling analysis it becomes clear that the task of replicating the fluid-boundary interactions in wind tunnels is difficult – especially when you cannot scale sand.

wind tunnel), so that the same physical processes of the full scale flow are exactly simulated in wind tunnel. The Froude number is defined as the ratio of inertial forces (defined here using shear velocity) to gravitational forces (defined here using the gravitational constant, *g*, and a length scale, *l*). There are a number of characteristic length scales we can use to calculate the Froude Number but boundary layer theory suggests that using the mixing length is a reasonable scale. The mixing length, used to parameterize the momentum transfer with a fluid boundary layer, defines the spatial and length scales of coherent turbulent structures that can occur for given boundary conditions and is estimated by multiplying the boundary layer height, δ, by the von Kármán constant (k = 0.4). Physically, similarity of the Froude Number ($F_r = U_z / (g\delta)^{1/2}$) cannot be satisfied during wind tunnel tests. For example, in order to satisfy the non-dimensional Froude number criterion for a 2 m boundary layer observed across a beach in a wind tunnel with a maximum boundary layer depth (δ) of 0.15 m, there are two options. First, the value of the numerator can be changed, in which case wind speed (U_z) needs to be slowed down considerably. The two consequences of this are (i) wind speed cannot be so small as to not satisfy Re >2.5 and (ii) the sample grain size also needs to be reduced considerably in order to decrease the critical threshold shear velocity and ensure sand is moving - but not to grain diameters so small that cohesive forces become important (White and Mounla, 1991). Second, the value of the denominator can be changed. If we assume that the boundary layer in a wind tunnel is approximately half the wind tunnel height, then a 4 m high wind tunnel is needed to simulate a 2 m high boundary layer. To the author's knowledge, there has not been any laboratory aeolian saltation research completed using wind tunnel heights exceeding 1.5 m. It is a fundamental concept that reduced scale models have inherent scaling constraints. Despite researchers continued efforts to refine our understanding of many of these, there has yet to be any consensus on the treatment of the 'unavoidable' constraints of sediment scaling, or the subsequent treatment of constrained particle trajectories.

Other differences between the two research environments is the propensity of some wind tunnel workers to measure saltation dynamics using very high wind speeds

and shear velocities. For example, maximum shear velocities of 1.20, 1.24, 2.33, and 2.36 m/s were reported in Williams (1964), Feng et al., (2009), Hotta et al., (2006), and Ni et al., (2002), respectively. Using the relationship of Hsu (1977), to convert shear velocity (u_*) to a wind speed at two meters elevation ($u_* = 0.044U_{2m}$), these equate to wind speeds of 27, 28, 53, and 54 m/s. The latter two wind speeds are Category 3 hurricane force (111-130 mph) using the Saffir-Simpson scale! Moreover, these wind speeds are being driven through a small tunnel. These ranges of shear velocity are seldom experienced, or measured, in the field.

The mean grain size distributions can sometimes be very different in wind tunnel and field experiments. Wind tunnel experiments, by design, use controlled sand samples that are, invariably, well sorted, uniform sized grain. This has implications for the characteristic representative grain trajectories that comprise the saltation layer. Conversely field locations can be poorly sorted, have a wide range of grain size populations, be positively or negatively skewed, and be comprised of different minerals and densities. Currently, there is no robust model that explains how a naturally mixed-sand population moves once the threshold shear velocity is exceeded for all available grain sizes. One approach to addressing this difficultly is to use a combination of numerical modeling and sets of observed vertical flux measurements to deduce what the launch parameters must be, at least in aggregate. The vertical grain size-sorting data and flux data provided in this study provide one such opportunity to the modeling community.

This review is not to question the validity of wind tunnel research. It is simply proposed that there are implicit scaling differences absorbed by wind tunnel studies and these have created fundamental differences between the two basic integral components of the saltation system: the boundary layer and the saltating layer. McKenna-Neuman and Maljaars (1997) surmise that these differences may scale with wind tunnel dimensions but because this facet of wind tunnel modeling has received little attention then, substantive differences will continue to occur in reported findings. Perhaps, somewhat ominously, Simiu and Scanlan (1997) state that "*the wind tunnel modeler has*

a series of inevitable compromises that render the task complex, revealing it as an art of both performance and interpretation rather than an exact science (p.274)". One fundamental part of this research is to address some of these scaling concerns in wind tunnels, and specifically to determine if the hypothesized scaling differences in saltation can be identified. In order to address this question quality vertical flux profile data from both environments are required. The data collected in the field experiment will complement the small number of commensurate laboratory data so that we can gain a measure of scaling differences between wind tunnel and field environments. For modeling, this research is important because it will provide field data to meet a critical need identified by Arnold (2002) "*numerical model predictions of the behavio(u)r of the sand transport system have advanced further than the available physical data required for their verification* (p.818)".

2.5 The Rouse model

Sediment suspension occurs when the upward velocity component of turbulent motion is greater than or equal to sediment fall velocity. Thus, the position of a particle in the fluid is supported by the fluid motion itself. This is a common mode of fine sediment transport in a number of aquatic environments and for dust in aeolian systems. The nature of the distribution of suspended particles above a surface has been a focus of research since the early years of the 20th Century. Schmidt (1925) was the first to suggest that the vertical distribution of suspended sediment can be defined by a balance between upward turbulent diffusion of sediment and its settling rate. He developed a theoretical relationship based upon turbulent mixing of particulates in the atmosphere. The basic premise is that the average *concentration* of sediments, defined as the volume of sediment per total volume of material (sediment + fluid), at any elevation is controlled by a balance between the gravity force on the particles (manifest as particle settling velocity) and the vertical component of turbulence (represented, more recently, as shear velocity). By assuming an equilibrium vertical distribution of sediment, the upward flux of suspended sediment driven by turbulence from high concentration (near the bed) to

low concentration (near the water surface) is perfectly balanced by the downward flux of suspended sediment under its own fall velocity (Parker, 2004). This relationship can is expressed as:

$$V_g C + \varepsilon_s \frac{dC}{dz} = 0 \quad (2\text{-}2)$$

where V_g is the downward flux of a particular volume of grains per unit volume, C is the volume concentration of suspended sediment at elevation z, ε_s is the diffusivity of suspended sediment, and dC/dz is rate of turbulent diffusion per unit volume (Schmidt, 1925; O' Brien, 1933; Rouse, 1937; Vanoni, 1946; Einstein and Chien, 1955; and Bridge, 2003). The second term derives from a gradient diffusion assumption, in that the turbulent flux is assumed to be equal to the concentration gradient (dC/dz) times an eddy diffusion coefficient (ε_s) for sediment. This latter coefficient, the ε_s term, is assumed to be equivalent to the kinematic eddy viscosity, or diffusivity, of the flow (ε_m) which defines the momentum transfer of the turbulent flow (and, by assumption, sediment) through the profile. It usually has a negative sign to indicate that there is a net flux from high to low concentration. This is the case as concentration is greatest near the bed (as sediment is always tends to settle out) and any upward turbulent eddy fluctuation will tend to carry more sediment than the equivalent downward fluctuation. Therefore, where a concentration gradient exists, turbulent diffusion leads to a net upward flux of material. The minus sign is balanced by the term on the left, representing the net downward flux.

This theory, described by Equation 2-2, was extended for application in water by Jakuschoff (1932) and Leighly (1924, 1932). O'Brien (1933) added the diffusivity term (ε_m) that related the distribution of sediment in the fluid based upon a linear decrease in shear stress distribution with distance from the bed (Shah-Fairbank, 2009):

$$\varepsilon_m = k u_* \frac{y}{h}(h - y) \quad (2\text{-}3)$$

where ε_m is the momentum exchange coefficient, h is the flow depth, and y is the vertical distance from the bed (Shah-Fairbank, 2009). This momentum exchange coefficient was related to the diffusivity of suspended sediment (ε_s) by:

$$\varepsilon_s = \beta\, \varepsilon_m \quad (2\text{-}4)$$

where β is a constant of proportionality, that is also called the Schmidt number or, more simply, a diffusion coefficient. The original approaches assumed β equal to unity. By assuming that β equals 1, and the law of the wall extends through the profile (in order to calculate ε_m), the Rouse equation was derived (Equation 2-5).

Rouse (1938) evaluated the exponential distribution in a series of laboratory experiments (in this case, using a blender-like stirring apparatus to keep sediments in suspension). He found that the concentration gradient, or slope, was a function of grain size and "frequency of agitation" in his apparatus – or shear velocity more generally. Specifically, for a given grain size, the slope of the concentration profile decreases with increased shear velocity. Physically, this means that the sediment is more uniformly distributed along the profile. Conversely, for a constant shear velocity, the slope of the concentration profile will increase with increased grain size. Note that the slope changes described here are reversed from those seen in Rouse's original paper (Rouse, 1938, Figures 4 and 5) because he reversed the independent and dependent variables in his analysis. Rouse combined the influence of grain size and shear velocity changes into a universal equation (Equation 3) for concentration gradients (now termed the Rouse Profile):

$$\frac{C_z}{C_a} = \left(\frac{h-z}{z}\frac{a}{h-a}\right)^{\frac{R}{\beta}} \tag{2-5}$$

where C_z is the sediment concentration at elevation z above the bed, C_a is a reference concentration at a reference elevation a above the bed, h is water depth, R is the Rouse number, and β is a constant of proportionality, typically assumed to be equal to 1 but with much larger values reported (Lees, 1981; van Rijn, 1984; Hill et al., 1988). The Rouse number relates sediment size (in the form of settling velocity, w_0) to shear velocity, u_* . Here, it is expressed in its full form:

$$R = \frac{W_0}{k u_* \beta} \tag{2-6}$$

where κ is the von Kármán constant (0.4) and u_* is the shear velocity. In practice the reference level, a, is established by measuring the sediment concentration and grain size distribution at some height off the bed in order to estimate the concentration profile at all

levels off the bed and derive a value for the total flux. The value of *a* cannot be zero in order for the equilibrium diffusion-sediment gradient concentration approach to be applicable as turbulence cannot persist all the way down to the sediment bed, or boundary, where laminar effects dominate. Also, if the reference height, *a*, is equal to zero, then Equation 2-5 predicts an infinite concentration which is physically incorrect. The value *a* has been given by half the flow depth, or 0.05*h* (Vanoni, 1946; Itakura and Kishi, 1980), half the bedform height (van Rijn, 1984), some small multiple of the grain size, *d*, (Lee et al, 2004), 100*d* (Shibayama and Rattanapitikon, 1993), the lowermost extent of direct observation (Lee et al, 2004) or the height of the roughness length (Smith and McLean, 1977; Dyer, 1986). The value of w_0 is derived using a sediment grain size relationship derived from empirical and theoretical models (Hallermeir, 1981; Dietrich, 1982; van Rijn, 1984; Cheng, 1997; Ahrens, 2003; Ferguson and Church, 2004). The shear velocity, u_*, is derived from experimental measurements. The value of the constant of proportionality, β, or the Schmidt number, that describes the relationship between the diffusion coefficients for suspended sediment and the turbulent fluid mass is mostly assumed to be unity – which is correct, but only in principal ($\varepsilon_s = \varepsilon_m$ in Equation 2-4).

The ***shape*** of the Rouse concentration profile which represents the characteristic distribution of sediment in the fluid is controlled by the exponent, or Rouse number, whose role can be understood in its limits (shown in Figure 2-4). When fall velocity is large, say for larger grain populations, or shear velocity is low, for smaller fluid velocities, the Rouse Parameter (*R*) is greater than one and the grains are concentrated near the bed and the upper flow is clear. As turbulence (near-bed turbulence intensity) increases or fall velocity decreases, *R* becomes less than one and the grains are spread more uniformly throughout the flow. From these relationships the Rouse number is also one way to quantify expected (dominant) modes of sediment transport, based upon empirical studies. For example, Metivier and Meunier (2003) indicate that bedload

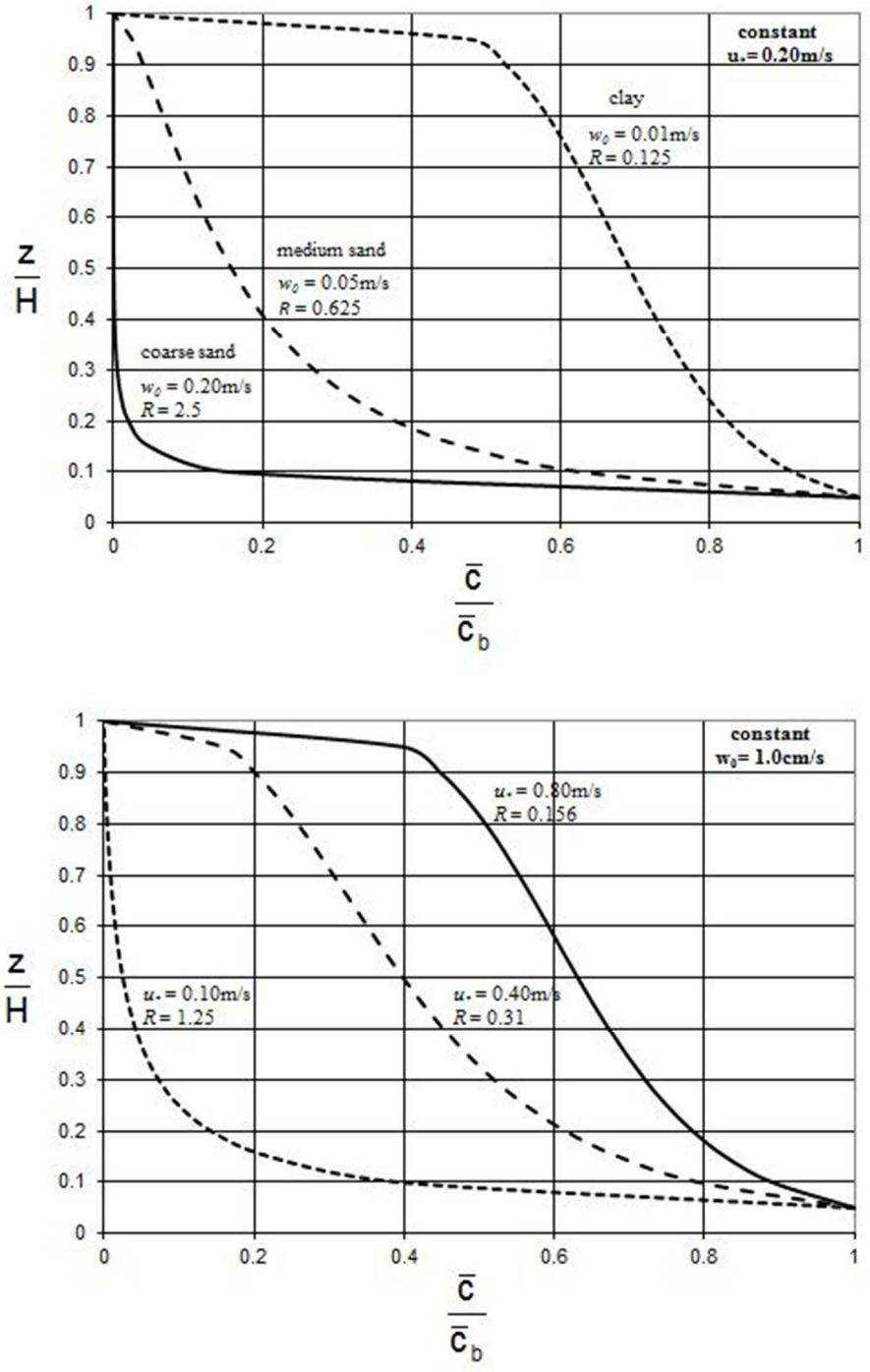

Figure 2-4. Controls on the shape of the concentration distributions. Holding the shear velocity constant (A, on top), the concentration becomes more uniform with decreasing fall velocity (grain size). Holding the grain size constant (B, on bottom), the concentration becomes more uniform with increasing shear velocity.

should dominate when the Rouse number is greater than 1. Lee and Hsieh (2003) indicate that the critical Rouse number to distinguish bedload from suspended load is 5 (bedload dominates with R > than 5). Although the absolute cutoffs described by these (and other) authors, are different, the concept is the same. As the value of the Rouse number increases, an increasing proportion of the sediment is moved closer to the bed.

The Rouse number controls the shape of the concentration profile. Of equal importance is the ***magnitude*** of the sediment in suspension. The suspended concentration C_z increases linearly with increases in C_a. Importantly, this mathematical model cannot be solved without using experimental results to evaluate the unknowns. The suspended sediment transport rate (Q_s) can be calculated from:

$$Q_s = u_s C \tag{2-7}$$

where u_s is the average speed of the sediment (approximately equal to the fluid velocity), which is calculated from an appropriate velocity profile law (e.g. the law of the wall) (Bridge, 2003). The depth-averaged volumetric suspended load transport can be calculated by integrating Equation 6 through the entire depth, from the bedload layer (z_{ref} = a) to the water surface (z = h), to yield:

$$Q_s = \int_{z_{ref}}^{h} Cu\, dz \tag{2-8}$$

The have been many reported cases of differences between the measured values of the Rouse number, obtained by fitting the Rouse model to observed data, and theoretical calculations of the Rouse number by solving Equation 2-6 (see Akalin, 2002 for background). There are many reasons why these differences occur - from questions regarding the nature of the assumptions used to construct the model to the correct parameterization and variability of the input variables that control the model output. For example, the Rouse model is that do not account for spatial variability in flow or bed sediment characteristics. This horizontal uniformity assumption ignores variability in the horizontal advection of water and/or sediment that will lead to differences in predicted and/or calculated values of the Rouse number (Orton and Kineke, 2001). Similarly, the assumption of identical eddy diffusion coefficients for mass and momentum transfers

has received a lot of attention and is discussed in Section 2.5.4. Besides these type of assumptions, trying to determine the correct parameterization of the values of the input variables in the Rouse number (w_0, k, , u_*, β) in response to changing environmental conditions has become an insurmountable task. The behavior of the input variables in response to different experimental and environmental conditions have been scrutinized by many workers in water research in order to provide some physical basis to correct for observed differences in measured and predicted values of the Rouse number. Numerous experiments have since been conducted to examine the impact of these on the values of the Rouse number (Parker and Coleman, 1986; Gelfenbaum and Smith, 1986; McLean, 1992). The next sections provide a brief synopsis of some of the physical and theoretical challenges in identifying representative and reliable values of the Rouse number variables in water research.

2.5.1 Rouse number: w_0, fall velocity

Fall velocity appears as the numerator in the Rouse number. It is fundamental to any discussion of sediment transport in environments where sediment transport occurs as suspended, or partially suspended, load in water or in air. It is one of the most important factors affecting the mode of sediment transport and the time a particle remains in suspension. Intuitively, hydrodynamic and aerodynamic properties of particles are best characterized using their fall velocities, which are strongly controlled by particle properties such as size, shape, and density, rather than a geometric grain size parameter which ignores potentially important controls on grain behavior. As such, sediment fall velocity has come to represent a characteristic of considerable practical as well as analytical value. There are many challenges for researchers trying to establish a representative value of fall velocity, also referred to as settling velocity or terminal velocity, to use in calculations of the Rouse number. These include, but are not limited to, (i) deciding which fall velocity equation to use; (ii) determining a representative particle diameter for a mixed sediment population; (iii) assessing the impact of environmental conditions on the value of the fall velocity; and, (iv) evaluating the

sensitivity of the Rouse model to changes in estimates of the fall velocity. Evaluating all these issues is beyond the scope of this research. However, a brief synopsis of the fall velocity of particles in water is provided here to provide the theoretical background used to derive a new empirical equation to estimate the fall velocity of particles in air, which is presented at the end of this section.

The relative motion between a sediment particle and the surrounding fluid under various conditions of entrainment, transport and deposition appears to depend upon the same factors as the velocity at which the particles would fall through the fluid under their own weight. Any object moving through a viscous fluid has a resistive drag force exerted on it by the fluid. This resisting force strengthens as the downward velocity increases. Eventually, a free falling object reaches its fall velocity when the downward force of gravity, or weight of the object, equals the upward force of drag, or fluid resistance. This causes the net force to be zero, resulting in an acceleration of zero. This is an important relationship as it prevents the object velocity from increasing without limit and it implies that there is a maximum fall velocity for a given set of conditions.

Experimentally, it is very difficult to measure the fall velocity *in situ* and so researchers have relied on laboratory experiments, theoretical models or combinations of the two, to derive relationships to calculate fall velocity (Jiménez and Madsen, 2003). Measuring the fall velocities of particles in water can be accurately done in settling tubes only a meter or two in length and a large number of formulas have been proposed. These are reviewed in detail in Clark and Quadir (1981), Dietrich (1982), Cheng (1997), Ahrens (2003), and Ferguson and Church (2004).

As stated previously, the fall velocity of particles can be estimated with reasonable accuracy by balancing relationships for the weight of a particle and fluid drag. For small particles, moving at slow rates, the Stokes Law is used (Equation 2-9). Stokes Law (1851) states that for ideal spheres, with a diameter, $d \approx 0.1$mm, at low values of particle Reynolds number ($R = w_s d/\nu < 1$), and falling at their fall velocity, the forces resisting gravity (mg) are balanced by the viscous forces (Krumbein and Pettijohn, 1938). A fundamental result of the theoretically derived Stokes Law is that fall velocity

increases as a square of the particle diameter, the density difference and inversely proportional to fluid viscosity, so that larger particles settle much faster than smaller particles *ceteris paribus*.

$$w_s = \frac{1}{18} g \frac{(\rho_s - \rho_f)}{\mu} D^2 \quad (2\text{-}9)$$

where the acceleration of gravity, g, is 9.81 m/s^2; the dynamic viscosity of air μ is 0.000018 kg/ms; the density of the particle (ρ_s) and fluid (ρ_f) are 2650 kg/m^3 and 1.2 kg/m^3, respectively and D is the particle diameter in meters. For larger grains settling at faster rates (i.e. higher particle Reynolds numbers) the inertial effects cannot be ignored, as particles are affected by turbulent (impact dominated) as well as viscous (friction dominated) forces. The drag forces are proportional to the square of the velocity and extending the Stokes relationship in accordance with general resistance (impact) equations based on Newton's Impact Law (1687) a general equation for the fall velocity of small and large particles can be derived:

$$w_s = \sqrt{\left(\frac{4g(\rho_s - \rho_f)D}{3C_D\rho_f}\right)} \quad (2\text{-}10)$$

Here, C_D is the dimensionless drag coefficient and is partly a function of fall velocity which leads to an *impasse*. It must be determined experimentally and is usually expressed as a function of the Reynolds number. Coarse sized sand particles fall with velocities which vary as the square root instead of square of the diameters. This relationship contains no empirical constants and comes close to measured data of quartz grains but not so closely with particles of different shapes and densities (Rubey 1933). To address this problem, workers such as Rubey (1933), Wadell (1934) and Rouse (1936) started to examine the behavior of the drag coefficient parameter (C_D) to account for the effect of the fluid for different types of particles. Many workers conducted experiments to develop empirical equations e.g. Rubey (1933, Equation 2-11), Rubey – Watson (1969), Janke (1965), Zanke (1977), Dietrich (1982) and van Rijon (1982) using different drag coefficients. These relationships were subsequently modified to account for different properties of the fluids and characteristics of the flow (e.g. density, specific weight, viscosity, average velocity) and particles (e.g. size shape and density).

$$w_s = \sqrt{(s-1)gd}\left(\sqrt{\frac{2}{3}+\frac{36v^2}{(s-1)gd^3}}-\sqrt{\frac{36v^2}{(s-1)gd^3}}\right) \quad (2\text{-}11)$$

where s is the relative sand density (ρ_s/ρ_a) and v is the kinematic viscosity of air. Gibbs et al., (1971, 1977) developed an empirical relationship for glass spheres falling in water with densities ranging from 2.24-2.488 g/cm^3 given by:

$$w_s = \frac{-3\mu+\sqrt{9\mu^2+gr^2\rho_a(\rho_s-\rho_a)(0.015476+0.19841r)}}{\rho(0.011607+0.14881r)} \quad (2\text{-}12)$$

where the fall velocity units are cm/s; μ is dynamic viscosity given in poises; g *is* the acceleration of gravity g is in cm/s^2; r is the particle radius in cm; and $\rho_s - \rho_a$ are the particle and fluid densities in g/cm^3. Komar (1981) illustrated that this relationship is only applicable to a very narrow range of particle properties.

One approach, suggested by Einstein (1950), has been to dismantle the concentration profiles into different size fractions. This is attractive as the bedload sediment is, invariably, much larger than the suspended material. This approach assumes that the different size fractions do not influence each other and can be much more complex than choosing one representative grain size (Van Rijn, 1984). Rose and Thorn (2004) used a depth-averaged approach (over the bottom 1 m) to calculate fall velocity using a median grain size and the empirical relationship given by Soulsby (1997), despite recognizing that the grain sizes were much larger for $z < 0.05$ m:

$$w_0 = \frac{v}{d_s}\left[(10.36^2 + 1.049D_*^3)^{1/2} - 10.36\right];\ D_* = \left[\frac{g(s-1)}{v^2}\right]^{1/3} d_s \quad (2\text{-}13)$$

where v is the kinematic viscosity, *ds*, is the depth-averaged *in situ* median grain size, obtained from adjusted acoustic estimates, and D_* is a particle parameter.

Besides the development of different empirical relationships that relate sediment fall velocity to different sediment characteristics, such as size, shape, density, there are a suite of added complications for estimating fall velocity for non-ideal conditions. For example, the influence of sediment concentration (McNown and Lin, 1952); water temperature (Burke, 1966), and turbulence (Coleman, 1970; Bechteler et al., 1983) have all been found to influence the fall velocity of sediments. Subsequently, many more different fall velocity equations have been derived for particles falling in water, e.g., van

Rijn (1984); Bouvard and Petkovic (1985), Zhang and Xie (1993), and Julien (1995). In many cases workers, recognizing the complexities of dismantling the problem, have chosen to apply a fall velocity derived in quiescent fluid in their models, e.g., Celik and Rodi, (1988), and applied sensitivity tests afterwards to examine the impact, if any, of changing fall velocity to the results. The fall velocity of particles falling in air is discussed next. The sensitivity of the Rouse model to different values of fall velocity will be discussed in Section 5 for particles falling in air.

Measuring the fall velocities of grains in air is much more difficult than in water as the particles require much longer distances to reach their terminal fall velocity. As Cui et al., (1983) state "*the scarcity of data of grain settling rates in air can certainly be attributed to the difficulty of making such measurements….. (sand grains settling in air) require timing over a vertical distance of some 10 m or more in order* (p.1205)". This is due to the different properties of the two media which lead to very different dynamical properties of the falling particles. For example, one fundamental difference is that the particle-to-fluid density is almost eight hundred times greater in air than in water, resulting in very different proportions in the different modes of transport for each medium and, subsequently, very different particle trajectories or paths.

Beside the logistical problems of measuring particle fall velocity in air there are other reasons why this parameter isn't commonly reported in aeolian research. First, the standard grain size distribution statistics used in wind blown transport studies are more easily obtained from sieve analysis widely available in most sedimentary laboratories. These resulting parameters (e.g. size, sorting, skewness, kurtosis) provide the important clues to the sediment provenance, transport history and depositional conditions (Folk and Ward, 1957; Friedman, 1979; Bui et al., 1990; Blott and Pye, 2001) that satisfies the needs for most aeolian studies. Secondly, an average mean grain size estimate is sufficient to characterize the sediment properties to satisfy the suite of empirical and numerical models used to predict short term sediment transport rates (Sherman et al., 1998; Dong et al., 2003; Sherman and Li, *in press*) or the longer term indices of sand mobility used to predict dune stability (Tsaor, 2005) and the evolution of sedimentary

environments (Alcántara-Carrió and Alonso, 2002). However, more recent saltation models, focused on understanding the physics of wind blown sand to describe grain trajectories and overall flux, require distributions of lift-off and fall velocities of particles in order to simulate the concentration profiles. Cheng et al. (2009) state "*fall velocities of saltating sand grains and their distributions are key parameters in determining how the collision processes lead to the development of saltation clouds and to their subsequent behavior* (p.99)". These approaches rely on an understanding of the aerodynamic behavior of particles. In these cases, knowing the fall velocity of the particles is air is more beneficial than a sediment sieve size. Further, in order to assess the application of the Rouse profile to aeolian flux profiles it is necessary to determine an accurate value of the fall velocity of sediment much coarser than are normally reported in studies of suspended load in water research. Besides these challenges, it is also clear that current theory does not adequately describe the complexities of the problem. For example, the influence of particle-particle interactions in sediment laden flows remains unclear. Nor is it clear how to estimate a representative fall velocity for a mixed grain population. The problem of estimating a representative fall velocity for sand sized particles in air is clearly a challenging task.

2.5.2 Rouse number: u_*, shear velocity

Estimates of shear velocity are calculated using the law of the wall from observed elevation-velocity measurements, assuming that these measurements are taken within a constant stress region. In practice, this depth range is difficult to determine, *a priori*, so workers have established post-observation, processing methods to select only those points that fit the *ideal* situation. Bauer (*in press*) provides a detailed description of the problem in aeolian environments. Further, measurements of the near bed velocity profiles have shown drastic differences between clear fluid cases(water or air) and studies where sediment is present (Vanoni and Nomicos, 1959; Bauer et al., 1994). It has been well documented that flow velocities increase if suspended sediment is present, *ceteris paribus*. This results in a steeper velocity gradient and a subsequent increase in

shear velocity and roughness length. As Rijn (1984) states, "*for very heavy sediment-laden flows, the application of (the law of the wall) may lead to serious errors* (p.1631-32)". The one concern for workers is that the flow velocity observations are usually measured in the outer part of the profile and, as a consequence, they may give an over estimate of the actual bed shear stress. Using this shear stress value in the Rouse model, results in concentration profiles that do not match the observed data.

2.5.3 Rouse number: *k*, apparent von Kármán constant

For sediment laden flows, applying the value of 0.40 for the apparent von Kármán constant has been questioned. In some cases, *k* has been reported to decrease with increasing suspended sediment concentrations (Vanoni, 1946; Einstein and Chien, 1955; Elata and Ippen, 1961; Wang and Qian, 1989). Lees (1981) found that the apparent von Kármán constant can decrease by over 100% as the concentration increases. Shah-Fairbank (1990) provides an insightful review of this complex relationship. The physical reasons purported to explain the decrease in *k*, include the presence of a wake layer (Coleman, 1981; Barenblatt, 1996); the presence of suspended sediment and channel patterns (Nouh, 1989); the effects of large near-bed suspended concentrations (Lyn, 1986, 1988; Kereseidze and Kutauaia, 1995); the presence of secondary currents (Dyer, 1986); or damping effects on the turbulent structures of the fluid by the suspended sediment (Van Rijn, 1984). Akalin (2002) reviewed the reported studies that analyzed how both the velocity and concentration profiles were impacted by changes in the von Kármán constant. He reports cases where the von Kármán constant has no dependency on concentration (Itakura and Kishi, 1980; Coleman, 1981) and concludes, based on Coleman (1986) that, "*the findings of the variation of the value of the von Kármán constant is misapplication of a curve-fitting method because the logarithmic velocity distribution with the various values of k fits only the lower 15 percent of the total water depth* (p.40)". In light of these findings, an alternative approach that uses a local constant *k* that is dependent on the local sediment concentration has been proposed (Yalin and Finlayson, 1972). Further, other workers

have reduced the value of k in order to compensate for the overestimates of the shear velocity measured in outer flow when applied to shear stress calculations to the near bed where there is a much higher concentration of suspended sediment. Dyer (1986) suggests that k is best represented using the ratio of fall velocity to shear velocity (w_0/u_*). Trying to resolve some of these issues is beyond the scope of this work. As Rijn (1984) states, "*a proper study of the influence of the sediment particles on the velocity and concentration profile requires the solution of the equations of motion and continuity applying a first order closure (mixing length) or a second order (turbulence energy and dissipation) closure* (p.1622)".

For sand moving in air, the value of k = 0.40 was evaluated by Li et al., (2011) using flux data collected in the field experiment described herein, Brazil (2008). They found an inverse linear relationship between the apparent von Kármán parameter (k_a) and sand transport rate (Q):

$$k_a = -3.028Q + 0.399 \quad (2\text{-}15)$$

,

2.5.4 Rouse number: β, Schmidt number

The constant of proportionality, or β, is a form of the Schmidt number and describes the difference in diffusion patterns of a fluid particle and a sediment particle, and is usually derived from theoretical relationships (Suleyman, 2002). The term Schmidt number is used herein but it is acknowledged that it should not be applied *sensu stricto*. It is defined in Equation 2-16 as the ratio of the sediment-mixing coefficient (ε_s) to the momentum exchange coefficient of water, also referred to as fluid viscosity (ε_f):

$$\beta = \frac{\varepsilon_s}{\varepsilon_f} \quad (2\text{-}16)$$

The constant has been applied to the Rouse model in order to balance the upward turbulent diffusion of sediment and its settling rate, by assuming that the former process emulates the momentum transfer of the turbulent flow, which can be measured. This assumption, of β equal to 1, implicit in the Rouse equation, has been scrutinized by many workers in water research (Parker and Coleman, 1986; Gelfenbaum and Smith, 1986; McLean, 1992). After eight decades of application in suspension studies, the

values and behavior of this parameter is still unresolved. As Bridge (2003, p.65) states "*perhaps the most serious concern with the Rouse equation is that the sediment diffusivity has rarely been calculated directly using quantitative observations of the motion of sediment in turbulent eddies. Thus, there is doubt about the vertical variation of* ε_s *and* β".

Lees (1981) found that the value of β increased with grain size, being approximately 1 for very fine sands, but reaching almost 10 for medium sand (Dyer, 1986). Similarly, Hill et al., (1988) report values of β equal to approximately 3 for medium sand. Others have also found β to be greater than unity but less than these values (Ismall, 1952; Colby and Hembree, 1955; Laursen, 1958; Nordin and Dempster, 1963; Ikeda and Asaeda, 1983). Equally, others have reported the value of β to be less than unity (Rouse, 1938; Kalinske and Pien, 1943; Hunt 1954). Wright and Parker (2004), commenting on the little agreement of the value of the Schmidt number and the significant debate on the topic, argued for choosing the simplest choice of unity to use for their modeling purposes. However, Teakle and Nielsen (2004, 1) report that despite the wide range of reported values of β that "*a universally observed feature is the strong dependence … of* β *on the ratio,* w_0/u_*".

Experimental approaches do suggest that the value of β is a function of turbulent characteristics of the flow and particle settling velocity. Hill et al., (1988) found that β could be solved using:

$$\beta = 1.45\left(\frac{w_0}{ku_*}\right)^{0.33} \tag{2-17}$$

where the constant of proportionality lies between 1.10 and 1.89 at the 95% confidence level and the exponent varies between 0.08 and 0.58 for the same confidence levels. Similarly, van Rijn (1984) used the data of Coleman (1981) and found that values of β could be computed, but not with high accuracy, using the empirical expression:

$$\beta = 1 + 2\left(\frac{w_0}{u_*}\right)^2 for\ 0.1 < \frac{w_0}{u_*} < 1 \tag{2-18}$$

Rose and Thorne (2001) provide an in depth analysis of the variability of the values of β and suggest, given the poorly understood contribution of the different

processes effecting the values of β, that the most pragmatic approach is to plot values of β as a function of a fall velocity – shear velocity ratio and empirically determine the trend of the data. They examined the variability in the Rouse number by comparing the straight line slopes of the temporally averaged, measured, concentration profiles (equivalent to the Rouse number), with values of the Rouse number calculated from sediment diffusivity profiles. Using this approach on tidal data they found reasonably good agreement with the empirical function given in Equation 2-19, but caution that more data are required with estimated error bars to further test this, and other, relationships:

$$\beta = 3.1exp\left(\frac{-0.17u_*}{w_0}\right) for\ 1 \leq \frac{u_*}{w_0} \leq 9.5 \qquad (2\text{-}19)$$

Weerappuli (1980) found, using multiple regression analysis on observed data, that the value of the Rouse number showed dependence on fall velocity and shear velocity, but also on average velocity (V), water temperature (T), concentration of suspended sediment at mid-depth ($C_{h/2}$), flow depth (h), and the particle size of sediment in suspension (d_s):

$$R = w_0^{0.52597}\ V^{0.0.55999}\ k^{-0.2742}\ u_*^{-1.06709}\ T^{-0.55875}\ C_{h/2}^{-0.02702}\ ds^{0.27613} \qquad (2\text{-}20)$$

He found that the value of the Rouse exponent calculated from this expression provided a better estimate than that from Equation (2-6).

The influence of bedforms on the vertical mixing patterns of the sediment have also been found to be important. Graf and Cellino (2002) directly measured the value of β experimentally using an Acoustic Particle Flux Profiler. They found that the values of β changed over plane beds and beds with bedforms. They argue that the existence of bedforms enhances sediment diffusion (at the crests) and suppresses turbulent diffusion, resulting in large values of β. They recommended a new empirical expression to calculate β based upon settling velocity and shear velocity. They found good agreement using this method against an independent method that fit the Rouse equation to measured concentration profiles. The spatial and temporal changes in the value of the Rouse number from the presence of different bedform types, was also studied by Dolphin and Vincent (2004).

Vanoni (1941) and Anderson (1942) found that the Rouse profile is satisfactory provided an appropriate value of the Rouse number in chosen. They conclude that the value of the Rouse number should be determined from measured data, and not from the expression given in Equation 2-6. Clearly, determining the controls and value of the Rouse exponent is a challenging, but enticing, task for water research. Clearly, differentiating the controls and changes of the four input variables in Equation 2-5 is an area of interest and concern in water studies. This has immediate ramifications for the task of applying the Rouse model to aeolian saltation.

2.6 Rouse number: aeolian studies

There has been limited application of the Rouse profile to aeolian research. Sundborg (1955) derived an almost identical expression for the vertical distribution of wind-blown dust (note: Sundborg's terminology has been changed to follow that of Rouse):

$$C = C_a \left(\frac{z}{z_a}\right)^{-R} \tag{2-21}$$

where $-R$ is the equivalent of the Rouse number described earlier. This is one of very few published applications of a Rouse type analysis to an aeolian system. There is an attribution of a similar, but less formalized, line of thinking to Schmidt (1925) by Kalinske and Hsia (1945). Anderson and Hallett (1986) use the Rouse number to describe the distribution of aeolian sediments in suspension (as have several other studies involving, mainly, dust), but present no empirical data to support this application. Scott et al., (1995) and Scott (1995) describe a mathematical treatment that define an equilibrium between the vertical distributions of mass flux, driven by sediment fall velocity, and turbulence - which formulates the Rouse approach - but without empirical evidence to support their interpretation. They imposed a Rouse number exponent (R) greater than 1 so that the majority of sediment is transported near the surface, thereby distinguishing between saltation and suspension ($R < 1$) modes of transport. Udo and Mano (2011) calculated equivalent concentration profiles from mass flux profiles by dividing the mean particle velocities by the mass flux (their Equation 1). They used the

flux data of Ni et al., (2002) and the particle velocity data of Dong et al., (2006). They justify this by stating that both experiments were completed in the same wind tunnel at the Shapotau Desert Research Station (Chinese Academy of Sciences) – a supposition that is difficult to critically assess. They surmise that the values of the Rouse number - used to define the transport mode - corresponded for fluvial and aeolian systems based upon the work of van Rijn (1993) and Shao (2000), respectively. Using these arguments they categorized the Ni et al., (2002) runs as either saltation, modified saltation, or suspension. They found only marginally good results - only one run, where the transport was categorized as modified saltation, had a good fit between the predicted Rouse profile and observed flux profile (their Figure 5b). It is noteworthy that these runs had a mean grain size of 0.17 mm and minimum shear velocities of 0.60 m/s, and as high as1.64 m/s - conditions that are seldom measured in field experiments. There are several theoretical and methodological uncertainties with the results from this research.

Tsaor and Pye (1987) used a modified Rouse number to theoretically derive the modes of transport of aeolian sediments: saltation, modified saltation or suspension, but with no distinct boundaries between the different modes. Clearly the physics of dust suspension in air are the same (in kind) as those of fine sediments suspended in water, although the magnitudes of some of the variables are substantially different; e.g., typical shear velocities and fluid densities. The application of the Rouse approach, especially as embodied in *R*, to aeolian sand systems requires estimations for both sediment fall velocity and shear velocity in fashions that are more complicated than those for fine grained sediments.

2.6.1 Rouse model: application in air *vs.* water

Bauer (2009) states, "*although apparent similarities exist between the mechanics of aeolian and fluvial transport, especially because many of the fluid mechanical laws and principles are thought to be universal, it is increasingly apparent that the dominance of saltation as the primary mode of transport in air leads to complexities that are not found in water. These are rooted in the extreme difference in density between the*

fluid (air) and the solid (sand), which leads to: (1) ballistic trajectories of grains that have the potential to impact the surface and cause cratering and the ejection of other surface particles (the "splash" process); and (2) mutually efficient exchange of momentum between the fluid and the grains (p.2)". There are many unresolved issues of the physical '*correctness*' of applying the Rouse model to construct vertical flux distributions of sediments moving by saltation dominantly in air.

First and foremost, the Rouse concentration model was developed to describe the vertical distribution of medium sized sands, silts and clays moving by suspension in water. This mode of transport is fundamentally different to saltation of particles in air. It may be argued that the bedload processes reported in fluvial research should be analogous to saltation processes in aeolian studies. In both cases, the transport grain population obtains part of its energy from repeated contact with the bed (rebound) or from the impact of moving grains (ejection). This is different to suspension processes where fine particles are moved by turbulent diffusion processes of the fluid rather than rebound or ejection from the mobile bed and are not in frequent contact with the bed.

For saltating particles in air, the particles move either by impacts from other grains already in saltation (for which splash functions have been developed) or, by momentum exchange with the ground, as particles already in motion rebound off the bed. Thus, the primary source of energy driving the transport is fundamentally different for both systems. Extending this argument, it implies that the Rouse approach, which depends upon a shear velocity parameter to define the turbulent characteristics and the positive energy driving the transport, is insufficient to describe the dynamics that drive aeolian saltation and produce characteristic vertical flux distributions. This argument will be re-visited in Section 5.

2.7 Key data sources

In order to test the hypotheses, data was gathered from a field experiment and supplemented with data from previously published research in the aeolian saltation literature. The literature was reviewed extensively to identify experiments that reported

vertical distributions of mass flux from wind tunnels or field environments where (i) sand sized material was measured, and (ii) saltation was the dominant transport mode. An initial search of published sources identified fifty one different studies with vertical flux data (Table 2-2). Thirty six of these studies were based in wind tunnel laboratories and fifteen studies were field-based experiments. A total of 651 vertical flux profiles were reported, 508 from wind tunnel studies, and 130 from field studies. A brief summary of all these experiments is provided in Appendix A.

Table 2-2. List of experiments reporting vertical mass flux profiles. In the table, *Source* refers to the author(s) and year of the research publication; *Site* describes the environment where the data were gathered (*B* = beach, *D* = Desert, *WT* = wind tunnel); *n* represents the number of profiles obtained; *d* is grain size in *mm*; *WT (LWH)* are the wind tunnel dimensions of length, width and height - the boundary layer height is provided in parentheses if reported; *Max and Min* u_* are the maximum and minimum shear velocities, in *m/*s, for the reported flux profiles, *Max and Min u* are the maximum and minimum wind speeds, in *m/*s, for the reported flux profiles shear velocity. Some of the field sources are from experiments conducted by the author, or colleagues. These include Guadalupe (1996), Portugal (2006), and Brazil (2008). The nomenclature refers to the location of the experiment and the year it was conducted.

Source	***Site***	***n***	***d*** ***(mm)***	***WT (LWH)*** ***(m)***	***Max*** u_* ***(m/s)***	***Min*** u_* ***(m/s)***	***Max U*** ***(m/s)***	***Min U*** ***(m/s)***
Arens and van der Lee (1994)	WT	**12**	0.24	15 x 0.60 x 0.90			6	13
Arens et al. (2002)	F	**9**	0.144 – 0.171				17.8	11.6
Brazil (2008)	F	**25**	0.235 – 0.408		0.54	0.41		
Butterfield (1999)	WT	**5**	0.184	8.2 x 0.3 x 0.3 (0.17m)	0.441	0.271		
Dong et al. (2002)	WT	**58**	0.10 – 0.80	21 x 1.2 x 1.2 (0.40-0.50m)			22	8
Dong et al. (2004a)	WT	**119**	0.18	21 x 1.2 x 1.2 (0.40-0.50m)			22	8
Dong et al. (2004b)	WT	**8**	0.18	21 x 1.2 x 1.2 (0.40-0.50m)	0.53	0.21		
Dong et al. (2006)	WT	**12**	0.10 – 0.40	16.2 x 1.0 x 0.6			14	8
				(0.12m)				
Dong et al. (2011)	F	**25**						
Dong and Qian (2007)	WT	**58**	0.10 – 0.80	21 x 1.2 x 1.2 (0.40-0.50m)	0.53	0.21	22	8

Table 2-2 continued.

Draga (1983)	F	4						
Feng et al. (2009)	WT	**9**	0.35	21 x 1.2 x 1.2 (0.2m)	1.24	0.56		
Gerety and Slingerland (1983)	WT	**4**	0.17 – 0.20	10 x 0.35 x 0.50	1.10	0.20		
Greeley et al. (1996)	F	10	0.23		0.54	0.312		
Guadalupe (1996)	F	13/11	0.39					
Hasi (1997)	F	6					11.5	9.1
Hotta and Horikawa (1991)	WT	**10**	0.30	20 x 1.0 x 1.1	1.0	0.30		
Hotta et al. (2006)	WT	**15**	0.15 – 0.68	20 x 1.0 x 1.1	2.33	0.40		
Kawamura (1951)	WT	**2**	0.248	1.5 x 0.05 x 0.80	0.732	0.488		
Kawamura (1951)	F	2	0.307				12.6	10.5
Leys and McTainish (1996)	WT	8						
Li and Ni (2002)	WT	12	0.35	21 x 0.4 - 1.2 x 1.2				
Liu and Dong (2004)	WT	25	0.1 – 0.6	16.23 x 1.0 x 0.8 (0.12m)			18	10
Liu et al. (2006)	WT	**5**	0.4 – 0.5	21 x 1.2 x 1.2	0.75	0.48		
Mikkelsen (1989)	WT	1						
Mikkelsen (1989)	F	1	0.40					
Mohammed et al. (1996)	WT	6	0.10 – 0.30				14.4	11.5
Namikas (2003)	F	**9**	0.25		0.63	0.27		
Namikas et al. (2009)	F	**9**	0.11 – 0.55		0.52	0.42		
Ni et al. (2002)	WT	**10**	0.17 - 0.35	21 x 1.2 x 1.2	2.36	0.47		
Portugal (2006)	F	**13**	0.27 – 0.35		0.41	0.35		
Rasmussen and Mikkelsen (1988)	WT	**4**	0.22	15 x 0.60 x 0.90	0.27			

Table 2-2 continued.

Rasmussen and Mikkelsen (1998)	WT	**3**	0.20	15 x 0.35 x 0.50 (0.07m)	0.63	0.27		
Rasmussen and Sørensen (1999)	F	**3**	0.32		0.20	0.177		
Rasmussen and Sørensen (2008)	WT	12	0.242 – 0.32	15 x 0.60 x 0.90 (0.15m)	0.74	0.27		
Rasmussen et al., (1985)	F	4						
Shao and Raupach (1992)	WT	12	0.20	17 x 1.15 x 0.90	0.60	0.34		
Sharp (1966)	F	4						
Sørensen (1985)	WT	**2**	0.106 - 0.211	15 x 0.60 x 0.90	0.46			
Weinan et al. (1996)	WT	6	0.11	16 x 6.0 x 1.0			19	6
Weinan et al. (1996)	F	5	0.09				11	6.1
White and Mounla (1991)	WT	4	0.25	7.32 x 0.80 x 0.47			11.94	6.405
Williams (1964)	WT	**6**	0.4	9.14 x 0.35 x 0.35	1.20	0.51		
Wu and Ling (1965)	F	3					13.3	4.5
Xing (2007)	WT	17		8 x 0.40 x 0.60			15.3	7.5
Xing et al. (2011)	WT	12	0.364 – 0.525	6.0 x 0.40 x 0.60 (0.15m)			14.5	8.5
Zhang et al. (2007a)	WT	2	0.01 – 0.03	1.0 x 0.20 x 0.01 (0.20m)			8.05	6.5
Zhou et al. (2002)	WT	14	0.211	21 x 1.2 x 1.2			20	8
Zingg (1953)	WT	23	0.20 -0.715	17 x 0.9 x 0.9				
Znamensky (1960)	WT	8					10.61	
Zou et al. (2001)	WT	**4**	0.20 – 0.30	16.2 x 1.0 x 0.60 (0.18m)	0.81	0.63		

III. DATA ACQUISITION AND METHODS

In order to test Hypotheses 1 and 2,

H1: *the average grain size of the sediments comprising the vertical mass flux profile become smaller with distance away from the bed*

H2: *the observed mass flux distribution profiles observed in wind tunnel and field environments all decay exponentially away from the bed but at different rates for each environment*

it was necessary to conduct a field experiment to measure vertical flux profiles where, optimally, a wide range of environmental conditions (grain size and wind speed) are experienced. This field data set supplemented a much larger data repository obtained from a comprehensive review of experiments that measured vertical flux profiles the past seven decades. These data were evaluated using a set of criteria based upon data representation and experiment methodology and design. The remaining datasets were stratified into two categories - field and laboratory results - which were then compared to test Hypothesis 2. The datasets were then re-evaluated to identify experiments that reported sufficient information on sediment (grain size) and wind (shear velocity) in order to test the application of the Rouse profile given by Hypothesis 3,

H3: *the rate of decay changes as a function of wind speed and/or grain size parameters and can be accounted for using a form of the Rouse Parameter.*

3.1 Data acquisition: field experiment

3.1.1 Field site location

Sediment transport data were collected October and November 2008 from three sedimentary sub-environments near Jericoacoara, in the state of Ceará in NE Brazil (Figure 3-1A and B). During these months there is minimal precipitation and consistently fast winds, averaging over 8 m/s in October, for example (Maia et al., 2005). The first two sub-environments were located at an inland sand flat (2.7955°S; 40.4920°W) in the deflation plain of a blown-out, parabolic dune system (Figure 3-1B, location B and Figure 3-2A). The site is approximately 40 m wide and bounded by parallel ridges formed by the inland migration of the dune. The wind directions at the site are constrained by the dune ridges, and blew mainly from east northeast during this study. The fetch is approximately 100m upwind from the instrumented sites. There was a distinct grading of bed texture across the sand flat, perpendicular to the wind direction. The southern side comprises well-sorted, medium-sized sand grains, and is referred to herein as sub-environment Cow Splat Flat Fine or CSFF (the designation of 'fine' being relative to the other sediments at the site). The northern side also has medium-sized sediments that were moderately well-sorted. This sub-environment is termed Cow Splat Flat Coarse or CSFC.

The second site was located on the foreshore of a beach (2.7959°S; 40.4713°W) approximately 1 km south of Jericoacoara (Figure 3-1B, location C and Figure 3-2B), and is herein designated "Beach". The tidal regime is semi-diurnal with a maximum range of approximately 2.5 m during the study period. Wind speeds were almost continuously above the threshold speed for dry sand. The source of sand blowing across the foreshore was a dry berm at the top of the Beach. The estimated fetch from the instruments to the berm exceeded 100 m and ran across the low angle, unobstructed inter-tidal zone. Because of the semi-diurnal tides and length of time needed for instrument deployment and removal, the periods for measurements were limited to a few hours just after the morning low tides.

The differences in bed textures between the three locations provide some control over the mean grain size of the flux profiles. This is advantageous to identify the changes, if any, that occur to the flux distributions in response to changes in a first order control variable. Additionally, by sampling in environments with different sediment grains size characteristics, a wider range of Rouse numbers can be tested.

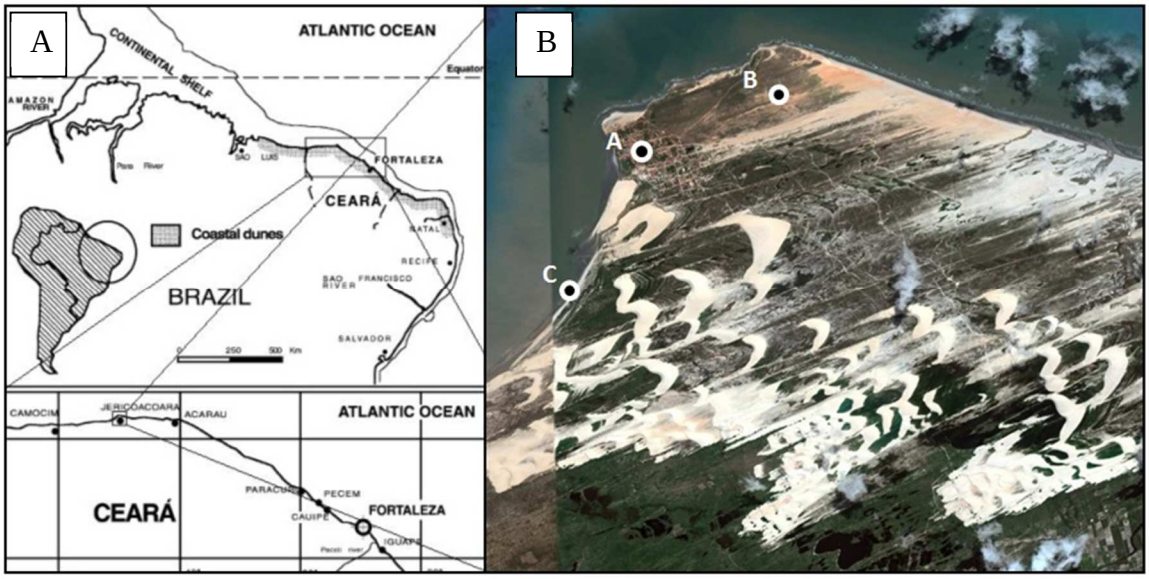

Figure 3-1. A. Regional location of the town of Jericoacoara, Brazil. **B.** Locations of the town of Jericoacoara (labeled A) and the inland (labeled B) and beach (labeled C) study sites (Adapted from Jeminez et al., 1999; Li, 2010; Google Earth, 2011).

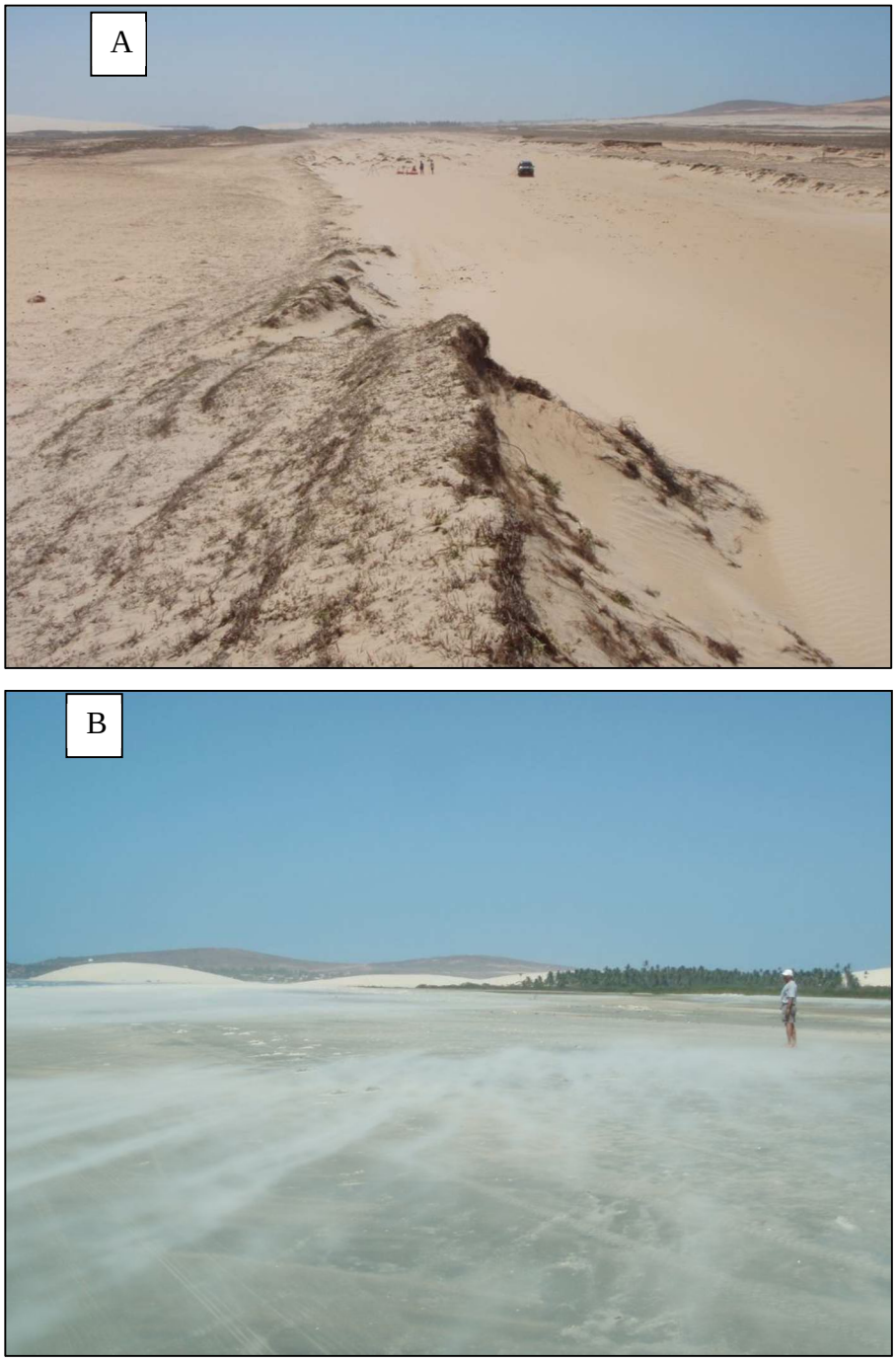

Figure 3-2. Field site photographs. Photo A: Cow Splat Flat, looking downwind to experiment setup. Photo B. Beach, looking upwind from experiment location.

3.1.2 Instrumentation

In order to test the hypotheses, the following variables are required to be measured in the field experiment: at one location, the instantaneous horizontal wind velocity (for the slope of velocity profile to calculate u_*), and the transport rate, or flux, at different elevations above a mobile bed (for the vertical flux profile) over a period of time (Figure 3-3).

Wind speed measurements were collected using an ultrasonic anemometer (R.M. Young 81000), with an internal sample rate of 160 Hz and 32 Hz output rate. The instrument was mounted 1 m above the bed and had sampling durations ranging from 120 s to 300 s. The sample rate was 96 Hz. These data were used to calculate shear velocity with a correction for variability, related to transport rate, in the von Kármán parameter as described in Li (2010) and Li et al., (2010).

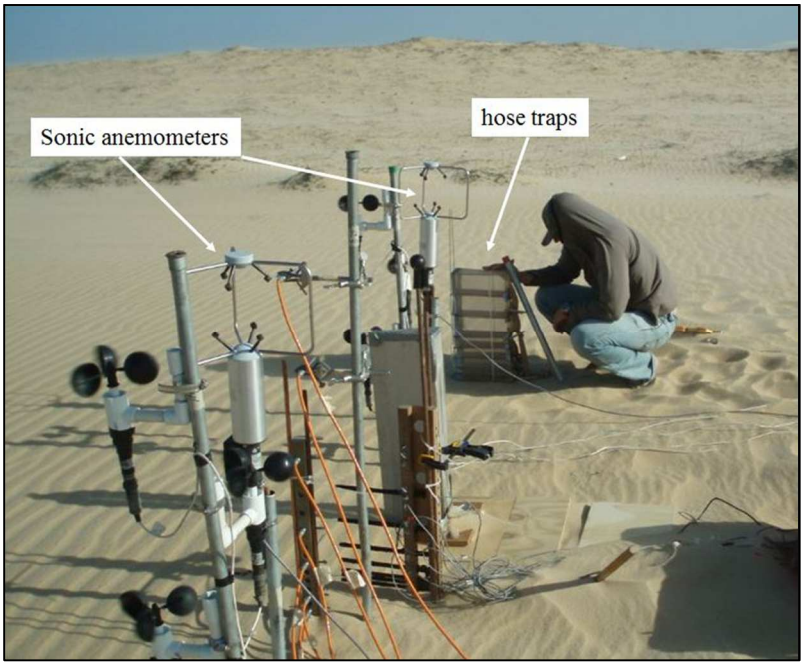

Figure 3-3. Field experiment instrument setup. This research was part of a larger field project (GRS NSF grant 0822482) that required more instruments to accomplish the research goals. The description here focuses on the sonic anemometers and hose traps.

Transport data were obtained for thirty runs using an array of eight, vertically-stacked, hose-style traps similar to those reported in Ellis et al. (2009) and Li (2010). Eighteen of the runs were from CSFF, four from CSFC, and three from the Beach. The vertical opening of the lowest two traps (traps 1 and 2) was 0.025 m. Openings of the higher traps were 0.050 m (traps 3 and 4) and 0.10 m (traps 5, 6, 7 and 8). The total stack height was 0.55 m. All traps were 0.10 m wide. Sand was collected in runs spanning 120 – 480 s depending on the transport rate. Shorter runs were associated with periods of more intense transport with contemporaneous ultrasonic anemometer deployment.

3.2 Data acquisition: published studies

Table 2-2 provides a list of the exhaustive literature review to identify previous studies that reported vertical distributions of mass flux. An initial search of published sources identified fifty one different studies with vertical flux data. Thirty six of the studies are based in wind tunnels laboratories and fifteen studies were based in field experiments. A total of 651 vertical flux profiles are reported, 508 from wind tunnel studies, and 143 from studies (Table 3-1).

Table 3-1. Summary of the initial archive of wind tunnel and field experiments reporting vertical flux profiles.

Experiment type	Number of studies	Number of profiles
Wind tunnel	34	508
Field	17	143
Total	51	651

3.3 Methods

3.3.1 Wind data

Analyses of the wind speed data have been described in detail in Li (2010) and Li et al., (2010), following the methods detailed in van Boxel et al., (2004). The sonic anemometer data were subsampled to 32 Hz from the original time series by selecting the median value of every 3-point block. If spikes existed after subsampling they were linearly interpolated using the neighbouring values. The Reynolds stress estimates, used to derive the shear velocity, are given by the numerator in Equation 3-1. The velocity fluctuation components, *u'* (horizontal velocity) and *w'* (vertical velocity), were calculated by subtracting the mean speeds from their instantaneous values after the data had been rotated to make the transverse velocity component, *v'*, equal to zero. The shear velocity was then calculated from:

$$u_* = \frac{\sqrt{-\rho \overline{u'w'}}}{\rho} \qquad (3\text{-}1)$$

where ρ is the fluid density (1.23 kg/m^3).

3.3.2 Sediment data

In the laboratory, sand samples were weighed, washed and oven dried, and then sieved at ¼ φ intervals using a sonic sifter (Model L3P, ATM Corp., Milwaukee, WI). Grain-size sorting properties were obtained using the freeware computer program GRADISTAT (Blott and Pye, 2001). These steps are also described in the accompanying paper, Farrell et al., (*accepted*) in Appendix 3.

As a means of facilitating the comparison of the vertical distributions of grain size, a mass-weighted, mean grain-size was calculated for each run, and those data were used to normalize grain sizes at each elevation from the different runs. In order to obtain the weighted means, the flux (Q_i) in each trap *i* (*i* = 1-6) was divided by the trap height ($h_{ti} - h_{bi}$), where h_{ti} and h_{bi} are the elevations (in mm) of the top (*t*) and bottom (*b*) of trap *i*. The representative flux per 1 mm ($Q_i/(h_{ti} - h_{bi})$) was divided by the total flux for each run ($\Sigma\, Q_{i(1\text{-}6)}$) to establish the normalized flux per 1 mm of trap opening (Q_{ni}):

$$Q_{ni} = \frac{Q_i/(h_{ti}-Q_{bi})}{\sum_{i=1}^{6}(Q_i)} \quad (3\text{-}2)$$

The normalized flux for each trap was multiplied by the mean grain size ($D_{50(i)}$) of the sand caught in that trap (listed in Table 1, Appendix 3). The representative, mean grain-sizes were summed to determine the weighted, mean grain-size, D_{wi}, for each run:

$$D_w = \Sigma\ (Q_{ni}\ D_{50(i)}) \quad (3\text{-}3)$$

These data were used to calculate the normalized, mean grain-size (D_i/D_{wi}) for each run, where D_i is the mean grain size of trap i. Samples with a mean grain-size equal to the weighted mean for their run have a value of unity ($D_i/D_w = 1$). Traps containing a coarser fraction of the sand have values greater than unity ($D_i/D_w > 1$) and, conversely, traps containing a finer fraction have values less than unity ($D_i/D_w < 1$). This procedure allows direct comparison of grain-size profiles from the three sub-environments and for different transport conditions. This approach also provides a more representative, mean grain-size for each run by weighting the calculations according to total mass trapped.

3.3.3 Literature studies

3.3.3.1. Data quality controls

The flux profiles in the literature were quality controlled to reduce the number of studies to those that, at the very least, had the minimum data requirements that allowed either of the two hypotheses to be tested; measurements that were applicable to the process being investigated (short term equilibrium saltation); and presentation of the results in a format that permitted the data to be reverse engineered. Following these basic requirements, the first set of criteria used to validate the suitability of the data sources listed in Table 2-2 included:

1. Data presentation and format: In many cases the graphical presentation of the flux profiles was too poor to allow the data to be extracted using an onscreen digitizing technique described in the next section. The primary reason was overlapping symbols from different profiles on the same graph made it

impossible to accurately identify the flux-elevation data for a complete profile. Examples include: Shao and Raupach (1992), Figure 3; Weinan et al., (1996), Figures 4 (depicted in Figure 3-4) and 5; Dong et al., (2004a) (depicted in Figure 3-4), Figure 3; Dong et al., (2004b), Figure 3; Dong et al., (2006), Figure 3, and Rasmussen and Mikkelsen (1998), Figure 5. Zingg (1953) used illegible, duplicating symbols that also prevented the profiles from being accurately identified. All these datasets were removed in the analysis.

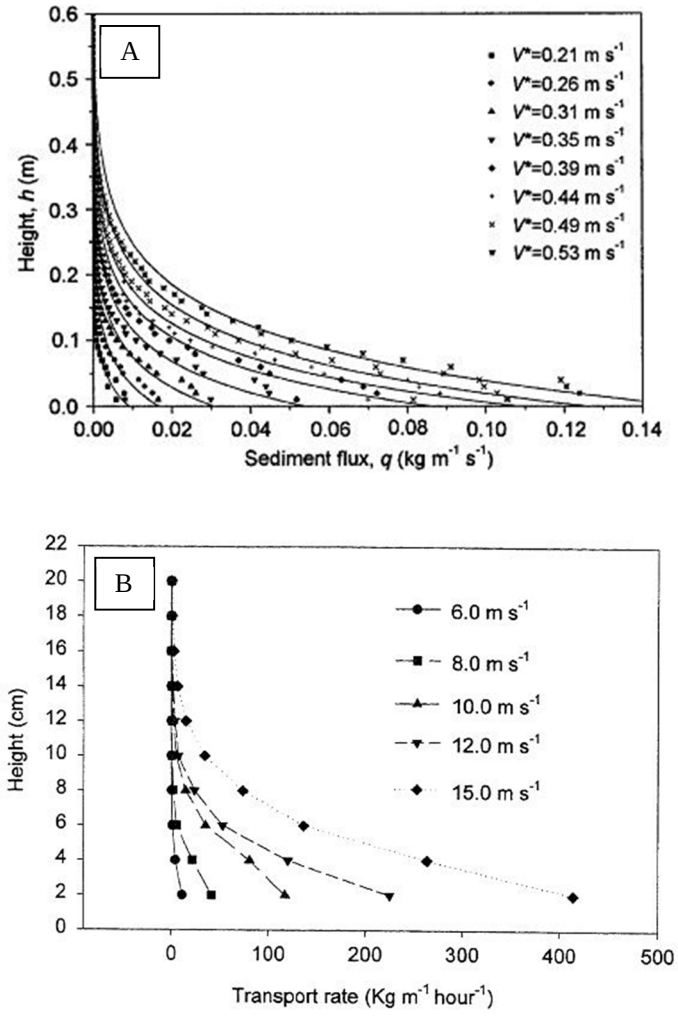

Figure 3-4. Examples of overlapping symbols presented in graphical presentation of vertical flux profiles from Dong et al., (2004) (A), Figure 3 and Weinan et al., (1996), Figure 4 (B).

Research methodology and design: In some studies the traps used to collect the vertical distribution of mass flux were very inefficient. For example, the traps used by Arens and van der Lee (1995), Arens et al., (2002) and Mohammed et al. (1996) had reported efficiencies of 7-27%, 15% and 3%, respectively. The only case that could be made to use these data is if every trap at each elevation underestimated the flux by the same amount thereby preserving the characteristic slope of the relative flux profile. White and Mounla (1991) used walnut shells as opposed to sand but did not report the density of the shells. Later, White (1996) described a similar experiment using walnut shells that had a density for 1.1 g cm^{-3} which is far less than that of quartz sand (2.65 g cm^{-3}). This dataset was subsequently ignored. The run durations in some experiments were too long to expect that an equilibrium flux profile was measured. Dong et al., (2011) provide flux profiles that are time averaged for eleven days of sampling. Similarly, Sharp (1964) and Leys and McTainish reported flux profiles that were averaged over long durations, up to 233 days and 2 days, respectively. These data were not used in the analysis.

2. Data Originality: The profiles reported in Dong and Qian (2007) were the same as those reported in Dong et al., (2002), Table 2 (p.224). The only differences are in the format of the data e.g. flux reported as $g\ cm^{-1}\ s^{-1}$ and corrected to four decimal places *vs.* kg $m\text{-}^{1}s^{-1}$ corrected to three decimal places. The creep fraction F_c reported in Dong et al (2002) is the *a* regression coefficient in Dong and Qian (2007). This set of profiles was only represented once in the analysis. The same issue may applies to Xing (2007, 2011).

Applying these basic criteria reduced the number of studies and profiles available to test Hypothesis 2 to 31 studies comprising 305 profiles. These are summarized in Table 3-2.

Table 3-2. Summary of data used to test Hypothesis 2.

Experiment type	Number of studies	Number of profiles
Wind tunnel	19	207
Field	12	98
Total	31	305

A similar approach was used to evaluate the suitability of these remaining datasets to test Hypothesis 2. Besides the basic criteria outlined above (data presentation and format, research methodology and design, data originality), there were two other fundamental data requirements necessary to test Hypothesis 3.

4. Data : In addition to providing the basic vertical distributions of mass flux, there were two other data requirements to test Hypothesis 3: estimates of shear velocity and grain size, both of which are essential for calculating the Rouse number. In some cases these studies reported a free stream velocity which is physically incommensurable with shear velocity for calculations of the Rouse number (Table 2-1). Applying these two fundamental data requirement criteria reduces the number of studies (listed in Table 3-2) available to test Hypothesis 3 to (Table 3-3):

Table 3-3. Summary of data used to test Hypothesis 3.

Experiment type	Number of studies	Number of profiles
Wind tunnel	12	78
Field	3	32
Total	15	110

3.3.3.2 Reverse engineering: Data Thief III© (2006)

After reducing the gathered datasets to those that were appropriate to test either Hypothesis 1 or 2, a number of tasks were completed to transform the published data to a format suitable for the analytical purposes of this research. The first task was to extract the data from the published sources. Flux profiles from the literature were scanned and the images processed using Data Thief III© (2006) software. The points and lines comprising the flux profiles and the axes of their graphs were converted to digital format using the tools in this shareware program. Using this tool, the flux profile points were reverse engineered to extract the coordinate information (Figure 3-5). Repeat tests of sample profiles indicated that digitization errors were, on average, less than 1% - although this may increase to 5% for cases where an axis has a logarithmic scale and the symbols are large. This method was successfully used by Sherman and Farrell (2008) to analyze wind velocity profiles. A second method to extract data was to fitting regression coefficients provided in the literature to construct the vertical flux profiles. For example, Figure 4 in Dong et al., (2004) was obtained from the regression results provided in their Table 1.

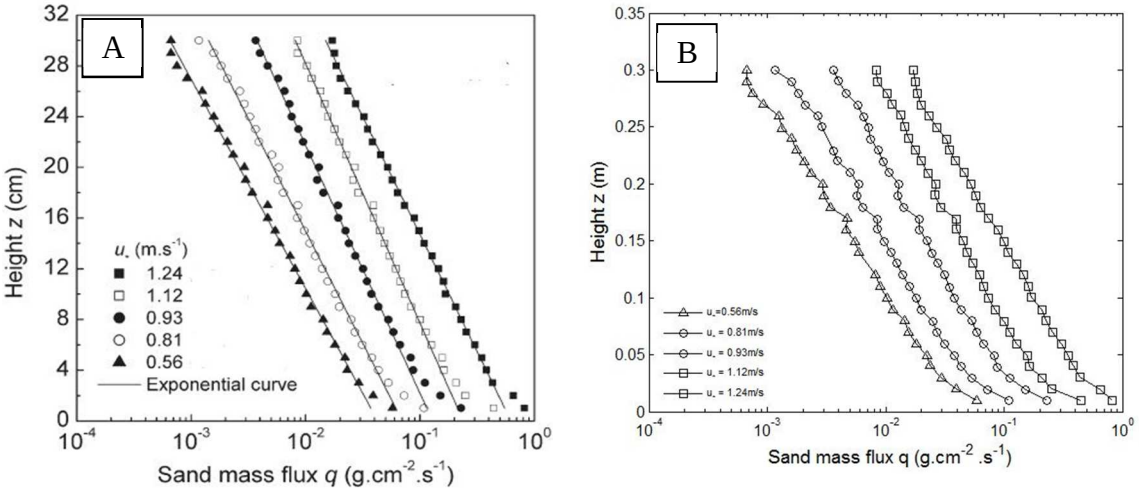

Figure 3-5. Example of reverse engineered data using the Data Thief III © (2006) software. A. Scanned image of Figure 6, Feng et al., (2009). B. Reverse engineered figure using the method described in Section 3.3.3.2.

3.4 Data normalization

In order to compare the flux profiles from different experiments, or indeed to compare profiles within individual experiments, it was necessary to normalize the data. The regression coefficients derived from the regression analysis of the exponential function ($q_z = \alpha\exp(bz)$) represent a scaling factor for "*a*", and the rate of decay (or slope) of the flux for "*b*". Intuitively, one would expect that the only difference between measured flux profiles for a range of different wind speeds should be a scaling factor if surface properties are consistent. The flux profiles were normalized by converting the absolute quantity of sand captured in each trap to a percentage relative to the total mass trapped for each run. In hydrological environments, normalization is typically based on a reference sediment concentration e.g. the C_a term in the Rouse model. In saltation studies, previous workers have normalized using the total flux (Chen et al., 1996; Dong and Qian, 2007; Namikas, 2003) or the flux measured nearest the bed (Butterfield, 1999). Ellis et al., (2009), in a review of mass flux analyses, proposed using the total flux method as a protocol to normalize flux profiles in aeolian environments. This method is used in this analysis. This approach or normalizing the traps to a proportional representation of the total flux has the advantage of removing any potential influence of spatial variability in total transport or influences from measuring in different environments and conditions (Namikas et al., 2009). The normalized profiles represent the proportion of total mass flux moving rather than an absolute flux. In some cases it is also necessary to also normalize the mass caught by trap size, in cases where traps of different dimensions were deployed. This was the case in Brazil (2008), Guadalupe (1996), and Portugal (2009). In these data, the flux caught in each trap was reduced to a mass in grams per 1 cm^2 per 1 second. Figure 3.6 illustrates the results of the normalization process for a set of five runs reported in Feng et al., (2009). The fact that the profiles overlay each other suggests that, for these five runs, the vertical distribution of sand has a characteristic distribution (discussed later) that is maintained for different transport rates.

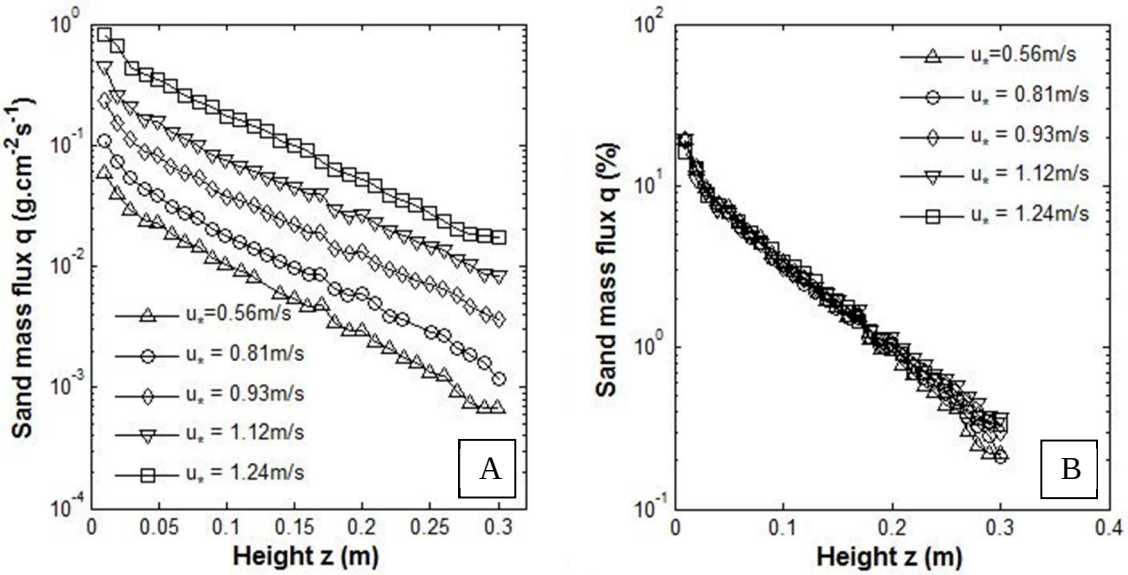

Figure 3-6. Data of Feng et al., (2009) for elevation (m) *vs.* flux (g/cm^2/s). A. Original published vertical mass flux profiles. B. Same flux profiles normalized by the total transport rate in for each run: elevation (m) *vs.* flux (%).

3.5 Curve fitting: elevation *vs.* flux

Applying curve fits to the vertical distributions of mass flux is typically accomplished using regression analysis to establish the statistical strength of the relationship between flux data and elevation. The recommended protocol of Ellis et al., (2009) was used to analyse the mass flux profiles. Elevation and flux were the independent and dependent variables. A non-linear, least squares, exponential curve was used to fit curves to the data (Equation 3-4). For comparative purposes, the performance of power (Equation 3-5) and logarithmic (Equation 3-65) curves were also tested using the goodness-of-fit (r^2) value.

$$q_z = ae^{bz} \tag{3-4}$$

$$q_z = az^b \tag{3-5}$$

$$q_z = \ln(z) + b \tag{3-6}$$

where, q_z is the transport rate at elevation z, a and b are the regression coefficients.

3.6 Fall velocity of sand sized particles in air

In order to examine the controls on fall velocity, the five known published data sets that reported direct measurements of particles fall velocity were analyzed. The details of these studies are described in Table 3-4. The fall velocity data sets were obtained using three different methods.

1. The published fall velocity graphs in Bagnold (1935), Cui et al., (1983) and Malcolm and Raupach (1991) were scanned and the images were processed using Data Thief III (2006) software (shareware from http://www.datathief.org). The fall velocity points and axes of the graphs were manually digitized using the suite of onscreen digitizing tools. Once this was done the coordinate information of each point was obtained digitally and the data set was reverse engineered.
2. The theoretically derived data in Chen and Fryrear (2001) and the experimental data in Wilson and Huang (1979) were reproduced by directly transposing from the tables in their published reports. The Chen and Fryrear data were reproduced from their Table 1 (p.368) and the Wilson and Huang data were taken from their Table 1 (p.314-316).
3. Finally, if neither of the first two options was sufficient the authors were contacted to request copies of the original data. Chen and Fryrear (2001) generously shared the data they used to create their Figure 6 (p.369).

Any data supplemental to the fall velocity graphs were obtained from the published sources. These mainly included details pertaining to experimental design (e.g. fall height) and sediment properties (e.g. diameter, density and shape). The results from these studies are shown in Figure 3-7A. Linear regression shows a strong relationship between grain size and fall velocity, with $r^2 = 0.87$:

$$w_0 = 3.34D + 0.3447 \qquad (3\text{-}7)$$

The goodness of fit for all the runs clearly indicates that grain size as expected exerts the first order control on the fall velocity. However, it was noted that the fall velocities of the coarsest grain fractions trail off to towards a critical maximum in the experiments of Bagnold (1941), Cui et al., (1983) and Chen and Fryrear (2001). Theoretical approaches

have shown that grain fall velocities are proportional to the square of diameter for smaller grains and the square root of grain diameter for larger grain diameters. This might partly explain the change in curves for the latter two studies but the not the very pronounced change in the Bagnold data set. Cui et al., (1983) argue that Bagnold fall height of 1.09 m was too short to allow the larger grains to attain their true fall velocity. In order to address this argument the height required for a range of different grain sizes (0.1 – 1.2 mm) to reach terminal velocity was calculated using the system of equations described in Baas (2004) to calculate the velocity of the spherical grains in time increments of 0.001 s from an initial acceleration of 0.001 m/s^2. The simulated fall velocities were calculated in time increment of 0.001 s until such time as there was no appreciable change in successive fall velocities. The fall distance at which this occurred was designated the critical/threshold height. The critical fall heights were then recalculated for a shape correction using the method described in Baas (2004), based upon the findings of Gibbs et al., (1971) and Cui et al. (1983). A second quality control was also implemented, whereby grain diameters had to range between 0.0625 and 2.0 mm, the range of very fine to very coarse sand – which reflect the range of grains sizes reported in saltation studies. The results of the quality controlled data are shown in Figure 3-7B. The goodness-of-fit test for the quality controlled data shows that there is a strong relationship between grain diameter and fall velocity (r^2 = 88) using the empirical relationship:

$$w_0 = 4.23D + 0.1956 \qquad (3\text{-}7)$$

This relationship provides the fall velocity, in *m/s*, for a mean grain size of D in *mm* and was used to calculate the fall velocities of different sized sand particles in this research.

Table 3-4. Details of published fall velocity experiments

Source	Fall Height (m)	Particle type	Particle diameter (mm)	Particle density (g cm^{-3})	Fall velocity (m/s)
Bagnold (1935)[1]	1.09	Desert sand (Western Desert, Egypt)	0.13 – 1.23	2.65	0.61 – 2.12
Chen & Fryrear (2001)[2]	6.2013	Glass spheres	0.15 – 0.55	2.49	0.06 – 2.30
		Dune sand (White Sands Desert, USA)	0.49 – 0.55	2.307 ± 0.045	0.23 – 2.22
		Desert sand (Central Takla Makan Desert, China)	0.49 – 0.55	2.56 ± 0.038	0.29 – 2.02
		Desert sand (North Takla Makan Desert, China)	0.49 – 0.55	2.56 ± 0.038	0.32 – 2.20
		Eolian sand (Big Spring, USA)	0.49 – 0.55	2.604 ± 0.094	0.12 – 2.53
Cui et al. (1983)[3]	7.55	Beach sand (Oregen, USA)	0.41 – 1.80	2.65	1.40 – 5.45
	11.20	Beach sand (Oregen, USA)	0.36 – 1.70	2.65	1.54 – 6.08
Malcolm & Raupach (1991)[4]	6.09	Glass beads	<0.044 - >0.50		0.22 – 2.67
		Bungendore sand (NSW, Australia)			
		(air dried)	0.05 – 0.46		0.27 – 3.22
		(oven dried)	0.06 – 0.46		0.29 – 2.98
Wilson & Huang (1979)[5]	0.317	Feldspar grains	0.035 – 0.475	2.65	0.09 – 2.17

Notes

1.Bagnold plotted the fall time of the sand particles against an 'equivalent grain diameter' that was an "*arbitrary shape factor* (p.347)" used to convert the irregular shaped grains to equivalent sized quartz spheres by multiplying by 0.75 (his Figure 3, p.347). The multiplier is removed in this analysis following the method of Cui et al. (1983).

2. The data used in their Figure 6 (p.369) was obtained from the authors upon request. They used a mean geometric grain size which was calculated as the mean of the opening of the last sieve through which the grains have passed through and the sieve on which they are retained.

3. From Cui et al. (1983), Figure 1 (p.1206).

4. The 0.210 – 0.177mm and 0.177 – 0.149 mm classes of glass beads were eliminated from the results by the authors because they "*contained too many irregular shapes* (p.15279)" after microscope analysis. Bugendore is located in New South Wales, Australia but it is unclear what type of deposit the sand was. The authors state they had problems with re-aggregation for the small sized sand samples. Samples were both air dried and oven dried to examine the role of water content. The reported data herein was obtained from their Figures 9 and 10 (p.15281). The authors use the arithmetic median sieve diameter which was found to be within 0.4% of the geometric median diameter.

5. The Wilson and Huang experiments were conducted in a settling tube 0.317m long that they deemed sufficient for particle up to 0.80 mm to reach terminal velocity based on Wilson (1973). Their data was taken from Table 1, p.315-316.

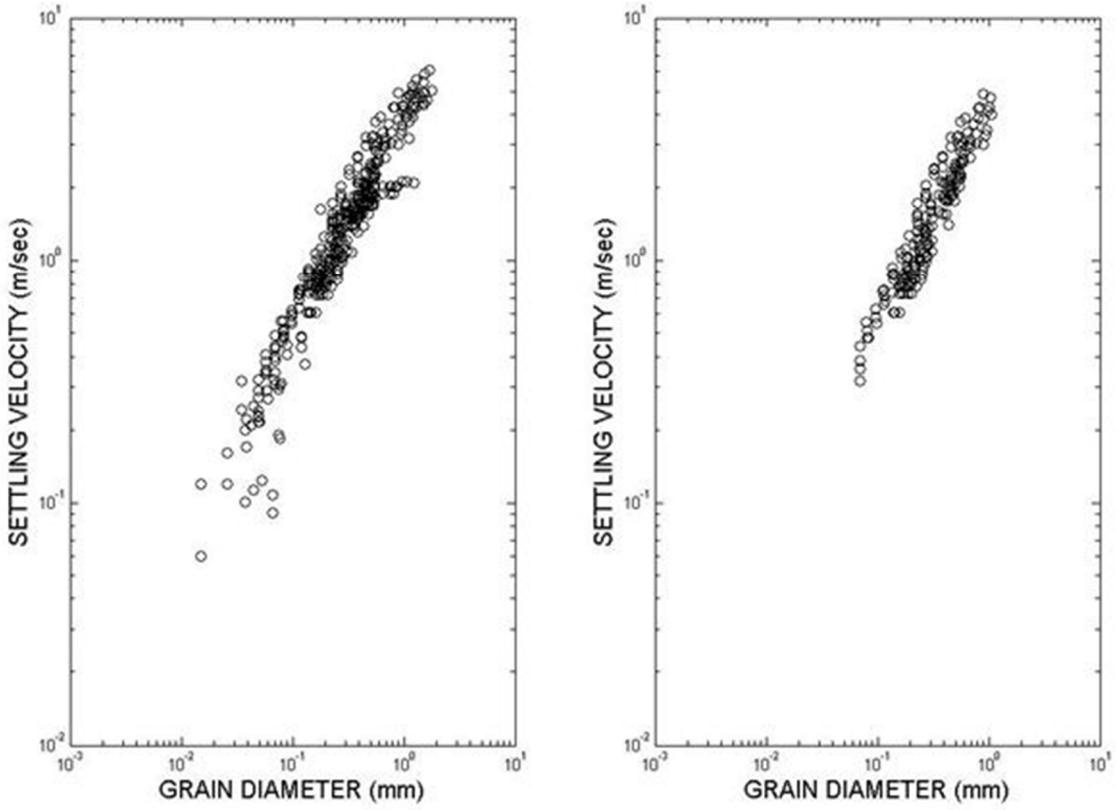

Figure 3-7. A. Relationship between grain diameter and fall velocity for all the grouped data (left). B. The data were quality controlled using two criteria and re-plotted (right).

3.7 The Rouse profile

The Rouse model was tested on vertical flux data from experiments that reported runs with shear velocity and grain size. Both these parameters are required to calculate the exponent in the Rouse model. A total of 110 runs from field and wind tunnel experiments were used in the analysis. These are summarized in Table 3-4. The details of run identification, shear velocity, and grain size are listed in Table 4-2. The flux – elevation data obtained from each experiment are provided in Appendix B.

Table 3-5. List of data sources for Rouse analysis. *n* is the number of runs used in each experiment.

Experiment type	***n***	**Source**
Field	32	Brazil, (2008); Greeley et al., (1996); Namikas (2003)
Large wind tunnels	56	Dong et al., (2004); Feng et al., (2009); Hotta & Horikawa (1991); Hotta et al., (2006); Ni et al., (2002); Zou et al., (2001)
Small wind tunnels	22	Butterfield (1999); Gerety & Slingerland (1983); Kawamura (1951); Rasmussen & Mikkelsen (1998); Sørensen (1985); Williams (1964)

The Rouse model requires the following inputs to calculate the vertical distribution of concentration:

- C_a, the reference concentration, C, at elevation a above the bed
- H, the total flow depth. was assumed to be the vertical distance from the surface ($z = 0$) to the elevation of the highest sampled point.
- The Rouse number, calculated using the sediment fall velocity (w_0), the von Kármán constant (k), the shear velocity (u_*) and the constant of proportionality (β).

Firstly, the reported flux and elevation of the bottom trap in each run were designated the values for C_a and a, respectively (reported in Appendix B). The appendix provides tables of data for each experiment listing the elevation and flux details that were obtained from the digitization method described in Section 3.3.3.2. The total flow depth,

H, was assumed to be the vertical distance from the surface (z =0) to the elevation of the highest sampled point. Again, the values of H can be obtained from the tables provided in Appendix 4-2. The fall velocity was calculated from Equation 3-7. For the first series of analyses, k and β were assumed to be 0.40 and 1.0, respectively. Shear velocity was obtained from the methods described in Section 3.2 for the Brazil (2008) data or using the reported values in all other studies.

3.7.1 Example: Applying the Rouse model to aeolian saltation

The following is an example of how the Rouse model was used with the vertical flux data using five profiles from Feng et al., (2009). Tables 3-5 and 3-6 contain the digitized data for the five runs and the details of the Rouse number calculations used to re-engineer their results. The *a/H* parameter was calculated from dividing the elevation of the lowest trap by the maximum sampled elevation. For example, the value for *a/*H for Run 1 is 1.0218/29.9563 = 0.03411.

Table 3-6. Summary of input parameters to Rouse models for Runs 1-5, Feng et al., (2009).

	U* (m/s)	D (mm)	w_0 (m/s)	Rouse Number	*a/H*
Run 1	0.56	0.35	1.676	7.480	0.03411
Run 2	0.81	0.35	1.676	5.170	0.03226
Run 3	0.93	0.35	1.676	4.510	0.03226
Run 4	1.12	0.35	1.676	3.740	0.03226
Run 5	1.24	0.35	1.676	3.380	0.03226

Table 3-7. Digitized data using Data Thief III© (2006) for Runs 1-5, Feng et al., (2009).

Run 1		Run 2		Run 3		Run 4		Run 5	
q (g/cm2/s)	z (cm)	q (g/cm2/s)	z (cm)	q (g/cm2/s)	z (cm)	q (g/cm2/s)	z (cm)	q (g/cm2/s)	z (cm)
0.0006673	29.9563	0.0011737	30.0101	0.0036319	30.0101	0.0084124	30.0101	0.0171	30.0101
0.0006676	28.9345	0.0015917	28.9345	0.0040212	29.042	0.008539	28.9882	0.0179	28.9882
0.0007499	27.9664	0.0018405	27.9664	0.0046501	27.9664	0.0103	27.9664	0.0184	27.9664
0.0009323	26.9983	0.0020977	26.9445	0.005781	26.9445	0.0113	26.9983	0.0201	26.9445
0.0012642	25.9765	0.0026845	25.9765	0.006494	25.9227	0.0134	26.0303	0.0232	25.9765
0.00134	24.9008	0.0028873	25.0084	0.00719	24.9546	0.0146	25.0084	0.0272	24.9546
0.0015953	23.9866	0.0036436	22.9109	0.0075128	23.9328	0.0157	23.9866	0.0324	23.9328
0.0017662	23.0185	0.0039189	21.9966	0.0086873	22.9647	0.0179	23.0185	0.0349	22.9647
0.0020722	21.9429	0.0050151	20.9748	0.0094802	21.9429	0.0198	21.9966	0.0386	21.9966
0.0023618	20.921	0.0058839	19.9529	0.0106	20.9748	0.0226	20.921	0.046	20.9748
0.0029361	20.0067	0.0057185	18.9311	0.013	19.9529	0.0265	19.9529	0.0524	19.9529
0.0029803	18.9849	0.0064239	17.9092	0.0127	18.9849	0.0262	19.0387	0.0572	18.9849
0.0033967	17.963	0.0085857	16.9412	0.0142	17.9092	0.0294	17.963	0.0633	17.963
0.0047414	16.995	0.0085893	16.0269	0.0193	16.9412	0.0393	16.9412	0.0732	16.995
0.0046754	15.9731	0.0097898	14.9513	0.0193	15.9731	0.0393	16.0269	0.0897	15.9731
0.0054853	14.9513	0.011	13.9832	0.0223	15.005	0.0448	15.005	0.0993	14.9513
0.0059859	13.9832	0.0124	13.0151	0.0244	13.9294	0.0489	13.9832	0.1084	13.9832
0.0081207	11.9933	0.0139	11.9933	0.0274	13.0151	0.0541	13.0151	0.129	12.9613
0.008991	11.0252	0.0158	10.9714	0.0317	11.9933	0.0617	11.9933	0.1449	11.9933
0.0102	9.9496	0.018	9.9496	0.0346	10.9176	0.0673	10.9714	0.1605	10.9714
0.0115	8.9277	0.02	8.9815	0.0377	10.0034	0.0745	9.9496	0.1701	10.0571
0.0145	7.9597	0.0252	7.9059	0.0436	8.9277	0.0837	8.9815	0.2084	8.9815
0.0156	6.9378	0.0271	6.9916	0.0535	7.9597	0.0996	7.9059	0.2275	7.9597
0.0183	5.9697	0.0313	5.9697	0.0592	6.9378	0.1119	6.9378	0.2593	6.9916
0.0225	4.9479	0.0384	4.9479	0.0675	5.916	0.1276	5.9697	0.3042	5.916
0.0235	4.0336	0.0431	3.9798	0.0827	4.9479	0.1563	4.9479	0.3517	4.9479
0.0296	2.958	0.0536	2.958	0.0876	3.9261	0.1633	3.9798	0.3838	4.0336
0.0395	1.9899	0.0727	1.9361	0.1121	2.958	0.209	2.958	0.4374	3.0118
0.0585	1.0218	0.109	0.9681	0.1521	1.9361	0.2524	1.9899	0.6565	1.9361
				0.2315	0.9681	0.4442	0.9681	0.8161	0.9681

The Rouse model calculates the flux distribution from three inputs: a/H, w_0 and u_*. The outputs are: (1) a relative flux (c/cb) and, (2) a relative elevation (a/H). The maximum flux ($c/cb = 1$) occurs at the reference elevation, a/H. This, in essence, states that flux decays away from the surface from this point. The rate of decay is exponential and is dependent upon the value of the exponent, or Rouse number. The Rouse model builds concentration profiles using the following boundary conditions (see Table 3-7):

- Bottom elevation: a/H

Table 3-8. Calculated Rouse profile based on input parameters derived from aeolian vertical mass flux profiles: a/H, w_0 and u_*.

Run 1: Input	
a/H	0.03411
w_0 (m/s)	1.6761
u_* (m/s)	0.56

c/cb	a/H
1	0.03411
0.00072	0.08495
1.4E-05	0.13578
8.3E-07	0.18662
8.4E-08	0.23746
1.2E-08	0.28829
2E-09	0.33913
3.9E-10	0.38996
8.1E-11	0.4408
1.8E-11	0.49164
3.8E-12	0.54247
8.1E-13	0.59331
1.6E-13	0.64415
2.9E-14	0.69498
4.3E-15	0.74582
5E-16	0.79665
3.6E-17	0.84749
1.1E-18	0.89833
4.2E-21	0.94916
0	1

Run 2: Input	
a/H	0.03226
w_0 (m/s)	1.6761
u_* (m/s)	0.56

c/cb	a/H
1	0.03226
0.00563	0.08319
0.00035	0.13413
4.9E-05	0.18506
1E-05	0.23599
2.5E-06	0.28693
7.4E-07	0.33786
2.4E-07	0.3888
8E-08	0.43973
2.8E-08	0.49066
9.6E-09	0.5416
3.3E-09	0.59253
1.1E-09	0.64346
3.3E-10	0.6944
8.8E-11	0.74533
2E-11	0.79627
3.2E-12	0.8472
2.9E-13	0.89813
6.1E-15	0.94907
0	1

Run 3: Input	
a/H	0.03226
w_0 (m/s)	1.6761
u_* (m/s)	0.56

c/cb	a/H
1	0.03226
0.01098	0.08319
0.00099	0.13413
0.00018	0.18506
4.4E-05	0.23599
1.3E-05	0.28693
4.6E-06	0.33786
1.7E-06	0.3888
6.6E-07	0.43973
2.6E-07	0.49066
1E-07	0.5416
4.1E-08	0.59253
1.5E-08	0.64346
5.5E-09	0.6944
1.8E-09	0.74533
4.8E-10	0.79627
9.8E-11	0.8472
1.2E-11	0.89813
4.2E-13	0.94907
0	1

Run 4: Input	
a/H	0.03226
w_0 (m/s)	1.6761
u_* (m/s)	0.56

c/cb	a/H
1	0.03226
0.0236	0.08319
0.00319	0.13413
0.00076	0.18506
0.00024	0.23599
9E-05	0.28693
3.7E-05	0.33786
1.6E-05	0.3888
7.4E-06	0.43973
3.4E-06	0.49066
1.6E-06	0.5416
7.3E-07	0.59253
3.3E-07	0.64346
1.4E-07	0.6944
5.4E-08	0.74533
1.8E-08	0.79627
4.9E-09	0.8472
8.7E-10	0.89813
5.3E-11	0.94907
0	1

Run 5: Input	
a/H	0.03282
w_0 (m/s)	1.6761
u_* (m/s)	0.56

c/cb	a/H
1	0.03226
0.03391	0.08319
0.00557	0.13413
0.00153	0.18506
0.00054	0.23599
0.00022	0.28693
9.9E-05	0.33786
4.7E-05	0.3888
2.3E-05	0.43973
1.2E-05	0.49066
5.8E-06	0.5416
2.9E-06	0.59253
1.4E-06	0.64346
6.4E-07	0.6944
2.7E-07	0.74533
1E-07	0.79627
3.1E-08	0.8472
6.5E-09	0.89813
5.2E-10	0.94907
0	1

- Maximum elevation: 1
- Bottom (and maximum) concentration: 1
- Top (and minimum) concentration: 0
- Number of points in profile: controlled by the user/modeler, in this case 19.

Figure 3.7 provides an example of plotted Rouse-type profiles based upon the saltation data. Note, for clarity, the plotted runs presented in Figure 3-7 are based upon a modified Rouse number calculation (for $\beta = 10$) which will be discussed in detail in Section 5. The shapes of the Rouse profiles provides a means to test, and compare, the performance of the Rouse model in replicating the response of vertical distributions of mass flux to different environmental and/or experimental conditions. For example, in Figure 3-7, Run 1 has the steepest slope with proportionally more flux moving closer to the bed

compared to Runs 2- 5. These steps were repeated for all the runs in each experiment, listed in Table 3-4.

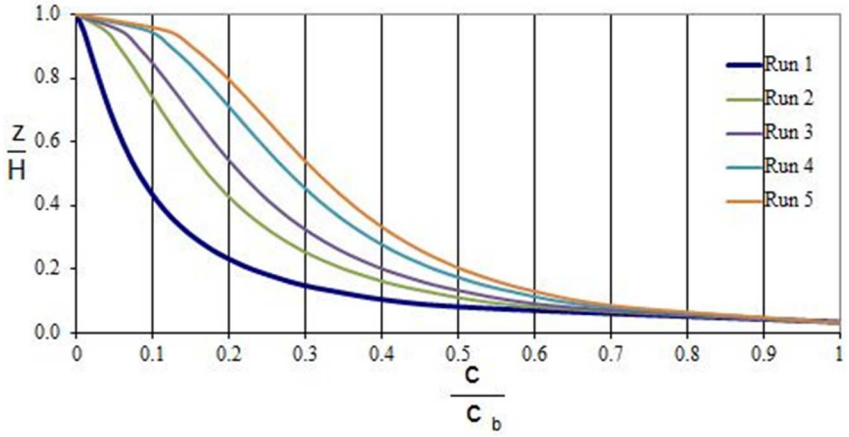

Figure 3-8. Example of Rouse profiles (using β = 10).

The original flux profiles can be reconstructed using the relative distributions predicted by the Rouse model (Table 3-8). The only input required to predict the transport profile is the measured flux at the reference elevation. The predicted flux profiles based upon this Rouse approach are shown in Table 3-9, where the Rouse number is based upon the original assumption of β = 1. These were compared with the observed transport rate calculated from the digitized data shown in Table 3-6 and Appendix B. These steps provided a means to compare the shape and magnitude of the Rouse profiles with the observed data measured in the experiments.

Table 3-9. Reconstructed flux profiles using the predicted Rouse vertical distributions.

Q (g/cm^2/s)	z (cm)	Q (g/cm^2/s)	z (cm)	Q (g/cm^2/s)	z (cm)	Q (g/cm^2/s)	z (cm)	Q (g/cm^2/s)	z (cm)
0.0585	0.5115	0.109	0.4634	0.2315	0.4936	0.4442	0.00412	0.8161	0.00399
4.23025E-05	2.54838	0.000613126	2.49579	0.002540861	2.49579	0.010481793	2.49579	0.027673612	2.49579
8.24927E-07	4.07347	3.85544E-05	4.0238	0.000228315	4.0238	0.00141746	4.0238	0.004541828	4.0238
4.85259E-08	5.59856	5.32933E-06	5.55181	4.07402E-05	5.55181	0.000338828	5.55181	0.001246946	5.55181
4.93595E-09	7.12365	1.08506E-06	7.07982	1.01858E-05	7.07982	0.000107172	7.07982	0.000440886	7.07982
6.89855E-10	8.64874	2.7631E-07	8.60783	3.0945E-06	8.60783	3.9852E-05	8.60783	0.000180415	8.60783
1.17537E-10	10.1738	8.08692E-08	10.1358	1.06128E-06	10.1358	1.63883E-05	10.1358	8.08541E-05	10.1358
2.2707E-11	11.6989	2.58514E-08	11.6639	3.93042E-07	11.6639	7.18332E-06	11.6639	3.83848E-05	11.6639
4.73369E-12	13.224	8.71806E-09	13.1919	1.52506E-07	13.1919	3.27282E-06	13.1919	1.8871E-05	13.1919
1.02514E-12	14.7491	3.02035E-09	14.7199	6.05796E-08	14.7199	1.52048E-06	14.7199	9.44224E-06	14.7199
2.23171E-13	16.2742	1.05065E-09	16.2479	2.41491E-08	16.2479	7.08459E-07	16.2479	4.73702E-06	16.2479
4.72922E-14	17.7993	3.58844E-10	17.7759	9.47433E-09	17.7759	3.2576E-07	17.7759	2.34824E-06	17.7759
9.4126E-15	19.3244	1.17391E-10	19.3039	3.58009E-09	19.3039	1.45192E-07	19.3039	1.13175E-06	19.3039
1.68239E-15	20.8495	3.56583E-11	20.8319	1.26821E-09	20.8319	6.13336E-08	20.8319	5.19664E-07	20.8319
2.53533E-16	22.3746	9.62754E-12	22.3599	4.05433E-10	22.3599	2.37928E-08	22.3599	2.20937E-07	22.3599
2.91486E-17	23.8996	2.15612E-12	23.888	1.10136E-10	23.888	8.06253E-09	23.888	8.31334E-08	23.888
2.13173E-18	25.4247	3.53221E-13	25.416	2.27862E-11	25.416	2.17919E-09	25.416	2.55025E-08	25.416
6.6345E-20	26.9498	3.20578E-14	26.944	2.81855E-12	26.944	3.84259E-10	26.944	5.31924E-09	26.944
2.45721E-22	28.4749	6.67933E-16	28.472	9.67728E-14	28.472	2.33752E-11	28.472	4.24273E-10	28.472
0	30	0	30	0	30	0	30	0	30

IV. RESULTS

4.1 Field experiment

A total of twenty-five usable samples of vertical flux profiles were available for laboratory analysis of the grain size data. The averaged, cumulative mass-flux distributions of the runs in each sub-environment (CSFF, CSFC, Beach) determined that the proportions of transport caught in the lowest trap (below 0.025 m) are 62%, 55% and 61% of the total load for CSFF, CSFC and the Beach environments, respectively – differences that are probably trivial. For the traps located more than 0.35 m above the surface the amount of sand caught was always less than 3% of the total. The absolute masses involved were small to make the results of sieving for grain-size analysis questionable. Therefore, samples caught at elevations above 0.35 m were excluded from the rest of the analyses. The standard, grain-size distribution statistics (mean, sorting, skewness, kurtosis) derived using the geometric method-of-moments, are provided in Table 4.1. Blank entries indicate contaminated samples (10/22 Run 3, Trap 2) or samples that were too small for grain-size analysis (10/24 Run 4, Trap 6). The estimates of shear velocity for fourteen of the runs are also provided in Table 4.1. Shear velocities for the three CSFC runs were 0.49, 0.50 and 0.50 m/s. The remaining shear velocities were all collected in CSFF and ranged from 0.41 - 0.54 m/s. Shear velocity was not measured during sampling at the Beach site, but was of comparable magnitude.

4.1.1 Field experiment: grain size-sorting variability

The sediment transport samples collected from three sedimentary sub-environments near Jericoacoara, Brazil were analyzed using the methods described in Section 3.3.2. The mean (D_{trap}), standard deviation (σ_g), skewness (Sk_g), and kurtosis (K_g) grain size statistics are plotted for all the samples in each sub-environment in Figures 4-1(A-D). This research will focus on the variability of grain size with elevation above the bed.

Table 4-1. Transport data collected using vertically integrating, passive traps. The trap heights (in *mm*) are provided for each trap. Each trap is 100 mm wide. The sediment mass (*g*) measured in each trap is reported for each run. Run duration is provided in seconds *(s).* Standard grain size distribution statistics using the geometric method of moments (mean (D_{trap}), sorting (σ_g), skewness (Sk_g), kurtosis (K_g)) are also listed for each sample. D_w is the weighted mean grain size (*mm*) calculated for each run. Shear velocities (u_*) are reported where applicable.

Run	Location		Trap 1 25mm	Trap 2 25mm	Trap 3 50mm	Trap 4 50mm	Trap 5 100mm	Trap 6 100mm	D_w *(mm)*
10/22 Run1	**CSFF**	***mass (g)***	105.1	73.9	64.1	36.4	31.6	38.7	
Duration: 120 *s*		D_{trap} ***(mm)***	0.334	0.271	0.264	0.261	0.270	0.285	0.309
U_* : 0.54 *m/s*		σ_g	1.554	1.526	.470	1.457	1.420	1.435	
		Sk_g	-0.460	0.012	0.112	-0.035	-0.0 5	-0.069	
		K_g	2.370	2.152	2.359	2.312	2.449	2.574	
10/22 Run 2	**CSFF**	***mass (g)***	206.5	121.0	92.5	45.6	40.2	32.1	
Duration: 180 *s*		D_{trap} ***(mm)***	0.266	0.225	0.228	0.240	0.244	0.251	0.253
U_* : 0.47 *m/s*		σ_g	1.571	1.426	1.400	1.425	1.402	1.418	
		Sk_g	0.295	0. 18	0.326	0.094	0.010	0.021	
		K_g	2.248	2.943	3.223	2.565	2.931	2.836	
10/22 Run 3	**CSFF**	***mass (g)***	139.0		112.7	54.7	40.9	22.2	
Duration: 240 *s*		D_{trap} ***(mm)***	0.273	0.244	0.241	0.251	0.248	0.252	0.26
U_* : 0.53 *m/s*		σ_g	1.554	1.487	1.432	1.422	1.417	1.4 0	
		Sk_g	0.096	0.198	0.251	0.060	0.011	-0.208	
		K_g	2.222	2.410	2.734	2.594	2.724	2.809	
10/24 Run 1	**CSFF**	***mass (g)***	148.8	76.5	89.1	45.1	17.8	16.7	
Duration: 170 *s*		D_{trap} ***(mm)***	0.340	0.296	0.292	0 296	0.295	0.307	0.325
U_* : 0.49 *m/s*		σ_g	1.441	1.402	1. 74	1.347	1.382	1.349	
		Sk_g	-0.478	-0.204	-0.244	-0.326	-0.564	-0.778	
		K_g	2.929	2.601	2.701	2.886	3.269	3.327	
10/24 Run 2	**CSFF**	***mass (g)***	165.8	91.6	104.1	52.0	30.1	27.3	
Duration: 240 *s*		D_{trap} ***(mm)***	0.325	0.288	0.276	0.292	0.292	0.285	0.311
U_* : 0.50 *m/s*		σ_g	1.432	1.385	1.380	1.341	1.335	1.457	
		Sk_g	-0.356	-0.135	-0.201	-0.359	-0.335	-0.796	
		K_g	2.567	2.662	2.808	2.853	2.883	3.403	
10/24 Run 3	**CSFF**	***mass (g)***	158.7	90.2	36.9	92.8	19.4	1 .9	
Duration: 240 *s*		D_{trap} ***(mm)***	0.308	0.269	0.267	0.275	0.289	0 297	0.296
U_* : 0.50 *m/s*		σ_g	1.469	1.409	1.373	1.339	1.325	1.317	
		Sk_g	-0.215	-0.085	-0.176	-0.249	-0.175	-0.506	
		K_g	2.451	2.566	2.587	2.786	2.630	3.490	
10/24 Run 4	**CSFF**	***mass (g)***	1 9.8	72.2	75.4	47.4	24.7	7.3	

Table 4-1 continued.

Duration: 240 *s*		D_{trap} *(mm)*	0.310	.273	0.291	0.286	0.303		0.298
U_* : 0.47 *m/s*		σ_g	1.484	1.417	1.401	1.356	1.349		
		Sk_g	-0.344	-0.094	-0.378	-0.178	-0.421		
		K_g	2.477	2.537	2.313	2.746	2.810		
10/24 Run 5	**CSFF**	***mass g)***	124.8	68.5	72.7	36.0	22.8	18.2	
Duration: 240 *s*		D_{trap} *(mm)*	.337	0.287	0.279	0.292	0.291	0.248	0.318
U_* : 0.45 *m/s*		σ_g	1.466	1.427	1.365	1.351	1.354	1.496	
		Sk_g	-0.432	-0.338	-0.137	-0.324	-0.349	-0.376	
		K_g	2.612	2.372	2.502	2.716	2.785	2.365	
10/24 Run 6	**CSFF**	***mass (g)***	167.3	77.1	93.3	33.1	25.1	19.6	
Duration: 240 *s*		D_{trap} *(mm)*	0.320	0.294	0.278	0.291	0.302	0.301	0.310
U_* : 0.51 *m/s*		σ_g	1.470	1.442	1.383	1.362	1.355	1.331	
		Sk_g	-0.166	-0.314	-0.302	-0.321	-0.399	-0.431	
		K_g	2.236	2.3 3	2.557	2.680	2.699	2.982	
10/25 Run 1	**CSFF**	***mass (g)***	52.0	36.2	44.2	28.1	18.5	16.2	
Duration: 150 *s*		D_{trap} *(mm)*	0.422	0.285	0.290	0.292	0.297	0.306	0.366
		σ_g	1.520	1.492	1.430	1.394	1.364	1.344	
		Sk_g	-0.872	-0.143	-0.085	-0.026	-0.067	-0.184	
		K_g	2.923	2.097	2.236	2.226	2.314	2.494	
10/25 Run 2	**CSFF**	***mass ( )***	82.8	62.5	77.4	36.2	25.2	21.5	
Duration: 300 *s*		D_{trap} *(mm)*	0.368	0.293	0.300	0.290	0.303	0.322	0.337
		σ_g	1.528	1.474	1.420	1.390	1.368	1.327	
		Sk_g	-0.554	-0.143	-0.160	-0.060	-0.133	- .168	
		K_g	2.405	2.073	2.259	2.404	2.489	2.329	
10/25 Run 3	**CSFF**	***mass (g)***	56.1	43.5	56.4	31.8	19.7	13.7	
Duration: 240 *s*		D_{trap} *(mm)*	0.332	0.291	0.279	0.292	0.291	0.335	0.312
		σ_g	1.520	1.447	1.409	1.375	1.357	1.290	
		Sk_g	-0.272	-0.092	0.056	-0.0 6	0.003	-0.281	
		K_g	2.136	2.166	2.212	2.437	2.356	2.671	
10/25 Run 4	**CSFF**	***mass (g)***	106.9	78.9	91.2	47.9	24.8	18.1	
Duration: 480 *s*		D_{trap} *(mm)*	0.257	0.229	0.239	0.250	0.254	0.271	0.248
		σ_g	1.497	1.380	1.347	1.324	1.337	1.329	
		Sk_g	0.324	0.135	0 162	0.166	0.020	-0.321	
		K_g	2.602	2.790	2.792	2.825	2.806	3. 77	
10/26 Run 1	**CSFF**	***mass (g)***	172.7	122.5	136.2	76.0	45.8	41.3	
Duration: 240 *s*		D_{trap} *(mm)*	0.356	0.287	0.287	0.296	0.290	0.323	0.329
U_* : 0.48 *m/s*		σ_g	1.598	1.523	1.467	1.427	1.391	1.35	
		Sk_g	-0.452	0.005	-0.017	-0.117	-0.030	-0.372	
		K_g	2.183	2.131	2.294	2.337	2.541	2.965	
10/26 Run 2	**CSFF**	***mass (g)***	160.0	136.4	153.1	77.9	35.5	27.8	
Duration:		D_{trap} *(mm)*	0.289	0.248	0.249	0.257	0.273	0.292	0.272

Table 4-1 continued.

300 *s*									
U_* : 0.41 *m/s*		σ_g	1.560	1 468	1.427	1.373	1.352	1.348	
		Sk_g	-0.026	0.250	0.125	0.028	-0. 50	-0.287	
		K_g	2.168	2.493	2.721	2.644	3.017	2.733	
10/29 Run 1	**CSFF**	***mass (g)***	78.7	51.4	57.1	33.1	18.0	10.0	
Duration:		D_{trap} ***(mm)***							
240 *s*			0.348	0.291	0.295	0.307	0.301	0.347	0.328
		σ_g	1.580	1.539	1.464	1.394	1.358	1.285	
		Sk_g	-0.602	-0.262	-0.26	-0.296	-0.108	-0.454	
		K_g	2.459	2.263	2.424	2.362	2.292	2.905	
10/29 Run 2	**CSFF**	***mass (g)***	63.2	41.7	50.6	26.1	12.9	9.5	
Duration:		D_{trap} ***(mm)***							
240 *s*			0.322	0.275	0.273	0.281	0.278	0.295	0.304
		σ_g	1.529	1.422	1.376	1.350	1.307	1.285	
		Sk_g	-0.184	- .133	0.048	-0.026	-0.017	-0.105	
		K_g	2.159	2.690	2.524	2.630	2.602	2.554	
10/29 Run 3	**CSFF**	***mass (g)***	51.1	42.3	45.7	25.3	13.9	9.5	
Duration:		D_{trap} ***(mm)***							
240 *s*			0.309	0.260	0.258	0.266	0.275	0.28	0.288
		σ_g	1.524	1.427	1.372	1.348	1.321	1.309	
		Sk_g	-0.110	0.061	-0.048	-0.044	0.005	-0.219	
		K_g	2.103	2.409	2.504	2.635	2.439	2.797	
10/26 Run 3	**CSFC**	***mass (g)***	93.3	79.8	100.5	71.7	44.2	47.2	
Duration:		D_{trap} ***(mm)***							
240 *s*			0.390	0.327	0.333	0.348	0 351	0.367	0.364
		σ_g	1.632	1.564	1.497	1.454	1.430	1.3 3	
		Sk_g	-0.444	-0.387	-0.345	-0.392	-0.439	-0.458	
		K_g	2.583	2.340	2.387	2.533	2.712	2.666	
10/30 Run 1	**CSFC**	***mass (g)***	114.9	77.8	105.6	68.8	44.3	47.1	
Duration:		D_{trap} ***(mm)***							
240 *s*			0.429	0.361	0.370	0.376	0.373	0.395	0.403
U_* : 0.50 *m/s*		σ_g	1.605	.606	1.510	1.495	1.442	1.413	
		Sk_g	-0.706	-0.446	-0.364	-0.435	-0.369	-0.446	
		K_g	2.836	2.114	2.145	2.277	2.329	2.556	
10/30 Run 2	**CSFC**	***mass (g)***	144.2	105.7	143.2	89.8	65.5	65.4	
Duration:		D_{trap} ***(mm)***							
300 *s*			0.445	0.358	0.360	0.372	0.368	0.386	0.408
U_* : 0.50 *m/s*		σ_g	1.579	1.622	1.512	1.492	1.467	1.400	
		Sk_g	-0.609	-0.403	-0.402	-0.322	-0.429	-0.337	
		K_g	2.596	2.111	2.313	2.236	2.546	2.333	
10/30 Run 3	**CSFC**	***mass (g)***	117.9	88.0	119.8	7 .5	54.4	54.6	
Duration:		D_{trap} ***(mm)***							
240 *s*			0.439	0.358	0.350	0.362	0.361	.396	0.402
U_* : 0.49 *m/s*		σ_g	1.642	1.627	1.550	1.505	1.462	1.379	
		Sk_g	-0.644	-0.431	-0.447	-0.413	-0.386	-0.361	
		K_g	2.649	2.118	2.319	2.317	2.347	2.244	
10/29 Run 4	**BEACH**	***mass (g)***	163.4	136.1	101.2	36.1	13.7	8.0	
Duration:		D_{trap} ***(mm)***							
240 *s*			0. 56	0.230	0.232	0.279	0.295	0.329	0.248

Table 4-1 continued.

		σ_g	1.674	1.565	1.609	1.599	1.538	1.446	
		Sk_g	-0.229	-0.034	-0.102	-0.495	-0.813	-1.106	
		K_g	1.914	2.099	1.960	2.331	2.977	3.922	
10/29 Run 5 Duration: 240 *s*	**BEACH**	***mass (g)***	134.3	144.1	112.6	45.8	20.6	13.3	
		D_{trap} ***(mm)***	0.240	0.232	0.221	0.243	0.251	0.276	0.235
		σ_g	1.598	1.549	1.537	1.526	1.507	1.475	
		Sk_g	-0.097	-0.122	-0.057	-0.248	-0.538	-0.835	
		K_g	1.951	2.043	2.146	2.313	2 551	3.252	
10/30 Run 4 Duration: 240*s*	**BEACH**	***mass (g)***	200.6	122.1	122.8	52.3	24.3	14.5	
		D_{trap} ***(mm)***	0.266	0.249	0.257	0.275	0.303	0.340	0.263
		σ_g	1.610	1.586	1.572	1.542	1.521	1.469	
		Sk_g	-0.052	0.111	0.078	-0.075	-0.282	-0.575	
		K_g	2.074	2.197	.182	2.203	2.275	2.732	

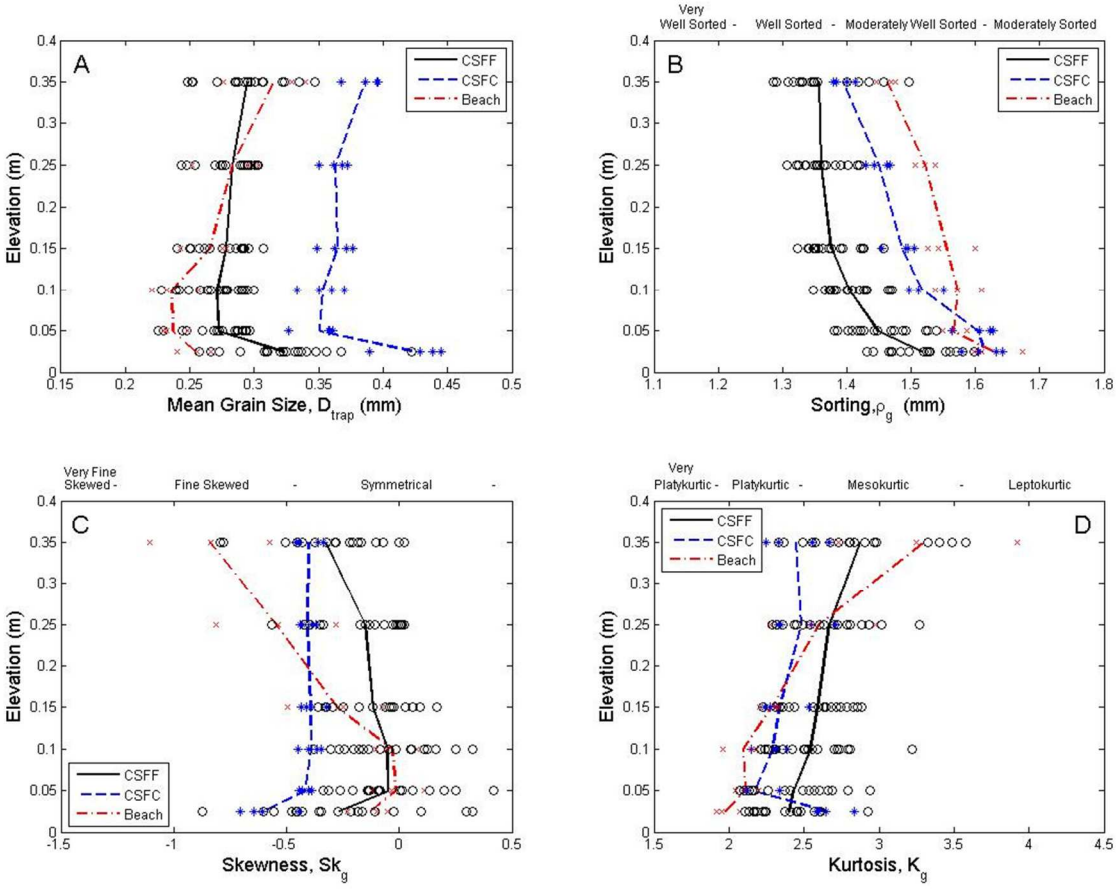

Figure 4-1. Grain size distribution plots. (Fig.A) The mean (D_{trap}), (Fig.B) standard deviation (σ_g), (Fig.C) skewness (Sk_g), and (Fig.D) kurtosis (K_g) statistics are plotted for all the samples in each sub-environment. The grouped averages of each sub-environment are plotted as lines.

Mean Grain Size: The three sub-environments have distinct grain-size characteristics that support our visual observations during the experiments. Figure 4.2A and Table 4.1 present the mean grain-sizes calculated from our samples and the grouped averages for each elevation for each sub-environment. The averages of the mean grain-size calculated for the lowest trap of each sub-environment were 0.42 mm for CSFC, 0.32 mm for CSFF and 0.25 mm for the Beach. These values were larger than the averages for the entire profiles in CSF (0.37 mm and 0.29 mm, respectively) but not for the Beach (0.27 mm). Above the lowest trap there is a marked decrease in grain size at the two Cow Flat Splat sub-environments, where the average mean grain-sizes for trap 2 are 0.35 mm and 0.27 mm at CSFC and CSFF. The decrease in the trap 2 grain size for the Beach is not as pronounced, decreasing only 0.01 mm. The mean grain-sizes for traps 3 (0.05 – 0.10 m) are identical to those for traps 2 in all three sub-environments. In each environment, a reversal in grain-size trends occurs above 0.10 m and mean grain-sizes increase continuously from traps 4 to traps 6.

As a means of facilitating the comparison of the vertical distributions of grain size, we calculated a mass-weighted, mean grain-size for each run, and used those data to normalize grain sizes at each elevation from the different runs (described in Section 3.3.2). The distributions of mean grain-size with elevation for each run are shown in Figure 4.2 (A-C) for each sub-environment. The lowest traps (traps 1) yielded the coarsest fraction of sand for the runs at location Cow Splat Flat (CSFF and CSFC in Figure 4.2) (D_i/D_w >1). Because the bottom trap contains the largest, normalized-mass, the greatest proportion of coarse grains occurs below 0.025 m. For traps 2, grain sizes do not change significantly. The smallest, normalized grain-sizes were almost always found in traps 2 (0.025 - 0.05 m) and traps 3 (0.05 – 0.10 m). Above these traps, grain sizes increased with elevation. This inflection, reflecting the grain-size reversal, is distinguishable in all runs and occurs in the range of 0.05 – 0.15 m, representing the range of elevations for traps 2 to 4. Above this inflection zone, mean grain-sizes increase consistently. The Beach location runs display a similar trend but the rates of change of

grain sizes are different. There are smaller decreases in mean grain-size from the bottom trap to the second trap than at the CSF sub-environments.

All the runs in each location (Figure 4-2A-C) were averaged to produce characteristic grain-size profiles shown in Figure 4-10D. In each case: 1) mean size decreases above the lowest traps; 2) there is an inflection in grain-size trends between 0.05 – 0.15 m, and 3) the rate of increase in mean size above the inflection zone is greater for the flux profiles from the Beach than from CSF.

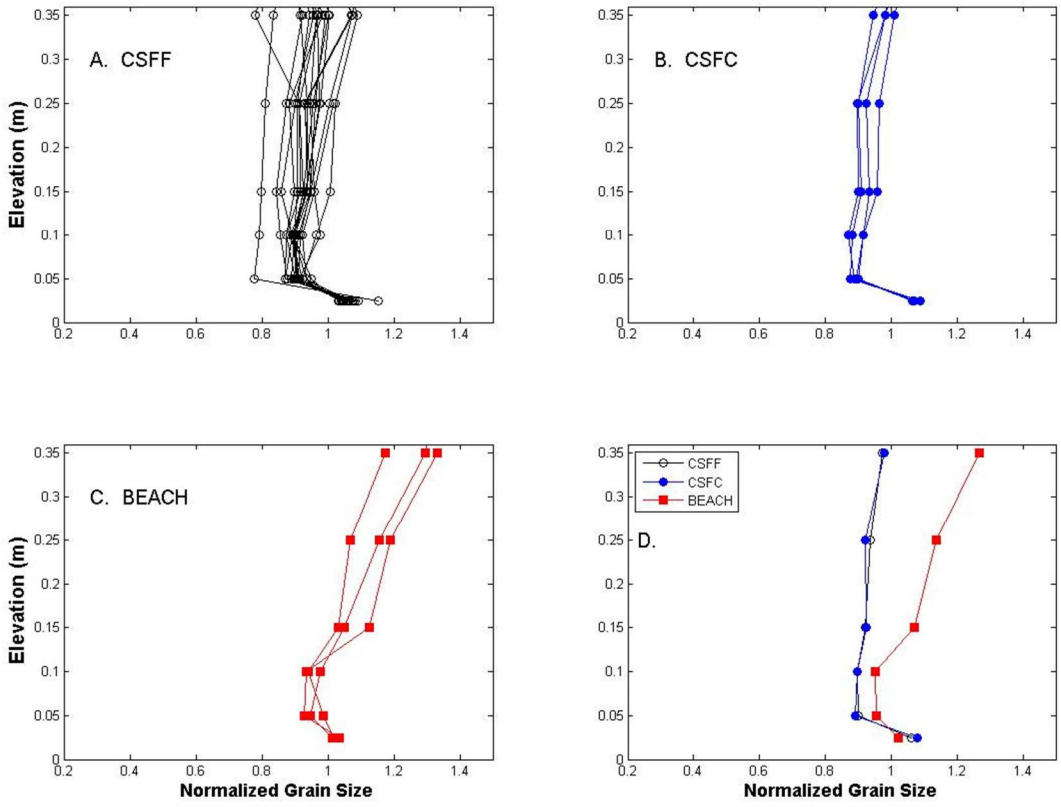

Figure 4-2. Relationship between normalised grain size and elevation for the different sub-environments (A-C). The runs in each sub-environment are averaged in Figure 4D. The CSF plots are superimposed.

This analysis of the grain-size statistics shows that a reverse in grain-size trends occurs at an inflection zone located 0.05 – 0.15 m above the bed. Below this inflection, mean grain-size decreases steeply with elevation in the near bed region dominated by reptation and saltation modes of transport. Above the inflection there is a coarsening of grain size with elevation. Sorting improves with elevation above the surface. There is not a strong relationship between skewness and kurtosis with elevation. The grain-size inflection above the surface is a characteristic of saltation in some natural environments, with important implications for numerical modeling of grain trajectories.

4.1.2 Field experiment: vertical distributions of mass flux

The vertical distribution of mass flux for each run was assessed using the protocol described in Ellis et al., (2009). Non-linear regression analyses, using exponential, logarithmic, and power functions (Equations 3-4, 3-5, and 3-6), were carried out on the observed field data. A comparison of the goodness-of-fit (r^2) values for each type of function (Table 4.2) indicates that in all thirty runs the exponential fit was superior to the power or logarithmic curves, with the exception of Run 18 (r^2 = 0.77). In all but four of the runs, the r^2 value for the exponential fit exceeds 0.98. For thirteen of the runs, r^2 rounds, at two decimal places, to 1.0.

4.2. Field and wind tunnel experiments

4.2.1. Best fit function: aggregate all experiments

A similar comparison of fitting exponential, logarithmic, and power function curves to vertical flux distributions from thirty one published studies was completed. This analysis comprised of twelve datasets from field experiments (including Brazil, 2008) and nineteen datasets from wind tunnel experiments (see Table 3-2). The performance of the curve fitting functions for all the field and wind tunnel profiles are plotted in Figure 4-3 (n = 305). The twenty five vertical flux profiles published in Liu and Dong (2004) were not included in the comparative analysis as these profiles were

constructed using their published regression coefficients, resulting in $r^2 = 1$ for the exponential curves. This procedure was followed because their graphical illustrations of the vertical flux profiles had too many overlapping points to digitize using the methods described in Section 3, discussed in Subsection 3.3.3.1. The six Hasi (1997) vertical flux profiles were also removed from the analysis because the average r^2 values for these profiles were 0.66, 0. 38 and 0.49 for the exponential, power and logarithmic fits, respectively. These results were much lower than the other thirty studies and, as such, it was thought prudent to ignore them in the analysis. Removing them does not impact the general findings reported in this section. There is little that can be done to eliminate the uncertainty associated with using statistical approaches to analyzing mass flux profiles. However, using a minimum r^2 threshold provides some limits on the uncertainty, and we have to presume that any remaining errors are distributed randomly (Sherman and Farrell, 2008).

The average r^2 value for the grouped exponential, logarithmic, and power function fits are 0.98, 0.85 and 0.91, respectively. A comparison of the r^2 values for each fitted function indicates that in 240 of the 274 cases the exponential fit was either superior, or equal, to the power or logarithmic curves. The results for each experiment are listed in Table 4-2. In some runs, there were no differences in the values of the goodness-of-fit between the exponential fit and the power fit (6 runs) or the exponential fit and logarithmic fit (7 runs). These runs did not overlap. In 85 cases, the exponential fit r^2 value rounds, at two decimal places, to 1.0. The power and logarithmic functions performed best in 23 and 12 of the tests, respectively. In one run both these tests performed better than the exponential curve fit. Two runs had exponential curves that were a poorer fit to both the power and logarithmic curves. Both these cases were profiles measured during field experiments. In the case of the profile measured in the Brazil (2008) experiment it is, most likely, a sample that was contaminated during field collection. The other profile was measured in the Rasmussen and Sørensen (1999) experiment and the same assumption is presumed to apply.

Table 4-2. Comparison of exponential, power, and logarithmic functions using vertical flux profiles collected in Brazil (2008) experiment.

Source	Run	u_* (m/s)	U_z (m/s)	d (mm)	Exponential Function A	B	r^2	Power Function A	B	r^2	Logarithmic Function A	B	r^2
Brazil, 2008 (F)	1	0.54		0.3090	11.8773	-11.0781	**0.98**	1.1226	-0.4428	0.85	-2.5380	-1.9199	0.95
	2				13.0366	-11.7285	**0.98**	1.1227	-0.4576	0.83	-2.7966	-2.3263	0.94
	3	0.47		0.2530	15.8051	-14.7620	**0.99**	0.9655	-0.5193	0.89	-3.3311	-3.2522	0.95
	4	0.53		0.2620	15.8051	-14.7620	**0.99**	0.9655	-0.5193	0.89	-3.3311	-3.2522	0.95
	5	0.49		0.3250	15.8051	-14.7620	**0.99**	0.9655	-0.5193	0.89	-3.3311	-3.2522	0.95
	6	0.50		0.3110	14.2427	-13.0286	**1.00**	1.0031	-0.4978	0.90	-3.0787	-2.8366	0.98
	7	0.50		0.2960	15.6668	-14.8041	**0.93**	0.9641	-0.5197	0.87	-3.3031	-3.1681	0.92
	8	0.47		0.2980	14.6522	-13.0957	**0.99**	1.0165	-0.5006	0.90	-3.1747	-2.9599	0.98
	9	0.45		0.3180	14.6733	-13.6138	**1.00**	0.9807	-0.5063	0.91	-3.1449	-2.9523	0.98
	10	0.51		0.3100	16.4305	-15.9000	**0.99**	0.8605	-0.5496	0.93	-3.4570	-3.5301	0.97
	11				10.0985	-8.8689	**1.00**	1.2139	-0.4041	0.84	-2.2013	-1.3402	0.97
	12				10.7553	-9.1783	**0.99**	1.2507	-0.4060	0.80	-2.3442	-1.5486	0.93
	13				10.0744	-8.3166	**1.00**	1.3079	-0.3871	0.78	-2.2069	-1.2967	0.93
	14				11.8640	-9.8564	**1.00**	1.2345	-0.4256	0.80	-2.6130	-1.9691	0.94
	15	0.48		0.3290	11.6311	-10.0128	**1.00**	1.1952	-0.4292	0.83	-2.5484	-1.8915	0.96
	16	0.41		0.2720	11.7063	-9.1735	**0.98**	1.3445	-0.4043	0.73	-2.5871	-1.8667	0.90
	17				8.4828	-6.8692	**0.99**	1.3902	-0.3457	0.74	-1.8265	-0.6740	0.91
	18				9.3840	-14.7239	*0.77*	0.9108	-0.4269	0.79	-1.6166	-0.6329	0.73
	19				17.4230	-14.8853	**0.99**	1.0008	-0.5291	0.86	-3.7258	-3.8707	0.94
	20				16.0364	-12.1491	**0.96**	1.2476	-0.4708	0.74	-3.5235	-3.3978	0.88
	21				13.2802	-9.8422	**0.90**	1.4522	-0.4045	0.62	-2.8987	-2.2885	0.79
	22				20.2110	-16.4994	**0.99**	0.9410	-0.5665	0.87	-4.3040	-4.8402	0.94
	23				12.9923	-10.9427	**1.00**	1.1526	-0.4564	0.85	-2.8709	-2.4080	0.97
	24				12.7550	-10.6539	**1.00**	1.1673	-0.4506	0.84	-2.8281	-2.3431	0.97
	25				12.8792	-10.6088	**1.00**	1.1910	-0.4482	0.83	-2.8555	-2.3591	0.96
	26				11.6196	-9.2094	**0.98**	1.3252	-0.4071	0.75	-2.5682	-1.8398	0.91
	27				15.8885	-13.3325	**1.00**	1.0519	-0.5064	0.86	-3.4685	-3.4261	0.96
	28	0.50		0.4030	9.6042	-8.2333	**1.00**	1.2329	-0.3946	0.84	-2.1180	-1.2050	0.97
	29	0.50		0.4080	9.0973	-7.6129	**1.00**	1.2927	-0.3752	0.81	-1.9953	-0.9833	0.96
	30	0.49		0.4020	8.9696	-7.4614	**1.00**	1.3074	-0.3702	0.80	-1.9637	-0.9275	0.95

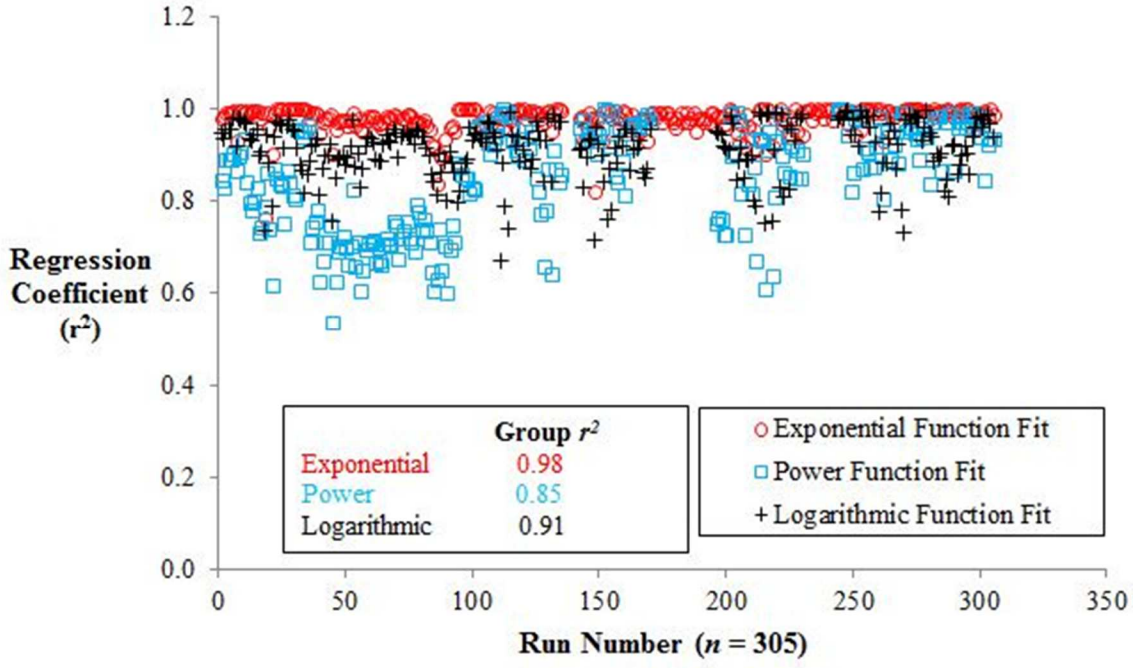

Figure 4-3. The goodness-of-fit (r^2) values for the curve fitting functions

Table 4-2 Comparison of non-linear regression analysis for all experiments.

Source	Run	u_* (m/s)	U_z (m/s)	d (mm)	Exponential Function A	Exponential Function B	Exponential Function r^2	Power Function A	Power Function B	Power Function r^2	Logarithmic Function A	Logarithmic Function B	Logarithmic Function r^2
Butterfield, 1999 (WT)	1	0.271		0.184	62.5700	-100.0000	0.9975	0.1965	-0.9426	0.9540	-13.6200	-39.4100	0.9141
	2	0.339		0.184	57.2300	-91.3700	0.9974	0.1892	-0.9523	0.9488	-11.1900	-29.7800	0.8781
	3	0.375		0.184	55.5900	-93.6400	0.9981	0.2283	-0.8861	0.9396	-10.3100	-26.6800	0.8636
	4	0.441		0.184	58.5800	-93.4200	0.9979	0.1623	-0.9818	0.9505	-9.8000	-24.1800	0.8181
	5	0.403		0.184	61.5300	-98.6100	0.9963	0.1444	-1.0190	0.9614	-11.4400	-30.5300	0.8584

Source	Run	u_* (m/s)	U_z (m/s)	d (mm)	Exponential Function A	Exponential Function B	Exponential Function r^2	Power Function A	Power Function B	Power Function r^2	Logarithmic Function A	Logarithmic Function B	Logarithmic Function r^2
Dong et al., 2002 (WT)	1		16	0.9	3.8310	-3.1960	0.9777			0.7101			0.8866
	2		18	0.9	3.8970	-3.275	0.9915			0.7433			0.9163
	3		20	0.9	3.875	-3.261	0.9931			0.7547			0.9236
	4		22	0.9	3.859	-3.249	0.9871			0.7799			0.9328
	5		14	0.715	3.745	-3.059	0.9452			0.6245			0.813
	6		16	0.715	4.112	-3.516	0.9688			0.6723			0.8688
	7		18	0.715	4.182	-3.626	0.9794			0.71			0.8988
	8		20	0.715	4.211	-3.616	0.9791			0.7096			0.8997
	9		22	0.715	4.198	-3.68	0.9856			0.7485			0.9228
	10		12	0.595	4.48	-3.791	0.9022			0.5368			0.7556
	11		14	0.595	4.563	-3.931	0.9533			0.6273			0.8491
	12		16	0.595	4.489	-3.844	0.9712			0.6923			0.889
	13		18	0.595	4.212	-3.64	0.9764			0.7035			0.8952
	14		20	0.595	4.175	-3.476	0.9769			0.7218			0.8989
	15		22	0.595	3.722	-3.074	0.9758			0.6984			0.8758
	16		12	0.53	5.769	-5.093	0.9633			0.6631			0.8919
	17		14	0.53	5.421	-4.83	0.9763			0.7014			0.9189
	18		16	0.53	5.695	-4.65	0.993			0.8244			0.973
	19		18	0.53	4.662	-4.143	0.9631			0.6584			0.873
	20		20	0.53	4.439	-3.92	0.9774			0.71			0.9029
	21		22	0.53	4.349	-3.583	0.9542			0.6071			0.8272
	22		10	0.45	7.681	-6.677	0.951			0.6516			0.8699
	23		12	0.45	6.659	-5.999	0.9738			0.6944			0.9195
	24		14	0.45	6.252	-5.749	0.9846			0.707			0.9385
	25		16	0.45	5.914	-5.454	0.9843			0.7119			0.9352
	26		18	0.45	5.312	-4.883	0.9827			0.7131			0.9259
	27		20	0.45	5.389	-4.435	0.9703			0.6678			0.8891
	28		22	0.45	4.811	-4.311	0.9677			0.6715			0.887
	29		10	0.325	8.468	-7.378	0.9591			0.6634			0.8866

Table 4-2 continued.

Source	Run	u_* (m/s)	U_z (m/s)	d (mm)	Exponential Function A	Exponential Function B	Exponential Function r^2	Power Function A	Power Function B	Power Function r^2	Logarithmic Function A	Logarithmic Function B	Logarithmic Function r^2
Dong et al., 2002 (WT)	30		12	0.325	7.361	-6.572	0.9715			0.705			0.9235
	31		14	0.325	6.91	-6.345	0.982			0.7205			0.9417
	32		16	0.325	6.521	-5.999	0.9774			0.7072			0.9306
	33		18	0.325	6.359	-5.877	0.9772			0.7037			0.9277
	34		20	0.325	6.27	-5.834	0.9877			0.7545			0.9534
	35		22	0.325	5.881	-5.308	0.9849			0.749			0.9459
	36		10	0.225	10.64	-9.247	0.9555			0.6738			0.8935
	37		12	0.225	8.877	-7.965	0.9781			0.7173			0.938
	38		14	0.225	8.544	-7.828	0.9796			0.7359			0.9454
	39		16	0.225	8.494	-7.883	0.9852			0.7546			0.9481
	40		18	0.225	7.59	-7.024	0.9858			0.7186			0.9432
	41		20	0.225	7.579	-7.027	0.9821			0.7092			0.9369
	42		22	0.225	7.238	-6.601	0.9727			0.6904			0.9231
	43		8	0.175	22.82	-18.76	0.9723			0.7906			0.955
	44		10	0.175	17.44	-14.63	0.9727			0.7739			0.9522
	45		12	0.175	14.61	-12.47	0.9687			0.7376			0.938
	46		14	0.175	14.38	-12.52	0.9753			0.7612			0.9381
	47		16	0.175	13.91	-11.87	0.9612			0.7338			0.9139
	48		18	0.175	13.42	-11.21	0.9562			0.7091			0.8997
	49		20	0.175	11.59	-10.24	0.9233			0.6445			0.856
	50		22	0.175	11.12	-9.709	0.919			0.6039			0.8408
	51		8	0.125	30.52	-23.5	0.8353			0.6277			0.8126
	52		10	0.125	32.51	-21.16	0.9008			0.7408			0.9011
	53		12	0.125	19.88	-16.34	0.8924			0.6518			0.8615
	54		14	0.125	21.03	-17.75	0.9335			0.7033			0.8839
	55		16	0.125	19.53	-14.64	0.8754			0.6016			0.8002
	56		18	0.125	13.24	-11.89	0.9602			0.6963			0.9052
	57		20	0.125	17.15	-15.46	0.9635			0.7462			0.8825
	58		22	0.125	15.43	-13.98	0.9511			0.7093			0.8603

Source	Run	u_* (m/s)	U_z (m/s)	d (mm)	Exponential Function A	Exponential Function B	Exponential Function r^2	Power Function A	Power Function B	Power Function r^2	Logarithmic Function A	Logarithmic Function B	Logarithmic Function r^2
Feng et al., 2009 (WT)	1	0.56		0.35	20.36	-19.43	0.9677	0.4688	-0.826	0.9529	-4.97	-7.093	0.9475
	2	0.81		0.35	20.48	-20.21	0.9625	0.446	-0.834	0.9608	-4.873	-6.981	0.9351
	3	0.93		0.35	19.66	-19.7	0.9543	0.4602	-0.817	0.9645	-4.708	-6.659	0.9344
	4	1.12		0.35	18.85	-18.95	0.9343	0.4629	-0.812	0.9701	-4.566	-6.348	0.9262
	5	1.24		0.35	16.96	-16.32	0.9752	0.5722	-0.745	0.9267	-4.428	-6.054	0.9693
	6	0.56		0.35	18.7000	-17.6200	0.9941	0.5471	-0.7683	0.8999	-4.8090	-6.8690	0.9671
	7	0.81		0.35	21.0300	-20.1800	0.9891	0.4854	-0.8111	0.9239	-5.0400	-7.3460	0.9457
	8	0.93		0.35	20.9900	-20.5500	0.9846	0.4715	-0.8163	0.9371	-4.9540	-7.1810	0.9396
	9	1.12		0.35	22.6300	-22.7900	0.9541	0.3956	-0.8690	0.9705	-5.0550	-7.3950	0.9098

Table 4-2 continued.

Source	Run	u_* (m/s)	U_z (m/s)	d (mm)	Exponential Function A	Exponential Function B	Exponential Function r^2	Power Function A	Power Function B	Power Function r^2	Logarithmic Function A	Logarithmic Function B	Logarithmic Function r^2
Gerety & Slingerland, 1983 (WT)	1	0.2		0.18	460.5000	-411.9000	0.9800	0.0001	-2.4900	0.9890	-28.5700	-97.1700	0.6700
	2	0.4		0.18	93.6400	-129.6000	0.9580	0.1548	-1.0750	0.9990	-20.6300	-64.7900	0.8800
	3	0.52		0.18	224.4000	-248.2000	0.9800	0.0064	-1.7350	0.9900	-26.5700	-88.4300	0.7900
	4	1.1		0.18	313.3000	-149.6000	0.9800	0.0030	-2.1610	0.9900	-32.2000	-93.8800	0.7390

Source	Run	u_* (m/s)	U_z (m/s)	d (mm)	Exponential Function A	Exponential Function B	Exponential Function r^2	Power Function A	Power Function B	Power Function r^2	Logarithmic Function A	Logarithmic Function B	Logarithmic Function r^2
Greeley et al., 1996 (F)	1	0.312		0.23	35.7900	-16.4300	0.9743	1.5530	-0.6888	0.9563	-10.6300	-16.7700	0.9925
	2	0.317		0.23	42.0500	-20.0300	0.9961	0.7585	-0.8783	0.9293	-9.8940	-14.0300	0.9432
	3	0.42		0.23	37.7300	-18.1100	0.9939	0.7072	-0.8857	0.9118	-8.4190	-10.5500	0.9194
	4	0.348		0.23	38.2300	-17.1300	0.9983	0.8276	-0.8587	0.8970	-8.8490	-10.8800	0.9363
	5	0.47		0.23	44.5800	-21.2600	0.9967	0.6457	-0.9268	0.9337	-8.9850	-11.3900	0.8868
	6			0.23	46.6900	-17.7900	0.9989	0.8801	-0.8399	0.8895	-10.0900	-12.6500	0.9113
	7	0.51		0.23	55.1000	-25.4100	0.9778	0.5853	-0.9823	0.9619	-10.4800	-13.2000	0.8867
	8	0.41		0.23	38.8700	-19.6400	0.9942	0.8295	-0.8083	0.9148	-8.6990	-11.5600	0.9323
	9	0.49		0.23	47.6400	-24.9600	0.9855	0.6058	-0.9090	0.9501	-8.9580	-11.6400	0.8695
	10	0.54		0.23	43.3800	-22.1000	0.9939	0.6595	-0.8926	0.9375	-8.6070	-10.8200	0.8887

Source	Run	u_* (m/s)	U_z (m/s)	d (mm)	Exponential Function A	Exponential Function B	Exponential Function r^2	Power Function A	Power Function B	Power Function r^2	Logarithmic Function A	Logarithmic Function B	Logarithmic Function r^2
Guadalupe, 1996 (F)	1			0.39	12.26	-12.78	0.99	1.227	-0.435	0.848	-2.5924	-3.093	0.97
	2			0.39	14.24	-14.09	0.99	1.383	-0.434	0.819	-3.476	-4.366	0.95
	3			0.39	13.07	-12.85	0.98	1.322	-0.428	0.77	-3.093	-3.419	0.93
	4			0.39	9.085	-8.431	0.97	1.6554	-0.322	0.66	-2.027	-1.147	0.84
	5			0.39	10.6	-10.96	0.99	1.229	-0.408	0.78	-2.42	-2.074	0.93
	6			0.39	12.49	-13.82	0.997	1.031	-0.471	0.87	-2.814	-2.899	0.979
	7			0.39	9.761	-9.269	0.95	1.326	-0.375	0.64	-2.182	-1.481	0.84
	8			0.39	21.38	-17.02	0.99	1.361	-0.515	0.91	-4.949	-6.355	0.989
	9			0.39	17.13	-15.22	0.999	1.323	-0.479	0.87	-4.006	-4.866	0.97
	10			0.39	14.61	-14.71	0.999	1.163	-0.473	0.84	-3.475	-4.276	0.969
	11			0.39	17.42	-19.15	0.995	1.9511	-0.536	0.858	-4.341	-4.341	0.97

Table 4-2 continued.

Source	Run	u_* (m/s)	U_z (m/s)	d (mm)	Exponential Function A	Exponential Function B	Exponential Function r^2	Power Function A	Power Function B	Power Function r^2	Logarithmic Function A	Logarithmic Function B	Logarithmic Function r^2
Hotta & Horikawa, 1993 (WT)	1	0.3		0.3	26.6400	-40.7900	0.9776	0.3388	-0.8100	0.9595	-5.5310	-10.1500	0.9117
	2	0.47		0.3	20.9200	-31.1800	0.9817	0.4452	-0.7048	0.9305	-4.2280	-4.2280	0.9144
	3	0.76		0.3	22.9900	-33.4000	0.9300	0.3177	-0.8041	0.9764	-3.8870	-5.3940	0.8296
	4	1		0.3	19.5600	-23.9400	0.9606	0.5024	-0.7177	0.9349	-3.8900	-5.0210	0.8930
	5	0.4		0.3	25.7600	-22.9900	0.9923	0.3137	-0.9856	0.9415	-6.1950	-9.9050	0.9305
	6	0.52		0.3	21.0000	-23.4500	0.9792	0.4228	-0.8157	0.9294	-4.9310	-7.6150	0.9323
	7	0.83		0.3	33.3100	-78.1300	0.8225	0.1696	-0.9286	0.9471	-4.0400	-5.7230	0.7130
	8	0.44		0.3	19.5700	-27.7600	0.9843	0.5758	-0.6479	0.9003	-4.5490	-7.7160	0.9578
	9	0.66		0.3	16.1900	-22.1000	0.9805	0.4595	-0.7037	0.9405	-3.4330	-4.4490	0.9238
	10	0.94		0.3	17.4500	-27.9200	0.9309	0.4613	-0.6625	0.9589	-3.3980	-4.5250	0.8976

Source	Run	u_* (m/s)	U_z (m/s)	d (mm)	Exponential Function A	Exponential Function B	Exponential Function r^2	Power Function A	Power Function B	Power Function r^2	Logarithmic Function A	Logarithmic Function B	Logarithmic Function r^2
Hotta et al., 2006 (WT)	1	0.63		0.15	98.2000	-67.0900	0.9971	0.1706	-0.7735	0.9986	-12.4400	-36.7900	0.8406
	2	1.01		0.15	120.3000	-77.6000	0.9976	0.1159	-1.2870	0.9951	-17.2600	-34.8000	0.7601
	3	1.74		0.15	56.7000	-20.5900	0.9855	0.4780	-1.1710	0.9186	-12.2300	-17.5200	0.8684
	4	0.61		0.25	117.5000	-130.6000	0.9797	0.1190	-1.1490	0.9942	-15.6600	-33.7200	0.7795
	5	1.15		0.25	39.5500	-22.6700	0.9933	1.0780	-0.7098	0.8519	-9.0360	-13.6900	0.9131
	6	1.77		0.25	31.2400	-16.3800	0.9831	1.0680	-0.7274	0.8403	-6.8300	-7.5820	0.8798
	7	0.87		0.28	49.3800	-45.7100	0.9786	0.7366	-0.7401	0.9591	-11.0300	-22.6100	0.9368
	8	1.48		0.28	33.7600	-22.4100	0.9968	1.2970	-0.6192	0.8874	-7.0240	-8.9860	0.9186
	9	2.16		0.28	24.0500	-12.9100	0.9911	2.0160	-0.4820	0.8114	-5.6350	-5.7090	0.9526
	10	0.4		0.48	34.2700	-22.6300	0.9538	1.1410	-0.6512	0.9450	-8.0270	-12.1200	0.9560
	11	1.21		0.48	35.6800	-22.8300	0.9621	0.7495	-0.8010	0.9685	-6.7720	-7.7320	0.8655
	12	1.93		0.48	25.2400	-13.6500	0.9857	1.2600	-0.6427	0.9183	-5.7620	-5.6180	0.9474
	13	0.84		0.68	28.4600	-18.3400	0.9716	0.9715	-0.7027	0.9635	-5.8470	-6.1340	0.9107
	14	1.67		0.68	28.8400	-18.4800	0.9535	1.1720	-0.6394	0.9587	-5.7400	-5.7990	0.9146
	15	2.33		0.68	24.9100	-14.4300	0.9500	1.1860	-0.6647	0.9625	-5.5600	-5.3290	0.9310

Source	Run	u_* (m/s)	U_z (m/s)	d (mm)	Exponential Function A	Exponential Function B	Exponential Function r^2	Power Function A	Power Function B	Power Function r^2	Logarithmic Function A	Logarithmic Function B	Logarithmic Function r^2
Kawamura, 1951 (WT)	1	0.488		0.25	0.9315	-278.4000	0.98	0.0051	-0.7120	0.9780	-0.1544	-0.4750	0.8600
	2	0.7321		0.25	2.4290	-269.2000	0.98	0.0196	-0.6612	0.9700	-0.3512	-0.9636	0.8500
Kawamura, 1951 (F)	1		10.5	0.31	0.1859	-174.4000	0.93	0.0020	-0.6445	0.9890	-0.0270	-0.0550	0.8700
	2		12.6	0.31	0.0660	-18.5000	0.99	0.0006	-1.1660	0.9700	-0.0169	-0.0240	0.9530

Table 4-2 continued.

Source	Run	u_* (m/s)	U_z (m/s)	d (mm)	Exponential Function A	Exponential Function B	Exponential Function r^2	Power Function A	Power Function B	Power Function r^2	Logarithmic Function A	Logarithmic Function B	Logarithmic Function r^2
Liu & Dong, 2004 (WT)	1		10	0.15		-19.259288	0.99						
	2		12	0.15		-13.174883	0.98						
	3		14	0.15		-12.538399	0.99						
	4		16	0.15		-12.663678	0.99						
	5		18	0.15		-12.336389	0.97						
	6		10	0.25		-8.5073078	0.99						
	7		12	0.25		-8.4160207	0.99						
	8		14	0.25		-8.9313625	0.98						
	9		16	0.25		-7.8065231	0.97						
	10		18	0.25		-6.9025022	0.96						
	11		10	0.35		-7.5574936	0.98						
	12		12	0.35		-6.5058846	0.99						
	13		14	0.35		-6.7767665	0.97						
	14		16	0.35		-5.9511411	0.99						
	15		18	0.35		-5.3502258	0.97						
	16		10	0.45		-6.9203673	0.98						
	17		12	0.45		-5.438566	0.99						
	18		14	0.45		-5.3503403	0.95						
	19		16	0.45		-4.9366382	0.98						
	20		18	0.45		-4.5807891	0.98						
	21		10	0.55		-4.6319027	0.97						
	22		12	0.55		-4.743068	0.98						
	23		14	0.55		-4.3406169	0.97						
	24		16	0.55		-4.2839028	0.99						
	25		18	0.55		-4.1089361	0.99						

Source	Run	u_* (m/s)	U_z (m/s)	d (mm)	Exponential Function A	Exponential Function B	Exponential Function r^2	Power Function A	Power Function B	Power Function r^2	Logarithmic Function A	Logarithmic Function B	Logarithmic Function r^2
Liu et al., 2006 (WT)	1	0.48		0.45	6.603	-5.923	0.9826	0.7145	-0.567	0.7501	-1.93	-1.108	0.9509
	2	0.54		0.45	6.245	-5.549	0.9818	0.7521	-0.55	0.7632	-1.825	-0.9214	0.9475
	3	0.64		0.45	5.618	-5.012	0.9819	0.7342	-0.503	0.7602	-1.641	-0.66	0.944
	4	0.7		0.45	5.273	-4.613	0.9671	0.7735	-0.515	0.7285	-1.537	-0.4917	0.9183
	5	0.75		0.45	5.438	-4.46	0.9661	0.8017	-0.52	0.7268	-1.593	-0.4673	0.9154

Table 4-2 continued.

Source	Run	u_* (m/s)	U_z (m/s)	d (mm)	Exponential Function A	Exponential Function B	Exponential Function r^2	Power Function A	Power Function B	Power Function r^2	Logarithmic Function A	Logarithmic Function B	Logarithmic Function r^2
Mikkelsen, 1989 (WT)	1				74.06	-47.39	0.999	0.036	-1.721	0.988	-15.22	-35.34	0.91
Mikkelsen, 1989 (F)	1				18.2	-18.49	0.9955	0.5364	-0.795	0.898	-5.722	-10.02	0.985

Source	Run	u_* (m/s)	U_z (m/s)	d (mm)	Exponential Function A	Exponential Function B	Exponential Function r^2	Power Function A	Power Function B	Power Function r^2	Logarithmic Function A	Logarithmic Function B	Logarithmic Function r^2
Namikas, 2003 (F)	1	0.32		0.25	33.6200	-31.5600	0.9829	1.2360	-0.5979	0.9065	-8.3150	-16.1000	0.9657
	2	0.32		0.25	52.4300	-61.7300	0.9460	0.4894	-0.8148	0.9907	-9.0450	-17.5900	0.8449
	3	0.27		0.25	38.7000	-41.7300	0.9255	0.7555	-0.7029	0.9764	-7.4610	-12.8400	0.8870
	4	0.3		0.25	29.3900	-25.5200	0.9667	1.3200	-0.5665	0.8182	-6.8170	-11.1100	0.9146
	5	0.63		0.25	29.8000	-25.3400	0.9172	1.4240	-0.5473	0.7263	-6.9100	-11.3700	0.8475
	6	0.37		0.25	40.2600	-40.6300	0.9884	0.7555	-0.7224	0.9331	-7.8840	-13.9000	0.8904
	7	0.38		0.25	33.4900	-30.5200	0.9624	1.0760	-0.6282	0.8383	-7.3800	-12.5600	0.8910
	8	0.38		0.25	30.0500	-26.0800	0.9391	1.2460	-0.5819	0.8181	-6.9670	-11.4900	0.8962
	9	0.47		0.25	49.9800	-52.7000	0.9540	0.6602	-0.7515	0.8751	-8.7100	-16.1900	0.7996

Source	Run	u_* (m/s)	U_z (m/s)	d (mm)	Exponential Function A	Exponential Function B	Exponential Function r^2	Power Function A	Power Function B	Power Function r^2	Logarithmic Function A	Logarithmic Function B	Logarithmic Function r^2
Namikas et al., 2009 (F)		0.42		0.55	53.8400	-22.8	0.9100	-0.3560	0.6700	0.6700	-12.8100	-21.0700	0.7880
		0.42		0.28	81.8200	-43.09	1.0000	-0.6660	0.9350	0.9350	-21.8900	-53.6000	0.9900
		0.42		0.11	87.8800	-45.22	0.9980	-0.7080	0.9300	0.9300	-23.8900	-59.7700	0.9850
		0.46		0.55	46.0400	-19.8	0.9000	-0.3450	0.6100	0.6100	-10.8100	-16.2300	0.7500
		0.46		0.28	63.4300	-32.03	0.9990	-0.5760	0.9100	0.9100	-17.4200	-38.4700	0.9890
		0.46		0.11	70.8400	-38.33	0.9970	-0.6320	0.9500	0.9500	-19.0300	-44.3600	0.9930
		0.52		0.55	37.8100	-15.92	0.9200	-0.2920	0.6380	0.6380	-8.0510	-7.9050	0.7540
		0.52		0.28	45.0500	-21.26	0.9800	-0.4069	0.8100	0.8100	-11.2600	-18.7200	0.9100
		0.52		0.11	55.4400	-29.7	0.9900	-0.5280	0.9300	0.9300	-14.7000	-30.6500	0.9900

Table 4-2 continued.

Source	Run	u_*	U_z	d	Exponential Function			Power Function			Logarithmic Function		
		(m/s)	(m/s)	(mm)	A	B	r^2	A	B	r^2	A	B	r^2
Ni et al., 2002 (WT)	1	0.61		0.17	115.2000	-111.8000	0.9992	0.0602	-1.3260	0.9880	-20.3400	-56.3000	0.8296
	2	0.47		0.35	14.3500	-15.9200	0.9655	0.8045	-0.5713	0.8962	-3.5970	-4.7310	0.9864
	3	0.86		0.17	55.0600	-53.9400	0.9749	0.3350	-0.9459	0.8618	-10.0400	-20.7900	0.8069
	4	0.77		0.35	16.3900	-18.0500	0.9401	0.7234	-0.6203	0.9370	-3.9310	-5.2810	0.9623
	5	1.184		0.17	38.3600	-39.3700	0.9845	0.4358	-0.8190	0.8521	-6.7750	-11.4600	0.8233
	6	1.11		0.35	15.0000	-18.1700	0.9392	0.7086	-0.6107	0.9195	-3.5950	-4.7860	0.9560
	7	1.64		0.17	25.5500	-26.3100	0.9986	0.6179	-0.6971	0.8486	-5.5740	-8.9150	0.9289
	8	1.53		0.35	13.9000	-14.8600	0.9501	0.8625	-0.5560	0.9116	-3.4700	-4.2910	0.9798
	9	2.36		0.17	17.3800	-17.8500	0.9902	0.7947	-0.5988	0.8482	-4.3040	-6.1150	0.9776
	10	2.31		0.35	11.7100	-11.9700	0.9433	0.9950	-0.5014	0.9009	-3.0200	-3.3060	0.9886

Source	Run	u_*	U_z	d	Exponential Function			Power Function			Logarithmic Function		
		(m/s)	(m/s)	(mm)	A	B	r^2	A	B	r^2	A	B	r^2
Portugal, 2006 (F)	1	0.49		0.31	22.771	-22	0.996						
	2	0.49		0.31	24.782	-24	0.994						
	3	0.41		0.31	19.006	-17	0.999						
	4	0.41		0.3	19.09	-13	0.974						
	5			0.32	23.106	-24	0.993						
	6			0.32	21.702	-18	0.999						
	7			0.35	17.478	-16	0.995						
	8	0.41		0.35	15.19	-12	0.98						
	9	0.35		0.34	17.402	-16	0.999						
	10	0.38		0.33	16.828	-14	0.995						
	11	0.39		0.33	16.098	-14	0.999						
	12			0.31	13.517	-10	0.975						
	13	0.38		0.27	15.653	-12	0.995						

Table 4-2 continued.

Source	Run	u_* (m/s)	U_z (m/s)	d (mm)	Exponential Function A	Exponential Function B	Exponential Function r^2	Power Function A	Power Function B	Power Function r^2	Logarithmic Function A	Logarithmic Function B	Logarithmic Function r^2
Rasmussen &	1	0.27		0.22	130.2000	-53.7600	1.0000	0.2892	-1.1870	0.9950	-36.7400	-95.3300	0.9731
Mikkelsen, 1988 (WT)	2	0.27		0.22	116.6000	-67.0400	0.9999	0.1928	-1.1060	0.9990	-31.8000	-88.0300	0.9846
	3	0.27		0.22	172.0000	-51.2400	0.9994	0.1478	-1.5240	0.9962	-49.9100	-133.6000	0.9785
	4	0.27		0.22	217.4000	-50.6300	0.9999	0.0784	-1.8180	0.9957	-60.4700	-164.0000	0.9911
Rasmussen &	1	0.27		0.2	46.7400	-78.1000	0.9686	1.4570	-0.4782	0.9426	-9.8140	-25.9500	0.9932
Mikkelsen, 1998 (WT)	2	0.49		0.2	45.8500	-95.2600	0.9937	2.0150	-0.4200	0.8223	-9.8390	-28.0500	0.9418
	3	0.63		0.2	40.6600	-75.9900	0.9894	1.7690	-0.4043	0.8623	-8.1650	-21.8500	0.9744
Rasmussen &	1	0.1761		0.32	78.4100	-179.2000	0.9440	0.2604	-0.8379	0.9795	-18.2000	-63.5000	0.9415
Sorensen, 1999 (F)	2	0.1782		0.32	91.4300	-213.9000	0.9940	0.1421	-0.9479	0.9885	-20.0100	-71.1300	0.9169
	3	0.1977		0.32	40.6400	-66.9300	0.9544	1.6200	-0.4950	0.9729	-10.4100	-28.9800	0.9959
Rasmussen et al., 1985 (F)	1	*0.63*		0.3	47.0300	-30.4300	0.9980	1.3390	-0.6216	0.8699	-11.9300	-24.4100	0.9782
	2	*0.63*		0.3	51.3600	-34.0400	0.9996	1.0400	-0.6952	0.9155	-12.9400	-27.1300	0.9827
	3	*0.26*			33.1300	-21.7000	0.9954	3.2180	-0.4124	0.9040	-8.2290	-13.6200	0.9815
	4	*0.36*			30.3600	-18.8600	0.9982	3.8540	-0.3656	0.8715	-7.1850	-10.0800	0.9579
Sorensen, 1985 (WT)	1	0.46		0.1175	38.0000	-41.1100	0.9894	0.7060	-0.7121	0.8741	-10.6200	-25.6800	0.9820
	2	0.46		0.2345	59.7600	-66.7700	0.9977	0.3200	-0.9099	0.9198	-14.0700	-36.8300	0.9267

Source	Run	u_* (m/s)	U_z (m/s)	d (mm)	Exponential Function A	Exponential Function B	Exponential Function r^2	Power Function A	Power Function B	Power Function r^2	Logarithmic Function A	Logarithmic Function B	Logarithmic Function r^2
Weinan et al., 1996 (WT)	1		6	0.11	188.7	-52.24	0.999	0.0666	-1.86	0.98	-25.28	-50.65	0.777
	2		8	0.11	149.7	-43.32	0.99	0.0977	-1.663	0.955	-24.78	-49.1	0.8178
	3		10	0.11	70.47	-25.04	0.93	0.4952	-1.148	0.8063	-19.26	-36.26	0.88
	4		12	0.11	105	-35.19	0.996	0.1965	-1.43	0.952	-21.7	-42.07	0.88
	5		15	0.11	78.45	-28.52	0.997	0.334	-1.259	0.939	-19.18	-36.15	0.9337
	6		19	0.11	58.18	-22.07	0.987	0.62	-1.059	0.889	-16.75	-30.22	0.965
Weinan et al., 1996 (F)	7		11	0.09	46.73	-18.93	0.984	0.8657	-0.938	0.924	-13.45	-22.17	0.95
	8		8.7	0.09	91.8	-33.37	0.99	0.247	-1.351	0.97	-18.89	-35.25	0.87
	9		9.5	0.09	62.43	-23.43	0.97	0.587	-1.083	0.88	-17.01	-30.66	0.924
	10		6.4	0.09	164.7	-49.77	0.997	0.068	-1.738	0.99	-22.94	-44.83	0.78
	11		6.1	0.09	232.3	-63.11	0.995	0.023	-2.034	0.99	-23.67	-46.94	0.73

Table 4-2 continued.

Source	Run	u_* (m/s)	U_z (m/s)	d (mm)	Exponential Function A	Exponential Function B	Exponential Function r^2	Power Function A	Power Function B	Power Function r^2	Logarithmic Function A	Logarithmic Function B	Logarithmic Function r^2
Williams, 1964 (WT)	1	0.51		0.4	73.2700	-37.9300	0.9999	1.3850	-0.7206	0.9489	-18.5800	-39.6800	0.9755
	2	0.53		0.4	56.2300	-33.8000	0.9984	1.4560	-0.6626	0.9488	-14.3600	-29.4700	0.9866
	3	0.72		0.4	77.0900	-41.5500	0.9998	1.1990	-0.7504	0.9580	-19.1000	-41.4800	0.9677
	4	0.78		0.4	68.4500	-34.2200	0.9994	1.6370	-0.6841	0.9461	-17.6000	-36.3600	0.9822
	5	1.13		0.4	69.7500	-34.2100	0.9996	1.5610	-0.7030	0.9334	-18.2200	-38.0800	0.9776
	6	1.2		0.4	59.2900	-26.1900	0.9974	2.4030	-0.5982	0.8906	-16.0100	-31.0000	0.9801

Source	Run	u_* (m/s)	U_z (m/s)	d (mm)	Exponential Function A	Exponential Function B	Exponential Function r^2	Power Function A	Power Function B	Power Function r^2	Logarithmic Function A	Logarithmic Function B	Logarithmic Function r^2
Zou et al., 2001 (WT)	1	0.63		0.25	32.5100	-15.2200	0.9949	1.8780	-0.6039	0.8434	-9.5910	-14.6700	0.9752
	2	0.64		0.25	36.0800	-17.7300	0.9824	1.5020	-0.6693	0.9211	-10.2700	-16.4800	0.9851
	3	0.74		0.25	53.3400	-26.5300	0.9992	0.8357	-0.8584	0.9324	-14.0900	-26.2300	0.9665
	4	0.81		0.25	48.7900	-25.7100	0.9861	1.0010	-0.7910	0.9333	-12.4200	-22.0600	0.9393

Source	Run	u_* (m/s)	U_z (m/s)	d (mm)	Exponential Function A	Exponential Function B	Exponential Function r^2	Power Function A	Power Function B	Power Function r^2	Logarithmic Function A	Logarithmic Function B	Logarithmic Function r^2
Hasi, 1997 (F)	1				16.43	-5.346	0.305	6.717	-0.152	0.08	-2.434	3.715	0.125
	2				20.95	-8.385	0.69	4.362	-0.312	0.38	-4.985	2.859	0.518
	3				18.54	-6.716	0.48	5.648	-0.217	0.17	-3.626	0.6319	0.26
	4				20.24	-8.009	0.88	4.147	-0.328	0.577	-4.882	-2.621	0.72
	5				22.23	-9.484	0.99	3.2	-0.417	0.83	-5.863	-5.144	0.94
	6				17.28	-5.99	0.61	5.626	-0.217	0.27	-3.257	1.578	0.37
Wu & Ling, 1965 (F)	1				79.24	-56.72	0.995	0.1479	-1.248	0.939	-19.5	-50.23	0.93
	2				54.59	-43.77	0.994	0.2965	-1.049	0.96	-15.02	-36.49	0.96
	3				26.42	-20.78	0.994	1.302	-0.63	0.9382	-8.223	-15.4	0.995
Znamensky, 1960 (F)	1				42.4	-36.81	0.953	0.4533	-0.917	0.99	-11.9	-27.02	0.94
	2				43.55	-37.37	0.97	0.4558	-0.916	0.982	-12.31	-28.3	0.958
	3				42.15	-35.63	0.99	0.5198	-0.884	0.96	-12.33	-28.37	0.979
	4				40.69	-34.32	0.99	0.5699	-0.859	0.94	-12.15	-27.86	0.985
	5				47.22	-40.33	0.985	0.398	-0.955	0.978	-13.07	-30.69	0.958

The results provide a strong evidence that curve fits to vertical flux data using the exponential function perform much better than either the power or logarithmic functions for a wide range of environmental conditions and different experimental methods and designs.

4.2.2. Best fit function: field *vs.* wind tunnel experiments

A difference in means test (*t*-test) was used to assess the statistical similarity of the populations (field and wind tunnel studies) using the exponential decay coefficient calculated from non-linear regression analyses of each normalized vertical flux profile. The data were first separated into two categories: (1) all field studies (98 profiles), and (2) all wind tunnel studies (207 profiles) (Table 3-2). A statistical difference of means *t*-test was done for these two datasets. The wind tunnel data were subsequently separated into two further groups: (3) large wind tunnel studies and, (4) small wind tunnel studies. The *large-small* boundary was delineated using the cross section area of the working section of the wind tunnel. Wind tunnels with cross sections less than 0.25 m^2 were designated as *small*. Selecting a critical cutoff for the cross section area was not difficult upon reviewing of the different tunnel dimensions. None of the tunnels designated as *small* had working sections over 0.60 m high. The one exception is Kawamura (1951) where the tunnel height is 0.80 m but the tunnel width was, reportedly, only 0.05 m. The dimensions of the wind tunnels used in the reported experiments are listed in Table 4-3. There were nine wind tunnels categorized as *small* wind tunnels and nine categorized as *large*.

A total of four different *t*-tests were designed:

Test 1. All field (n = 98) *vs.* all wind tunnel studies (n = 201)

Test 2. All field (n = 98) *vs.* large wind tunnel studies (n = 150)

Test 3. All field (n = 98) *vs.* small wind tunnel studies (n = 45)

Test 4. Large wind tunnel (n = 150) *vs.* small wind tunnel studies (n = 45)

Prior to the statistical tests, the six profiles of Hasi (1997) were removed in the analysis because of the very low r^2 values for the exponential curve fits (average r^2 = 0.66). The

six laboratory-based, wind tunnel profiles of Znamensky (1960) were not included in Tests 2, 3 and 4 because the wind tunnel dimensions of their study were not available. This reduced the wind tunnel profiles from 201 to 195 for these tests.

Table 4-3. Wind tunnel dimensions for experiments measuring vertical mass flux profiles. Categories are designated *large* or *small* based on a critical cross section area of 0.25 m^2.

Source	Wind tunnel dimensions				Category
	length (m)	Width (m)	Height (m)	Cross section (m^2)	
Butterfield 1999	8.20	0.30	0.30	0.09	Small
Dong et al. (2002)	21.00	1.20	1.20	1.44	Large
Feng et al. (2009)	21.00	1.20	1.20	1.44	Large
Gerety & Slingerland (1983)	10.00	1.10	0.20	0.22	Small
Hotta & Horikawa (1993)	20.00	1.00	1.10	1.10	Large
Hotta et al. (2006)	20.00	1.00	1.10	1.10	Large
Kawamura (1951)	1.50	0.05	0.80	0.04	Small
Liu & Dong (2004)	16.23	1.00	0.80	0.80	Large
Liu et al. (2006)	21.00	1.20	1.20	1.44	Large
Mikkelsen (1989)	15.00	0.35	0.50	0.18	Small
Ni et al., (2002)	21.00	1.20	1.20	1.44	Large
Rasmussen & Mikkelsen (1988)	15.00	0.35	0.50	0.18	Small
Rasmussen & Mikkelsen (1998)	15.00	0.35	0.50	0.18	Small
Sorensen (1985)	15.00	0.35	0.50	0.18	Small
Weinan et al. (1996)	1.60	0.60	1.00	0.60	Large
Williams (1964)	9.14	0.35	0.35	0.13	Small
Xing (2007)	8.00	0.40	0.60	0.24	Small
Znamensky (1960)	unknown	unknown	unknown	unknown	-
Zou et al. (2001)	16.20	1.00	0.60	0.60	Large

An *F*-test was used to determine if variances of the decay coefficients in each category were equal. This was done in order to determine which *t*-test is appropriate. Two populations were designated as having unequal variances if the *P* value in the *F*-test was less than 0.05. The results from each *F*-test are listed in Table 4-4. The results from the *F*-tests are that each group of decay coefficients has unequal variances to all the other groups. This supports using the 'two sample *t*-test assuming unequal variances' to compare the different groups. The results of the four difference-in-means *t*-tests are shown in Table 4-4. For the two grouped categories, '*all field*' and '*all wind tunnels*', the

t-test found that the two populations are ***not*** statistically different, $P > 0.05$. Conversely, the field-based population is statistically different to both, the large and small, wind tunnel populations for $P < 0.05$ and $P < 0.01$ (not shown). There is less than a 1% chance that the decay coefficients, which define how rapidly the mass flux decays away from the bed, obtained in the field and the wind tunnels are derived from the same population. Interestingly, the *large* and *small* wind tunnel data are also statistically different at the 95% and 99% significance levels.

In summary, from the two sample *t*-test, assuming unequal variances, analyses:

- All field *vs.* all wind tunnel studies: *statistically the same (P>0.05)*
- All field *vs.* large wind tunnel studies: *statistically different (P<0.05)*
- All field *vs.* small wind tunnel studies: *statistically different (P<0.05)*
- Large wind tunnel *vs.* small wind tunnel studies: *statistically different (P<0.05)*

The extent to which these relationships (or lack thereof) are controlled by environmental conditions and/or experimental methods and design is investigated in the next section.

Table 4-4. Results of the *F*-tests and *t*-tests.

Test 1: All field studies *vs.* All wind tunnel studies

FIELD vs WIND TUNNEL (ALL)

F-Test Two-Sample for Variances

	Variable 1	*Variable 2*
Mean	-24.55628004	-31.245
Variance	799.5669377	2362.83
Observations	98	201
df	97	200
F	0.338394261	
P(F<=f) one-tail	6.09337E-09	
F Critical one-tail	0.742782257	

t-Test: Two-Sample Assuming Unequal Variances

	Variable 1	*Variable 2*
Mean	-24.556	-31.2451
Variance	799.567	2362.827
Observations	98	201
Hypothesized Mean Difference	0	
df	288	
t Stat	1.49888	
P(T<=t) one-tail	0.0675	
t Critical one-tail	1.65016	
P(T<=t) two-tail	0.135	
t Critical two-tail	1.96824	

Test 2: Field studies *vs. large* wind tunnel studies

FIELD vs LARGE WIND TUNNEL (ALL)

F-Test Two-Sample for Variances

	Variable 1	*Variable 2*
Mean	-24.55628004	-15.689
Variance	799.5669377	244.548
Observations	98	150
df	97	149
F	3.269567403	
P(F<=f) one-tail	3.87385E-11	
F Critical one-tail	1.34860745	

t-Test: Two-Sample Assuming Unequal Variances

	Variable 1	*Variable 2*
Mean	-24.556	-15.6895
Variance	799.567	244.5482
Observations	98	150
Hypothesized Mean Difference	0	
df	136	
t Stat	-2.834	
P(T<=t) one-tail	0.00265	
t Critical one-tail	1.65613	
P(T<=t) two-tail	0.0053	
t Critical two-tail	1.97756	
t Critical two-tail	1.970	

Test 3: Field studies *vs. small* wind tunnel studies

FIELD vs SMALL WT (ALL)

F-Test Two-Sample for Variances

	Variable 1	*Variable 2*
Mean	-24.55628004	-80.262
Variance	799.5669377	6401.4
Observations	98	45
df	97	44
F	0.124905076	
P(F<=f) one-tail	0	
F Critical one-tail	0.665792513	

t-Test: Two-Sample Assuming Unequal Variances

	Variable 1	*Variable 2*
Mean	-24.556	-80.2618
Variance	799.567	6401.397
Observations	98	45
Hypothesized Mean Difference	0	
df	49	
t Stat	4.5421	
P(T<=t) one-tail	1.8E-05	
t Critical one-tail	1.67655	
P(T<=t) two-tail	3.6E-05	
t Critical two-tail	2.00958	

Test 4: *Large* wind tunnel studies *vs. small* wind tunnel studies

LARGE WT vs SMALL WT

F-Test Two-Sample for Variances

	Variable 1	*Variable 2*
Mean	-15.68949914	-80.262
Variance	244.548235	6401.4
Observations	150	45
df	149	44
F	0.038202325	
P(F<=f) one-tail	0	
F Critical one-tail	0.685802031	

t-Test: Two-Sample Assuming Unequal Variances

	Variable 1	*Variable 2*
Mean	-15.689	-80.2618
Variance	244.548	6401.397
Observations	150	45
Hypothesized Mean Difference	0	
df	45	
t Stat	5.3832	
P(T<=t) one-tail	1.3E-06	
t Critical one-tail	1.67943	
P(T<=t) two-tail	2.5E-06	
t Critical two-tail	2.0141	

4.3 Controls on the vertical distributions of mass flux

4.3.1 Field experiments

The field experiments were used to investigate the influence of, if any, environmental and experimental controls on the observed mass flux decay rates. Within each experiment, the percentage variations between the slopes of the flux profiles from the experiment mean were 22, 12, 4, 29 and 21% for Brazil (2008), Greeley et al., (1996), Namikas (2003), Namikas et al., (2009) and Portugal (2006), respectively. Identifying possible reasons for these departures are investigated here. The slopes of the flux profiles in each experiment were regressed on (i) shear velocity, (ii) grain size, (iii) average transport rate, (iv) maximum sample elevation, and (v) sampling resolution. The maximum sampled elevation was defined as the highest point in the observed mass flux profile where sediment was trapped. It corresponds to the elevation of the highest digitized point in the flux profiles. The sampling resolution is the maximum sampled elevation divided by the number of traps that were used to obtain the representative vertical flux profile. This is a reference parameter to determine if the trap design influences the characteristics of observed mass flux profile. The experiments chosen had at least nine profiles to test for correlations. The Brazil (2008) data were reduced to a subset of fourteen profiles where shear velocity was reported. Results from the regression analyses are provided in Table 4-5. Some of these variables did not change value, e.g., reported grain sizes in Greeley et al., (1996) and Namikas (2003) or maximum sampling elevation in Brazil (2008), Namikas (2003) and Namikas et al., (2009). Correlation analyses were not done in these cases and are marked (-) in Table 4-5. Relationships that were significant at the 95% confidence level ($P < 0.05$) are in bold.

Table 4-5. Field data: results of regression analyses between the slopes of the flux profiles and different environmental and experimental conditions.

	u_* (m/s)	d (mm)	ave. Q (g/cm^2/s)	Max. Sample Elev., H (m)	Sample Resolution, H/#traps (m)
All field data	0.0007	**0.22**	0.02	**0.55**	**0.47**
Brazil (2008)	0.02	**0.51**	0.008	-	-
Greeley et al. (1996)	**0.65**	-	**0.66**	0.30	0.176
Namikas (2003)	0.27	-	0.0042	-	-
Namikas et al. (2009)	0.35	**0.57**	0.34	-	-
Portugal (2006)	**0.64**	0.003		**0.77**	**0.596**

Shear velocity: Two experiments, Greeley et al., (1996) and Portugal (2006), show significant relationship between the slope and shear velocity. Both these relationships have a high goodness-of-fit, with r^2 values equal to 0.65 and 0.64, respectively (Table 4-5) and are statistically significant. Both datasets predict that the rate of decay of sediment away from the surface becomes less steep as shear velocity decreases (Figure 4-4). It should be noted that the overall variability in slope within each experiment is low (12 and 21%).

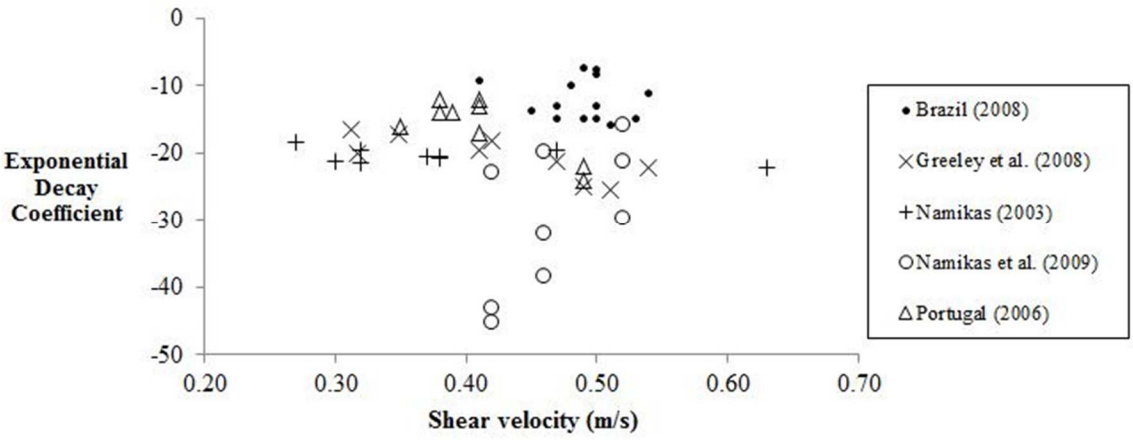

Figure 4-4. Shear velocity *vs.* slope for field experiments.

This trend is opposite to that reported in Dong et al., (2002) and Liu and Dong (2004) who report steeper slopes for mass flux profiles as wind speed decreases. This is the case for the data of Namikas et al., (2009) shown in Figure 4-4. As shear velocity decreases from 0.52 m/s to 0.42 m/s the value of the exponential decay coefficient changes from -16 to -45, indicating a steepening of the flux profiles. However this relationship is statistically insignificant at the 95% confidence level. In contrast, both the Namikas (2003) and Brazil (2008) have no significant relationship or trends between shear velocity and the decay coefficient. The data of Namikas (2003) show only a 4% variability in slope despite measuring a large range of shear velocities, from 0.27 to 0.63 m/s. Namikas (2003, p.311) states that "*the slope of the vertical distribution of mass flux is either independent of shear velocity, or that any dependence is so weak as to be obscured by natural variability and/or measurement error*". The Namikas et al., (2009) data is significant because it is one of the very few field studies reported where there was a grain size control. This experiment also reports a much wider range of slope values than are reported in any of the other field experiments where grain size is not highly variable. They report flux profile slopes with variation of up to 65% from the experiment mean.

Grain size: Both the Brazil (2008) and Namikas et al., (2009) data have significant relationships between the exponential decay coefficient and grain size (Figure 4-5). In both experiments the rates of decay of flux steepen as grain size decreases. The goodness-of-fit of these relationships is good, with r^2 values of 0.51 and 0.57, respectively (Table 4-5). This type of grain size steepening of the flux profiles is also reported in wind tunnel studies of Dong et al., (2002), Liu and Dong (2004), Ni et al., (2002) and Dong et al., (2006). The runs reported in Greeley et al., (1996) and Namikas (2003) have no substantial change in mean grain size at their field sites. Interestingly, both these studies were conducted at the same location in Pismo Dunes, California, USA. They report mean grain sizes of 0.23 and 0.25 mm, respectively. The field data,

aggregated as a single group of decay coefficients and regressed on mean grain size, has an r^2 value of 0.22 which is significant at the 95% confidence level.

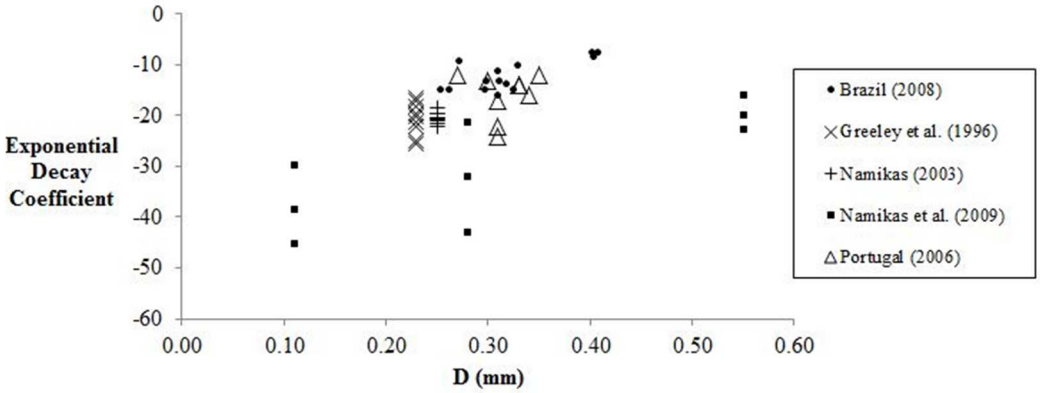

Figure 4-5. Grain size *vs.* slope for field experiments.

Transport rate: With the exception of Greeley et al., (1996) there are no significant relationships between the decay coefficient and the average rate of transport (Figure 4-6). The Greeley et al. (1996) have a strong relationship (r^2 = 0.66) for the relatively low transport rates observed. None of the other field experiments show any significant trends.

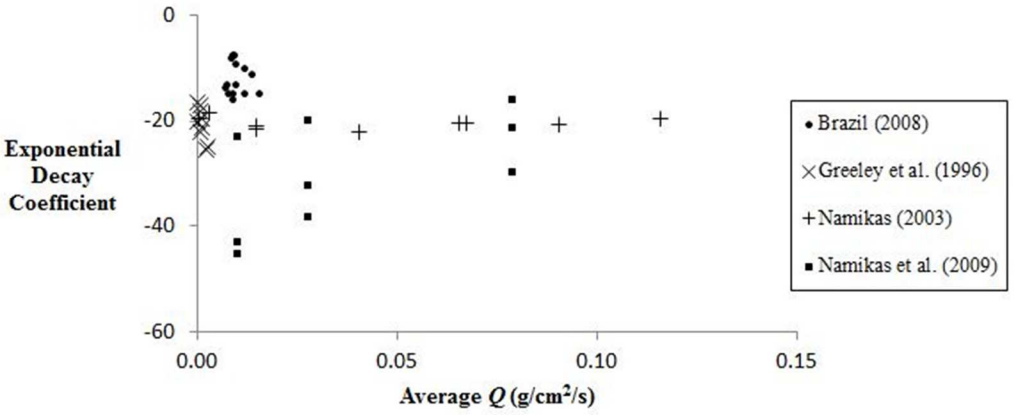

Figure 4-6. Average transport rate *vs.* slope for field experiments.

Maximum sampling elevation: The field data, aggregated as a single group of decay coefficients and regressed on the maximum sampled height, has an r^2 value of 0.55 and is significant at the 95% confidence level (Table 4-5). As sampled height increases the rate of decay of flux becomes less steep (Figure 4-7). Intuitively, we would expect this to occur as more of the flux is being measured at higher elevations above the bed, thereby extending the vertical flux profile. This has implications for comparing the rates of decay of mass flux from experiments with different trap designs. It is important to note that the Namikas et al., (2009) data was only reported for the lowest 0.10 m.

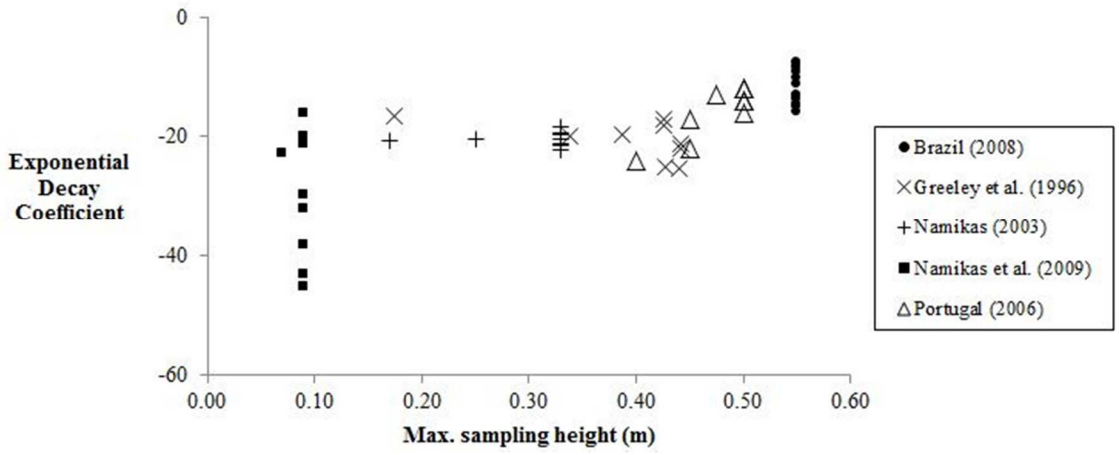

Figure 4-7. Maximum sampled height *vs.* slope for field experiments.

Sampling resolution: The sampling resolution was calculated by dividing the maximum sampled elevation by the number of traps used to measure flux. Clearly a flux profile with only one trap lying on the bed and a few traps higher up will 'observe' a very steep slope. The experiments of Greeley et al., (1996), Namikas (2003) and Namikas et al., (2009) all used collectors with small dimensions. Greeley used a vertical stack that was 0.45 m high with a continuous array of collectors each with an opening 0.01 m^2. Namikas (2003) and Namikas et al., (2009) used versions of a vertical trap that comprised of wedge-shaped sediment with openings 60 mm wide and varying vertical

openings of 10, 20 or 40 mm. Neither of these experiments varied their sample height to any great degree which precludes correlation analysis. Only the mass flux measurements from Portugal (2006) show a significantly strong relationship (Figure 4-8). As the number of traps increases (maximum sampling height / # traps decreases), the measured slopes steepen.

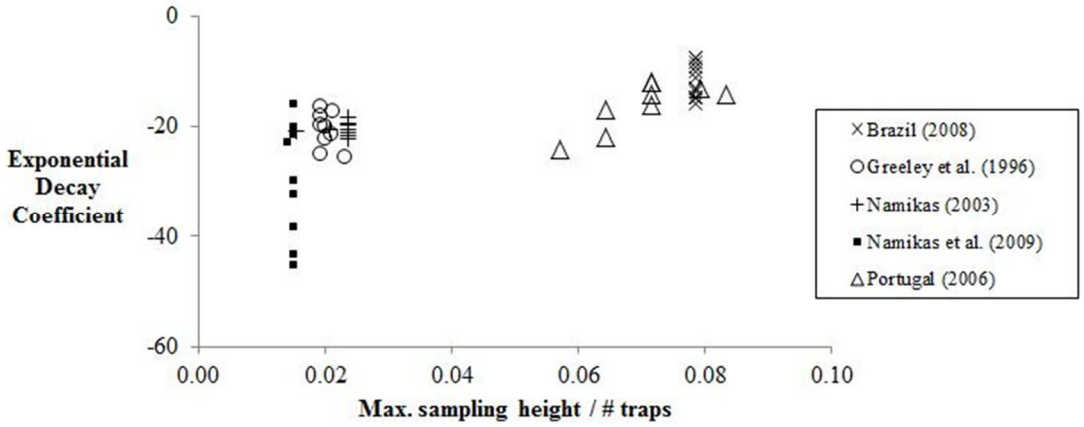

Figure 4-8. Sampling resolution *vs.* slope for field experiments.

4.3.2 Wind tunnel experiments

Following the methods used to analyze the field data, the decay coefficient, or slope, values in each wind tunnel experiment were regressed on (i) shear velocity, (ii) grain size, (iii) average transport rate, (iv) maximum sampled elevation, and (v) sampling resolution. The results are listed in Table 4-6. In some of these reported studies correlation analyses were not done if the studies did not have more than three reported runs. This was the case for Kawamura (1951), Rasmussen and Mikkelsen (1998) and Sørensen (1985) and are marked (-) in the table. Relationships that were significant at the 95% confidence level ($P< 0.05$) are in bold. Overall, there was a much wider range in the variability of slopes within the wind tunnel studies than observed in the field experiments (Table 4-7). This should be expected as there were much better controls on experimental conditions. For example the slopes of the runs observed in Hotta et al.

(2006) and Ni et al. (2002) had 69% and 65% variability from the mean. Hotta et al. (2006) conducted tests using samples ranging in grain size from 0.15 – 0.68 mm and shear velocities from 0.61 – 2.33 m/s. Similarly, Ni et al., (2002) used two different grain sizes, 0.17 and 0.35 mm, and a range of shear velocities from 0.47 – 2.36 m/s. These wide ranges of conditions are not usually experienced in field experiments.

Table 4-6. Wind tunnel data: results of regression analyses between the slopes of the flux profiles and different environmental and experimental conditions.

	$u*$ (m/s)	d (mm)	ave. Q (g/cm^2/s)	Max. Sample Elev., H (m)	Sample Resolution, H/#traps (m)
All wind tunnel data	0.003	**0.09**	0.01	**0.32**	**0.09**
Butterfield (1999)	0.15	0.26	0.01	0.26	0.04
Dong et al. (2002)	**0.20**	**0.60**	0.06	**0.80**	0.02
Dong et al. (2004)	**0.88**	(-)	**0.76**	0.03	0.04
Feng et al. (2009)	0.0007	(-)	0.17	(-)	0.00
Gerety & Slingerland (1983)	0.39	0.54	0.19	0.56	0.19
Hotta & Horikawa (1993)	0.03	(-)	0.04	0.04	0.02
Hotta et al. (2006)	**0.34**	0.20	0.17	**0.57**	**0.57**
Kawamura (1951)	(-)	(-)	(-)	(-)	(-)
Liu et al. (2006)	**0.99**	0.05	**0.99**	0.06	0.06
Ni et al. (2002)	0.20	0.34	0.20	**0.93**	0.19
Rasmussen & Mikkelsen (1988)	0.81	0.81	**0.95**	0.18	0.17
Rasmussen & Mikkelsen (1998)	(-)	(-)	(-)	(-)	(-)
Sorensen (1985)	(-)	(-)	(-)	(-)	(-)
Williams (1964)	0.40	(-)	0.16	0.03	0.03
Zou et al. (2001)	0.83	0.14	0.34	0.14	0.14

Table 4-7. Summary statistics for the mass flux profile experiments.

	Field		**Wind Tunnel**	
	$u*$ (m/s)	**d (mm)**	**$u*$ (m/s)**	**d (mm)**
Maximum	0.63	0.55	2.36	0.9
Minimum	0.27	0.11	0.2	0.118
Average	0.44	0.29	0.64	0.336
Std. dev.	0.075	0.09	0.065	0.24

Shear velocity: Only two experiments have strong statistical relationships for the decay coefficient and shear velocity. Both Dong et al., (2004) and Liu et al., (2006) have high r^2 values of 0.88 and 0.99, respectively. Both sets of experiments show a steepening of the flux profile slope as shear velocity decreases (Figure 4-9). It is important to note that the shear velocities presented in Liu et al., (2006), Figure 4 (p.665) have an inverse relationship with the rate of flux. The lowest shear velocity, 0.48 m/s, has the highest flux. Similarly the highest shear velocity, 0.75 m/s, has the lowest observed flux rates. There is no physical reasoning why this should occur – other than it was a mistake in the legend. Here, the lowest to highest shear velocities are associated with the lowest to highest flux rates in these analyses.

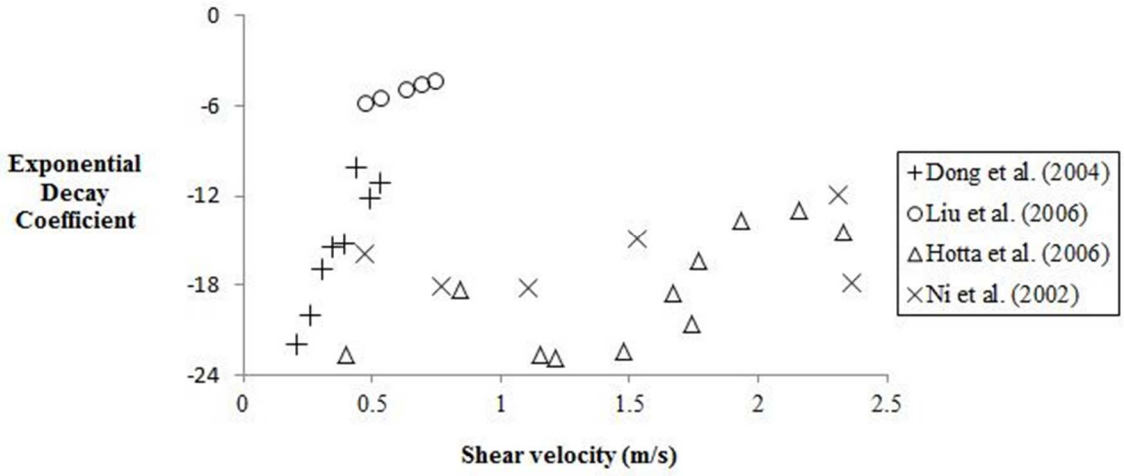

Figure 4-9. Shear velocity *vs.* slope for wind tunnels experiments of Dong et al., (2004), Liu et al., (2006), Hotta et al., (2006) and Ni et al., (2002).

The data of Dong et al., (2002) are illustrated in Figure 4-10 using the representation of their 58 mass flux profiles in Dong and Qian (2007). This figure provides an excellent reference to assess the characteristics of the mass flux profiles with changing grain size and wind speed (*not* shear velocity). In this figure the flux profiles are normalized using the total mass caught in each run, similar to the approach described in the Section 3, subsection 3.4. The significant findings from analyzing the runs in this

experiment are (i) flux decreases more rapidly as wind velocity decreases (i.e. steeper rates of decay for lower shear velocities), (ii) an increase in wind speed decreases the relative proportion of the sediment in moving near the bed, but increases the proportion moving at higher elevations (profile slopes become *less* steep), (iii) the flux decreases more rapidly as grain size decreases (smaller grain size have steeper slopes than larger grains, *ceteris paribus*), (iv) smaller grain sizes are more susceptible to changes in wind speed (and do not normalize as conveniently!).

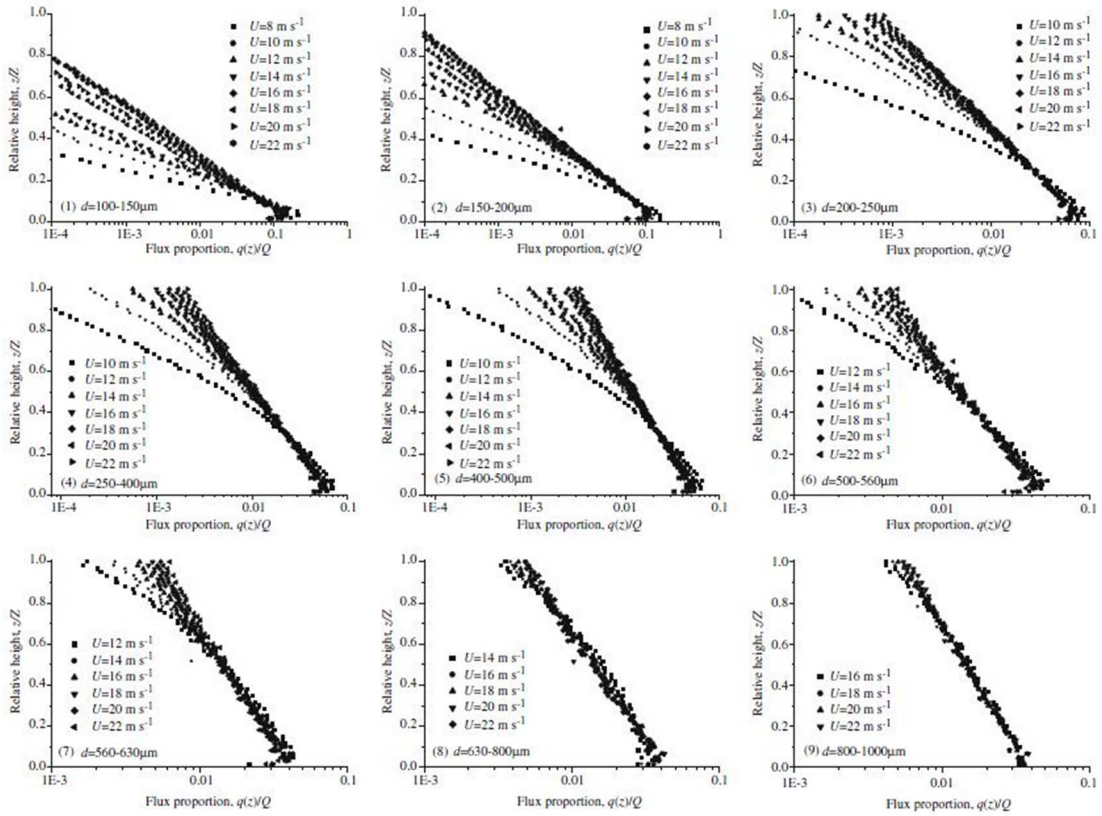

Figure 4-10. Wind speed and grain size controls on the normalized flux profiles of Dong et al., (2002).

Grain size: The high correlation of the Dong et al., (2002) data (r^2 = 0.60) in Table 4-6 provides insight into the influence of different grain sizes on the vertical distributions of

mass flux. Their data, shown in Figure 4-11, indicate that flux profiles steepen as grain size decreases. It is peculiar that this study is the only strong statistical relationship between grain size and slope.

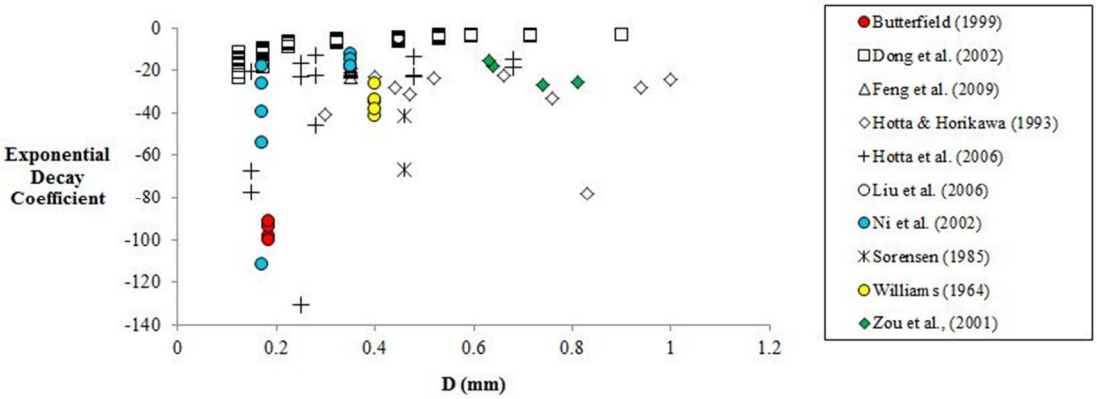

Figure 4-11. Grain size *vs.* slope for wind tunnels experiments

Maximum sampling elevation: Three wind tunnel experiments have strong statistical relationships between the maximum sampled elevation and the decay coefficient (Dong et al., 2002; Ni et al., 2002; Hotta et al., 2006). All three experiments had a wide range of wind speeds and grain sizes (Table 4-6) which is reflected in the different elevations from which flux was observed. The very steep slopes are correlated with small grain sizes and low wind speeds. In these conditions the small amount of sand moving is close to the surface. Therefore the decay rates are very steep as there is not enough energy for the sand to move higher above the surface. Conversely for higher wind speeds and coarser sands the sands reach much higher elevations and result in an increase in the decay coefficient. The points with high decay coefficients shown in Figure 4-12 correspond closely with the lowest mean grain sizes and shear velocities (or wind speeds), respectively. For example the Dong et al., (2002) slope values with maximum sampling elevation less than 0.25 m are for the smallest grains sizes and lowest wind speeds they tested: 0.125 – 0.175 mm and 8 – 10 m/s. Similarly the Hotta et al. (2006)

slope values greater than -40 correspond to their smallest grain sizes (0.15 – 0.25 mm) and lowest shear velocities (0.63 – 1.0 m/s). The Ni et al., (2002) points are for their small grain sizes (0.17 mm) and lowest shear velocities (0.47 – 0.86 m/s).

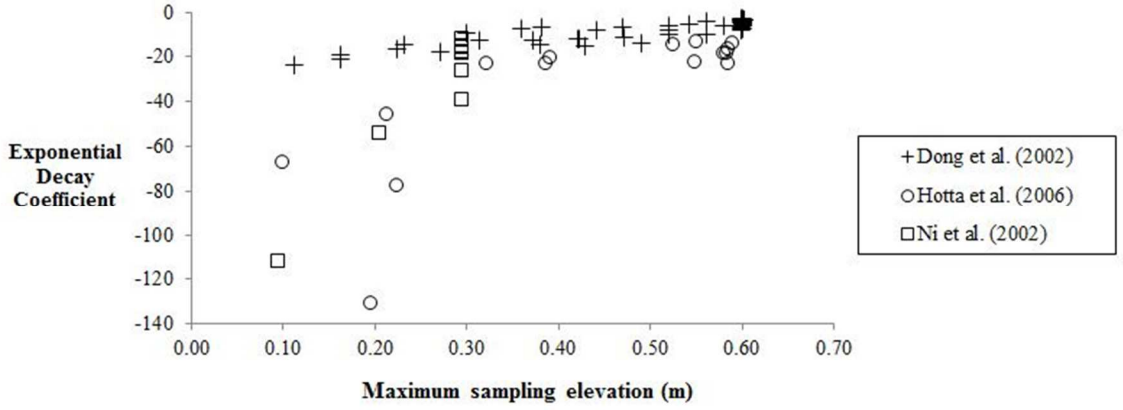

Figure 4-12. Maximum sampled height *vs.* slope for wind tunnel experiments.

Sampling resolution: On first inspection of the linear regression results listed in Table 4-6, the data show no indication that sampling the flux profiles using a high number of small traps influences the measured slope. There was one significant relationship for the Hotta et al., (2006) profiles (r^2 = 0.56). The very steep slopes in Figure 4-13, from the Hotta et al. (2006), correspond with flux profiles measured a very short distance above the bed. In these cases the grain sizes are usually very small and/or the shear velocities or wind speeds are lowest relative to other runs in the experiment. For example, the four decay coefficient values of -130, -77, -67 and -45 shown in Figure 4-9 correspond with the lowest grain sizes (0.25, 0.15, 0.15 and 0.28), lowest reported shear velocities (0.61, 1.01, 0.63, 0.87 m/s) and lowest sampled elevations (0.311, 0.11, 0.07, and 0.10 m) compared with the rest of the runs. The runs with the higher value decay coefficients (approximating -20) were measured up to 0.30 m above the bed with shear velocities in excess of 1.75 m/s and grain sizes greater than 0.50 mm. Physically, we would expect this, as less grains are reaching higher elevations for the lower shear velocities.

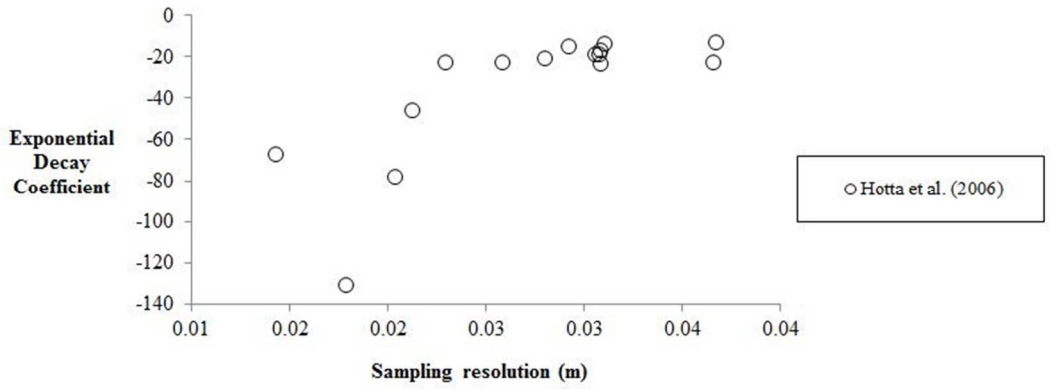

Figure 4-13. Sampling resolution *vs.* slope for runs reported in Hotta et al., (2006).

The following is a summary of the main findings from investigating potential environmental and experimental controls on the vertical distributions of mass flux.

Field experiments:

1. In field experiments shear velocity has different reported impacts on the distribution of mass flux. In two experiments decreasing the shear velocity flattens the observed slopes, although the variability in slopes was not large in these experiments: 12% and 21% in Greeley et al., (1996) and Portugal (2006), respectively. In one experiment (Namikas et al., 2009), decreasing the shear velocity results in a steepening of the slope. This study had the large variability of slopes within a field experiment (up to 30%) which is probably a result of these researchers controlling for grain size. In two experiments there is no relationship between shear velocity and slopes of the mass flux profiles.
2. In field experiments, where there were significant changes in grain size, decreasing grain size resulted in steeper slopes, *ceteris paribus*.

Wind tunnels:

1. In wind tunnel experiments, as shear velocity decreases, the slope of the vertical mass profile steepens. This trend is seen in the data of Dong et al., (2002, 2004), Liu et al., (2006), Hotta et al., (2006) and Ni et al., (2002). The relationships are

statistically strong for all studies. In some cases there is no change in slope despite varying shear velocity, e.g., Hotta and Horikawa (1993) and Feng et al., (2009).

2. In wind tunnel experiments the influence of grain size on flux profile slope is ambiguous. In Dong et al., (2002), as grain size decreases, the slope of the vertical mass profile steepens. This relationship is the only statistically strong and significant relationship for grain size and slope ($r^2 = 0.60$). Varying the grain does not impact the slope value is other experiments (e.g. Hotta and Horikawa, 1993). In other cases, the same grain size has different slopes, inferring that there are other controls on slope (e.g. Ni et al., 2002).

With these findings it was decided to re-visit the difference in means test (*t*-tests) described in Section 4.2.2 to re-assess the statistical similarity of the calculated slopes for flux profiles between field and wind tunnel experiments. For this part of the analysis, the mass flux profiles from each experiment were assessed to establish commensurable sets of reported shear velocities and grain sizes upon which to compare the slope characteristics. Table 4-7 provides a summary of the range of shear velocities and grain sizes reported in the different experiments. The range of field data was used as the boundary conditions for this analysis. Any wind tunnel study that did not meet the requirements: $0.27 < u_* < 0.63$ m/s for shear velocity, and $0.11 < d < 0.55$ mm for grain size, were removed from this statistical comparison.

This resulted in 56 wind tunnel profiles being removed from the analysis. An *F*-test was used to determine if the variances of the decay coefficients in each category were equal. The *P* value in the *F*-test was less than 0.05 (Table 4-8) so the two populations were designated as having unequal variances. The results of the difference in means *t*-test assuming unequal variances are provided in Table 4-8. For the grouped categories ‘all field’ and ‘all wind tunnels’, the *t*-test calculated that **the two populations are not statistically different**, $P > 0.05$.

Table 4-8: Results of *F*-tests and *t*-tests using field and wind tunnel runs with the same range of shear velocities and grain sizes.

F-Test Two-Sample for Variances		
	Variable 1	*Variable 2*
Mean	-24.556	-32.027
Variance	799.567	2231.066
Observations	98	145
df	97	144
F	0.358	
P(F<=f) one-tail	8.69444E-08	
F Critical one-tail	0.731862534	

t-Test: Two-Sample Assuming Unequal Variances		
	Variable 1	*Variable 2*
Mean	-24.556	-32.027
Variance	799.567	2231.066
Observations	98	145
Hypothesized Mean Difference	0	
df	238	
t Stat	1.540	
P(T<=t) one-tail	0.063	
t Critical one-tail	2.342	
P(T<=t) two-tail	0.125	
t Critical two-tail	2.597	

The wind tunnel data were separated into two categories according to the same cross section cutoff described in Section 4.1.3. A series of *F*-tests and *t*-tests were used to compare the slopes of the vertical flux profiles between each group (Table 4-9). Using a 95% significance level, it was found that:

Test 1. All field *vs.* large wind tunnel studies: *statistically different (P<0.05)*

Test 2. All field *vs.* small wind tunnel studies: *statistically different (P<0.05)*

Test 3. Large wind tunnel *vs.* small wind tunnel studies: *statistically different (P<0.05)*

These replicate the findings in Section 4.2.2. This provides some support to questions or criticisms that the findings reported in Table 4-4 (that the slopes of vertical flux profiles measure din field and wind tunnel environments are different, at least statistically) are a result of different sampling designs or conditions. These differences are all reported at the 95% significance level i.e. **there is less than a 5% chance that the decay coefficients, which describe how rapidly the sediment decays away from the bed, obtained in the field and wind tunnels are derived from the same population.** However, comparing the field and wind tunnel groups for a 99% significance level, it is interesting to note that the slopes of the flux profiles from the large wind tunnel studies do in fact produce similar distributions to those observed in the field. The other groups are still different at the 99% significance level.

Test 4. Field *vs.* large wind tunnel studies: *statistically the same (P>0.01), P=0.022*

Test 5. Field *vs.* small wind tunnel studies: *statistically different (P<0.01)*

Test 6. Large *vs.* small wind tunnel studies: *statistically different (P<0.01)*

The following is a summary of the results comparing the slopes of the vertical flux profiles measured in field and wind tunnels, in experiments that were within the designated range of shear velocities and grain sizes:

1. The slopes of the mass flux profiles measured in the field are statistically different to the large wind tunnel slopes at the 95% significance level, but not at the 99% confidence level.
2. The slopes of the mass flux profiles measured in the field are statistically different to the small wind tunnel slopes at the 95% and 99% significance level.
3. The slopes of the mass flux profiles measured in the large wind tunnels are statistically different to the small wind tunnel slopes at the 95% and 99% significance level.

Table 4-9. Results of the *F*-tests and *t*-tests: same range of u_* and d.

Test 1: Field studies *vs. Large* wind tunnel studies

FIELD vs LARGE WT (QA/QC)

t-Test: Two-Sample Assuming Unequal Variances

	Variable 1	*Variable 2*
Mean	-24.556	-16.480
Variance	799.567	406.250
Observations	98	102
Hypothesized Mean Difference	0	
df	175	
t Stat	-2.318	
P(T<=t) one-tail	0.011	
t Critical one-tail	1.654	
P(T<=t) two-tail	0.022	
t Critical two-tail	1.974	

Test 2: Field studies *vs. Small* wind tunnel studies

FIELD vs SMALL WT (QA/QC)

t-Test: Two-Sample Assuming Unequal Variances

	Variable 1	*Variable 2*
Mean	-24.556	-73.269
Variance	799.567	5192.861
Observations	98	43
Hypothesized Mean Difference	0	
df	48	
t Stat	4.290	
P(T<=t) one-tail	0.000	
t Critical one-tail	1.677	
P(T<=t) two-tail	8.59373E-05	
t Critical two-tail	2.011	

Test 3: *Large* wind tunnel *vs. Small* wind tunnel studies

LARGE WT vs SMALL WT (QA/QC)

t-Test: Two-Sample Assuming Unequal Variances

	Variable 1	*Variable 2*
Mean	-16.480	-73.269
Variance	406.250	5192.861
Observations	102	43
Hypothesized Mean Difference	0	
df	45	
t Stat	5.085	
P(T<=t) one-tail	3.46971E-06	
t Critical one-tail	1.679	
P(T<=t) two-tail	6.93941E-06	
t Critical two-tail	2.014	

4.4 The Rouse profiles

4.4.1 Rouse profile shape

The Rouse profiles constructed using the methods described in Section 3.7 have very distinct L-shapes. Physically, these profiles predict that a miniscule amount of mass flux is moving above the reference elevation. For example, the absolute values of the predicted fluxes for each elevation for the Rouse profiles constructed for Runs 1-5 of Feng et al., (2009) are shown in Table 4.10. Run 1 has 0.0585 g/cm^2/s moving at an elevation of 0.5115 cm – both of which are inputs to the model taken directly from the digitized data. The Rouse model predicts the next point at an elevation of 2.55 cm with a predicted flux of 0.000042 g/cm^2/s. The predicted fluxes for elevation above the reference for Runs 2-5, in Table 4.10 show similar decreases in flux magnitudes: 0.00061, 0.00254, 0.0104 and 0.0277 g/cm^2/s, respectively. Physically, these flux predictions are implausible and do not agree with observations. These five runs of Feng et al., (2009) are shown in Figure 4-14 and are typical for all the experiments. The plots of all the experiments are provided in Appendix C.

Table 4-10. Rouse profiles for Feng et al., (2009), Runs 1-5.

Q (g/cm^2/s)	z (cm)	Q (g/cm^2/s)	z (cm)	Q (g/cm^2/s)	z (cm)	Q (g/cm^2/s)	z (cm)	Q (g/cm^2/s)	z (cm)
0.0585	0.5115	0.109	0.4634	0.2315	0.4936	0.4442	0.00412	0.8161	0.00399
4.23025E-05	2.54838	0.000613126	2.49579	0.002540861	2.49579	0.010481793	2.49579	0.027673612	2.49579
8.24927E-07	4.07347	3.85544E-05	4.0238	0.000228315	4.0238	0.00141746	4.0238	0.004541828	4.0238
4.85259E-08	5.59856	5.32933E-06	5.55181	4.07402E-05	5.55181	0.000338828	5.55181	0.001246946	5.55181
4.93595E-09	7.12365	1.08506E-06	7.07982	1.01858E-05	7.07982	0.000107172	7.07982	0.000440886	7.07982
6.89855E-10	8.64874	2.7631E-07	8.60783	3.0945E-06	8.60783	3.9852E-05	8.60783	0.000180415	8.60783
1.17537E-10	10.1738	8.08692E-08	10.1358	1.06128E-06	10.1358	1.63883E-05	10.1358	8.08541E-05	10.1358
2.2707E-11	11.6989	2.58514E-08	11.6639	3.93042E-07	11.6639	7.18332E-06	11.6639	3.83848E-05	11.6639
4.73369E-12	13.224	8.71806E-09	13.1919	1.52506E-07	13.1919	3.27282E-06	13.1919	1.8871E-05	13.1919
1.02514E-12	14.7491	3.02035E-09	14.7199	6.05796E-08	14.7199	1.52048E-06	14.7199	9.44224E-06	14.7199
2.23171E-13	16.2742	1.05065E-09	16.2479	2.41491E-08	16.2479	7.08459E-07	16.2479	4.73702E-06	16.2479
4.72922E-14	17.7993	3.58844E-10	17.7759	9.47433E-09	17.7759	3.2576E-07	17.7759	2.34824E-06	17.7759
9.4126E-15	19.3244	1.17391E-10	19.3039	3.58009E-09	19.3039	1.45192E-07	19.3039	1.13175E-06	19.3039
1.68239E-15	20.8495	3.56583E-11	20.8319	1.26821E-09	20.8319	6.13336E-08	20.8319	5.19664E-07	20.8319
2.53533E-16	22.3746	9.62754E-12	22.3599	4.05433E-10	22.3599	2.37928E-08	22.3599	2.20937E-07	22.3599
2.91486E-17	23.8996	2.15612E-12	23.888	1.10136E-10	23.888	8.06253E-09	23.888	8.31334E-08	23.888
2.13173E-18	25.4247	3.53221E-13	25.416	2.27862E-11	25.416	2.17919E-09	25.416	2.55025E-08	25.416
6.6345E-20	26.9498	3.20578E-14	26.944	2.81855E-12	26.944	3.84259E-10	26.944	5.31924E-09	26.944
2.45721E-22	28.4749	6.67933E-16	28.472	9.67728E-14	28.472	2.33752E-11	28.472	4.24273E-10	28.472
0	30	0	30	0	30	0	30	0	30

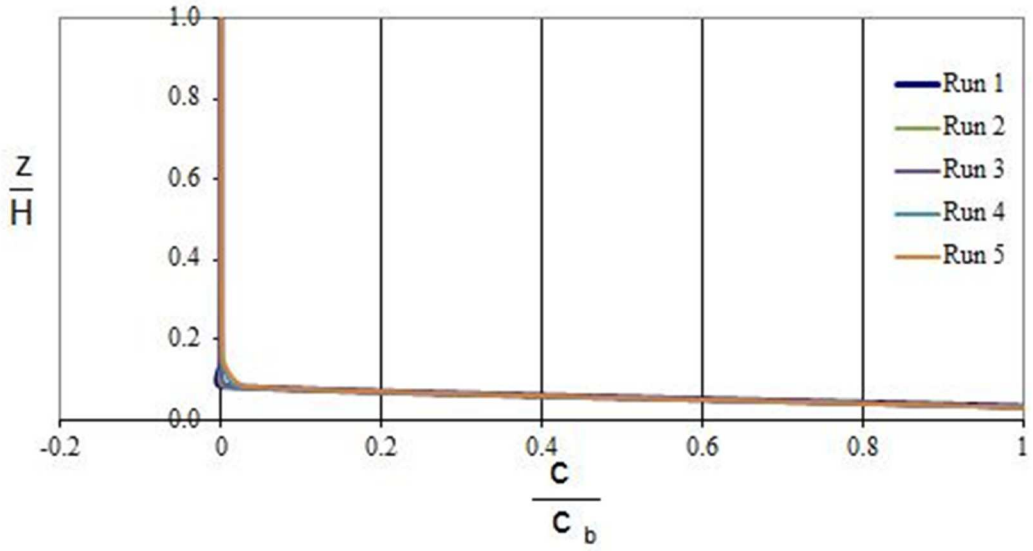

Figure 4-14. Predicted Rouse profiles for Feng et al., (2009), Runs 1-5. The Rouse number uses w_0 based on Equation 3-7, k = 0.40, u_* as reported or measured and β = 1.0.

These trends are the result of the very high estimates of fall velocity. Compared to sediment fall velocity in water, the fall velocities od sand-sized particles falling in air are orders of magnitude higher. The Rouse model was developed to give a general distribution of suspended concentration gradients for medium sands, silts and clays moving in suspension. In these transport systems reported fall velocities for particles 0.0625 – 2.0 mm range from, approximately (depending on the empirical relationship), 0.0033 – 0.28 m/s. The equivalent range of fall velocities of this range of sand size falling in air is 0.46 – 8.60 m/s using Equation 3-7. This approach will be re-visited in Section 5.

4.4.2 Rouse profile magnitude

The predicted fluxes from the Rouse approach were compared with the observed fluxes obtained from the digitized flux profiles. These are two independent methods to calculate estimates of total flux – although, importantly, they do share the reference flux and elevation which is invariably obtained very near the bed. The predicted total flux was calculated by adding the each predicted flux, for each elevation, within each run.

The equivalent observed total flux was calculated using the same method for the digitized data. The total fluxes have units of $g/cm^2/s$. Figure 4-15 plots the predicted *vs.* observed fluxes (both in $g/cm^2/s$) for all the data in Table 3-4. The relationship is very strong and statistically significant ($r^2 = 0.95$, $P < 0.05$). However the Rouse approach clearly under predicts the observed flux by nearly an order of magnitude.

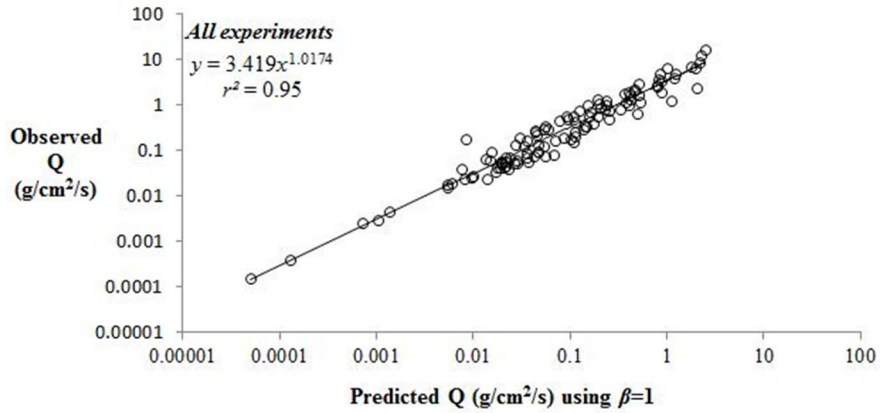

Figure 4-15. Predicted total flux using the unadjusted Rouse Parameter (k=0.40; B=1.0) for all experiments

The data were separated into two categories, field and wind tunnel studies, to test the predictive power of the Rouse approach in each environment performance. Again, and not surprisingly, the relationships are very strong ($r^2 = 0.98$ and 0.92) and are statistically significant (Figure 4-13). Still, the difference in the magnitude of the predicted flux remains large. This is clearly illustrated by examining the range of the log-X and log-Y axes. Figure 4-14 shows the percentage of transport observed (Q_{obs}.) predicted by the Rouse profiles. The field and wind tunnels, on average, predict 38% (+/- 8%) and 18% (+/- 86%) of the observed transport rate. The predictive powers of the Rouse model will be re-visited in the next Section.

From the analyses of the Rouse profile shapes, the Rouse model is not a viable approach to replicate distribution of mass flux above the bed for aeolian transport. This

is due to the dependency of the profile shape on the Rouse number – which is considerably larger for sediments moving in air than in water due to differences in fall velocities of particles in the two environments. In water, these high fall velocities would be manifested in all the sediment moving as bedload. Clearly, this is not the case for the observed flux profiles that are strongly exponential but still observe a proportion of sediment at higher elevations above the bed. Therefore, the Rouse profiles are physically incorrect and do not replicate the saltation process. Linked closely with this problem, is the very low predictions of flux magnitudes. The Rouse model has little or no sediment moving above the reference height, therefore the predicted fluxes are, in essence, the reference flux (C_a) i.e. the bottom trap. In aeolian transport most of the sediment moves close to the bed so it is, perhaps, not surprising that there is a very strong relationship between the predicted flux and observed flux ($r^2 = 0.92$ in Figure 4.12) – but the former is lower by nearly an order of magnitude. One possible solution to this was tested by adjusting the regression coefficient of the power relationships. The variability of Rouse number will be further investigated in Section 5.

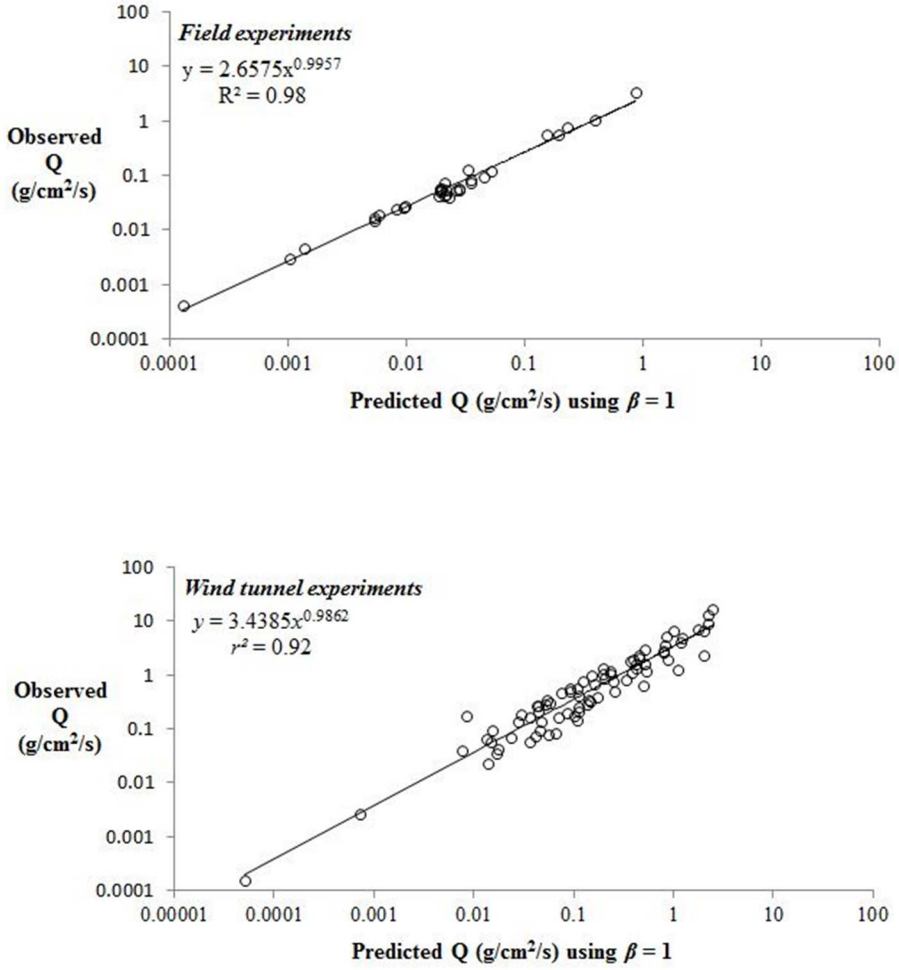

Figure 4-16. Predicted total flux using the unadjusted Rouse Parameter (k=0.40; B=1.0) for field (top) and wind tunnel (bottom) experiments.

V. DISCUSSION

Most wind-blown sand moves *via* saltation (Bagnold, 1936). Research of the characteristics of saltation can be separated into two broad categories: the first concerns the movement of individual particles based on equations of motion and analysis of forces exerted on the particles (Dong et al., 2006); the second concerns the resultant characteristics of the aggregate of the saltation trajectories, manifested as the saltation layer. Both these processes are inextricably linked in current modelling approaches.

5.1 Grain size-sorting variation in the vertical mass flux profiles

Despite the considerable work that has been done on the size and trajectory characteristics of saltating grains, there is still no consensus about what the shape of the vertical profile of the distribution of grain sizes should be. The analysis of the grain-size statistics for the flux caught in each trap of the vertical flux profiles shows that a reverse in grain-size trends occurs at an inflection zone located 0.05 – 0.15 m above the bed. Below this inflection, mean grain-size decreases steeply with elevation in the near bed region dominated by reptation and saltation modes of transport. Above the inflection there is a coarsening of grain size with elevation; as saltation becomes the dominant transport mode. These results indicate that the coarsest grains are found close to and farthest from the bed. The grain-size inflection above the surface is a characteristic of saltation in some natural environments (Draga 1983, Van Dijk, 1990; Greeley et al., 1996; van der Wal, 2000; Arens et al., 2002; and Xing, 2007, with important implications for numerical modeling of grain trajectories. Previously, only a few studies have reported vertically distributed grain-size characteristics for mass flux profiles.

Understanding how grain sizes in a saltating population vary with elevation is fundamental to physics-based modeling of the sand transport process, especially as numerical modeling relies on trajectory calculations. Recent models of terrestrial and extra-terrestrial dune processes also rely on models of the physics of aeolian transport at the levels of grains and grain trajectories (Andreotti, 2004; Duran and Hermann, 2006; Bourke et al., 2010) that subsequently drive dune-forming processes in different physical

conditions. Changing grain sizes will influence particle trajectories and transport rates and, in turn, modify the near-bed airflow. Saltation models developed over the last three decades typically contain four elements: calculations of 1) conditions for aerodynamic entrainment; 2) geometries of particle trajectories; 3) the dynamics of grain-bed collisions; 4) the physics of particle-wind feedback (Anderson and Haff, 1986; Anderson et al., 1991; McEwan and Willetts, 1991; Namikas, 2003; Spies and McEwan, 2000; Andreotti, 2004; Kok and Renno, 2009). When combined, these elements represent the self-limiting saltation process from entrainment to equilibrium. Vertical size-sorting has implications for all four elements in a modeling context. However, testing the models requires direct observations of both the distribution of the fluid shear stresses or wind profiles that force the transport, and the consequent distribution of the saltating grain population (the vertical flux profile) above the surface.

5.1.1 Theoretical controls on saltation trajectories

Establishing a physical rationale for the presence of the inflection is problematic. The dynamics of saltation are complex and contradictory findings on the physical controls of grain trajectories have been reported from different studies. Whether the ambiguity stems from different theoretical approaches or from experimental designs and methodology is difficult to discern. However, at the most fundamental level we know that grain trajectory is controlled by the launch velocity (speed and angle) and the acceleration of the grains by the wind. The lift and Magnus forces can be ignored without serious error and the grains in flight are assumed to be influenced mainly by gravity and the drag of the wind (Hunt and Nalpanis, 1985; Anderson and Hallet,1986; Werner, 1990). If all grains leave the surface at the same velocity, then larger grains should move higher in the wind profile. This is because the drag force on the grains is a function of its surface area, assumed to be proportional to the radius squared. The inertia of a grain is proportional to its radius cubed. Therefore the ratio of drag force to inertia becomes smaller for increasingly larger grain sizes. This requires that larger grains must travel higher and farther than smaller grains if their launch velocities are the same.

Bagnold (1935, his figure 5) was the first to apply this reasoning when describing the characteristic trajectory of different sized grains moving in air. His argument describes the grain-size distributions by assuming that the initial lift-off velocities of the grains are equal. However, it is known that a wide range of lift-off velocities can occur although there is no consensus on what the distribution of these velocities should be. For example, the range of particle liftoff velocities has been described using distributions that include *normal* (Anderson and Haff, 1988, 1991; Sørensen 1991; Nalpanis et al., 1993; Zhu et al., 2001), *log-normal* (Nalpanis et al., 1993), *exponential* (Sørensen, 1985; Raupach 1991, Zou et al., 1992; Anderson and Hallet, 1986; Dong and Liu, 1997; Sun and Wang, 2001, Dong et al., 2002; Xie and Zheng 2003), and *gamma* (Anderson and Hallet, 1986; Cheng et al., 2006). The disagreement is partly because of the difficulty in obtaining reliable measurements of trajectories near the bed where the largest concentration of flux occurs. We still do not fully understand the controls of lift-off velocities because of the complicated nature of grain impacts and ejections (Xing and Guo, 2004; Cheng et al., 2006; Feng et al., 2009; Kok and Renno, 2009; Kang and Liu, 2010). There is no robust model that explains how a naturally mixed-sand population moves once the threshold shear velocity is exceeded for all available grain sizes. One approach to addressing this difficultly is to use a combination of numerical modeling and sets of observed vertical flux measurements to deduce what the launch parameters must be, at least in aggregate. The vertical grain size-sorting data and flux data provided in this study provide one such opportunity to the modeling community.

5.1.2 Possible explanations for observed saltation trajectories

Bagnold (1935) argued that larger grains can travel higher, and longer, paths than finer grains provided both have the same launch velocity. Using this logic, it is equally valid to assume a uniform decrease in grain-size with elevation would be caused by larger grains leaving the bed with smaller velocities than finer grains. Namikas (2006) built on this this argument to develop and test his conceptual grain-bed collision model with vertical flux profiles collected in the field. His results suggested that the coarse

fraction of moving sand is restricted to near-bed elevations and with greater finer fractions moving at higher elevations. Similar fining upward trends were reported in Jensen et al. (1984) and Chen et al. (1995). Intuitively, we would expect this trend to occur as the inertia of the larger grains would make it more difficult for them to attain the same launch velocities of smaller grains. There should be a higher probability that more, larger grains will move as reptation rather than saltation. For this reason the transport population should have most of the larger particles close to the bed. This is commonly reported for mixed grain populations and in agreement with our observations. However, above the inflection zone described above, there is a coarsening of mean grain-size with elevation (see Figure 4.3A-C). This requires that coarser grains must have higher launch velocities to those of than finer grains. The mechanism for this is unclear.

Bagnold (1941), Sharp (1964) and Namikas et al. (2009) found that grains rebound higher and farther off bed with coarse texture. Namikas et al. (2009) conclude that surfaces comprising finer sands extract more energy from the moving grains through the mechanism of bed deformation, which reduces the impact energy available for grain rebound or ejection. This argument cannot be applied to the profiles gathered at Cow Splat Flat, *sensu stricto*, as the mean flux profiles exhibited very similar behavior despite having different bed compositions (Figure 4-3D). However, this coupling between bed deformation, collision dynamics, and grain rebound and ejection may explain some of the differences between the characteristic grain-size profiles at Cow Splat Flat and the Beach (Figure 4-3D). The beach experiments were carried out on a foreshore with sediments that were wet and immobile during our trapping experiments. The sand streamers that originated from the dry berm crest did not exchange sediment with the wet foreshore and there was no visible bed deformation (see Figure 3-2B). In contrast, the bed surface at the CSF locations was dry and there was active exchange of grains between the surface and saltating populations. The Beach profiles indicate that a larger proportion of the coarsest fraction of the grain population is moving at higher elevations above the bed than at CSF. These observations support the findings of

McKenna-Neuman and Scott (1998) who found that surface moisture impacts saltation by facilitating the formation of a hard surface, resulting in increased saltation heights and trajectory lengths as particles retain a higher proportion of their impact energy. Nield and Wiggs (2011), in their field experiments, also found that grains had higher trajectories above wet surfaces than for dry, rippled sand surfaces.

Visual inspection of the grain-size data depicted in Figure 4-2 suggests that there are also differences in sorting, skewness and kurtosis at different elevations. There have been few studies attempting to quantify such changes. Williams (1964), in his studies with symmetrically distributed sands, found that sorting decreased (i.e., improved) with height, while there was very little vertical variation of skewness. Li et al. (2008) examined changes in sorting with height, also finding that it improved with elevation. In the only other field study that we are aware of, van der Wal (2000) found that there was no statistically significant, vertical difference in the standard deviation, skewness or kurtosis of her trapped sands. A *t*-test was performed on data from different heights and found significant differences ($P \leq 0.01$) in the sorting and kurtosis of sands caught in Traps 1, 2, and 3 compared to those caught in Traps 6. Changes in sorting between Traps 2 and 3 and Traps 6 were more subtle ($P \leq 0.05$), but there was no statistically significant difference in sorting between traps 1 and 6.

It was mentioned before that grain size data such as those presented here could be used to support numerical modelling as a means to deduce some of the complex relationships that control grain trajectories. This supposition is supported by preliminary work of Kok (*pers. comm.*), who used a sub-set of the data presented in Table 4-1 and the model described in Kok and Renno (2009) to reproduce vertical grain-size distributions similar to those shown in Figure 4-2, including the distinctive inflection point. The results from these preliminary applications are encouraging and validate a coupled approach to modelling the vertical distribution of the different grain-size fractions of a mobile sediment population.

5.2 Vertical distributions of mass flux

Most research on vertical mass-flux profiles assesses either the rate of decay of saltation above the mobile bed or the environmental controls that influence the flux distribution. Wind tunnel studies have been successful in elucidating the influence of controls such as grain size and wind speed on characteristics of flux profiles. The results described in this research provide strong empirical evidence that the vertical distribution of mass flux is best described using an exponential decay function. In a comparison test using 305 vertical mass flux profiles obtained from 31 different studies, from field and wind tunnel-based experiments, the exponential fit was superior 89% of the time, compared with curve fits calculated using power or logarithmic functions. Rasmussen and Mikkelsen (1998) criticize this approach of using an analytical expression, such as an exponential function, to extrapolate a flux profile to the bed using flux measurements from a few prescribed locations away from the bed. This approach assumes that there is no change in flux gradient as one approaches the bed, and the model becomes bias towards flux measurements that are a small fraction of the total. Weinan (1996) found that the magnitude of flux predicted by the power function approaches infinity as elevation approaches zero which, physically, is not reasonable. Butterfield (1999) criticized using the exponential function curve fitting approach to model vertical flux distributions. He found that the relationships, using the exponential function, (i) are not well constrained by flow variables; (ii) become increasingly uncertain at wind speeds near threshold; and (iii) have parameters that cannot be easily determined in any '*a priori*' way. These reasons, in essence, provide strong theoretical validation to test the Rouse profile approach for saltation in air. The Rouse profile, well accepted in describing concentration profiles for sediments in water and fine sediments (dust) in air, includes the physical relationships that have been identified as controls on the character of the aeolian saltation layer. The Rouse profile is, therefore, more physically meaningful than current approaches that use standard curve fitting functions to fit to the vertical flux. Further, because it contains a shear velocity term, it can include boundary conditions for the application of the model depending on potential transport conditions.

Finally, the exponent in the Rouse model - the Rouse number - can be derived *'a priori'* based upon environmental conditions.

The high regression coefficients for the functions fitted to the vertical flux distributions suggest that an equilibrium flux profile existed during all the runs. From the arguments of Namikas (2003), this indicates first that there was a common process (saltation) driving the grain-size distributions across the entire range of transport rates observed. Second, it can be inferred that there was a relatively stable probability distribution of particle trajectories and lift off velocities (after Dong et al., 2004). The results suggest that the sample durations of the field experiments were sufficiently long to average out most of the small-scale spatial and temporal variability normally observed in the field. Finally, the protocol to analyze mass flux profiles described in Ellis et al. (2009) has now been verified using three vertical flux datasets measured in field experiments: Guadalupe (1996), Namikas (2003) in their research paper and Brazil (2008) described herein.

5.2.1 Field observations *vs.* wind tunnel simulations

The rates of exponential decay measured in field and wind tunnel experiments are statistically different – especially for small wind tunnels, defined here as a cross section <0.25 m^2 compared with larger wind tunnels and field environments. This infers, most likely, that these small wind tunnel dimensions do not permit the saltation layer to grow vertically. The differences between the flux profiles measured in larger wind tunnels and field environments are more difficult to substantiate. The same argument attributing differences to wind tunnel constraints is still valid as previous work has illustrated that all wind tunnels can affect the fundamental interaction between the wind and sand systems. Sherman and Farrell, (2008) examined the saltation-enhanced roughness length calculated from 291 wind profiles, measured in wind tunnels or in the field, for conditions where sand transport occurred. They found that the field roughness, which is a manifestation of the saltation layer, was about an order of magnitude larger in the field than in the laboratory. This is tangible evidence that the heights of grain

trajectories are either suppressed in the wind tunnel or exaggerated in the field. They attributed the differences to the constraints on the development of coherent turbulent structures in the wind tunnel relative to field environments. Similarly, Mikami et al., (2005, p.2) note that "*the turbulent structures within a wind tunnel is not a natural condition because of the size limitations of the width and height of the tunnel. In such a condition the saltation structure does not well represent the natural saltation that is heterogeneous in nature*". This argument endorses the conclusions of Sherman and Farrell (2008). It also advocates that vertical mass flux profiles measured in controlled wind tunnel studies with uniform particle sizes may not be representative of natural, or heterogeneous, processes measured in the field. Whether or not this provides explanatory power to explain the differences between the field and wind tunnel results is arguable.

An important implication of the results – that distributions of flux are different in wind tunnel and field environments – is that many numerical models have been tested and/or calibrated using results from small wind tunnels. Data from small wind tunnels, used for the development and training of numerical and abstracted models, introduces potentially large sources of error (Sauermann et al., 2001; Hatano et al., 2004; Dong et al., 2006; Xing, 2007 and Zheng et al., 2004). There is less concern with larger wind tunnels, but ultimately the optimal testing and calibration of models would compare field derived relationships with field data.

5.2.2 Controls on the vertical distribution of mass flux

The two primary environmental controls on the form, or character, of the vertical mass flux profile are shear velocity and grain size. Increasing shear velocity increases the proportion of flux moving at higher elevations and the distribution profile becomes flatter. Conversely, as shear velocity decreases, less flux is moved to higher elevations and the profiles become steeper. The results from this research partly confirm previous findings that there are well defined controls of shear velocity on the characteristic slope of the vertical flux profiles. These relationships, not surprisingly, are better defined in

controlled wind tunnel studies where the researcher has physical control of the important variables of the transport system and can test a wider range of transport conditions. As shear velocity, or wind speed, decreases the flux decreases more rapidly which results in a steeper rate of decay. The flux profiles of Hotta and Horikawa, (1993); Weinan et al., (1996); Butterfield (1999); Dong et al., (2002); Ni et al., (2002); Dong et al., (2004b); Hotta et al., (2006); and Liu et al., (2006), plotted in Appendix A, all exhibit this behavior. Similarly, decreasing grain size causes the flux profile to steepen. This was observed in the field experiment (Brazil, 2008) and also reported in the wind tunnel studies of Dong et al., (2002), Ni et al., (2002), Liu and Dong (2004), Hotta et al., (2006) and Dong et al., (2006), which are presented in Appendix A. Both these variables, shear velocity and grain size, are incorporated into the Rouse model though the exponent (Equations 3 and 4). This makes the Rouse approach an appealing line of enquiry to test for aeolian saltation. Further, the results of grain size controls indicate that coarser grains move higher up in the profile, resulting in flatter slopes. However, field studies are also important to understand how mixed grain populations behave. Understanding the behavior of different grain size populations, manifested as a saltation layer, is paramount to be able to apply saltation models to field applications.

5.3 The Rouse model

The vertical flux profiles measured for aeolian transport were adapted to Rouse profiles using the method described in Section 3, Subsection 3.7. The results are presented in Section 4, Subsection 4.4. The Rouse model performed very poorly in replicating the vertical distributions of the observed flux. The shapes of the distributions were distinctly L-shaped (Figure 4-14), indicating that the predicted mass fluxes did not extend higher than the reference elevation, designated as the elevation of the bottom trap. This is physically implausible and must be considered a point-of-failure if the Rouse model is to be considered in applications of aeolian saltation. Testing numerical saltation models relies on direct observations of both the distribution of the fluid shear stresses or wind profiles that force the transport, and the consequent distribution of the

saltating grain population (the vertical flux profile) above the surface. Without an appropriate, physically representative, vertical distribution of mass flux, the modeled flux profiles using a Rouse type approach cannot be used as input to test the numerical models.

Another concern is the prediction of the magnitude of flux derived from the Rouse model. Overall, the field and wind tunnel Rouse profiles consistently underestimated the observed flux: averaging 38% and 33% of the observed flux, respectively. Ellis et al., (2012) evaluated the spatial and temporal variations in the magnitude of fluxes caught in different traps that were located within meter scales of one another. They found, using data collected from a field experiment (Brazil, 2008) and from published experiments (Gares et al., 1996; Jackson et al., 2006), that fluxes can differ by up to 100% even over these small spatial scales. They state "(O)*ur results indicate that, because of the horizontal variability in transport rates, studies using transport rate measurements made at only one point should commonly expect mismatches between observations and predictions of the order of 100%, assuming all other variables are perfectly represented and measured* (p.385)". The predicted fluxes of the Rouse profiles are within this acceptable range of error. This is not surprising as the Rouse profiles are based on the flux measured at the bottom reference elevation. Reported values of flux in wind tunnel studies suggest that the proportion of sediment moving in the near-bed region ranges from 80-90% below 2cm (Butterfield, 1993; Rasmussen and Mikkelsen, 1998); 75% below 1.3cm (Gillette and Walker, 1977) and 50% below 1cm (Chiu, 1972; Zingg, 1953) or 1.5cm (Gerety, 1984). However, despite the immediate failures of the Rouse model to aeolian transport systems, the very strong statistical relationships between the predicted and observed fluxes (Figures 4-15 and 4-16) warrants further investigation.

The shape of the Rouse concentration profile, which represents the distribution of sediment in the fluid, is controlled by the exponent, or Rouse number. The Rouse number relates sediment size (in the form of settling velocity, w_0) to shear velocity, u_*, and is expressed as:

$$R = \frac{W_0}{ku_*\beta} \quad (5\text{-}1)$$

where β is a constant of proportionality, typically assumed to be equal to 1. The input parameters required to calculate Rouse profiles are shown in Table 5-1 for five flux profiles from Feng et al., (2009) - are shown in Figure 4-14. As described before these Rouse profiles do not provide an accurate representation of the mass flux distributions. This is explained by the high values of the calculated Rouse numbers, ranging from 3.38 to 7.48, which, for a grain size of 0.35mm, are at least an order of magnitude higher than those commonly observed in water studies. The sensitivity of the Rouse number, and subsequently the shape of the Rouse profile, to the variability of input parameters (fall velocity (w_0), shear velocity (u_*), von Kármán *constant* (*k)* and the constant of proportionality, β) was investigated next.

Table 5-1. Input parameters to Rouse profiles for Feng et al., (2009).

	u_* (m/s)	D (mm)	w_0 (m/s)	z/H	Rouse Number (β=1)
Run 1	0.56	0.35	1.68	0.034	7.48
Run 2	0.81	0.35	1.68	0.032	5.17
Run 3	0.93	0.35	1.68	0.032	4.50
Run 4	1.12	0.35	1.68	0.032	3.74
Run 5	1.24	0.35	1.68	0.032	3.38

Fall velocity: The fall velocity used in the Rouse analysis was calculated using the results of research described earlier in Section 3.6. Equation 3-7 was derived after the valuation of results from five previous fall velocity studies (Bagnold, 1935; Wilson and Huang, 1979; Cui et al., 1983; Malcolm and Raupach, 1991; and Chen and Fryrear, 2001) that measured the fall velocity of sand sized particles falling in air. This relationship, which is statistically significant with a goodness-of-fit (r^2) of 0.88, was used to calculate the fall velocities in this research. These predicted fall velocities were compared with four other equations (Gibbs et al., 1971 (spheres); Gibbs et al., 1971

(natural sediment); Cui et al., 1983; and Baas, 2004) for a range of grain sizes 0.125 – 2.0 mm, representing fine to very coarse sands. The comparison between the predicted fall velocities are shown in Figure 5-1A. These fall velocities were used to calculate the Rouse numbers for an arbitrary chosen shear velocity of 0.50 m/s. The results are shown in Figure 5-1B. The differences in the calculated Rouse numbers are small for the range of grains sizes commonly observed in saltation studies, $D < 0.50$ mm. The range of Rouse numbers predicted from the four fall velocity equations have no impact on the shape of the Rouse profiles nor do they change the large under predictions of estimated transport rates.

Shear velocity: The shear velocity variable cannot be adjusted. We have to accept that any variability derives from measurement error, which should never exceed 5%. Readjusting the profiles by this error margin has no impact on the shape or magnitude of the Rouse profiles.

von Kármán constant (*k*): The value of the von Kármán is generally assumed to be a constant equal to 0.40. The extent to which this holds true for aeolian transport was evaluated by Li (2010) and Li et al., (2011) using the vertical flux data collected in Brazil (2008). They found an inverse linear relationship between the apparent von Kármán parameter and sand transport rate:

$$k_a = -3.028Q + 0.399 \quad (5\text{-}2)$$

where Q is the transport rate (kg/m/s). The impact of this predicted change in the von Kármán constant to the Rouse profiles was examined for the Brazil (2008) data. These results are described in Li et al., (2011). On average, the von Kármán constant decreased in value by 30% (Table 5-1). Again, this change did not have any significant impact on the predicted flux of the Rouse profiles (less than 1%). Clearly the variability of this paramter is not large enough to change the characteristics of the Rouse profiles.

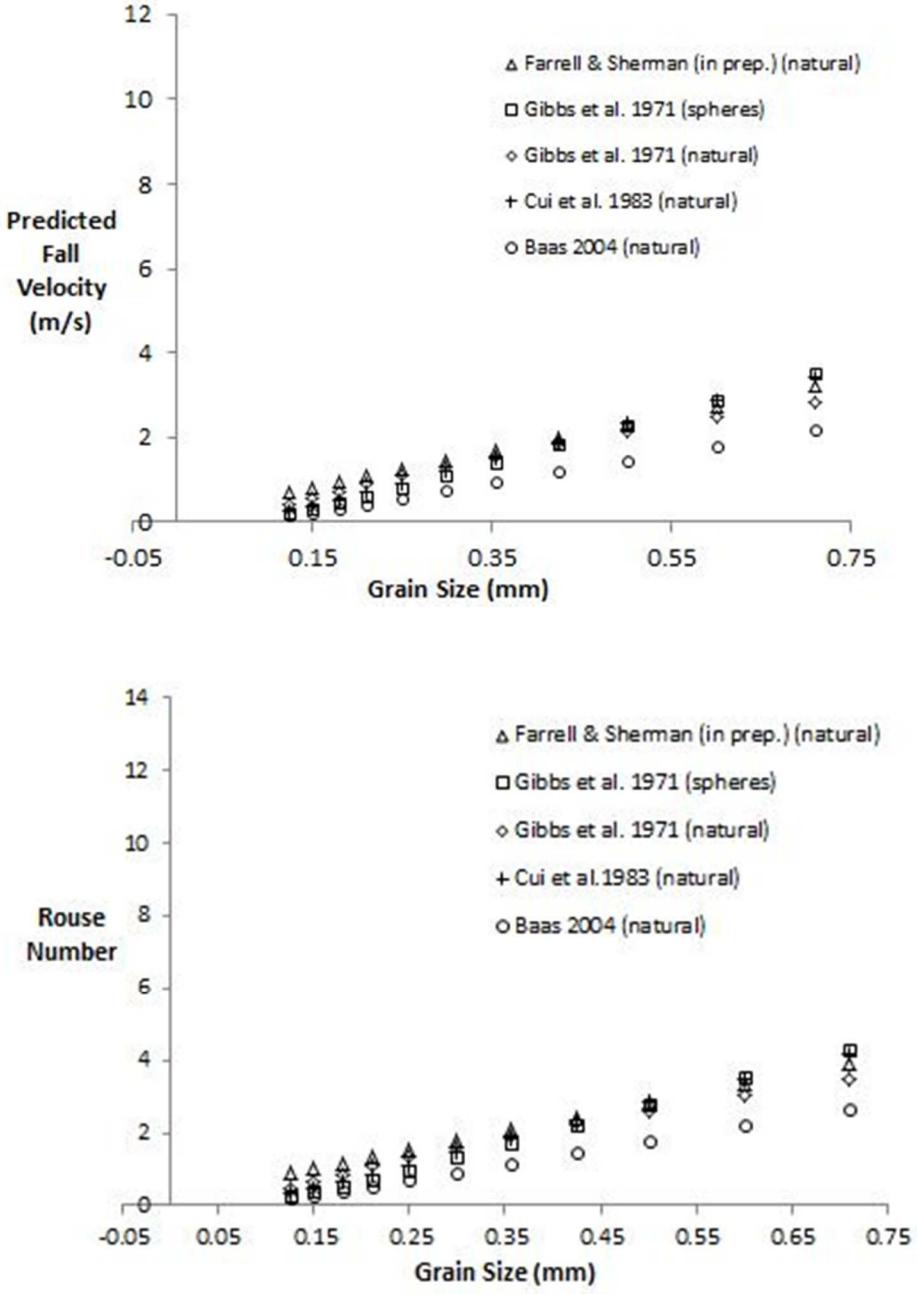

Figure 5-1. A. Comparison between predicted fall velocities of five equations for sand sized particles falling air. B. Comparison on Rouse numbers using different fall velocity equations and a shear velocity of 0.50 m/s.

Table 5-2. Predicted variability of the von Kármán constant based upon the inverse linear relationship between the apparent von Kármán parameter and sand transport rate.

	Run 1	Run 2	Run 3	Run 4	Run 5	Run 6	Run 7
Q (*grams*)	349.8	537.9	369.5	394	470.9	414.9	356.8
Q (*kg/m/s*)	0.029	0.045	0.031	0.033	0.039	0.035	0.030
k	0.40	0.40	0.40	0.40	0.40	0.40	0.40
k_a	0.31	0.26	0.31	0.30	0.28	0.29	0.31

	Run 8	Run 9	Run 10	Run 11	Run 12	Run 13	Run 14
Q (*grams*)	343	415.5	594.5	590.7	458.5	613.8	510.2
Q (*kg/m/s*)	0.029	0.035	0.050	0.049	0.038	0.051	0.043
k	0.40	0.40	0.40	0.40	0.40	0.40	0.40
k_a	0.31	0.29	0.25	0.25	0.28	0.24	0.27

The Schmidt number, β: The Schmidt number is the ratio of sediment diffusivity to fluid eddy diffusivity (viscosity). The number was introduced into the Rouse model in order to balance the upward turbulent diffusion of sediment and its settling rate, by assuming that the former process emulates the momentum transfer of the turbulent flow, which can be measured. This assumption implicit in the Rouse equation has been scrutinized by many workers in water research (Parker and Coleman, 1986; Gelfenbaum and Smith, 1986; McLean, 1992). In water, the two diffusivities are, reportedly, very close as the sediment travels with water. However, the Schmidt number is not 1.0 during aeolian salation. In air flow, the sediment diffusivity is greater than eddy viscosity during aeolian saltation. This results in a much higher value of β. Resolving values of the Schmidt number has been the focus of attention in water studies for decades where it is now accepted that the Schmidt number is not equal to 1.0 and is not constant (see Section 2.5.4) There are number of methods to calculate the value of the Schmidt number.

Method I

The most direct method to calculate the Schmidt number, β, is to derive it using temporally averaged concentration profiles and assume a Rouse concentration profile is an appropriate fit to the data (Rose and Thorn, 2001). The exponent of the power function fit ($y = x^b$) obtained by regression of the relative concentration on relative height is the Rouse number. The value of β can be easily resolved using the regression coefficient b, assuming that fall velocity (w_0), the von Kármán constant (k) and shear velocity (u_*) are known, where:

$$\beta = \frac{w_0}{k u_* b} \tag{5-3}$$

There are two major obstacles in applying this method to aeolian vertical flux profiles.

1. For aeolian studies, a major problem in trying to calculate the Schmidt number using the measured flux profiles is that a flow depth, or, in this case, a boundary layer height is required. In water studies the flow depth is easily determined. For aeolian studies it much more difficult to determine *a priori* the upper and lower limits of the boundary layer. Physically, the limits of the boundary layer are defined by the region where the Law of the Wall can be applied and there is constant stress with elevation. One approach workers have used to identify this region and establish a boundary layer height is by post processing the velocity data and identifying the range of points in the velocity profiles where the log law is appropriate. This usually means discarding points closest to the bed, where the presence of a saltation layer hinders the application of the log law (Bauer, *in press*).
2. The Rouse model was developed to describe the vertical distribution of concentration of sands, silts and clays moving by suspension in water. *Concentration is defined as the volume of sediment per total volume of material* (fluid + sediment). For aeolian studies, sediment transport is usually reported as a mass flux. *Mass flux is defined as the mass of sediment caught per unit area per unit time*. One approach to resolve this is to convert the mass flux rate to an equivalent concentration by calculating the volume of air passing through each

trap. In order to do this, the velocity profile needs to be accurately measured in order that the Law of the Wall to be applied. However, this approach is complicated because the Law of the Wall is not valid closest to the bed where the most sediment is moving. It becomes a complex series of theoretical and methodological problems to resolve this issue that are beyond the scope of this research. However, it should be noted that the Rouse model is based upon a normalized concentration. The concentration at each elevation is expressed as a ratio of the maximum concentration, defined as the highest concentration (equal to 1.0) observed nearest the bed. Similarly, the steps outlined in Section 3.4 illustrate how aeolian mass flux profiles can be normalized by converting the absolute quantity of sand captured in each trap to a percent relative to the total trapped (equal to 100%) for each run. The normalized mass flux profiles approach can be easily adapted to equivalent concentration-type ratios by converting the percentages to fractions of 1.0.

By resolving the challenges of estimating a boundary layer height and an appropriate representation of the relative transport at each elevation, then the Rouse equation can be applied to solve for β by fitting a power function, of the form $y = ax^b$, to the relationship:

$$\frac{C_z}{C_a} = \left(\frac{h-z}{z}\frac{a}{h-a}\right)^{\frac{w_0}{ku_*\beta}} \quad (5\text{-}4)$$

The slope of the fit (b) can be used to solve for the Schmidt number, β as long as the values of fall velocity (w_0), the von Kármán constant (k) and shear velocity (u_*) are known.

Method II

Another method to derive a value of the Schmidt number is described in Li (2010) who examined the variation of the von Kármán parameter based upon the stratification effects of the air-sediment mixture density gradient, which were adopted from the protocols of the thermally stratified atmosphere. He used a Richardson number approach and Law of the Wall stratification correction parameter (Φ_m) to quantify the vertical mixing and turbulence characteristics observed in sediment laden flows. Using

mathematical treatments, he derived relationships between important fluid-boundary correction parameters (κ_a and Φ_m) and Richardson numbers (R_i and R_f) in sediment laden flow:

$$\Phi_m = \frac{k}{k_a} = \frac{1}{1-\lambda R_f} = \frac{1}{1-\beta\lambda R_i} \quad (5\text{-}5)$$

where k_a is the apparent von Kármán constant, λ is the damping coefficient, R_f and R_i are the density-flux and density-gradient Richardson numbers within the saltation layer, respectively, and β is the Schmidt number. Here, R_i represents the sedimentological stratification effect due to a mixture density gradient, which is was deemed analogous to stably thermal stratification in the atmospheric boundary layer.

Li (2010) tested this approach on vertical aeolian flux profiles collected in the Brazil experiment (described herein) and found β =11.22. However, he was also forced to make a number of assumptions regarding the treatment of the wind velocities within the saltation layer to describe concentrations. This approach requires direct measurement of the instantaneous streamwise and vertical fluctuation components (u' and *w'*), the velocity profile and the vertical mass flux profile. Until such time as we can correctly parameterize the velocity profile from the surface of the mobile bed, through the saltation layer and into the free stream then this method is not attractive.

5.3.1 Re-analysis of aeolian flux profiles to obtain values of the Schmidt number

The aeolian vertical mass flux profiles were re-analyzed using Method I to derive values of the Schmidt number. The height parameter (*h*) was designated as the highest reported elevation where flux was caught in each run. The normalized mass flux data were converted to equivalent transport flux ratios based upon the total transport equal to 1.0. For example, if the normalized transport sampled at elevation *z* (q_z) equals 40%, the equivalent transport flux ratio is 0.40 or, q_z/Q_{total}, where Q_{total} = 100%. The sampled elevations were converted to equivalent reference elevations using the same approach as the Rouse model:

$$\left(\frac{h-z}{z}\frac{\frac{a}{h}}{1-\frac{a}{h}}\right) \quad (5\text{-}6)$$

where a/h is the reference elevation, h is the maximum sampled elevation and z is sample elevation. The Rouse number was derived by obtaining the slope from fitting a power regression to each run. The values of β were then calculated using Equation 5-3. An example of this approach outlining each step is provided next using five runs from Feng et al., (2009). The two most important considerations are to assess if the ***shape*** and ***magnitude*** of the Rouse profiles provide accurate representation of: (i) the vertical distributions of mass flux for different environmental conditions, and (ii) provide accurate estimates of total transport rates compared with the observations.

Step 1. Plot the relative elevation *vs.* the converted mass flux ratio. The relative elevation is similar to the method used to represent elevation in the Rouse model, where h = maximum sampled elevation, a = elevation bottom trap and z = elevation. The mass flux is converted to a ratio by dividing the mass flux at each elevation (q_z) by the total flux (Q_{total}). The first five runs of Feng et al., (2009) are shown.

Step 2. Fit a power function to the data to obtain the slope coefficient, where $y = ax^b$. The results of the regression analysis (a and b coefficients and the goodness-of-fit, r^2) for each run are shown in the inset table.

Step 3. Calculate the value of β, based upon the fall velocity (w_0), the shear velocity (u_*), and the slope (b) of the power function using Equation 5-3. The values of β are shown in the inset table for each run.

Step 4. Re-plot the Rouse profiles by using the derived value of β to adjust the values of the Rouse number. For comparison the original Rouse profiles derived using β =1 to calculate the Rouse numbers are also shown (Figure ??A). These profiles have the characteristic L-shapes. These profiles are re-plotted using the β values derived from Step 3 (Figure ??A).

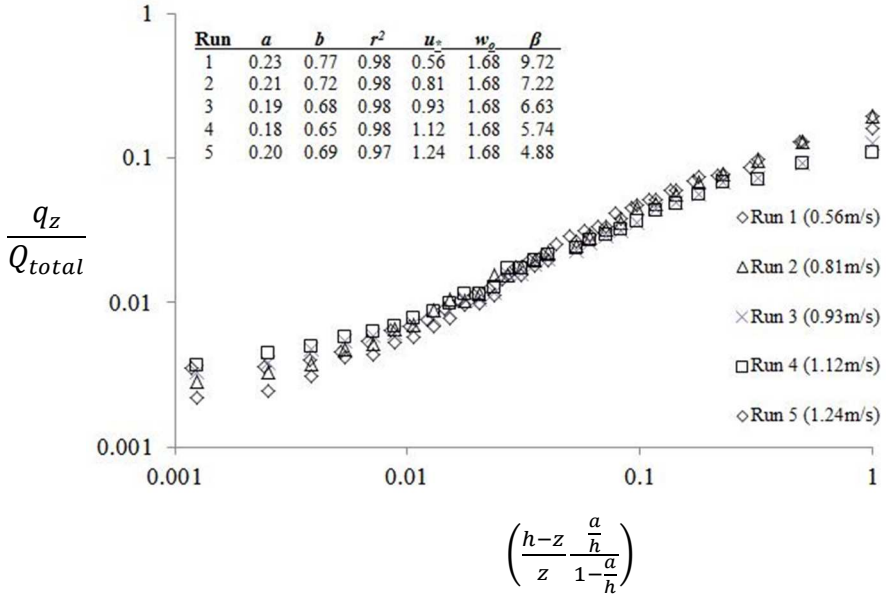

Figure 5-2 Adapting the vertical mass flux profiles in aeolian transport to Rouse-type relationship.

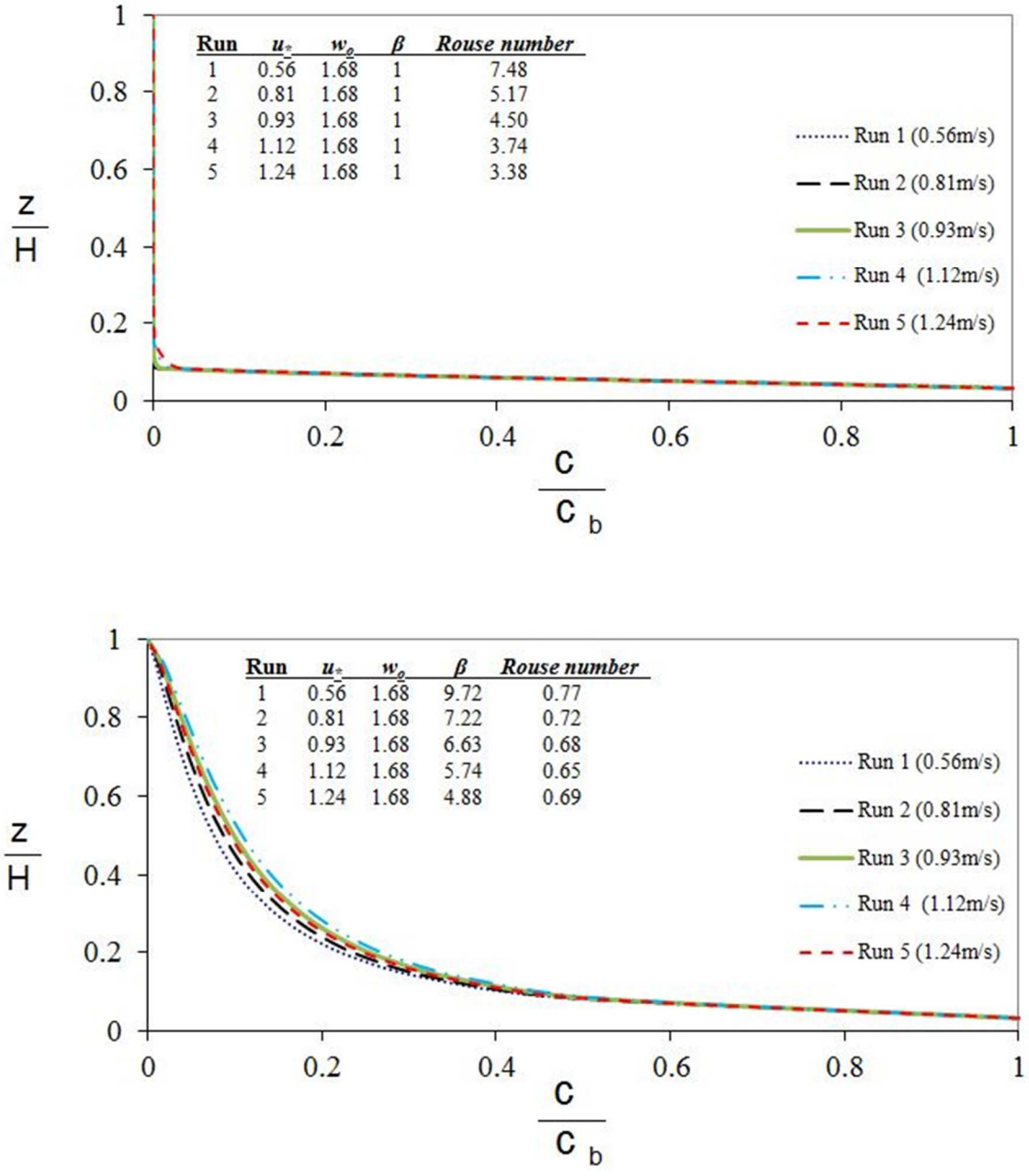

Figure 5-3: The predicted distributions of mass flux using the Rouse model for β =1 and the adjusted, variable β values based on the slopes of the flux profiles.

Step 5. Compare the predicted *vs.* observed transport rates. The predicted transport rates from the profiles using β =1 are shown (in blue) below for the first 5 runs of Feng et al., (2009). These profiles have no sediment moving above the reference elevation and, therefore, under predict the observed transport rates by 81% (on average). The predicted transport rates of the adjusted Rouse profiles (in red), using the variable Schmidt number values described in Step 3, predict transport rates much closer to the observed transport rates, within 39 % (on average).

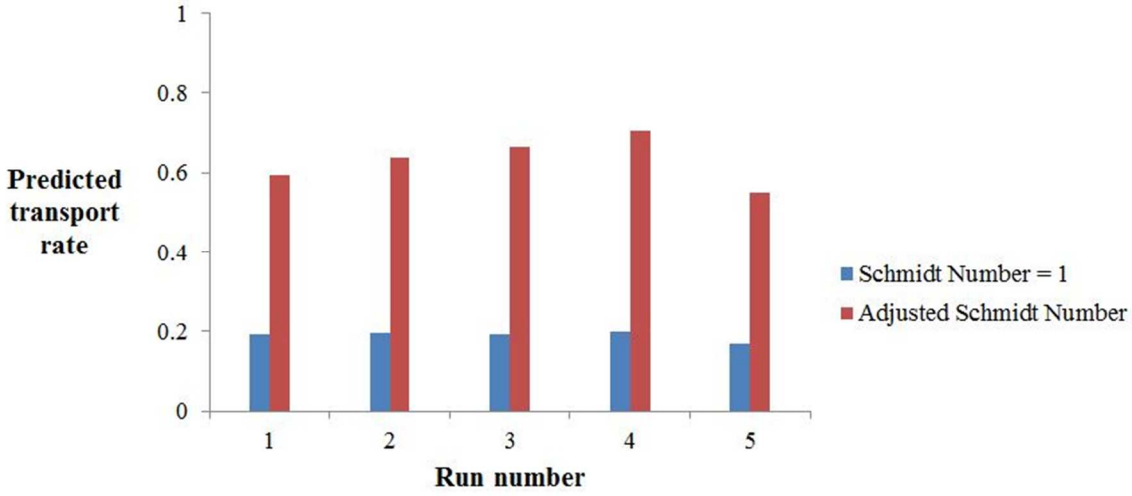

Figure 5-4: Comparison between the predicted transport rates using the Rouse model for β =1 and an adjusted β based on the slopes of the vertical flux profiles.

Step 6. Compare the shapes of the profiles. In order to compare the predicted flux distributions, the aeolian vertical flux profiles were re-constructed using the distributions predicted by the Rouse model for β =1 and then the adjusted β values from Step 3 . The only inputs to construct the profiles are (i) the magnitude of observed flux at the reference elevation, and (ii)

the maximum sample height. For comparison purposes the predicted distributions for β =1 are shown in Figure 5-5 It is clear that these profiles do not accurately reflect the observed distributions (profile slopes). Conversely, the adjusted Rouse slopes (Figure 5-5), based on the derived value of β, have very similar shaped distributions to the observed profiles.

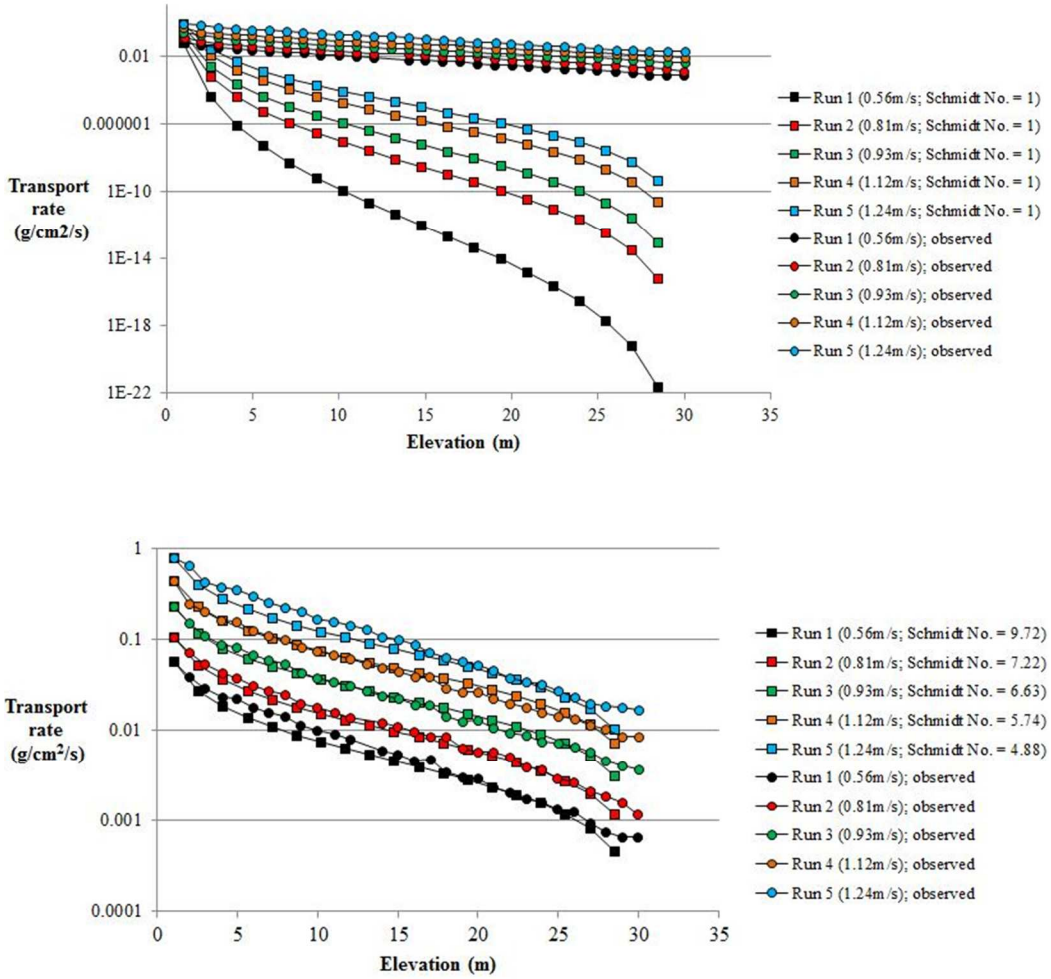

Figure 5-5: Reconstructing the vertical mass profiles using the predicted distribtuions of the Rouse model for β =1 (top) and an adjusted β based on the slopes of the vertical flux profiles (bottom).

5.3.2 What value of β should be used?

Steps 1-6 described above contain a circular argument. The adjusted values of β were obtained from regression analyses on the observed vertical mass flux profiles. Therefore, the slope values obtained from the fitted power functions (*b*) are based upon a prior knowledge of the vertical flux distribution. It should be no surprise then, that the Rouse approach provides accurate representations of the observed vertical flux profiles. However, in order for the Rouse approach to be of practical use it is necessary to know *a priori* the value of β. Many previous workers have tried to resolve this issue for different experimental conditions on water. Teakle and Nielsen (2004) report that, despite the wide range of reported values of β, "*a universally observed feature is the strong dependence … of β on the ratio, w_0/u_** (p.1)". This relationship was explored for the aeolian mass flux profiles described in this research.

5.3.3 The relationship between β, fall velocity and shear velocity

The variability of the Schmidt number was examined to investigate its dependency on the fall velocity and shear velocity parameters. Clearly, there is a mathematical relationship whereby increasing the fall velocity, which appears as the numerator, results in a subsequent increase in the value of β. Conversely, increasing the shear velocity, which appears in the denominator, results in lower values of β. The sensitivity of the values of β to these changing environmental conditions is investigated here.

Figure 5-6A shows the dependency of β with shear velocity and fall velocity for field studies. The shear velocity correlation is much stronger than fall velocity. However in two of these experiments, Greeley et al., (1996) and Namikas (2003), the reported grain size did not change. Therefore any changes in β are, in these cases, contributable to changes in shear velocity. Subsequently, both these studies have very strong correlations between β and shear velocity, with r^2 of 0.98 and 0.93, respectively (Figure 5-6C). There is no dependency of β on shear velocity for the Brazil (2008) data (r^2 = 0.08). However,

there is a very strong dependency of β on the fall velocity in this dataset (r^2 = 0.79) (Figure 5-6E).

Similar patterns are seen in the wind tunnel studies. The values of β in experiments with uniform grain sizes have a very strong dependency on the value of the shear velocity. Conversely, experiments with variable grain sizes have lower correlations with shear velocity. Table 5-2 shows the results of linear regressions (β regressed on shear velocity) for wind tunnel experiments with four runs or more. The r^2 values are all 0.89 or higher except for two experiments: Hotta et al. (2006) and Ni et al. (2002). It is hardly a coincidence that these two studies were the only ones that used variable grain sizes. However, unlike Brazil (2008), the dependency of β on grain size in these experiments is weak (Figure 5-6E) with r^2 values of 0.24 and 0.28, respectively. The strength of these correlations improves from the reported values if the data are segregated by grain size. For example, if the Ni et al (2002) data are analyzed using two different datasets, based upon the two reported grain sizes (d =*0.17* and 0.35 mm), the r^2 values are 0.85 and 0.79, respectively.

The evidence here suggests that shear velocity plays a more important role than grain size, for which fall velocity is a surrogate, in determining the value of β. However this requires further investigation as the results from the Brazil (2008) field experiments show an opposite trend. These results establish that both parameters impact the value of β. It was therefore deemed appropriate to assess the variability of β on the ratio w_0/u_*.

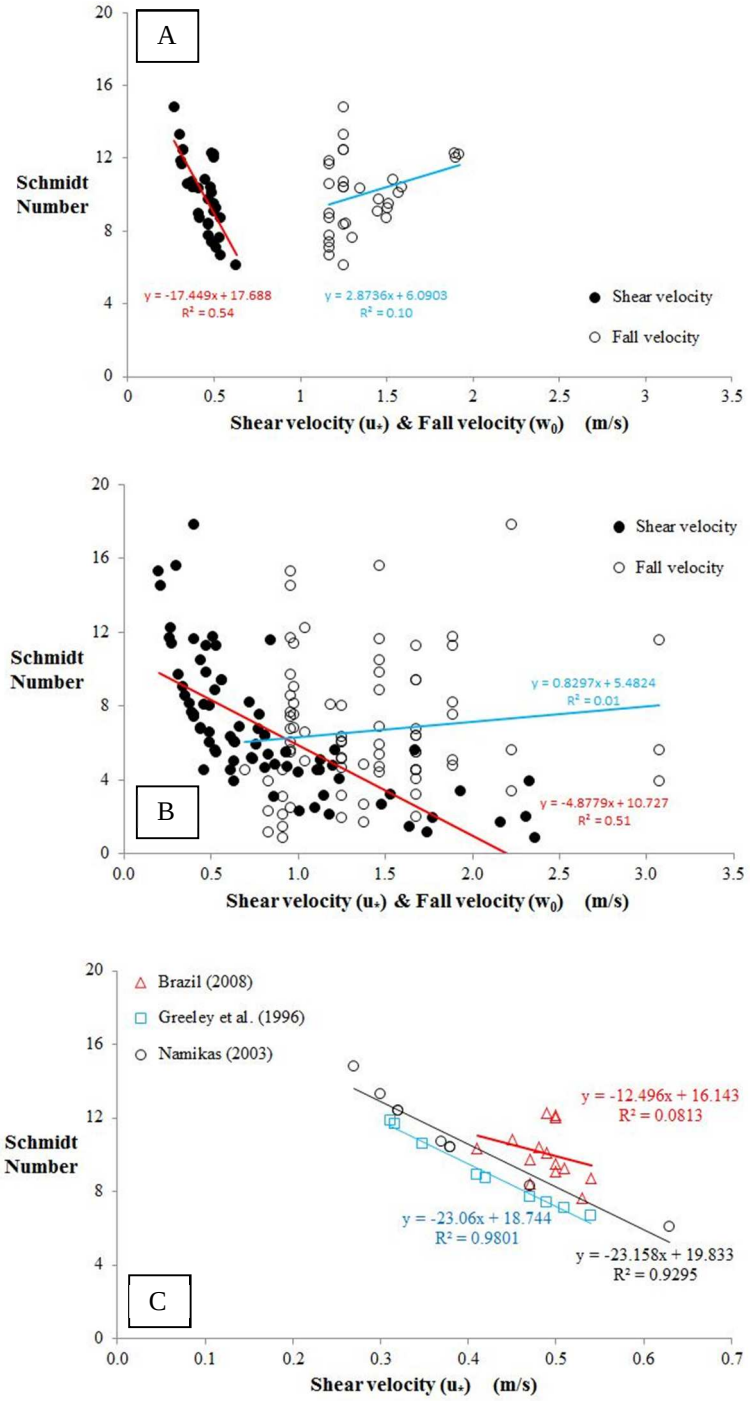

Figure 5-6. Variability of β: with (A) shear velocity and fall velocity for all field studies; (B) shear velocity and fall velocity for all wind tunnel studies; (C) shear velocity only for field studies; (D) shear velocity only for wind tunnel studies; (E) studies with variable grain size.

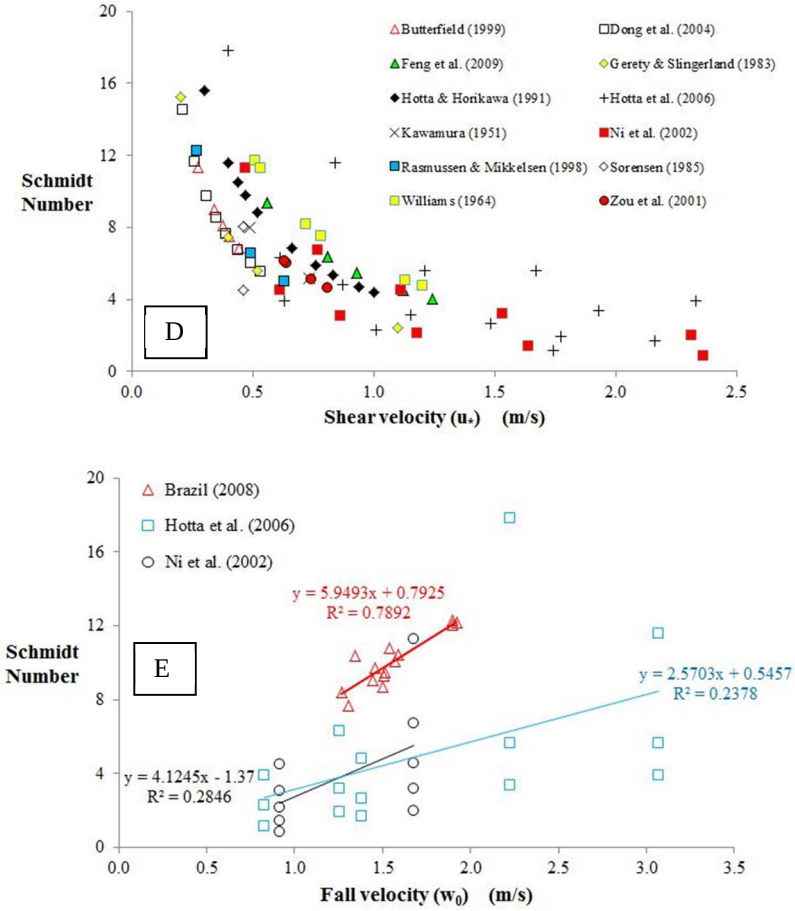

Figure 5-6 continued.

Table 5-2 Results of linear regressions using data in Figure 5-6D showing dependency of β on shear velocity for wind tunnel experiments with four or more runs.

Source	*a*	*b*	r^2
Butterfield (1999)	-26.84	18.38	0.98
Dong et al. (2004)	-26.59	18.69	0.93
Feng et al. (2009)	-8.11	13.45	0.95
Hotta & Horikawa (1991)	-14.03	-4.38	0.89
Hotta et al. (2006)	-4.38	10.84	0.36
Ni et al. (2002)	-3.44	8.38	0.54
Williams (1964)	-9.82	16.05	0.95
Zou et al. (2001)	-8.12	11.20	1.0

Table 5-3. Details of shear velocity, fall velocity, regression coefficients and goodness of fit, and the adjusted β values from Steps 1-3. Three values of β are listed: β_1 is the assumed value of $\beta = 1$; β_2 is the adjusted β from Steps 1 – 3; and β_3 is the modeled β based upon the β_2 relationship with the w_0/u_* ratio. The predicted transport, as a fraction of 1.0, using each approach is given as q_1, q_1, and q_3.

	Run	Label	u_* (m/s)	D (mm)	w_0 (m/s)	a	b	r^2	β_1	β_2	β_3	q_1	q_2	q_3
Brazil (2008)	Run 1	10/22 - run 1	0.54	0.309	1.503	0.621	0.593	0.90	1	11.74	8.71	0.41	1.08	0.74
	Run 2	10/22 - run 3	0.47	0.253	1.266	0.787	0.722	0.94	1	9.33	8.41	0.49	0.99	0.88
	Run 3	10/22 - run 4	0.53	0.262	1.304	0.919	0.674	0.86	1	9.13	7.65	0.57	1.26	1.02
	Run 4	10/24 - run 1	0.49	0.325	1.570	0.785	0.698	0.88	1	11.48	10.09	0.49	1.03	0.88
	Run 5	10/24 - run 2	0.5	0.311	1.511	0.836	0.724	0.91	1	10.43	9.49	0.47	0.95	0.85
	Run 6	10/24 - run 3	0.5	0.296	1.448	0.887	0.781	0.91	1	9.27	9.08	0.48	0.90	0.88
	Run 7	10/24 - run 4	0.47	0.298	1.456	0.929	0.793	0.84	1	9.77	9.74	0.47	0.86	0.85
	Run 8	10/24 - run 5	0.45	0.318	1.541	0.809	0.715	0.92	1	11.97	10.81	0.48	0.98	0.87
	Run 9	10/24 - run 6	0.51	0.31	1.507	0.853	0.757	0.93	1	9.76	9.27	0.52	0.99	0.93
	Run 10	10/26 - run 1	0.48	0.329	1.587	0.670	0.609	0.89	1	13.58	10.43	0.30	0.74	0.54
	Run 11	10/26 - run 2	0.41	0.272	1.346	0.840	0.718	0.83	1	11.43	10.35	0.33	0.68	0.60
	Run 12	10/30 - run 1	0.5	0.403	1.900	0.585	0.529	0.88	1	17.96	12.04	0.37	1.12	0.68
	Run 13	10/30 - run 2	0.5	0.408	1.921	0.555	0.503	0.85	1	19.10	12.18	0.35	1.13	0.64
	Run 14	10/30 - run 3	0.49	0.402	1.896	0.559	0.507	0.87	1	19.08	12.27	0.35	1.11	0.63

	Run	Label	u_* (m/s)	D (mm)	w_0 (m/s)	a	b	r^2	β_1	β_2	β_3	q_1	q_2	q_3
Greeley et al. (1996)	Run 1	1 (2)	0.312	0.23	1.169	9.051	1.980	0.99	1	4.73	11.86	0.31	0.52	1.29
	Run 2	2 (4)	0.317	0.23	1.169	1.041	0.778	0.96	1	11.84	11.67	0.34	1.06	1.04
	Run 3	3(6B)	0.42	0.23	1.169	0.681	0.580	0.95	1	12.00	8.71	0.31	1.26	0.87
	Run 4	4 (3)	0.348	0.23	1.169	0.752	0.608	0.95	1	13.80	10.59	0.31	1.21	0.89
	Run 5	5 (1A)	0.47	0.23	1.169	0.783	0.618	0.96	1	10.05	7.74	0.35	1.30	0.95
	Run 6	7 (1B)	0.51	0.23	1.169	0.757	0.626	0.96	1	9.16	7.10	0.43	1.54	1.14
	Run 7	8(6A)	0.41	0.23	1.169	0.757	0.714	0.95	1	9.98	8.93	0.33	0.98	0.86
	Run 8	9(5B)	0.49	0.23	1.169	0.757	0.671	0.96	1	8.89	7.40	0.39	1.20	0.96
	Run 9	10(5A)	0.54	0.23	1.169	0.851	0.686	0.95	1	7.88	6.68	0.36	1.09	0.90

	Run	Label	u_* (m/s)	D (mm)	w_0 (m/s)	a	b	r^2	β_1	β_2	β_3	q_1	q_2	q_3
Namikas (2003)	Run 1	P5	0.32	0.25	1.253	0.367	0.605	0.94	1	16.18	12.42	0.64	1.08	0.79
	Run 2	P4	0.32	0.25	1.253	0.576	0.894	0.98	1	10.95	12.42	0.43	0.82	0.95
	Run 3	P3	0.27	0.25	1.253	0.702	0.967	0.93	1	12.00	14.80	0.36	0.45	0.51
	Run 4	P8	0.3	0.25	1.253	0.735	1.016	0.92	1	10.28	13.28	0.26	0.40	0.53
	Run 5	P14	0.63	0.25	1.253	0.883	1.115	0.90	1	4.46	6.11	0.25	0.35	0.48
	Run 6	P6	0.37	0.25	1.253	0.680	1.057	0.96	1	8.01	10.69	0.34	0.52	0.71
	Run 7	P9	0.38	0.25	1.253	0.714	1.058	0.94	1	7.79	10.40	0.29	0.43	0.59
	Run 8	P10	0.38	0.25	1.253	0.814	1.064	0.91	1	7.75	10.40	0.28	0.41	0.56
	Run 9	P13	0.47	0.25	1.253	0.727	1.083	0.97	1	6.15	8.33	0.39	0.55	0.76

Table 5-3 continued.

	Run	u_* (m/s)	D (mm)	w_0 (m/s)	a	b	r^2	β_1	β_2	β_3	q_1	q_2	q_3
Butterfield (1999)	Run 1	0.271	0.184	0.97392	1.1236	1.3807	0.96	1	6.51	11.37	0.48	0.96	1.74
	Run 2	0.339	0.184	0.97392	1.1223	1.3979	0.98	1	5.14	9.00	0.43	0.54	0.93
	Run 3	0.375	0.184	0.97392	1.4703	1.4425	0.97	1	4.50	8.10	0.44	0.62	1.13
	Run 4	0.441	0.184	0.97392	1.2782	1.5649	0.97	1	3.53	6.83	0.44	0.53	0.96
	Run 5	0.403	0.184	0.97392	0.7579	1.2778	0.98	1	4.73	7.51	0.44	0.60	0.96
Dong et al. (2004)	Run 1	0.210	0.18	0.957	2.0611	2.0332	0.95	1	5.60	14.52	0.19	0.47	1.10
	Run 2	0.260	0.18	0.957	1.0734	1.6466	0.96	1	5.59	11.65	0.16	0.47	0.91
	Run 3	0.310	0.18	0.957	0.8259	1.4991	0.96	1	5.15	9.71	0.16	0.47	0.83
	Run 4	0.350	0.18	0.957	0.7346	1.4349	0.96	1	4.76	8.55	0.16	0.47	0.79
	Run 5	0.390	0.18	0.957	0.6825	1.395	0.96	1	4.40	7.63	0.16	0.47	0.77
	Run 6	0.440	0.18	0.957	0.6148	1.3392	0.96	1	4.06	6.72	0.16	0.47	0.73
	Run 7	0.490	0.18	0.957	0.4662	1.1957	0.96	1	4.08	5.99	0.15	0.47	0.66
	Run 8	0.530	0.18	0.957	0.3783	1.0918	0.96	1	4.13	5.51	0.15	0.47	0.60
Feng et al. (2009)	Run 1	0.56	0.35	1.6761	0.2339	0.7701	0.98	1	9.72	9.40	0.19	0.59	0.57
	Run 2	0.81	0.35	1.6761	0.2108	0.7169	0.98	1	7.22	6.37	0.20	0.64	0.55
	Run 3	0.93	0.35	1.6761	0.1922	0.6792	0.98	1	6.63	5.49	0.19	0.67	0.53
	Run 4	1.12	0.35	1.6761	0.184	0.6522	0.98	1	5.74	4.49	0.20	0.71	0.53
	Run 5	1.24	0.35	1.6761	0.2037	0.6922	0.97	1	4.88	4.02	0.17	0.55	0.44
	Run 6	0.56	0.35	1.6761	0.2476	0.8	0.97	1	9.35	9.40	0.17	0.48	0.49
	Run 7	0.81	0.35	1.6761	0.2248	0.764	0.98	1	6.77	6.37	0.18	0.56	0.52
	Run 8	0.93	0.35	1.6761	0.2015	0.717	0.97	1	6.28	5.49	0.19	0.61	0.52
	Run 9	1.12	0.35	1.6761	0.1974	0.7071	0.97	1	5.29	4.49	0.22	0.71	0.59
Gerety & Slingerland (1983)	Run 1	0.20	0.18	0.957	0.0879	0.5148	0.83	1	23.24	15.27	0.80	5.59	3.87
	Run 2	0.40	0.18	0.957	0.1994	0.6023	0.95	1	9.93	7.43	0.61	3.46	2.66
	Run 3	0.52	0.18	0.957	0.1816	0.9355	1.00	1	4.92	5.62	0.79	2.78	3.16
	Run 4	1.10	0.18	0.957	0.1875	0.8946	0.91	1	2.43	2.44	0.87	2.04	2.05
Hotta & Horikawa (1991)	Run 1	0.3	0.3	1.4646	0.3009	0.8717	0.94	1	14.00	15.59	0.25	0.52	0.59
	Run 2	0.47	0.3	1.4646	0.512	1.0841	0.95	1	7.19	9.80	0.21	0.28	0.38
	Run 3	0.76	0.3	1.4646	0.4938	1.0982	0.96	1	4.39	5.90	0.24	0.31	0.41
	Run 4	1	0.3	1.4646	0.4203	0.9819	0.96	1	3.73	4.39	0.20	0.30	0.35
	Run 5	0.4	0.3	1.4646	0.2905	1.0661	0.96	1	8.59	11.59	0.20	0.54	0.75
	Run 6	0.52	0.3	1.4646	0.3105	0.9562	0.98	1	7.36	8.82	0.18	0.39	0.48
	Run 7	0.83	0.3	1.4646	0.4337	1.0283	0.96	1	4.29	5.37	0.32	0.42	0.52
	Run 8	0.44	0.3	1.4646	0.353	0.8311	0.96	1	10.01	10.50	0.20	0.39	0.41
	Run 9	0.66	0.3	1.4646	0.3971	1.0523	0.96	1	5.27	6.86	0.16	0.23	0.30
	Run 10	0.94	0.3	1.4646	0.449	0.9406	0.96	1	4.14	4.69	0.21	0.32	0.36
Hotta et al. (2006)	Run 1	0.63	0.15	0.8301	1.266	1.0567	0.95	1	3.12	3.91	0.77	0.87	1.01
	Run 2	1.01	0.15	0.8301	0.9095	1.4556	0.99	1	1.41	2.28	0.85	1.07	1.74
	Run 3	1.74	0.15	0.8301	0.8223	1.7569	0.96	1	0.68	1.15	0.84	0.58	0.97
	Run 4	0.61	0.25	1.2531	0.8464	1.1107	0.98	1	4.62	6.32	0.72	1.16	1.64
	Run 5	1.15	0.25	1.2531	1.4064	1.4332	0.92	1	1.90	3.16	0.34	0.42	0.68
	Run 6	1.77	0.25	1.2531	1.3474	1.6044	0.93	1	1.10	1.91	0.29	0.30	0.48
	Run 7	0.87	0.28	1.38	0.8476	1.0698	0.95	1	3.71	4.79	0.45	0.72	0.96
	Run 8	1.48	0.28	1.38	1.375	1.3317	0.92	1	1.75	2.64	0.31	0.36	0.49
	Run 9	2.16	0.28	1.38	0.8679	0.988	0.88	1	1.62	1.68	0.25	0.32	0.34
	Run 10	0.4	0.48	2.226	0.5848	0.82	0.95	1	16.97	17.83	0.34	0.97	1.03
	Run 11	1.21	0.48	2.226	0.6523	1.1054	0.98	1	4.16	5.62	0.33	0.48	0.66
	Run 12	1.93	0.48	2.226	0.5348	0.9371	0.96	1	3.08	3.37	0.25	0.42	0.47
	Run 13	0.84	0.68	3.072	0.4209	0.8436	0.99	1	10.84	11.57	0.27	0.52	0.56
	Run 14	1.67	0.68	3.072	0.4184	0.7458	0.98	1	6.17	5.62	0.29	0.58	0.52
	Run 15	2.33	0.68	3.072	0.2605	0.6181	0.98	1	5.33	3.91	0.24	0.76	0.52
Kawamura (1951)	Run 1	0.488	0.25	1.2531	0.2923	1.0386	0.99	1	6.18	8.00	0.31	0.42	0.54
	Run 2	0.732	0.25	1.2531	0.2961	0.8929	0.99	1	4.79	5.20	0.30	0.42	0.45

Table 5-3 continued.

	Run	u_* (m/s)	D (mm)	w_0 (m/s)	a	b	r^2	β_1	β_2	β_3	q_1	q_2	q_3
Ni et al. (2002)	Run 1	0.61	0.17	0.9147	0.6342	1.2305	0.98	1	3.05	4.50	0.71	1.48	2.25
	Run 2	0.47	0.35	1.6761	0.2233	0.5918	0.97	1	15.06	11.28	0.15	0.48	0.34
	Run 3	0.86	0.17	0.9147	0.5112	1.1649	0.95	1	2.28	3.07	0.42	0.67	0.93
	Run 4	0.77	0.35	1.6761	0.1991	0.5549	0.98	1	9.81	6.72	0.18	0.62	0.39
	Run 5	1.18	0.17	0.9147	0.5132	1.1182	0.95	1	1.73	2.13	0.33	0.46	0.57
	Run 6	1.11	0.35	1.6761	0.1766	0.5415	0.97	1	6.97	4.54	0.16	0.57	0.34
	Run 7	1.64	0.17	0.9147	0.5216	0.9905	0.95	1	1.41	1.41	0.29	0.38	0.39
	Run 8	1.53	0.35	1.6761	0.1757	0.4958	0.97	1	5.52	3.18	0.15	0.59	0.30
	Run 9	2.36	0.17	0.9147	0.3278	0.7351	0.96	1	1.32	0.86	0.29	0.41	0.25
	Run 10	2.31	0.35	1.6761	0.1559	0.4421	0.97	1	4.10	1.97	0.15	0.59	0.24
Rasmussen & Mikkelsen (1998)	Run 1	0.27	0.2	1.0416	0.6369	0.5396	0.96	1	17.87	12.23	0.05	0.13	0.08
	Run 2	0.49	0.2	1.0416	0.6848	0.6517	0.91	1	8.15	6.55	0.42	0.91	0.70
	Run 3	0.63	0.2	1.0416	0.7011	0.5628	0.89	1	7.34	5.01	0.41	0.90	0.58
Sorensen (1985)	Run 1	0.46	0.1175	0.692625	0.6733	0.9509	0.94	1	3.96	4.52	0.34	0.84	0.98
	Run 2	0.46	0.2345	1.187535	0.6272	1.061	0.95	1	6.08	8.05	0.45	1.03	1.41
Williams (1964)	Run 1	0.51	0.4	1.8876	0.7965	0.8457	0.94	1	10.94	11.72	0.60	1.65	1.79
	Run 2	0.53	0.4	1.8876	0.7074	0.7099	0.95	1	12.54	11.26	0.48	1.58	1.39
	Run 3	0.72	0.4	1.8876	0.8144	0.8718	0.95	1	7.52	8.18	0.63	1.64	1.81
	Run 4	0.78	0.4	1.8876	0.703	0.7314	0.95	1	8.27	7.52	0.57	1.88	1.69
	Run 5	1.13	0.4	1.8876	0.7459	0.8121	0.94	1	5.14	5.06	0.59	1.72	1.69
	Run 6	1.2	0.4	1.8876	0.6529	0.6692	0.91	1	5.88	4.74	0.52	1.89	1.48
Zou et al. (2001)	Run 1	0.64	0.25	1.2531	0.3651	0.5738	0.96	1	8.53	6.00	0.28	1.38	0.97
	Run 2	0.63	0.25	1.2531	0.3505	0.557	0.93	1	8.93	6.11	0.32	1.63	1.11
	Run 3	0.81	0.25	1.2531	0.5027	0.8196	0.98	1	4.72	4.66	0.52	1.68	1.69
	Run 4	0.74	0.25	1.2531	0.3438	0.5997	0.87	1	7.06	5.14	0.40	1.82	1.31

Tables 5-3 provides details of shear velocity, fall velocity, regression coefficients and goodness of fit, and the adjusted β values from Steps 1-3. The relationship between the adjusted β values and the w_0/u_* ratio is shown in Figure 5-7. The relationship is strong (r^2 =0.65), but not statistically significant (P =*0.50*). However, this fit provides an independent means (based on fall velocity and shear velocity) to estimate a value β without having to collect vertical mass flux profiles. Comparison tests show that this independent approach predicts the field values of β within, on average, 20% (+/-11% standard deviation) of the adjusted values and wind tunnel values of β within, on average, 33% (+/- 29% standard deviation) of the adjusted values.

The relationship is much stronger and statistically significant within some individual experiments. For example, the relationship is shown for the three field experiments in Figure 5-8. The goodness-of-fit (r^2) values are 0.81, 0.70 and 0.64 but only the Brazil relationship is statistically significant. It is noted here that the first run in the Greeley et al. (1996) was removed from this analysis as it was an outlier for all the

data. One possible reason for this is that the observed transport rate in this run was orders of magnitude less than all others. Clearly, in order for the Rouse approach to be practical, a universal relationship is required to derive a value of β. The relationship found in Figure 5-7 was used in the next analyses, where:

$$\beta = 3.277\left(\frac{w_0}{u_*}\right) - 0.4133 \qquad (5\text{-}7)$$

The following steps provide a guide to the Rouse analysis for the vertical mass flux profiles collected in the Brazil (2008) experiment. This analysis was repeated for each experiment and the results are all provided in Appendix C. Steps 1-6 are similar to those described previously. The additional steps include a description of results of the Rouse model using the value of β based upon Equation 5-7. For comparison purposes, the results from using three different values of β are described:

1. β = 1: assumption based upon the original Rouse model and widely accepted in water studies.
2. Adjusted β: variable values that are experiment and run dependent. The adjusted β values are derived from fitting a power function to the adapted vertical mass flux data and using the regression slope coefficient, fall velocity and shear velocity to calculate β using Equation 5-3 (Steps 1-3).
3. Modeled β: variable values that are experiment and run dependent. The modeled β values are obtained independently of the mass flux data and are based upon the relationship between β and the ratio w_0/u_* (Equation 5-7).

As expected the predicted transport is under estimated by, on average, 57% using β = 1. The predicted transport rates are much closer using the adjusted and modeled β values, 99% and 79%, respectively. These results are shown in Table 5-3. The results from the Brazil (2008) experiment are presented next. Table 5-4 shows the comparison of predicted transport rates using the three values of β. These tabular results are presented graphically in Figure 5-9. The re-constructed profiles are then presented in Figure 5-10 to establish if the modeled approach can replicate the vertical distributions of mass flux.

The results from Greeley et al., (1996) and Namikas (2003) are also presented for comparative purposes in Figures 5-11 and 5-12 respectively.

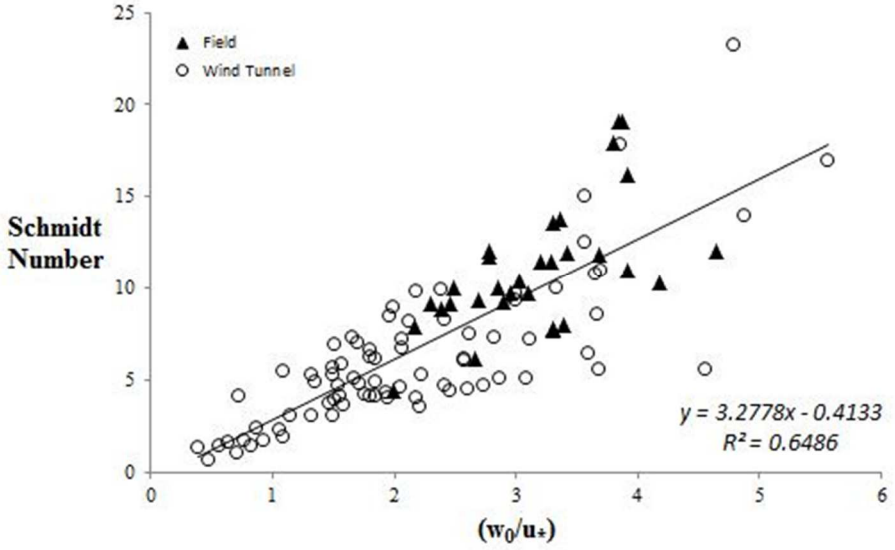

Figure 5-7: Relationship between the calculated Schmidt Number and w_0/u_*.

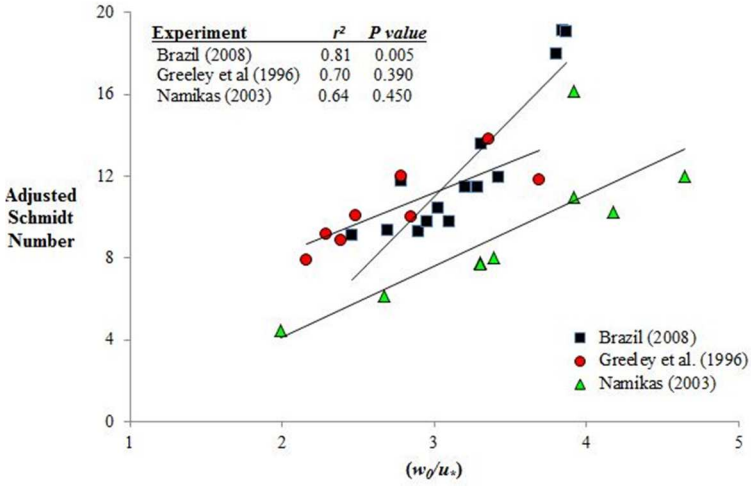

Figure 5-8: Relationship between the adjusted Schmidt Number and w_0/u_*. Results of the linear regression are shown in the inset table.

Table 5-4. Comparison of predicted transport rates using three values of β for the Brazil (2008) data.

	Run 1	Run 2	Run 3	Run 4	Run 5	Run 6	Run 7
Observed transport rate (g/cm^2/s)	0.0846	0.0937	0.0405	0.0721	0.0591	0.0545	0.0459
Predicted transport rate ($Q_{pre.}/Q_{obs.}$)							
β= 1	0.41	0.49	0.57	0.49	0.47	0.48	0.47
β adjusted	1.08	0.99	1.26	1.03	0.95	0.90	0.86
β modeled	0.74	0.88	1.02	0.88	0.85	0.88	0.85

	Run 8	Run 9	Run 10	Run 11	Run 12	Run 13	Run 14	
Observed transport rate (g/cm^2/s)	0.0437	0.0539	0.0721	0.0577	0.0517	0.0546	0.0566	
Predicted transport rate ($Q_{pre.}/Q_{obs.}$)								*Average*
β= 1	0.48	0.52	0.30	0.33	0.37	0.35	0.35	***0.43***
β adjusted	0.98	0.99	0.74	0.68	1.12	1.13	1.11	***0.99***
β modeled	0.87	0.93	0.54	0.60	0.68	0.64	0.63	***0.79***

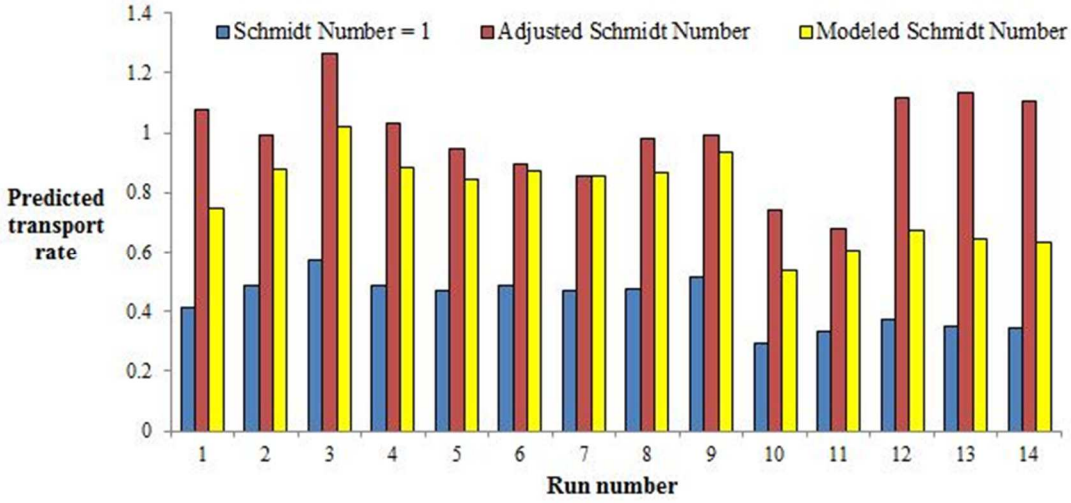

Figure 5-9. Comparison of predicted transport rates using three values of β for the Brazil (2008) data.

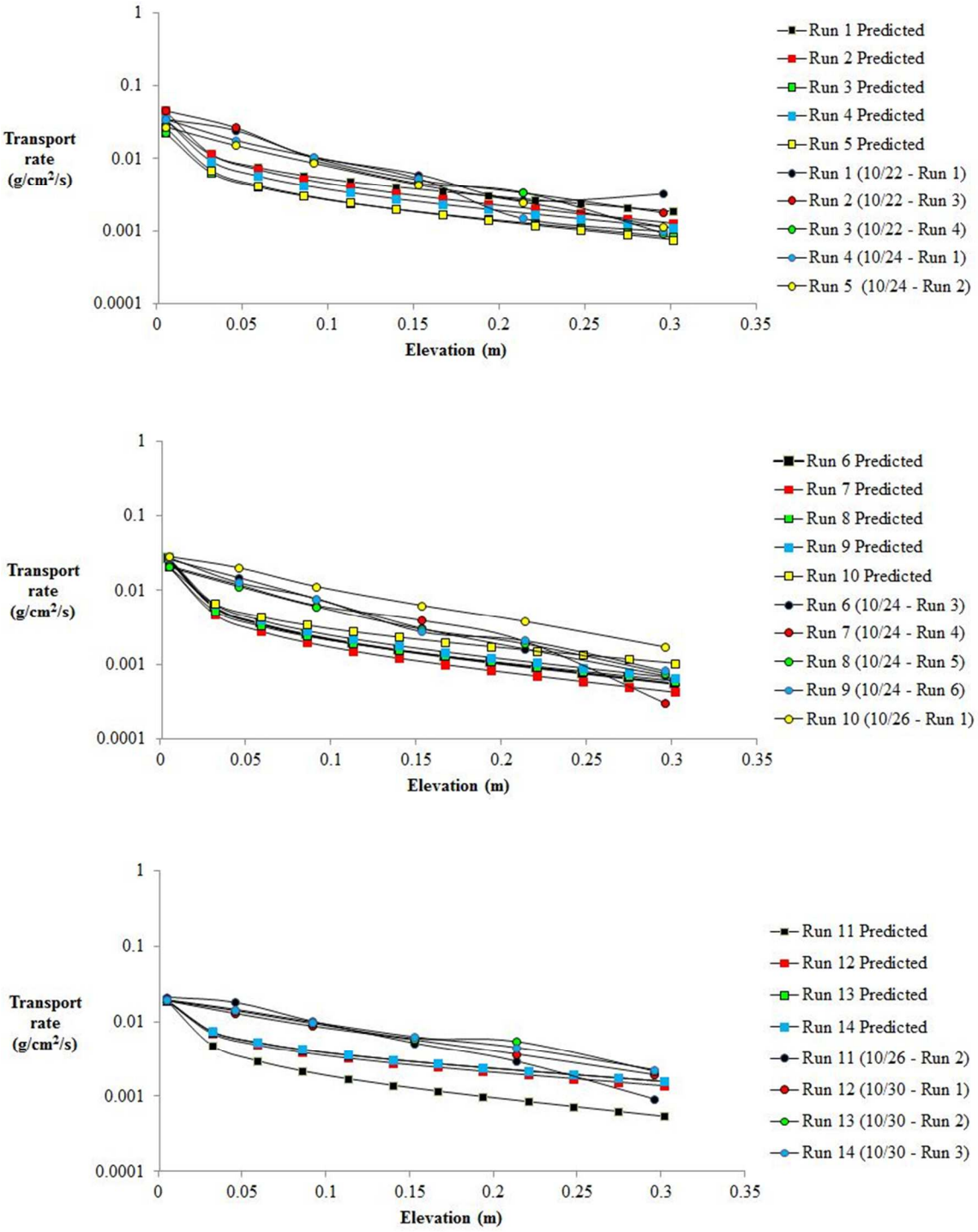

Figure 5-10 Testing the performance of the predicted vertical distributions based upon the modeled value of β for the Brazil (2008) data.

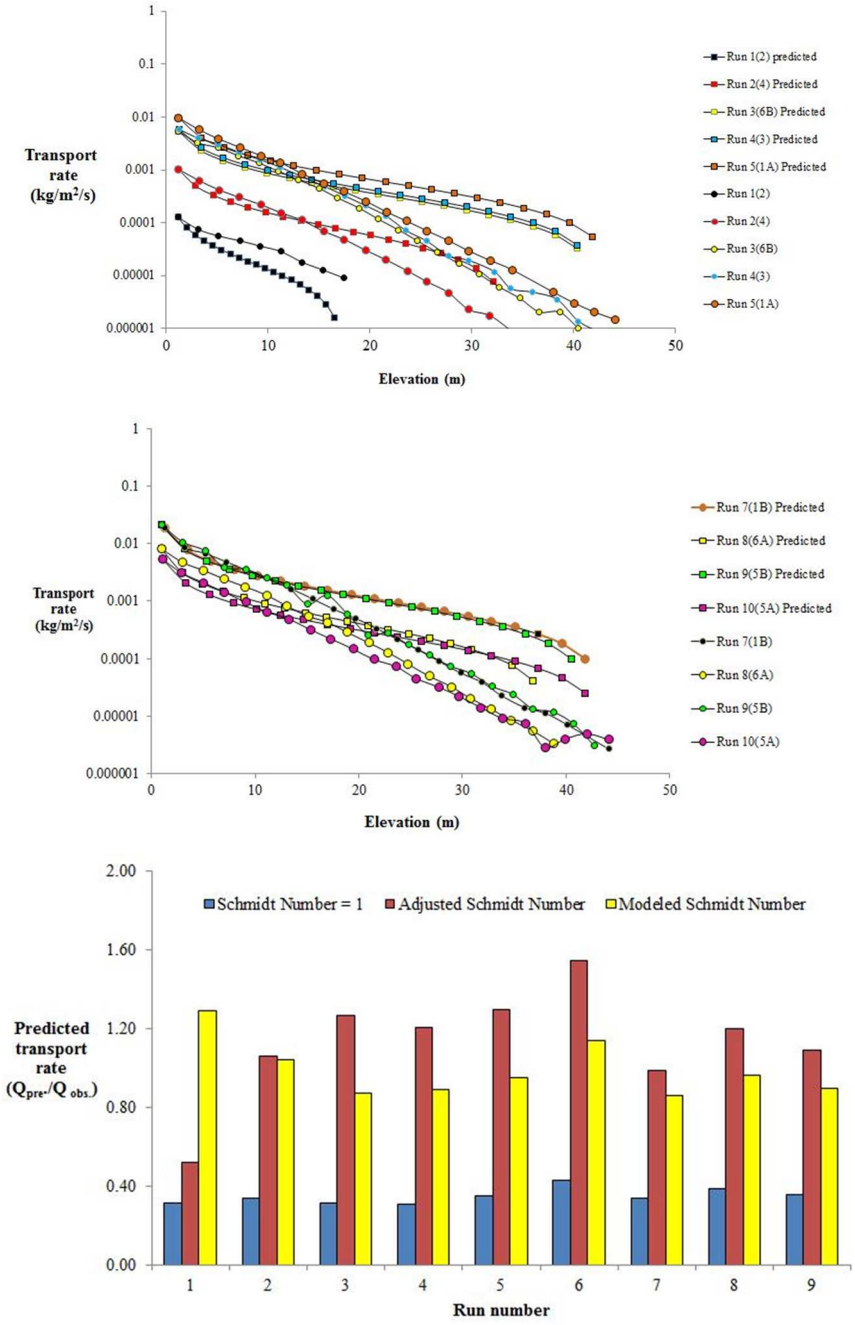

Figure 5-11 Testing the performance of the predicted vertical distributions based upon the modeled value of β for the Greeley et al., (1996) data. The predicted flux is compared with the observed flux for each approach in the bar graph.

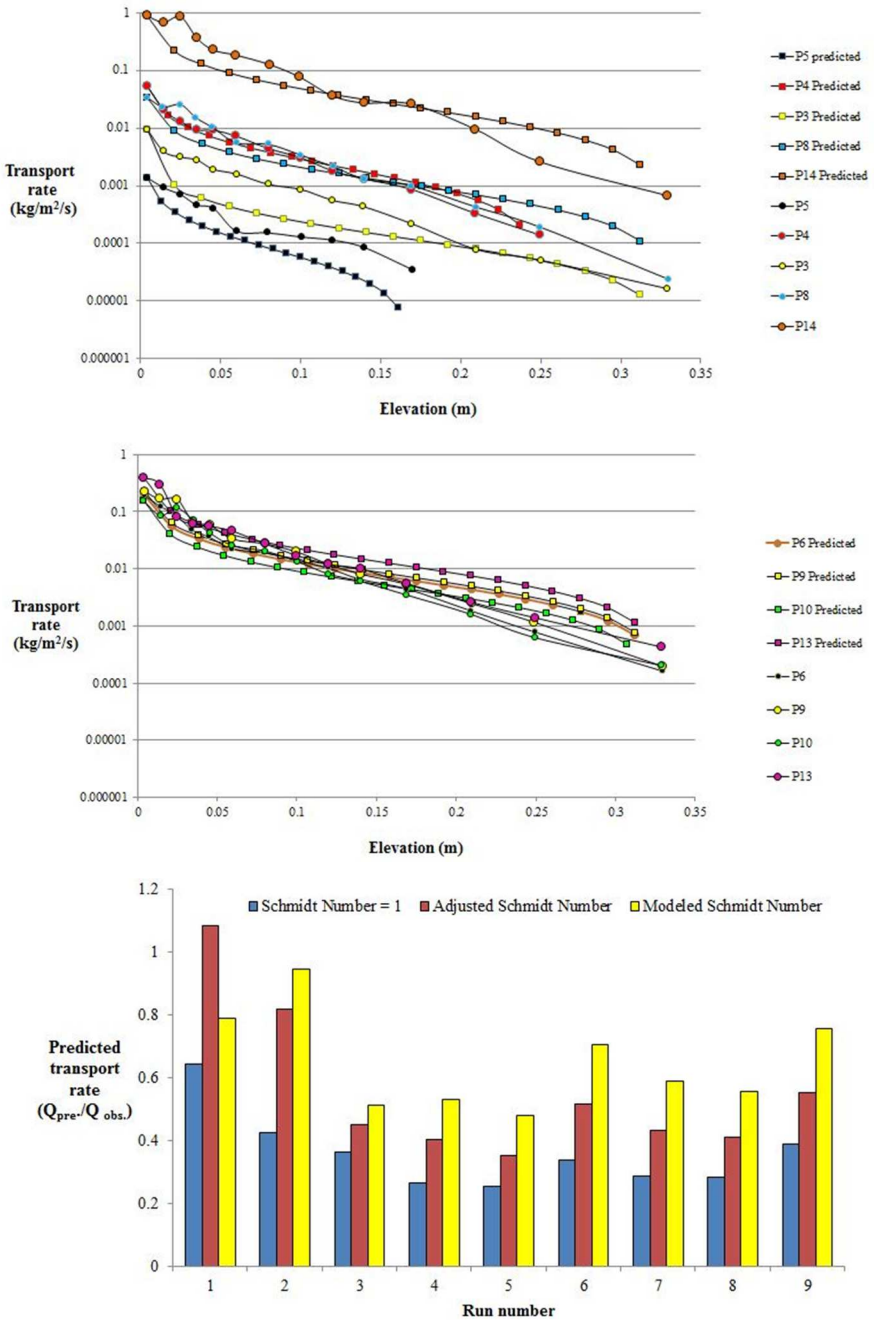

Figure 5-12. Testing the performance of the predicted vertical distributions based upon the modeled value of β for the Namikas (2003) data. The predicted flux is compared with the observed flux for each approach in the bar graph.

It is clear that the Rouse distributions are very similar to the observed profiles. This provides confidence in the application of the model to aeolian saltation. The second test for the model is the accuracy of transport predictions. Figure 5-13 provides a summary of the field and wind tunnel results where the predicted transport rates are presented as fraction of the observed value. Perfect correlation with the observed data would have values of 1.0. There are much better predictions of the total transport rates. In the field and wind tunnel experiments the modeled Rouse approach predicts, on average 86% and 81% of the observed transport rate, respectively (field: $\mu = 86\%$, $\sigma = 71\%$; wind tunnels: $\mu = 81\%$, $\sigma = 19\%$). In Section 4.2.2. it was found that the Rouse profiles using β =1 did not replicate the saltation process and estimated very low predictions of flux magnitudes. The Rouse model predictions had little or no sediment moving above the reference height, and the predicted fluxes were, in essence, the reference flux (C_a) i.e. the bottom trap. However, there was a very strong relationship between the predicted flux and observed flux ($r^2 = 0.92$ in Figure 4.12) – but the former is lower by nearly an order of magnitude. This analysis was repeated for the transport predictions based on the modeled values of modeled values of β. Figure 5-14 shows that there is still a strong relationship between the predicted and observed transport but the scaling differ3nce has been removed. The field and wind tunnel relationships have very strong correlations with r^2 values of 0.98 and 0.84, respectively.

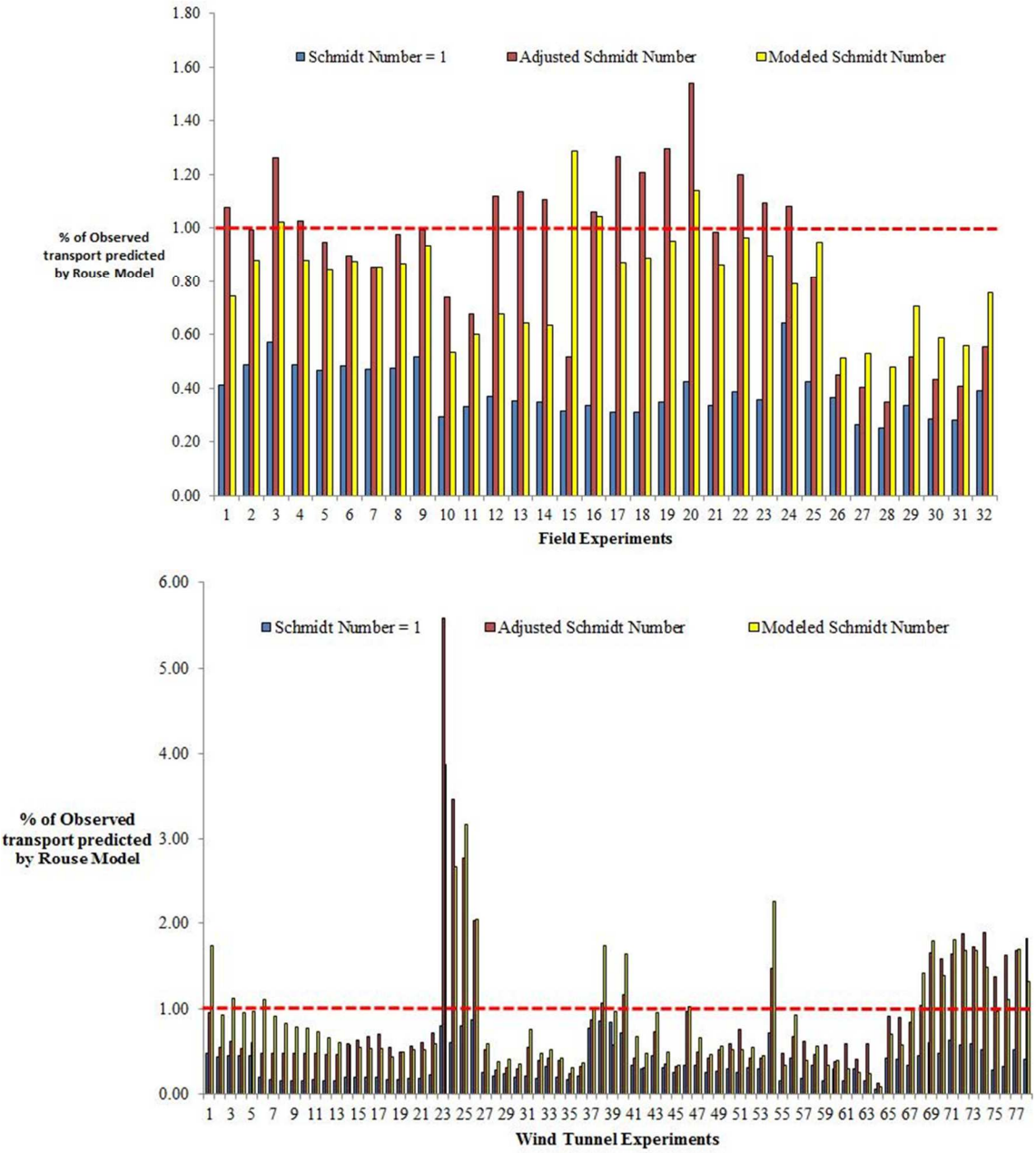

Figure 5-13. The performance of the Rouse model in predicting the observed transport rates for field and wind tunnel experiments. A value of 1.0 represents perfect prediction.

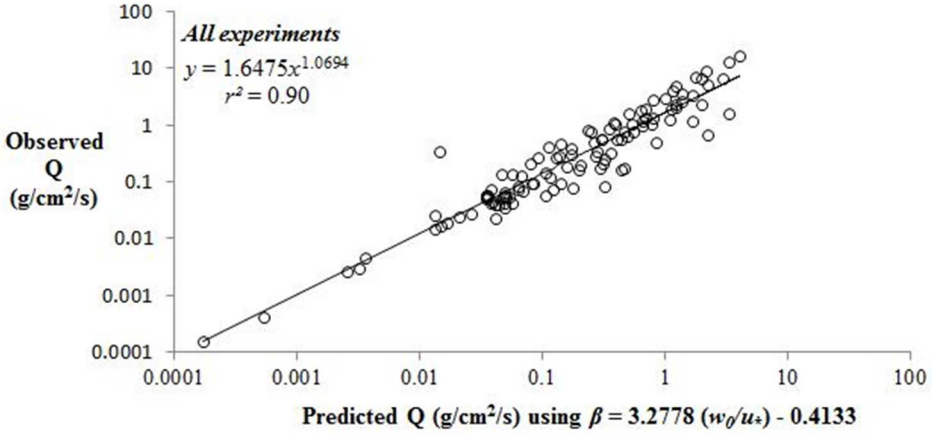

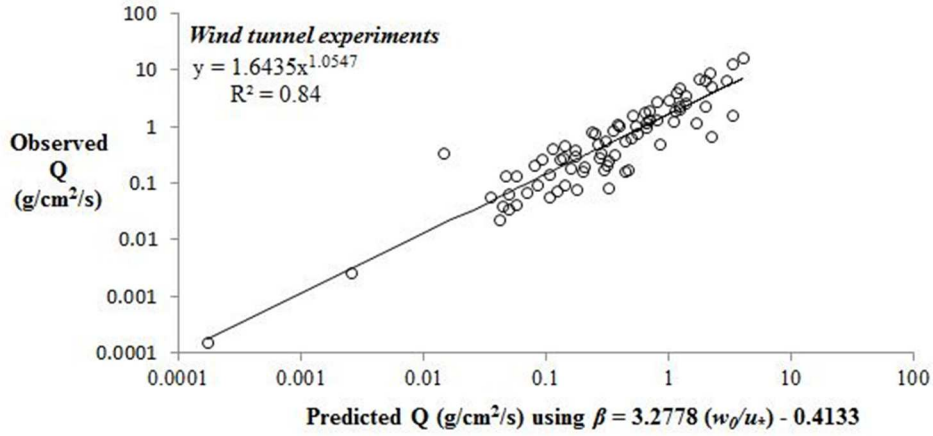

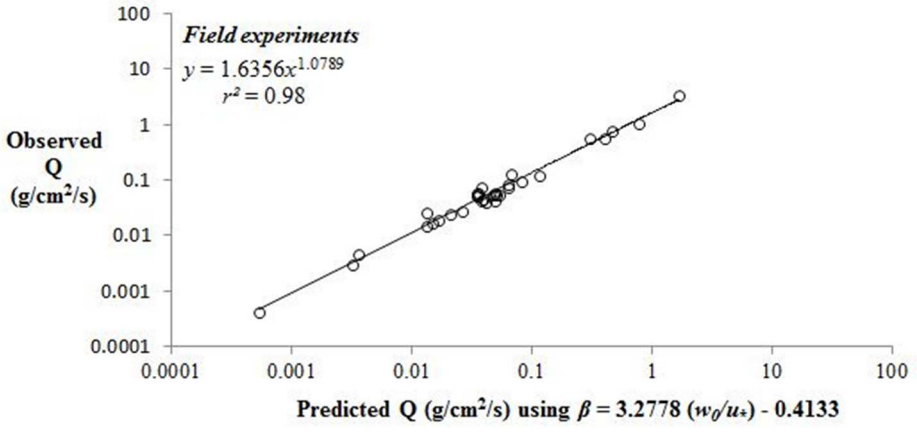

Figure 5-14. Predicted *vs.*Observed transport rates using the modeled β approach.

5.3.4 Main findings from the Rouse model analysis

1. The Rouse model performs very poorly when the value of $\beta = 1.0$ in the Rouse number exponent. This is because the high values of the Rouse number, which controls the shape of the profiles, results in profiles that are strongly L-shaped. This implies that no sediment is moving above the reference elevation. This is physically implausible and not in agreement with observations. Subsequently, the profiles also consistently under predict the magnitude of the transport. In the field and wind tunnel experiments the Rouse model predicts, on average 38% and 18% of the observed transport rate, respectively (field: $\mu = 38\%$, $\sigma = 8\%$; wind tunnels: $\mu = 18\%$, $\sigma = 86\%$).

2. The performance of the Rouse model is not sensitive to changes in the range of variability we can expect to observe in values fall velocity, shear velocity and the von Kármán constant. It is very sensitive to changes in the observed range of values of the Schmidt number, β.

3. The values of observed β were derived by adapting the aeolian vertical mass flux profiles to equivalent concentration-type ratios and obtaining the slopes values of the fitted power functions. The slope values, representing the vertical flux distributions, are equaivalent to the Rouse number. The value of β can be calculated as long as the values of fall velocity (w_0), the von Kármán constant (k) and shear velocity (u_*) are known. In field and wind tunnel experiments, the values of β ranged from 4.46 - 19.10 and 0.68 - 23.24, respectively (field: $\mu = 10.81$, $\sigma = 3.56$; wind tunnels: $\mu = 6.22$, $\sigma = 3.94$). These adjusted β values have a large impact on the values of the Rouse number. This results in Rouse profiles that predict very similar vertical distributions to the observed data and much

better predictions of the total transport rates (field: $\mu = 82\%$, $\sigma = 29\%$; wind tunnels: $\mu = 90\%$, $\sigma = 88\%$).

4. The observed values of β are strongly related to the w_0/u_* ratio ($r^2 = 0.65$). This relationship provides an independent method to estimate a value of β without the need for measuring vertical flux profiles. This modeling approach produces values of β that range from 6.11 – 14.80 and 0.86 – 17.83, for field and wind tunnel experiments, respectively (field: $\mu = 10.0$, $\sigma = 2.06$; wind tunnels: $\mu = 6.64$, $\sigma = 3.54$). These adjusted β values have a large impact on the values of the Rouse number. This results in Rouse profiles that predict very similar vertical distributions to the observed data and much better predictions of the total transport rates. In the field and wind tunnel experiments the modeled Rouse approach predicts, on average 86% and 81% of the observed transport rate, respectively (field: $\mu = 86\%$, $\sigma = 71\%$; wind tunnels: $\mu = 81\%$, $\sigma = 19\%$).

5. There is a strong relationship between the predicted and observed transport rates using the Rouse model approach for $\beta = 1$ and the calculated value of β using the w_0/u_* relationship. In the field experiments these relationships are strong and statistically significant: $\beta = 1$, $r^2 = 0.98$ and $P = 0.048$; β modeled, $r^2 = 0.97$ and $P = 0.042$. In the wind tunnel experiments these relationships are also strong but not statistically significant: $\beta = 1$, $r^2 = 0.80$ and $P = 0.424$; β modeled, $r^2 = 0.69$ and $P = 0.163$. For an aggregate of all the experiments the relationships between predicted and observed fluxes are also strong but not statistically significant: $\beta = 1$, $r^2 = 0.82$ and $P = 0.34$; β modeled, $r^2 = 0.72$ and $P = 0.124$.

6. The Rouse model is more sensitive to the variability we can expect to observe in values of fall velocity, shear velocity and the von Kármán constant provided that the appropriate value of value β is used. For example, the variability of the

apparent von Kármán parameter reported for the Brazil experiments can change the predicted transport rates by up to 16%. Similarly, doubling the value of the calculated fall velocity, results in up to 17% variability in the predicted transport rates.

7. In an independent method, Li (2010) derived values of the Schmidt number using the profiles collected in the Brazil (2008) experiment. He found $\beta = 11.22$ which is close to the predictions of β based on the two methods described here: 12.43 for the calculation based on calculating β using the observed slopes and 10.04 for the modeling approach based on the w_0/u_* ratio.

5.4 Critique of the Rouse approach for saltation in air

There are still many unresolved issues to using the Rouse approach for saltation. First and foremost, the Rouse concentration model was developed to describe the vertical distribution of sands, silts and clays moving by suspension in water. This mode of transport is fundamentally different to the saltation of particles in air. As Bauer (2009) states, "*although apparent similarities exist between the mechanics of aeolian and fluvial transport, especially because many of the fluid mechanical laws and principles are thought to be universal, it is increasingly apparent that the dominance of saltation as the primary mode of transport in air leads to complexities that are not found in water. These are rooted in the extreme difference in density between the fluid (air) and the solid (sand), which leads to: (1) ballistic trajectories of grains that have the potential to impact the surface and cause cratering and the ejection of other surface particles (the "splash" process); and (2) mutually efficient exchange of momentum between the fluid and the grains* (p.2)". Suspended sediment moves in response to the turbulent motion of the fluid and rarely has contact with the bed. Conversely, saltating sand in air, moves either by impacts from other grains already in saltation (for which splash functions have been developed) or by momentum exchange with the ground as particle already in

motion rebound off the bed. This infers that, unlike suspension, shear velocity alone cannot explain the energy balance driving the vertical flux distributions. The extent to which these differences in the two transport modes impacts the application of the Rouse model will require more investigation.

Similarly, the extent to which the variability of the Rouse number, which controls the shape of the mass flux distributions, is sensitive to changes in the von Kármán constant, the fall velocity and, especially, the constant of proportionality (β) needs to be resolved. This is especially the case for the Schmidt number, or β, whose value had the greatest impact on the form of the modeled Rouse profiles for saltation. The Rouse model only becomes sensitive to values of the von Kármán constant, fall velocity and shear velocity only after an appropriate β was established. Investigating these dependencies should be explored. It was shown that the fall velocity of sand sized particles can vary by up to 100% depending on which empirical expression is used. Further, it is not clear how the particle fall velocity will vary in sediment laden loads in water or air that comprise of mixed grain size populations and have particle-particle interactions. Current theory is inadequate to address this process. Therefore, it is clear that obtaining a representative and accurate fall velocity value for the Rouse model is a very challenging task.

The presence of a sediment load has been shown to changes values of the von Kármán constant in water and air. The von Kármán constant changed up to 30% during the Brazil experiment depending on transport conditions. This subsequently changes the values of the velocity and eddy viscosities. It is important that these potential sources of variability are accounted for when newer analytical expressions for the equilibrium-transport models are developed.

There is no prescribed approach for applications of the Schmidt number for sand particles moving in air. Indeed the value of β is still unresolved in water studies – despite decades of being scrutinized. The initial findings presented here are promising. This work presents an empirical adjustment of β based upon the observed variability of shear velocity and fall velocity in field and wind tunnel experiments. This approach follows

findings in water studies that have successfully elucidated the behavior of β in different transport environments. However, other potential controls should be investigated, including the impact of the absolute transport rates and grain size distributions on the values of β in the Rouse number. After eight decades of application in suspension studies, the values and behavior of this parameter is still unresolved. As Bridge (2003, p.65) states "*perhaps the most serious concern with the Rouse equation is that the sediment diffusivity has rarely been calculated directly using quantitative observations of the motion of sediment in turbulent eddies. Thus, there is doubt about the vertical variation of* ε_s *and* β". However, the strong statistical relationships between the predicted and observed fluxes, and the shapes of the reconstructed vertical flux profiles, using the Rouse model based on values of β from fitting (to the slope of the adapted vertical flux profiles) and modeling (using the ratio w_0/u_*) methods, suggest that the Rouse model can be used for aeolian sand transport. The shape and magnitude of the predicted Rouse profiles performed consistently well when compared to the vertical mass flux distributions observed in field and wind tunnel experiments. Therefore, the results do not appear to be fortuitous. From these analyses, the most pragmatic approach is to estimate β based on the w_0/u_* ratio.

The research findings here confirm that there is a positive dependence between β and the fall velocity. In water, this implies that larger, more inert particles are mixed more efficiently by turbulence than smaller sized particles environments (Teakle and Nielsen, 2004). An analogous example can be applied to sand transport in air whereby larger grains were observed to be moving at higher elevations for the vertical mass flux profiles measured during the Brazil field experiment. It remains clear, however, that greater detail of the characteristics of the vertical structure of the saltation field, including the grain-size characteristics is needed. Such characteristics represent the integration of complex processes through space and time, and thus provide key information concerning the nature and magnitude of those processes.

5.5 Hypotheses testing

Based upon the data analyses performed; a review of the relevant literature and a series of statistical tests, hypothesis 1 was rejected and hypotheses 2 and 3 were accepted.

Evaluating Hypothesis 1:

> *The average grain size of the sediments comprising the vertical mass flux profile become smaller with distance away from the bed*

Findings: **Hypothesis 2 is rejected**

The analysis of the grain-size statistics for the flux caught in each trap of the vertical flux profiles collected in the field experiment shows that a reverse in grain-size trends occurs at an inflection zone located 0.05 – 0.15 m above the bed. Below this inflection, mean grain-size decreases steeply with elevation in the near bed region dominated by reptation and saltation modes of transport. Above the inflection there is a coarsening of grain size with elevation; as saltation becomes the dominant transport mode. These results indicate that the coarsest grains are found close to and farthest from the bed.

Hypothesis 1: Implications of rejection

Aeolian research has established that the coarsest fraction of a grain-size population should move near the bed because the largest grains are least susceptible to lifting (Bagnold, 1941; Willets and Rice, 1986a; Anderson and Hallet, 1986; Shao, 2000). It is commonly assumed, for that reason, grain size should decrease with elevation above the bed surface. The findings of this research provide contradictory evidence. This discrepancy between theory and observation deserves further attention because of the importance of understanding distributions of grain trajectories during saltation. Understanding how grain sizes in a saltating population vary with elevation is fundamental to physics-based modeling of the sand transport process, especially as

numerical modeling relies on trajectory calculations. To date, the mechanisms by which saltating grains leave the surface and the velocities and angles that they attain are still not fully understood. Establishing these relationships can provide important boundary conditions for a suite of transport models (Anderson and Haff, 1991; McEwan and Willetts, 1991; Shao and Li, 1999; Doorschot and Lehning, 2002; Almeiada et al. 2006; Kok and Renno, 2009). An understanding of the distribution of trajectory heights and lengths for different grain sizes should be an integral part of the new saltation models (Namikas, 2003, 2006; Rasmussen and Sørensen, 2008; Namikas et al., 2009). Indeed, it would be the ability of a numerical model to replicate the size-sorting characteristics with elevation that provides one means of evaluating that model's performance. Unfortunately, there are few examples of quality data sets gathered from field experiments. As stated by Mikami et al. (2005, p. 2), "*field data, which include information of the whole saltation process and can be used for verifying the (heterogeneous saltation) theory, are lacking*". A primary contribution of this work is to provide data that describe the grain size and sorting characteristics of vertical flux distributions observed during transport events with a naturally mixed-size grain population.

Evaluating Hypothesis 2:

> *The observed mass flux distribution profiles observed in wind tunnel and field environments all **decay exponentially** away from the bed but at **different rates** for each environment.*

Findings: Hypothesis 2 is accepted

The vertical distribution of mass flux is best described using an exponential decay function, compared with curve fits calculated using power or logarithmic functions. The populations of the exponent coefficients, representing the relative rate of decrease with height above the surface, or slope of the vertical mass flux profiles, are statistically different in wind tunnels and field experiments. Small wind tunnels have, on

average, much lower values for the exponent coefficient. Physically, this indicates that small wind tunnels have steeper slopes, *ceteris paribus*.

Hypothesis 2: Implications of acceptance

The results from testing Hypothesis 1 substantiate the, partly surreptitious, doctrine in aeolian research that wind tunnels simulate boundary layer - surface interactions that are fundamentally different. Wind tunnels are important for the recognition and description of fundamental interactions, but are subject to constraints that limit substantially the vertical dimensions of the wind velocity profile (e.g., Owen and Gillette, 1985; Scott et al., 1995; Sherman and Farrell, 2008). Increasing efforts the past decade have been directed at probing and modeling the dynamics of the boundary layer in wind tunnels (Spies et al., 1995; Butterfield, 1999; Bauer et al., 2004). Surprisingly, as researchers continue to dismantle the boundary layer processes, the equivalent attention to the saltation dynamics has not been forthcoming. Rather, it has been implicit in saltation studies that these scaling constraints of the boundary layer will be manifested in smaller and shorter grain trajectories. The extent to which this holds true has never been tested. Sherman and Farrell (2008) formalized an approach to partly test it by evaluating one fundamental interaction between wind and sand, the apparent enhancement of the boundary roughness length associated with the presence of a saltation layer. They found that the saltation layer roughness *form* is about an order of magnitude higher in the field than in wind tunnels. This was the first tangible evidence that saltation trajectories were suppressed in wind tunnels. If the interpretation of their results was to be tested (*i.e.* saltation is suppressed in wind tunnels) then one would expect this anomalous behavior between the two systems, or environments, to be manifested in the characteristics of mass flux profiles. A constrained or suppressed saltation system should have proportionally more mass flux moving at lower elevations, resulting in a faster decay of flux away from the bed, and steeper profile. The extent to which this holds true was the focus of the first part of this research. The results confirm that small wind tunnels do, in fact, have statistically significant faster decay rates of

mass flux with elevation above the bed. These differences are magnified in wind tunnels with small working cross section areas, and in wind tunnel experiments that use extreme environmental conditions, e.g., hurricane wind speeds. The differences are modulated in wind tunnels that are large and test ranges of controls that are commonly observed in the field.

The primary implication of these results is to provide caution to the numerical modeling community who calibrate their saltation models using empirical relationships derived from wind tunnel experiments. Bauer et al. (2004) conclude their wind-tunnel study of saltation by acknowledging the potential limits caused by scaling issues. They caution that "*the extent to which any of these wind-tunnel results are applicable to equilibrium saltation systems in natural environments remains to be investigated* (p.97)*"*. Sherman and Farrell (2008) found …"*scaling differences in the representation of the two basic components of the saltation system: the boundary layer and the saltating grains.*…[and that]…*that the application of results obtained from research in wind tunnels to real-world saltation systems requires critical assessment of the nature and magnitude of error that might follow*". Nevertheless, the use of wind tunnel data for modeling is still the rule rather than the exception. These results may finally provide the empirical evidence for modelers to scale their saltation models for these differences.

Evaluating Hypothesis 3:

> *The rate of decay changes as a function of wind speed and/or grain size parameters and can be accounted for using a form of the* ***Rouse Parameter***.

Findings: Hypothesis 3 is accepted

The Rouse model, using values of β based upon the w_0/u_* ratio, performs well in predicting the vertical distributions of mass flux and transport rates for the series of runs reported form field and wind tunnel experiments. The vertical mass flux profiles were re-constructed using the predicted distributions calculated from the Rouse model. In

most cases, the profiles have very similar slopes to the observed profiles. The magnitude of the predicted transport rates was also very similar. In the field and wind tunnel experiments the modeled Rouse approach predicts, on average 86% and 81% of the observed transport rate, respectively. These results were confirmed independently by calculating the values of β in the Rouse number based upon the observed vertical mass flux data. The predicted values of β for the Brazil (2008) field experiment are in close agreement with an independent method to calculate β described in Li (2010), based upon the stratification effects of the air-sediment mixture density gradient.

Hypothesis 3: Implications of acceptance

It is assumed that the distribution of saltation flux is established, in a bulk (averaged) sense, by a set of physical relationships that can be defined, measured and described quantitatively. Yet such description has proven elusive. The Rouse profile, well accepted in describing concentration profiles for sediments in water and fine sediments (dust) in air, includes the physical relationships that have been identified as controls on the character of the aeolian saltation layer. The Rouse profile is, therefore, more physically meaningful than current approaches that use standard curve fitting functions to represent the vertical flux data. Further, the Rouse model successfully predicts, within the range of acceptable error, the observed transport rates and reproduces the response of the flux distributions to changes in forcing controls, *vis*-à-*vis,* shear velocity and grain size (for which fall velocity is a surrogate). The application of this accepted protocol in water studies, to aeolian research can remove serious obstacles and ambiguity that have challenged researchers for decades. In terms of fundamental generality and accuracy, as well as practicality and application, there is absolutely no physical reasoning that would preclude the widespread induction and application of the Rouse approach to aeolian research. It represents a universal flux-profile configuration.

VI. CONCLUSIONS

This dissertation evaluates characteristics of the vertical distribution of mass flux in field and laboratory experiments. Using an initial data set comprising 651 vertical flux profiles measured in wind tunnels or in the field, the different characteristics of distributions of vertical mass flux were tested. This dataset included data collected during a field experiment in Jericoacoara, Brazil (2008) that also detailed grain size-sorting statistics for each flux sampled elevation within the profiles. The Rouse model was applied to the vertical flux data to determine if it could reproduce the vertical distributions of mass flux for changing environment condition and also predict the total observed flux within an acceptable range of error.

An analysis of the grain-size statistics shows that a reverse in grain-size trends occurs at an inflection zone located 0.05 – 0.15 m above the bed. Below this inflection, mean grain-size decreases steeply with elevation in the near bed region dominated by reptation and saltation modes of transport. Above the inflection there is a coarsening of grain size with elevation. This led to a rejection of hypothesis 1 and led to the following conclusions:

1. The grain-size inflection above the surface is a characteristic of saltation in some natural environments, with important implications for numerical modeling of grain trajectories.
2. There is no consensus in current saltation theory to describe the saltation trajectories of a mixed grain size population. Recent modelling approaches, coupling bed deformation, collision dynamics, and grain rebound and ejection, may provide the theoretical framework to further investigate these results.
3. A primary contribution of this work is to provide data that describe the grain size and sorting characteristics of vertical flux distributions observed during transport events with a naturally mixed-size grain population.

All the vertical mass flux profiles were segregated into field based and laboratory based studies in order to test hypothesis 2. This hypothesis was accepted which led to the following conclusions:

1. The populations of the exponent coefficients, representing the relative rate of decrease with height above the surface, or slope of the vertical mass flux profiles, are statistically different in wind tunnels and field experiments.
2. These differences are magnified in wind tunnels with small working cross section areas, and in wind tunnel experiments that use extreme environmental conditions.
3. This is one of the first studies to provide tangible evidence that the saltation layer is suppressed in wind tunnels. This work complements research done by Sherman and Farrell (2008) who found that the enhanced roughness associated with the saltation layer was an order of magnitude large in the field than in wind tunnels.
4. This scaling constraint requires specific and explicit analytical and theoretical treatment in the next generation of saltation models.

The Rouse model was tested using data collected in the field experiment and the subset of experiments that collected vertical mass flux profiles but also reported shear velocity and grain size for each run. This hypothesis was accepted which led to the following conclusions:

1. The Rouse model performs very poorly when the value of $\beta = 1.0$ in the Rouse number exponent. The profiles are strongly L-shaped which indicates that no sediment is moving above the reference elevation. This is physically implausible and not in agreement with observations. Subsequently, the profiles also consistently under predict the magnitude of the transport. In the field and wind tunnel experiments the Rouse model predicts on average 38% and 18% of the observed transport rate, respectively.

2. The values of β can be calculated from the observed vertical flux profiles by adopting the data to Rouse-type distributions and deriving the slopes of the profiles. The calculated values of β are strongly related to the w_0/u_* ratio (r^2 = 0.65). This dependency provides an independent method to estimate a value of β without the need for measuring vertical flux profiles. This approach produces values of β that range from 6.11 – 17.83 for all the experiments and result in very different values of the Rouse number exponent in the Rouse model. The Rouse profiles calculated using this approach predict very similar vertical distributions to the observed data and perform much better predictions of the transport rates. In the field and wind tunnel experiments the modeled Rouse approach predicts, on average 86% and 81% of the observed transport rate, respectively.
3. The Rouse profile is more physically meaningful than current approaches that use standard curve fitting functions to represent the vertical flux data. There is absolutely no physical reasoning that would preclude the widespread induction and application of the Rouse approach to aeolian research. It represents a universal flux-profile configuration.

REFERENCES

Ahrens, J.P., 2003. Simple equations to calculate fall velocity and sediment scale parameter. J. Waterw. Port. C-ASCE, May/June 2003, 146-150.

Akalin, S., 2002. Water temperature effect on sand transport by size fraction in the lower Mississippi River. Ph.D. Thesis, Colorado State University, Fort Collins, Colorado. USA.

Alcántara-Carrió, J., Alonso, I., 2002. Measurement and prediction of aeolian sediment transport at Jandía Isthmus (Fuerteventura, Canary Islands). J. Coastal Res. 18, 300–315.

Almeiada, M.P., Andrade, J.S., Herrmann, H.J., 2006. Aeolian transport layer. Phys. Rev. Lett. 96, 1-4.

Anderson, R.S., Haff, B., 1986. Sediment transport by wind: Toward a general model. Geol. Soc. Am. Bull. 97, 523-535.

Anderson, R.S., Haff, P.K., 1988. Simulation of aeolian saltation. Science, 241, 820-823.

Anderson, R.S., Haff, P.K., 1991. Wind modification and bed response during saltation of sand in air. Acta Mech. [Suppl.] 1, 86-103.

Anderson, R.S., Hallet, B., 1986. Sediment transport by wind. Geol. Soc. Am. Bull. 97, 523-535.

Anderson, R.A., Sørensen, M., Willetts, B.B., 1991. A review of recent progress in our understanding of aeolian sediment transport. Acta Mech. [Suppl.] 1, 1-19.

Andreotti, B., 2004. A two-species model of Aeolian sand transport. J. Fluid Mech. 510, 47-70.

Arens, S.M., Van der Lee, G.E.M., 1994. Saltation sand traps for the measurement of aeolian transport into the foredunes. Soil Tech. 8, 61-74.

Arens, S.M., Van Boxel, J.H., Abuodha, J.O.Z., 2002. Changes in grain size of sand in transport over a foredune. Earth Surf. Processes and Landforms 27, 1163-1175.

Arnold, S., 2002. Development of the saltation system under controlled environmental conditions, Earth Surf. Processes and Landforms, 27, 817-829.

Baas, A.C.W., 2004. Evaluation of saltation flux impact responders (Safires) for measuring instantaneous aeolian sand transport intensity. Geomorphology 59, 99-118.

Bagnold, R.A., 1935. The movement of desert sand. Geogr. J. 85, 342-365.

Bagnold, R.A., 1936. The movement of desert sand. Proc. R. Soc. London. Ser. A. Mathematical and Physical Sciences, 157, 594-620.

Bagnold, R.A., 1941. The physics of blown sand and desert dunes. Meuthen, London.

Bauer, B.O.B., in press. Fundamentals of aeolian sediment transport: boundary layer processes. Elsevier Treatise on Geomorphology.

Bauer, B.O.B., 2009. Contemporary research in aeolian geomorphology. Geomorphology 105, 1-5.

Bauer, B.O.B, Houser, C.A., Nickling, W.G., 2004. Analysis of velocity profile measurements from wind tunnel experiments with saltation. Geomorphology, 59, 81-98.

Bechteler, W., Farber, K., Schrimpf, W., 1983. Settling velocity measurements in quiescent and turbulent water. 2nd Int. Symp. On River Sed., Nanjing, China, 1983.

Blott, S.J., Pye, K., 2001. Gradistat: a grain size distribution and statistics package for the analysis of unconsolidated sediments. Earth Surf. Processes and Landforms 26, 1237-1248.

Bouvard, M., Petkovic, S., 1985. Vertical dispersion of spherical heavy particles in turbulent open channel flow. J. Hydr. Res. 23, 5-20.

Bridge, J.S., 2003. Rivers and floodplains: forms, processes, and sedimentary record. Blackwell Science, Oxford., MA, USA.

Bui, E.N., Mazullo, J., Wilding, L.P., 1990. Using quartz grain size and shape analysis to distinguish between aeolian and fluvial deposits in the Dallol Bosso of Niger (West Africa). Earth Surf. Processes and Landforms 14, 157–166.

Burke, P. P., 1966. Effect of Water Temperature on Discharge and Bed Configuration – Mississippi River at Red River Landing, Louisiana. Tech. Rept. No. 3, Committee on Channel Stabilization, U.S. ACE.

Butterfield, G. R., 1991. Grain transport rates in steady and unsteady turbulent airflows. Acta Mech. [Suppl.] 1, 97-122.

Butterfield, G.R., 1999. Near-bed mass flux profiles in aeolian saltation: high resolution measurements in a wind tunnel, Earth Surf. Processes and Landforms 24, 393-412.

Celik, I., Rodi, W., 1988. Modeling suspended sediment transport in nonequilibrium situations. J. Hydr. Eng. 114, 1157-1191.

Chen, W., Fryrear, D.W., 2001. Aerodynamic and geometric diameters of airborne particles, J. Sed. Res. 71, 365-371.

Cheng, N-S., 1997. Simplified settling velocity formula for sediment particle. J. Hydr. Eng. 123, 149-152.

Chen, W., Yang, Z., Dong, Z., 1995. Vertical distribution of grain-size parameters of drifting particles during sand storms in the Taklamakan Desert, Central Asia. Phys. Geogr. 16, 503-523.

Cheng, H., Zou, X-Y., Zhang, C-L., 2006. Probability distribution functions for the initial liftoff velocities of saltating sand grains in air. J. Geophys. Res. 111, D22205, doi:10.1029/2006JD007069.

Cheng, H., Zou, X-Y., Zhang, C-L., Quan, Z-J., 2009. Fall velocities of saltating sand grains in air and their distribution laws. Power Tech. 192, 99-104.

Chepil, W.S., 1945. Dynamics of wind erosion: nature of movement of soil by wind. Soil Sci. 60, 305-320.

Chiu,. T.Y., 1972. Sand tranport by wind. University of Florida (Gainesville), Dept. Coastal and Oceanographic Engineering, Tech. Rept. TR-040.

Clark, P.E., Quadir, J.A., 1981. Prop transport in hydraulic fractures: a critical review of particle settling velocity equations. SPE/DOE Low Permeability Symposium, Denver, Colorado, 27-29 May, Paper SPE/DOE 9866.

Colby, B.R., Hembree, C.H., 1955. Computation of total sediment discharge, Niobrara River near Cody, Nebraska, U.S. Geol. Surv. Water Supply Paper 1357.

Coleman, N. L., 1970. Flume studies of the sediment transfer coefficient. Water Res. 6, 801-809.

Coleman, N. L., 1981. Velocity profiles with suspended sediment. J. Hydr. Res. 19, 211-229.

Cui, B., Komar, P.D., Baba, J., 1983. Settling velocities of natural sand grains in air. J. Sediment. Petrol. 53, 1205–1211.

Dietrich, W. E., 1982. Settling velocity of natural particles. Water Resour. Res., 18, 1615–1626.

Dong, F., Liu, D., 1997. Intellection about the vertical profiles of particle concentration and mass flux in the blown sand layer (in Chinese). Mech Pract. 19, 42-44.

Dong, Z., Liu, X., Wang, H., Wang, X., 2002. Aeolian sand transport: a wind tunnel model. Sediment. Geol. 161, 71-83.

Dong, Z., Liu, X., Li, F., Wang, H., and Zhao, A., 2002. Impact-entrainment relationship in a saltating cloud. Earth Surf. Processes and Landforms 27, 641-658.

Dong, Z., Lu, J., Man, D., Lv, P., Qian, G., Zhang, Z., Luo, W., 2011. Equations for the near-surface mass flux density profile of wind-blown sediments. Earth Surf. Processes and Landforms 36, 1292-1299.

Dong, Z, Sun, H., Zhao, A., 2004a. WITSEG sampler: a segmented sand sampler for wind tunnel test. Geomorphology 59, 119-129.

Dong, Z., Wang, H., Liu, X., and Wang, X., 2004b. The blown sand flux over a sandy surface: a wind tunnel investigation on the fetch effect. Geomorphology 1363, 1 - 11.

Dong, Z., and Qian, G., 2007. Characterizing the height profile of the flux of wind-eroded sediment. Environ Geol. 51, 835-845.

Dong Z, Qian G, Luo W., Wang H. 2006. Analysis of the mass flux profiles of an aeolian saltating cloud. J. Geophys. Res. Atmos. 111, doi: 10.1029/2005JD006630.

Doorschot, J.J.J., Lehning, M., 2002. Equilibrium saltation: mass fluxes, aerodynamic entrainment, and dependence on grain properties. Bound.-Lay. Meteorol. 104, 111-130.

Draga, M., 1983. Eolian activity as a consequence of beach nourishment – observations at Westerland (Sylt), German North Sea coast. Z. Geomorphol. [Suppl.] 45, 303-319.

Duran, O. Herrmann, H., 2006. Modelling of saturated sand flux. J. Stat. Mech. Theory. E. 07, 1-15.

Dyer, K.R., 1986. Coastal and estuarine sediment dynamics. John Wiley & Sons, Chichester, UK.

Einstein, H. A., Chien, N., 1955. Effects of Heavy Concentration near the Bed on the Velocity and Sediment Distribution. Rept. 8, U.S. Corp of Engineers, Uni. Cal. Inst. Eng. Res., 25pp.

Ellis, J.T., Li, B., Farrell, E.J., Sherman, D.J., 2009. Protocols for characterizing aeolian mass-flux profiles. Aeolian Res. 1, 19-26.

Farrell, E.J., Sherman, D.J., 2004. Process-scaling issues for aeolian transport modelling in field and wind tunnel experiments: roughness length and mass flux distributions. J. Coast. Res. SI39, 384-389.

Feng, D.J., Li, Z.S., Ni, J.R., 2009. Launch velocity characteristics of non-uniform in aeolian saltation. Physica A 388, 1367-1374.

Ferguson, R.I., Church, M., 2004. A simple universal equation for grain settling velocity. J. Sediment. Res. 74, 933-937.

Folk, R.L., Ward, W.C., 1957. Brazos River bar: a study in the significance of grain size parameters. J. Sediment. Petrol. 27, 3-26.

Foucaut, J.-M., Stanislaus, M., 1997. Experimental study of saltating particle trajectories. Exp. Fluids 22, 321-326.

Friedman GM., 1979. Differences in size distributions of populations of particles among sands of various origins. Sedimentology 26, 3–32.

Gares, P.A., Davidson-Arnott, R.G.D., Bauer, B.O., Sherman, D.J., Carter, R.W.G., Jackson, D.W.T., Nordstrom, K.F., 1996. Alongshore variations in aeolian sediment transport: Carrick Finn Strand, Ireland. J. Coast. Res. 12, 673-682.

Gelfenbaum, G., Smith, J. D., 1986. Experimental evaluation of a generalized suspended-sediment transport theory. In: Knight, R. J., McLean, J. R., (Eds.), Shelf and Sandstones, Canadian Society of Petroleum Geologists Memoir II, pp. 133-144.

Gerety, K.M., 1985. Problems with determination of u_* from wind velocity profiles measured in experiments with saltation. Proc. Int. Workshop on the Physics of Blown Sand, Dept. Theor. Stat., Aarhus Uni., Denmark, pp. 271-300.

Gerety, K.M., Slingerland, R., 1983. Nature of the saltating population in wind tunnel experiments with heterogenous size-density sands. In: Brookfeld, M.E., Ahlbrand, T.S. (Eds.), Eolian sediments and progresses: developments in sedimentology. Elsevier, Amsterdam, pp. 115-131.

Gibbs, R.J., Mathews, M.D., Link, D.A., 1971. The relationship between sphere size and settling velocity. J. Sediment. Petrol 41, 7-18.

Gillette, D. A., Walker, T. R., 1977. Characteristics of airborne particles produced by wind erosion of sandy soil, high plains of West Texas, Soil Sci. 123, 97-110.

Graf, W.H., Cellino, M., 2002. Suspension flows in open channels; experimental study. J. Hydr. Res. 40, 435-447.

Grams, P.E., P.R. Wilcock, Wiele, S.M., 2006. Entrainment and non-uniform transport of fine-sediment in coarse-bedded rivers. In: Parker, G., Garcia, M.H. (Eds.), River, Coastal and Estuarine Morphodynamics: RCEM 2005, Taylor and Francis Group, London, pp. 1073-1081.

Greeley, R., Blumberg, D.G., Williams, S.H., 1996. Field measurements of the flux and speed on wind-blown sand. Sedimentology 43, 41-52.

Greeley, R., Sullivan, R., 1992. Aerodynamic roughness measured in the field and simulated in a wind tunnel. NASA CR 4422, 50pp.

Haff, P.K., Anderson, R.S., 1993. Grain scale simulations of loose sedimentary beds: the example of grain-bed impacts in aeolian sedimentation. Sedimentology 40, 175-198.

Hallermeier, R. J., 1981. Terminal settling velocity of commonly occurring sand grains. Sedimentology 28, 859–865.

Hasi, W., 1997. Preliminary study on the vertical distributions of wind dust over Bashang Plateau, Hebei Province. J. Desert Res. 17, 9 – 14 (in Chinese).

Hatano, Y., Kanda, Y., Udo, K., Takewaka, S., Ueki, R., Hatano, N., Mouri, H., Chiba, M., Kurihara, K., Nishimura., H., 2004. A wind tunnel experiment of sand transport and its comparison with the Werner model. J. Geophys. Res. 109, F01001, doi:10.1029/2002JF000015.

Hill, P.S., Nowell, A.R.M., Jumars, P.A., 1988. Flume evaluation of the relationship between suspended sediment concentration and excess boundary shear stress. J. Geophys. Res. 93, C10, 12499-125099.

Hotta, S., Horikawa, K., 1993. Vertical distribution of sand transport rate by wind, Coastal Eng. 36, 91– 110.

Hotta, S., S. Kubota, N. Nakamura, K. Hosaka, K., 2006. Wind tunnel study of vertical distribution of sand transport rate by wind. In: Smith, J.M (Ed.), Proc. 30th Int. Conf. Coast. Eng., ASCE, New York, pp. 2604-2616.

Hughes, S. A., 1983. Movable-bed modeling law for coastal dune erosion. J. Water. Port, C. Div., ASCE, New York, 109, No. 2.

Hunt, J. N ., 1954. The turbulent transport of suspended sediment in open channels, Proc. Roy. Soc. London Ser. A, 24, 322-335.

Hunt, J.C.R., Nalpanis, P., 1985. Saltating and suspended particles over flat and sloping surface. In: Barndorff-Nielsen, O.E., Moller, J.T., Rasmussen, K.R., and Willetts, B.B. (Eds.), Proceedings on international workshop on the physics of blown sand, Aarhus University, Denmark, pp. 9-36.

Ikeda,S., Asaeda, T., 1983. Sediment suspension with rippled bed. J. Hydr. Eng., Proceedings of ASCE, 109, 409-442.

Ishihara,T., Iwagaki, Y., 1952. On the effect of sand storm in controlling the mouth of the Kiku river. Disas. Prev. Res. Inst., Kvoto Universitv Bull. No.2.

Ismail, H . M ., 1952. Turbulent transfer mechanism and suspended sediment in closed channels. T. ASCE 117, 409-446.

Itakura, T., T. Kishi, 1980. Open Channel Flow with Sediment Transport. J. Hydr. Div., ASCE, 106, 1345-1352.

Jackson, N.L., Sherman, D.J., Hesp, P.A., Klein, A.H.F., Ballasteros Jr., F., Nordstrom, K.F., 2006. Small-scale spatial variations in aeolian sediment transport on a fine-sand beach. J. Coast. Res. SI39, 379-383.

Jakuschoff, P., 1932. The movement of suspended matter in rivers in theory and practice. Rept. No. 5-6, Die Wasserwirtschaft.

Janin, L.G., Cermak, J.E., 1988. Sediment-laden velocity profiles developed in a long boundary-layer wind tunnel. J. Wind Eng. Ind. Aerod. 28, 159– 168.

Jensen, J.L., Sørensen, M., 1986. Estimation of some saltation transport parameters: a re-analysis of Williams' data. Sedimentology 33, 547 - 558.

Jensen, J.L., Rasmussen, K.R., Sørensen, M., Willetts, B.B., 1984. The Hantsholm Experiment 1982: Sand grain saltation on a beach. Uni. Aarhus Dept. Theor. Stat. Res. Rept. No. 125.

Jiménez, J.A., Madsen, O.S., 2003. A simple formula to estimate settling velocity of natural sediments. J. Water. Port. C. Div. ASCE, March/April 2003, 70-78.

Julien, P.Y., 1995. Erosion and Sedimentation. Cambridge University Press, Cambridge, UK, 279pp.

Kalinske, A. A ., C . L . Pien, 1943. Experiments on eddy diffusion and suspended material transportation in open channels, Eos Trans. AGU, 24, 530-536.

Kang, L., Liu, D., 2010. Numerical investigation of particle velocity distributions in aeolian sand transport. Geomorphology 115, 156-171.

Kawamura, R., 1951. Study on sand movement by wind. Kagaku 18, 24-30 (in Japanese).

Kok, J.F., Renno, N.O., 2009. A comprehensive numerical model of steady state saltation (COMSALT). J. Geophys. Res. 14, D17204, doi: 10.1029/2009JD011702.

Krumbein W.C., F.J. Pettijohn, 1938, Manual of sedimentary petrography. Appleton-Century-Crofts, New York.

Laursen, E. M., 1958. The total sediment load of streams. J. Hydraul. Div. ASCE. 84, 1-36.

Lees, B.J., 1981. Relationship between eddy viscosity of seawater and eddy diffusivity of suspended particles. Geo-mar. Lett. 1, 249-254.

Lee, G.-H., Dade, W.B., Friedrichs, C.T., and Vincent, C.E., 2004. Examination of reference concentration under waves and currents on the inner shelf. J. Geophys. Res.109, 1–10.

Lee H.Y., Hsieh, H.M., 2003. Numerical simulations of scour and deposition in a channel network. Int. J. Sediment. Res. 18, 32-49.

Leighly, J., 1932. Toward a theory of the morphologic significance of turbulence in the flow of water in streams. University of California Publication in Geography 6, 1-22.

Leighly, J., 1932. Turbulence and the transportation of rock debris by streams. Geogr. Rev. 24, 453-464.

Leys, L., McTainish. T., 1996. Sediment fluxes and particle grain-size characteristics of wind-eroded sediments in southeastern Australia. Earth Surface Proc. and Landforms 21, 661-671.

Li, B., 2011. Evaluating the von Kármán constant in sediment-laden air flow. PhD thesis, Texas A&M University, 97pp.

Li, X., Dong, Z., Zheng, X., 2005. Experimental analysis of sand particles' lift-off and incident velocities in wind-blown sand flux. Act. Mech. Sin. 21, 564-573.

Li, Z.S., Feng, D.J, Wu, S.L., Borthwick, A.G.L., Ni, J.R., 2008. Grain size and transport characteristics of non-uniform sand in aeolian saltation. Geomorphology 100, 484-493.

Li, Z.S., Ni, J.R. 2002. Sampling efficiency of vertical array aeolian sand traps. In: Lee, J.A., Zobeck, T.M. (Eds.), Proceedings of ICAR5/GCTE-SEN Joint Conf., Int. Center for Arid and Semiarid Lands Studies, Texas Tech Uni., Lubbock, Texas, USA, pp. 45-18.

Li, Z.S., Ni, J.R., 2003. Sampling efficiency of vertical array aeolian sand traps. Geomorphology 52, 243-252.

Li., B., Sherman, D.J., Ellis, J., Farrell, E.J., 2010. Variability of the apparent von Kármán parameter during aeolian saltation. J. Geophys. Res. 37, L15404, doi:10.1029/2010GL044068.

Liu, X., Dong, Z., 1994. Experimental investigation of the concentration profile of a blowing sand cloud. Geomorphology 60, 371-381.

Liu, X., Dong, Z., 2004. Experimental investigation of the concentration profile of a blowing sand cloud. Geomorphology 60, 371-381.

Liu, X., Dong, Z., Wang, X., 2006. Wind tunnel modeling and measurements of the flux of wind-blown sand. J. Arid Env. 66, 657-672.

Maia, L.P., Freire, G.S.S., Lacerda, L.D., 2005. Accelerated dune migration and aeolian transport during El Niño events along the NE Brazilian Coast. J. Coast. Res. 21, 1121-1126.

Malcolm, L.P., Raupach, M.R., 1991. Measurements in an air settling tube of the terminal velocity distribution of soil material. J. Geophys. Res. 96, 15275-15286.

McEwan, I.K., Willetts, B.B., 1991. Numerical model of the saltation cloud. Acta Mech. [Suppl.], 1, 53-66.

McKenna Neuman, Maljaars, C.M., 1997. Wind tunnel measurement of boundary layer response to sediment transport, Bound. Lay. Meteorol. 84, 67–83.

McKenna Neuman, C., Nickling, W.G., 1994. Momentum extraction with saltation: implications for experimental evaluation of wind profile parameters. Bound. Lay. Meteorol. 68, 35-50.

McKenna Neuman, C., Scott, M.M., 1998. A wind tunnel study of the influence of pore water on aeolian sediment transport. J. Arid Env. 39, 403–419.

McLean, S. R., 1992. On the calculation of suspended load for noncohesive sediment. J. Geophys. Res. 97, 5759-5770.

McNown, J. S., P. N. Lin, 1952. Sediment concentration and fall velocity. Proc. 2nd Midwestern Conf. Fluid Mech., Ohio State University, Columbus, OH, pp. 401-411.

Metivier, F., Meunier, P., 2003. Input and output flux correlations in an experimental braided stream. Implications on the dynamics of the bed load transport. J. Hydrol. 271, 22–38.

Mikami, M., Yamada, Y., Ishizuka, M., Ishimaru, T., Gao, W., Zeng, F., 2005. Measurement of saltation process over gobi and sand dunes in the Taklimakan desert, China, with newly developed sand particle counter. J. Geophys. Res. 110, doi: 10.1029/2004JD004688.

Mikkelsen, H.E., 1989. Wind flow and sediment transport over a low coastal dune, Geoskrifter, 32, 2-47.

Mohammed, A.E., C.J. Stigler, Adam, H.S., 1996. Moving sand and its consequences on

a severely desertified environment and a protective shelterbelt, Arid Soil Res. Rehab. 9, 423-435.

Nalpanis, P., 1985. Saltating and suspended particles over flat and sloping surfaces. Experiments and numerical simulations. In: Barndorff-Nielsen, O.E., Moller, J.T., Rasmussen, K.R., Willetts, B.B. (Eds.), Proceedings on international workshop on the physics of blown sand, Aarhus University, Denmark, pp. 37-66.

Nalpanis, P., Hunt, J.C.R., Barrett, C.F., 1993. Saltating particles over flat beds. J. Fluid Mech. 251, 661-685.

Namikas, S.L., 2003. Field measurement and numerical modeling of aeolian mass flux distributions on a sandy beach. Sedimentology 50, 303-326.

Namikas, S.L., 2006. A conceptual model of energy partitioning in the collisions of saltating grains with an unconsolidated sediment bed. J. Coast. Res. 22, 116-125.

Namikas, S.L., Bauer, B.O., Edwards, B.L., Hesp, P.A., Zhu, Y., 2009. Measurements of aeolian mass flux distributions on a fine-grained beach: implications for grain-bed collision mechanics. J. Coast. Res. SI 56, 337-341.

Ni, J.R., Li, Z.S., Mendoza, C., 2002. Vertical profiles of aeolian sand mass flux. Geomorphology 49, 205-218.

Nielsen, P., Teakle, I.A.L., 2004. Turbulent diffusion of momentum and suspended particles: a finite-mixing length theory. Phys. Fluids 16, 2342-2348.

Nishimura, K., Hunt, J.C.R., 2000. Saltation and incipient suspension over a flat

particle bed below a turbulent boundary layer. J. Fluid Mech. 417, 77-102.

Nordin CF, Dempster GR (1963) Vertical distribution of velocity and suspended sediment, middle Rio Grande, New Mexico. U.S. Geological Survey Professional Paper 462 B, USGS, Washington D.C.

O'Brien, M.P., 1933. Review of the theory of turbulent flow and its relations to sediment transport. T. Am. Geophys. Union 14, 487–491.

Orton, P.M., Kinke, G.C., 2001. Comparing calculated and observed vertical suspended-sediment distributions from a Hudson River estuary turbidity maximum. Estuar. Coast. Shelf S. 52, 401-410.

Owen, P.R. (1964) Saltation of uniform grains in air. J. Fluid Mech. 20, 225-242.

Owen, P., Gillette, D., 1985. Wind tunnel constraint on saltation. In Proceedings on international workshop on the physics of blown sand. In: Barndorff-Nielsen, O.E., Moller, J.T., Rasmussen, K.R., Willetts, B.B. (Eds.), Proceedings on international workshop on the physics of blown sand. Aarhus University, Denmark, 253-269.

Parker, G., 2004. 1D Sediment Transport Morphodynamics with Applications to Rivers and Turbidity Currents. http://vtchl.uiuc.edu/people/parkerg/morphodynamics_e-book.htm. Last accessed: 20 January 2012.

Parker, G., Coleman, N. L., 1986. Simple-model of sediment-laden flow. J. Hydraul. Eng. 112, 356-375.

Rasmussen, K.R., Mikkelsen, H.M, 1988. Development of a boundary layer wind

tunnel for aeolian studies. Geoskrift no. 27. Department of Earth Sciences, Aarhus Univeristat. Denmark, 35pp.

Rasmussen, K.R., H.E. Mikkelsen, H.E., 1998. On the efficiency of vertical array aeolian field traps. Sedimentology 45, 789-800.

Rasmussen, K.R, Sørensen, M., Willetts, B.B., 1985. Measurement of saltation and wind strength on beaches. In: Barndorff-Nielsen, O.E., Moller, J.T., Rasmussen, K.R., Willetts, B.B. (Eds.), Proceedings on international workshop on the physics of blown sand. Aarhus University, Denmark, 301-326.

Rasmussen, K.R., M. Sørensen, M., 1999. Aeolian mass transport near the saltation threshold, Earth Surf. Processes and Landforms 24, 413-422.

Rasmussen, K. R., Sørensen, M., 2005. Dynamics of particles in aeolian saltation. In: Garcia-Rojo, R., Herrmann, H.J. McNamara, S. (Eds.), Powders and Grains, 967–971.

Rasmussen, K.R., Sørensen, M., 2008. Vertical variation of particle speed and flux density in aeolian saltation: measurement and modeling. J. Geophys. Res. 113, F02S12, doi: 10.1029/2007JF000774.

Raupach, M.R., 1991. Saltation layers, vegetation canopies and roughness lengths. Acta Mech. 1, 83-96.

Rice, M.A, Willetts, B.B., McEwan, I.K., 1995. An experimental study of multiple grain-size ejecta produced by collision of saltating grains with a flat bed. Sedimentology 42, 695-706.

Rose, C., Thorne, P., 2001. Measurements of suspended sediment transport parameters in a tidal estuary. Cont. Shelf Res. 21, 1551–1575.

Rouse, H., 1936. Nomogram for the settling velocity of spheres. National Research Council Committee on Sedimentation Publication, 57–64.

Rouse, H., 1937. Modern Conceptions of the Mechanics of Fluid Turbulence. T. ASCE 102, 463-543.

Rouse H., 1938. Experiments on the mechanics of sediment suspension. Proceedings of the 5th International Congress for Applied Mechanics, Cambridge, MA, 550-554.

Rubey, W.W., 1933. Settling velocities of gravel, sand, and silt particles. American J. Sci. 25, 325-338.

Rumpel, D.A., 1985. Successive aeolian saltation: studies of idealized collisions. Sedimentology 32, 267-280.

Sauermann, G., Kroy, K., Herrmann, H.J., 2001. A continuum saltation model for sand dunes, Phys. Rev. E 64, 31305-31316.

Schmidt, W., 1925. Der Massenaustausch in freier Luft und verwandte Erschinungen. In Probleme der Kosmischen Physik, Bd, 7, Hamburg.

Scott, W.D., 1995. Measuring the erosivity of the wind. Catena, 24, 163-175.

Scott, W.D., J.M. Hopwood, K.J. Summers, K.J., 1995. A mathematical model of suspension with saltation, Act. Mech. 108, 1-22.

Shah-Fairbank, S.C., 2009. Series expansion of the modified Einstein procedure. Ph.D.

Thesis, Colorado State University, Fort Collins, Colorado, USA.

Shao, Y., 2000. Physics and modeling of wind erosion. Kluwer, Dordrecht.

Shao, Y., Li, A., 1999. Numerical modelling of saltation in the atmospheric surface layer. Bound. Lay. Meteorol. 91, 199-225.

Shao, Y.P., Mikmai, M., 2005. Heterogenous saltation: theory, observation and comparison. Boundary-Layer Meteorology, 115, 359-379.

Shao, Y., Raupach, M.R., 1992. The overshoot and equilibration of saltation. J. Geophys. Res. 97, 20559-20564.

Sharp, R.P., 1964. Wind-driven sand in the Coachella Valley, California. Geol. Soc. Am. Bull. 75, 785-804.

Sharp, R.P., 1966, Kelso Dunes, Mohave Desert, California. Geol. Soc. Am. Bull. 77, 1045–1074,

Simiu, E., Scanlon, R.H., 1997. Wind effects on structures. In: Fundamentals and Applications to Design, 3rd ed. John Wiley, New York.

Sherman, D.J., Farrell, E.J., 2008. Aerodynamic roughness lengths over movable beds: comparison of wind tunnel and field data. J. Geophys. Res. 113, F02S08, doi: 10.1029/2007JF000784.

Sherman, D. J., Jackson, D. W. T., Namikas S. L., Wang, J., 1998. Wind-blown sand on beaches: an evaluation of models. Geomorphology 22, 113–133.

Sherman, D.J., Li, B., in press. Predicting aeolian sand transport rates: a reevualtion

of models. Aeolian Res.

Shibayama, T., and Rattanapitikon, W., 1993. Vertical distribution of suspended sediment concentration in and outside the surf zone. Coast. Eng. in Japan, JSCE, 36, 49-65.

Smith, J. D., McLean, S. R. 1977. Spatially Averaged Flow over a Wavy Surface. J. Geophys. Res. 82, 1735-1746.

Sorensen, M., 1985. Estimation of some aeolian saltation transport parameters from transport rate profiles. In: Barndorff-Nielsen, O.E., Moller, J.T., Rasmussen, K.R., Willetts, B.B. (Eds), Proceedings on international workshop on the physics of blown sand,. Aarhus University, Denmark, 141-190.

Sorensen, M., 1991. An analytic model of wind-blown sand transport. Act. Mech. 1, 67-81.

Sorensen, M., 2004. On the rate of aeolian sand transport. Geomorphology 59, 53–62.

Spies, P.J., McEwan, I.K., 2000. Equilibration of saltation. Earth Surf. Processes and Landforms 25, 437-453.

Spies, P.J, McEwan, I. K., Butterfield, G.R., 1995, On wind velocity profile measurements taken in wind tunnels with saltating grains, Sedimentology 42, 515– 521.

Spies, P. J., McEwan, I.K., Butterfield, G. R., 2000. One-dimensional transitional behavior in saltation, Earth Surf. Processes and Landforms, 25, 505– 518.

Sterk, G., Raats, P.A.C., 1996. Comparison of models describing the vertical distribution of wind-eroded sediment, Soil Sci. Soc. Am. J. 60, 1914-1919.

Stout, J.E., Zobeck, T.M., 1996. The Wolfforth Field Experiment: a wind erosion study, Soil Sci. 161, 616-632.

Sun, Q.C., Wang, G.Q., 2001. Simulation of dynamic behavior of saltating grains from loose sedimentary bed. J. Desert Res. [Suppl.] 21, 17-21 (in Chinese).

Sundborg, A., 1955. Meteorological and climatological conditions for the genesis of aeolian sediments, Geograf. Ann., 37, 94-111.

Tsaor, H., 2005. Sand dunes mobility and stability in relation to climate. Physica A, 50-56.

Tsaor, H., Pye, K., 1987. Dust transport and the question of desert loess formation. Sedimentology 34, 139-153.

Tsuchiya, Y., 1970. Successive saltation of a sand grain by wind. Coast. Eng. Conf. ASCE III, 1417-1427.

Udo, K., Mano, A., 2009. Application of Rouse's sediment concentration profile to aeolian transport: is the suspension system for sand transport in air the same as that in water? J. Coast.Res. SI64, 2079-2083.

Van Boxel, J. H., Sterk, G., Arens, S. M., 2004. Sonic anemometers in aeolian sediment transport research, Geomorphology 59, 131-147, doi: 10.1016/j.geomorph.2003.09.011.

Van der Wal, D., 2000. Grain-size-selective aeolian sand transport on a nourished beach. J. Coast. Res. 16, 896-908.

Van Dijk, P.M., 1990. Wind erosion measurements on Schiermonnikoog: a study with acoustic sensors and sediment catchers. Rept. No. 1. Department of Irrigation and Soil and Water Conservation, Wageningen Agricultural University, 23pp.

Van Rijn, L. C., 1984. Sediment transport, Part II: suspended load transport. J. Hydraul. Eng. ASCE, 110, 1613-1641.

Van Rijn, L. C., 1993. Principles of sediment transport in rivers, estuaries and coastal seas. Aqua Publications: Amsterdam.

Vanoni, V. A., 1941. Some experiments on the transportation of suspended load. T. 22nd Annual Meeting, AGU, 22, 608-628.

Vanoni, V.A. 1946. Transportation of suspended sediment by water. T. ASCE, 111, 67-133.

Vanoni, V.A., Nomicos, G.N., 1960. Resistance properties of sediment-laden streams. T. ASCE 125, 1140-1175.

Vories, E.D., Fryrear, D.W., 1991. Vertical distribution of wind-eroded soil over a smooth, bare field. T. Am. Soc. Agric. Eng. 34, 12763-1768.

Weerappuli, D. P., 1980.Velocity and Suspended Sediment Distributions in a Missouri River Reach. M.S. Thesis, Dept. of Civil Engr., Colorado State Univ., Fort Collins, CO.

Weinan, C., Zuotao, Y., Jiashen, Z., Zhiwen, H., 1996. Vertical distribution of wind blown sand flux in the surface layer, Taklamakan Desert, Central Asia. Phys. Geogr. 17, 193-218.

Werner, B.R., 1990. A steady-state model wind blown sand transport. J. Geol. 98, 1-17.

White, B. R., 1996. Laboratory simulation of aeolian sand transport and physical modeling of flow around dunes, Ann. Arid Zone 35, 187– 213.

White, B. R., Mounla, H., 1991. An experimental study of Froude number effect on wind tunnel saltation, Act. Mech. [Suppl.] 1, 145– 157.

White, B.R., Schulz, J.C., 1977. Magnus effect in saltation. J. Fluid Mech. 81, 497-512.

Willetts, B.B., Rice, M.A., 1985. Inter-saltation collsions. In: Barndorff-Nielsen, O.E., Moller, J.T., Rasmussen, K.R., Willetts, B.B., (Eds.), Proceedings on international workshop on the physics of blown sand, Aarhus University, Denmark, pp. 83-100.

Willetts, B.B., Rice, M.A., 1986a. Collisions in aeolian saltation. Act. Mech. 63, 255-265.

Willetts, B.B., Rice, M.A., 1986b. Collisions in aeolian transport: the saltation/creep link. In: Aeolian Geomorphology, Nickling, W.G., (Ed.), Allen and Unwin, Boston, 1-17.

Williams, G.P., 1964. Some aspects of the eolian saltation load. Sedimentology 9, 89-104.

Wilson, L., Huang, T.C., 1979. The influence of shape on the atmospheric settling velocity of volcanic ash particles. Earth Planet. Sci. Lett. 44, 311–324.

Wu, Z., Ling, Y.Q., 1965. A preliminary study of wind-blown sand movement and sand disaster prevention. Res. Sand Disaster Prev., 7, 7 – 14 (in Chinese).

Xie, L., Zheng, X.J., 2003. Distribution of initial velocity of lift-off sand particles in aeolian saltation. J. Desert Res. 23, 637-641 (in Chinese).

Xing, M., 2007. The harmonious character in equilibrium aeolian transport on mixed sand bed. Geomorphology 86, 230-242.

Xing, M., Guo, L., 2004. A modified probability distribution of ejection state of sand grains in equilibrium aeolian sand transport. Phys. Lett. A 332, 389-397.

Xing, M., Wu, C., Adams, M.J., 2011. The saltations of different sized particles in aeolian sand transport. Geomorphology 134, 217-223.

Yang, P., Dong, Z., Qian, G., Luo, W., Wang, H., 2007. Height profile of the mean velocity of an aeolian saltating cloud: wind tunnel measurements by particle image velocimetry. Geomorphology, 89, 320-334.

Youssef, F., Erpul, G., Bogman, P., Cornelis, W.M., Gabriels, D., 2008. Determination of efficiency of vaseline slide and Wilson and Cooke sediment traps by wind tunnel experiments. Environ Geol. 55, 741-750.

Zhang, W., Wang, Y., Lee, S.-J., 2007a. Two-phase measurements of wind and saltating sand in an atmospheric boundary layer. Geomorphology 88, 109-119.

Zhang, W., Kang, J.H., Lee, S.J., 2007b. Visualization of saltating sand particle movement near a flat ground surface. J. Visual. 10, 39-46.

Zhang, W., Kang, J.H., Lee, S.J., 2008. Simultaneous PIV and PTV measurements of wind and sand particle velocities. Exp. Fluids 45, 241-256.

Zhang, R., Xie, J., 1993. Sedimentation research in China: systematic selections. China Water and Power Press, Bejing.

Zheng X., He, H., Zhou, Y. H., 2004. Theoretical model of the electric field produced by charged particles in windblown sand flux, J. Geophys. Res. 109, D15208, doi:10.1029/2004JD004863.

Zhou, Y., Guo, X., Zheng, X. J., 2002. Experimental measurement of wind-sand flux and sand transport for naturally mixed sands, Phys. Rev. E 66, 0213505, 1-9.

Zhu, J.J., Qi, L.X., Kuang, Z.B., 2001. Velocity distribution of particle phase in saltating layer of wind-blown-sand two phase flows. Act. Mech. Sin. 13, 36-45.

Zingg, A.W., 1953. Wind tunnel studies of the movement of sedimentary material. In: Hydraul. Conf. Proc., Uni. Iowa Studies in Eng. 24, 111-135.

Znamensky, A.I., 1960. Experimental Research of Wind Erosion on Sands and Questions of Protection Against Sand Drifts. Science Press, Beijing. 120 pp., (in Chinese).

Zobeck, T.M., Fryrear, D.W., 1986. Chemical and physical characteristics of windblown sediment, II. Chemical characteristics and total soil and nutrient discharge. T. ASAE 29, 1037-1041.

Zou, X.Y., Dong, G.R., Liu, Y.Z., 1992. Vertical initial velocity distribution function of saltating sand grains in wind-sand current structure. Chinese Sci. Bull. 37, 2175-2177 (in Chinese).

Zou, X., Hao, Q., Zhang, C., Yang, B., Liu, Y., Dong, G., Zhou, S., 1999. The trajectory parameters analysis of saltating sand grains driven by wind. Chinese Sci. Bull. 44, 1681-1685.

Zou, X.Y., Wang, Z.L., Hao, Q.Z., Zhang, C.L., Liu, Y.Z., Dong, G.R., 2001. The distribution of velocity and energy of saltating grains in a wind tunnel. Geomorphology 36, 155-165.

APPENDIX A

Experiments Descriptions

This appendix contains a brief summary of the all the experiments in the literature that reported measuring mass flux profiles. These experiments are listed in Table 2-2, Section 2. The vertical flux profiles used to test Hypothesis 2 are also provided for the datasets that met the criteria (discussed in Section 3).

Arens and Lee (1995) used scale models of omnidirectional vertical sand traps deployed in field environments to measure sand transport in a wind tunnel. The traps comprised of compartments, or trays, separated by a vertical distance of 0.05 m which were stacked 0.25m and 1.50 m high when deployed on the beach and dune respectively. The trap efficiency was between 7-27% depending on wind speed, the grain-size distribution and the moisture content. Efficiency was reduced at higher wind speeds due to sediment loss by blowout and for lower wind speeds when creep processes became increasingly important. A scale model of the traps was tested in a wind tunnel with a working section 15 m long and a cross section 0.60 m wide and 0.90 m high (described in Rasmussen and Mikkelsen, 1988). Four flux profiles are shown in their Figure 6 (1:1 model) representing wind tunnel tests of the trap using commercial sand with a mean grain size 0.24 mm at four different wind speeds: 6, 8, 10 and 13 m/s. The run lengths were reported to be ten minutes. They found an exponential decrease of sand with height and with a more pronounced decrease for lower wind speeds. They also reported eight sediment curves for different scale models (1:1, 1:2 and 1:2.5) for two different wind speeds (8 and 13 m/s) and two different sands (called Schiermonnikoog and commercial sand) with means particle sizes of 0.18 and 0.24 mm respectively (their Figure 8).. They reported six profiles from a beach-dune environment (their Figure 10).

Arens et al. (2002) examined vertical and horizontal variability in grain-size distributions across a beach and foredune on Wadden Island, The Netherlands. They

placed an array of omnidirectional sand traps with 0.05 m high compartments at eleven positions across a beach-dune environment (to a maximum height of 1.5 m). The efficiency of the traps was estimated to be 15% from wind tunnel tests. The sampling duration ranged from 52 minutes to nine hours depending on sand transport rates. The average wind speed during their experiment was 15.2 m/s with a maximum and minimum of 17.8 m/s and 11.6 m/s respectively and a maximum gust (5 s) of 24 m/s. Nine vertical flux profiles measured were plotted in their Figure 4. The textural grain size parameters of mean grain size, standard deviation, skewness and kurtosis are plotted for all their runs and locations in their Figure 5. However it was not possible to identify these values for the vertical flux profiles. In general, they found that 99.5% of the sand was moving below 0.30 m on the beach.. The height of the transport *cloud* increased over the foredunes which they deduce is associated with modified saltation or short-term suspension processes developing as sand moves landward from the beach, where saltation dominates, to the dunes. They also found a reversal in grain size trends at a height about 0.15 – 0.20 m above the bed at their beach site.

Brazil (2008) was a series of experiments, described in Section 3, that examined the characteristics of the vertical flux profile over three surfaces with different grain size distributions. Transport data was collected using an array of eight, vertically-stacked hose-style traps (see Li, 2010). All the traps were 0.10 m wide. The vertical opening of the two lowest traps was 0.025 m high (trap 1 and 2). The openings of the next highest traps were 0.05 m high (trap 3 and 4) and 0.10 m high (traps 5 – 8). The flux profiles were measured in 25 runs spanning 120 - 480 seconds depending on wind speed. Shear velocities were measured for fourteen of the runs and ranged from 0.41- 0.54 m/s. The weighted mean grain size ranged from 0.235-0.248, 0.402-0.408 and 0.248-0.366 mm at the three study locations. The results from this experiment are presented and discussed in Sections 4 and 5.

Butterfield (1999) conducted near-bed mass flux experiments in a wind tunnel with a working section 8.2 m long and a cross-section 0.3 m high and 0.3 m wide. Sand transport was measured using an optical sensor for the near-bed region (<17 mm) and a conventional vertically segmented trap. The segmented trap had 27 collection chambers with an aperture opening 5 mm wide and 6.5 mm high (total height of 175.5 mm). The small capacity of the chambers meant that sampling durations were restricted to period of 10 to 30s. Five profiles were reported for sand with a mean grain size of 0.184 mm in Figure 7 for different shear velocities: 0.271, 0.339, 0.375, 0.403 and 0.441 m/s. These profiles were also reported in Li and Ni (2003) Figure 5B. The Li and Ni figure was used in this analysis.

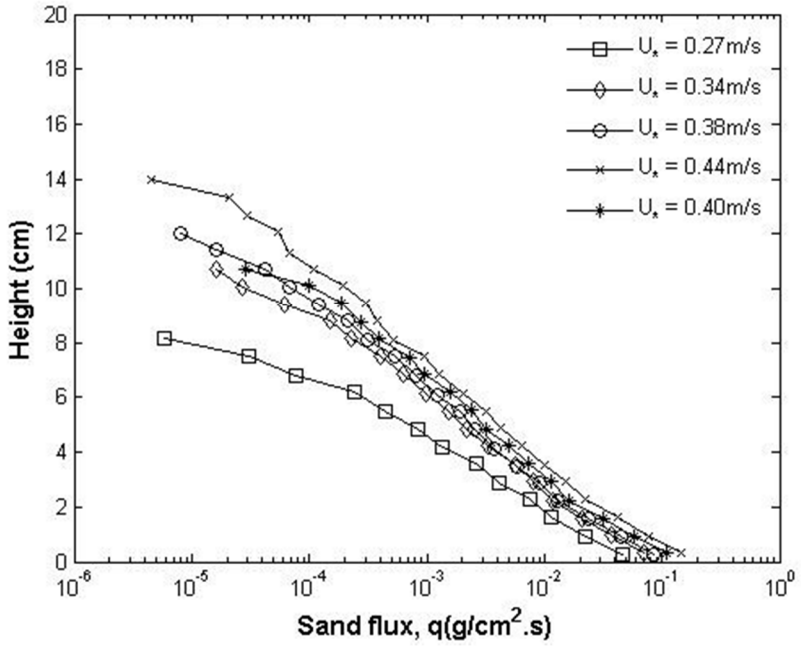

Figure A-1. Data of Butterfield (1999) obtained from Li and Ni (2003).

Dong et al., (2002) describe a series of wind tunnel experiments that examined the variability of the flux profile for differing wind speeds and grain sizes. The working section of the wind tunnel was 21 m long and had a cross section of 1.2 m x 1.2 m. They used free stream wind velocities of 8, 10, 12, 14, 16, 18, 20, and 22 m/s depending on

the grain size. The range of grain sizes used in the tests had means of 0.80-1.00, 0.63-0.80, 0.56-0.63, 0.50-0.56, 0.40-0.50, 0.25-0.40, 0.20-0.25, 0.15-0.20, and 0.10-0.15mm (see their Table 2, p.224). The vertically segmented trap was 0.60 m high comprised of 60 segments with openings 10 mm high and 5 mm wide. Run duration depended on wind speed and until 0.02 m of the sand in the test tray had been removed. Of note is that Dong et al. (2004b) used the same wind tunnel facility and very similar experimental design and free stream wind velocities. Dong et al., (2004b) note that the eight free-stream wind velocities (8, 10, 12, 14, 16, 18, 20 and 22 m/s) velocities corresponded to wind friction speeds of 0.21, 0.26, 0.31, 0.35, 0.39, 0.44, 0.49 and 0.53 m/s. We will use these shear velocities (carefully). They fit curved to the flux data using: $q_h = \alpha e(-h/\beta)$.

Figure A-2. Vertical mass flux data from Dong et al., (2002)

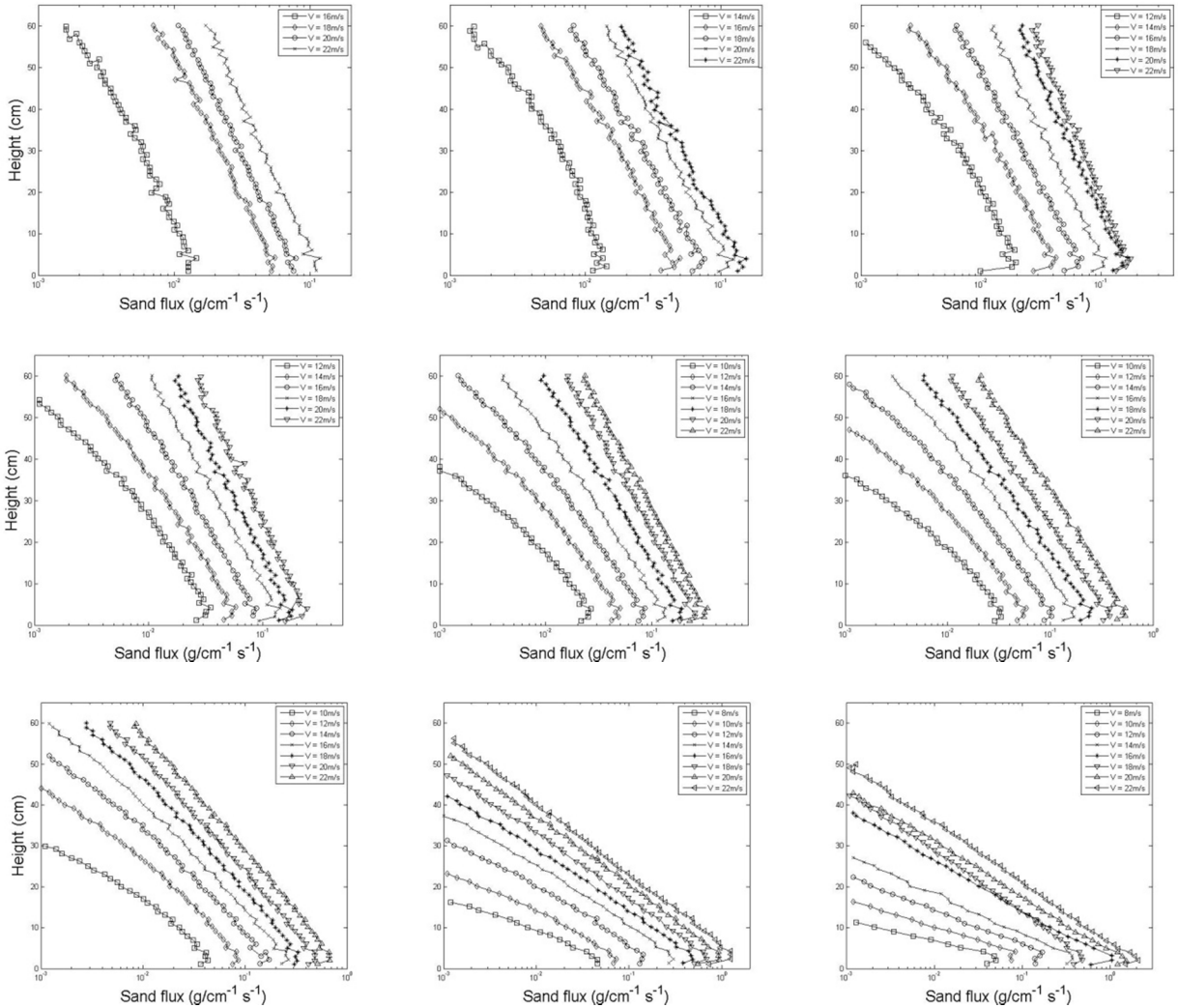

Dong et al., (2004a) details wind tunnel tests to examine the fetch effect on a sandy surface on a saltation cloud blowing over it. The experimental design was similar to that detailed in Dong et al., (2002). It was not possible to extract the 119 vertical flux profiles shown in their Figure 3 (p.120-121) due to the many overlapping points for the low fluxes measured at higher elevations. They found that the decay of flux with height above the bed could be described using and exponential function. Importantly they also observed that the "*vertical distribution of sand reach a kind of equilibrium flux profile characterized by a constant relative decay (p.122)*" which implies that a relatively stable probability distribution of particle trajectories and lift-off velocities.

Dong et al. (2004b) measured vertical flux profiles using a similar experimental design described in Dong et al., (2002). Both the wind tunnel working section dimensions and the sampler (WITSEG) are identical. They report a trap efficiency of 91%. They used dunes sands with a mean grain size of 0.18 mm. They reported (their Table 1, p.125) the exponential regression parameters for eight runs of friction velocity: 0.21, 0.26, 0.31, 0.35, 0.39, 0.44, 0.49 and 0.53 m/s. The published flux profiles provided in their Fig 2 (p.124) could not be digitized as they had too many overlapping points. However, the flux data were replicated using the data presented in their Table 1 (p.125) where V_* is friction wind speed, Q_o is the total flux, r^2 is the correlation coefficient and α and β are the fitted parameters from their equation 1 ($q_h = \alpha e(-h/\beta)$) – see Table A1.

Table A-1. Dong et al., (2004b) Table 1 (p.125)

V_* (m/s)	Q_0(kg m^{-1} s^{-1})	α	β	r^2
0.21	0.037	0.0090	0.049	0.92
0.26	0.086	0.0166	0.0610	0.89
0.31	0.178	0.0306	0.067	0.92
0.35	0.325	0.0538	0.070	0.92
0.39	0.55	0.0861	0.072	0.95
0.44	0.721	0.1084	0.075	0.96
0.49	0.952	0.1258	0.084	0.92
0.53	1.261	0.1525	0.092	0.87

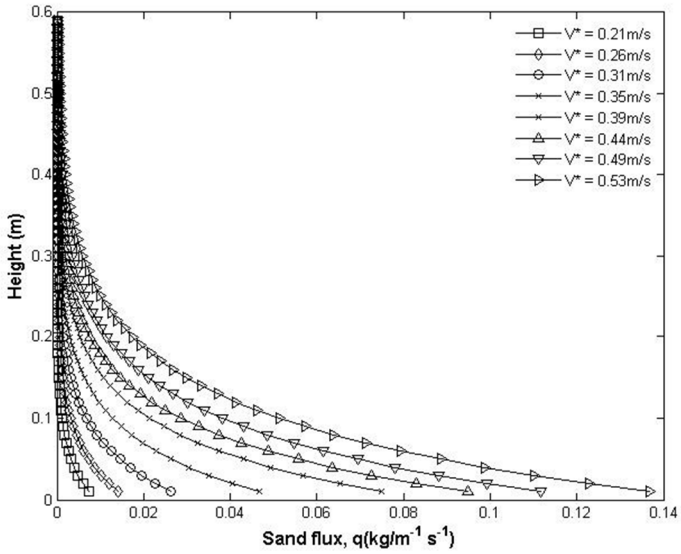

Figure A-3. Dong et al., (2002), Figure 2.

Dong et al., (2006) used particle image velocimetry to construct profiles of mean particle velocity and relative particle concentration. The vertical mass flux profiles were obtained by multiplying the mean particle velocity by the concentration profiles. They characterized their flux profiles into three regions: a near-bed region where mass flux increase with height; an upper layer where mass flux decays exponentially with height; and a region in between where a peak flux occurs but whose height varies with wind speed (height increases with higher wind speeds) and grain size (height decreases with increasing grain size). They used a wind tunnel with a working section 16.2 m long and a cross section 0.6 m high and 1.0 m wide. They used three different sized well-rounded artificial spherical quartz sands: 0.10-0.20 mm, 0.20-0.30 mm and 0.30-0.40 mm. The tests were carried out using four different free stream wind velocities: 8, 10, 12, and 14 m/s. The maximum normalized height reported was the height of the boundary layer, equal to 0.120 m. Their Figure 7 (p.7) shows 12 vertical flux profiles by combining the fitted coefficients from their Tables 3 and 4 representing the mean particle velocity and concentration respectively. They found that the average saltation height increase with

increasing wind speed and decreases with increasing grain size (their Figure 4). They also found that mass flux decays more rapidly as wind velocity decrease and particle size increases.

Dong et al., (2011) collected field data to compare the performance of seven different functions that describe the vertical distribution of mass flux above the surface. They used a 1.0 m tall vertical segment sampler (called the LDDSEG) that was divided into 50 openings 20 mm wide and 20 mm high. Wind speeds were recorded at an elevation of 10 m above the surface in 10 minute intervals from a wind tower placed 200 m away from the sampling locations. The sampling locations have four different surface types: biological crust-fixed dunes; reactivated dunes; semi-fixed dunes; and shifting dunes. Their Figure 5 (p.1297) contains 25 vertical flux profiles for sampling durations that ranged from 11 minutes (shortest, u_*= 1.18 m/s) to 21 days (longest, u_*= 0.17 m/s) depending on transport rates. These flux profiles are the mean values of all observations (85 transport events) for each month.

Dong and Qian (2007) data reported in Table 1 (p.839) is the same as those reported in Dong et al., (2002), Table 2 (p.224). The only differences are in the format of the data e.g. flux reported as g cm^{-1} s^{-1} corrected to four decimal places vs. kg $m^{-1}s^{-1}$ corrected to three decimal places. The creep fraction F_c reported in Dong et al (2002) is the *a* regression coefficient in Dong and Qian (2007). The creep is defined as the sand transport on the surface and is obtained by having $h = 0$ in the fitted exponential function: $q_h = \alpha e(-h/\beta)$, as reported in Dong et al., (2002) and Dong et al (2004b) .

Feng et al., (2009) examined the sidewall effects of a wind tunnel on wind velocity and mass flux by conducting a series of experiments with varying tunnel widths and measurements taken at different tranverse distances (0.05, 0.15, 0.30 and 0.50 m) from a sidewall. Their test section was 21 m long with a cross section 1.2 m high and 1.2m wide. They used naturally mixed dune sands that had a mean diameter of 0.35 mm.

The sand trap was vertically segmented with 30 collection chambers, each 1 cm high and 1 cm wide. The sampling durations were 3, 2, 1, 0.5 and 0.33 minutes. Their Figure 6 (p.258) reports nine different flux profiles with five different shear velocities: 0.56, 0.81, 0.93, 1.12, and 1.24 m/s. The modal shape of the mass flux profile did not change with varying wind tunnel widths or at different transverse locations. Therefore we used all nine profiles.

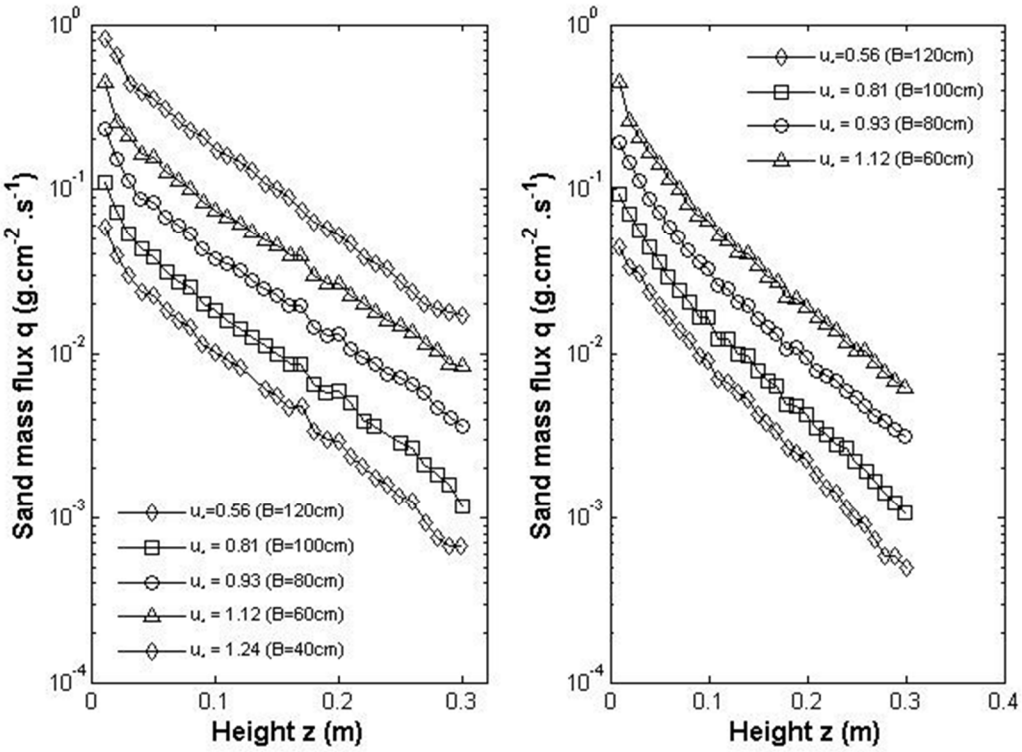

Fig A-4. Vertical mass flux profiles from Feng et al., (2009).

Gerety and Slingerland (1983) examined the distribution of particles above a surface comprised of a mixture of different mineral types in a wind tunnel 10 m long with a cross section 0.35 m wide and 0.50m high. Their stock sand was comprised of three minerals (crushed quartz, garnet and olivine) that were combined in the transport experiments. The three minerals had mean grain sizes of 0.18, 0.20 and 0.17 mm for the crushed quartz, garnet and olivine, respectively. They used an L-shaped suction tube

with an inside diameter of 4 mm to collect the samples at six different heights above the bed. Their Figure 7 (p.126) provides 4 vertical flux profiles with shear velocities of 0.20, 0.40, 0.52 and 1.10 m/s. They found that the mass flux decreases exponentially with height above the bed for all their experiments and that 60-90% of the sand moves within 20 mm of the bed surface. Their profiles were also plotted in Ni et al., (2002), figure 14, p.215 and Li and Ni (2003), figure 2, p.246. We used the four profiles in Li and Ni (2003).

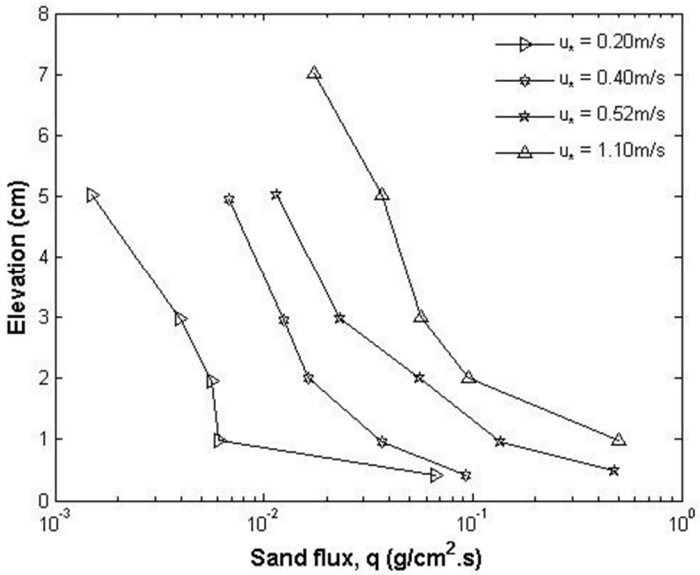

Fig A-5. Vertical mass flux profiles from Gerety and Slingerland (1983).

Greeley et al., (1996) carried out a field experiment to examine sand flux using both vertical and horizontal traps and particle speeds using high speed motion pictures from a particle velocimeter. Their Figure 11 (p.48) has 10 vertical flux profiles collected using the Ames type trap. This trap was a 0.45 m high array of stacked collectors each with an opening 0.01 m^2. The modal grain size was 0.23 mm. Wind data were not provided explicitly for each flux profile but are listed in their Table 1 (p.43) for the their trench and hycam runs. The flux runs were labeled: 1A, 1B, 1C, 2, 3, 4, 5A, 5B, 6A, 6B. The shear velocities for 1A, 1B, 5A, 5B, 6A and 6B were reported in the hycam runs in

Table 1 as 0.47, 0.51, 0.54, 0.49, 0.41 and 0.42 m/s. Runs 2, 3 and 4 are taken from the trench runs 0.312, 0.348 and 0.317 m/s respectively. These shear velocities will be used with caution for the reported flux profiles.

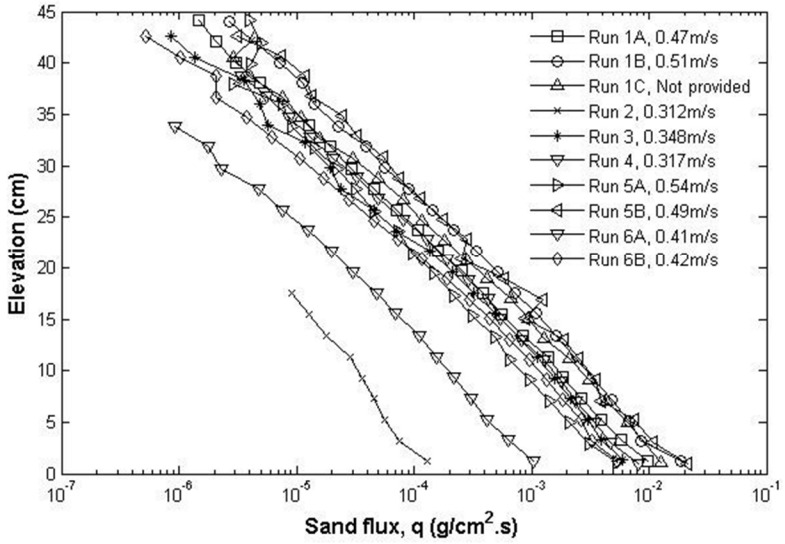

Fig A-5. Vertical mass flux profiles from Greeley et al., (1996).

Guadalupe (1996) was a field experiment that conducted to examine turbulent boundary layer dynamics across a beach and the subsequent surface response. The field site and flux experiments are described in Bauer et al (1998) and Ellis et al. (2009), respectively. A vertical stack of hose-style hose traps were used to collect 11 flux profiles. All the traps were 0.10 m wide. The vertical opening of the lowest trap was either 10 or 25 mm, depending on each particular deployment. Openings of the other traps ranged from 25 to 100 mm, with the size of the opening increasing upward. Total stack height of the traps ranged from 0.375 to 0.600 m above the bed (see Ellis et al., 2009 for description). The vertical opening of the two lowest traps was 0.025 m high (trap 1 and 2). The openings of the next highest traps were 0.05 m high (trap 3 and 4) and 0.10 m high (traps 5 – 8). The flux profiles were measured in 25 runs spanning 200 - 800 seconds depending on wind speed. The mean grain size for the site was 0.39 mm.

No wind data was collected during the collection of flux profiles which were fifteen minute durations.

Hasi (1997) reported two sets of experiments taking measurements ranging from 0 – 0.20 m and 0 – 1.0 m. They report the wind velocity and flux (in g/m in). There are limited details on grain sizes, sampling durations or sampler dimensions. The six profiles from these experiments plotted in Li and Ni (2003) are used here. These profiles extend up to 0.20m with 10 sample intervals. Wind speed (at 2m elevation) ranged from 0.98 – 11.5 m/s for the experiments. There is a pronounced deviation from the straight line in a log-linear plot (flux *vs.* elevation) at the bottom trap. In all cases the bottom trap underestimates the flux.

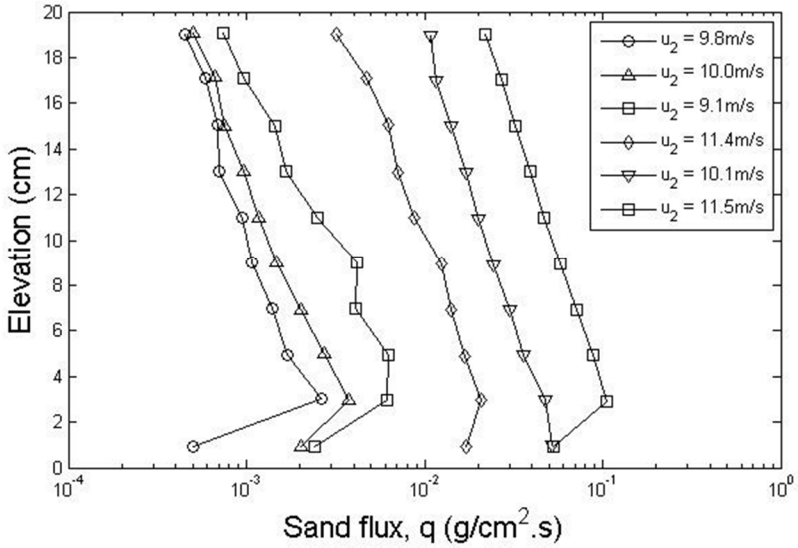

Fig A-6. Vertical mass flux profiles from Hasi (1997).

Hotta and Horikawa (1993) examined the vertical distribution of aeolian sand transport in a wind tunnel. The tunnel had a test section 20 m long and a cross section 1.1 m high and 1.0 m wide. The median grain diameter was 0.30 mm. Shear velocities ranged from 0.03 to 1.0 m/s. Run durations ranged from two to twenty two minutes. The

dimensions of their vertical trap are shown in their Figure 1 (p.94) but are still difficult to discern the details. Trap efficiency, given in their Figure 3 (p.96), ranges from 0.50-0.70 approximately. Their Figure 4 (p.97) has 10 vertical flux profiles for a range of shear velocities from 1.0 – 0.30 m/s. They compared their experimental data with the predicted theoretical curves generated from Kawamura (1951) and Ishihara and Iwagaki (1952). The former equation is listed on p.??, The latter model used the balance of gravitational settling and turbulent diffusion of sediments to develop a relationship:

$$\boldsymbol{q(z) = c\varphi_0 u e^{-\frac{w_0}{\eta}z}}$$

where φ is the sediment mass contained in a unit volume at elevation z =0, w_0 is the fall velocity of a sand grain, η is the coefficient of eddy viscosity. The Kawamura model works well but it is difficult to empirically derive the coefficient and parameter values whereas the Ishihara and Iwagaki model underestimates the near-bed transport but is easier to derive the values.

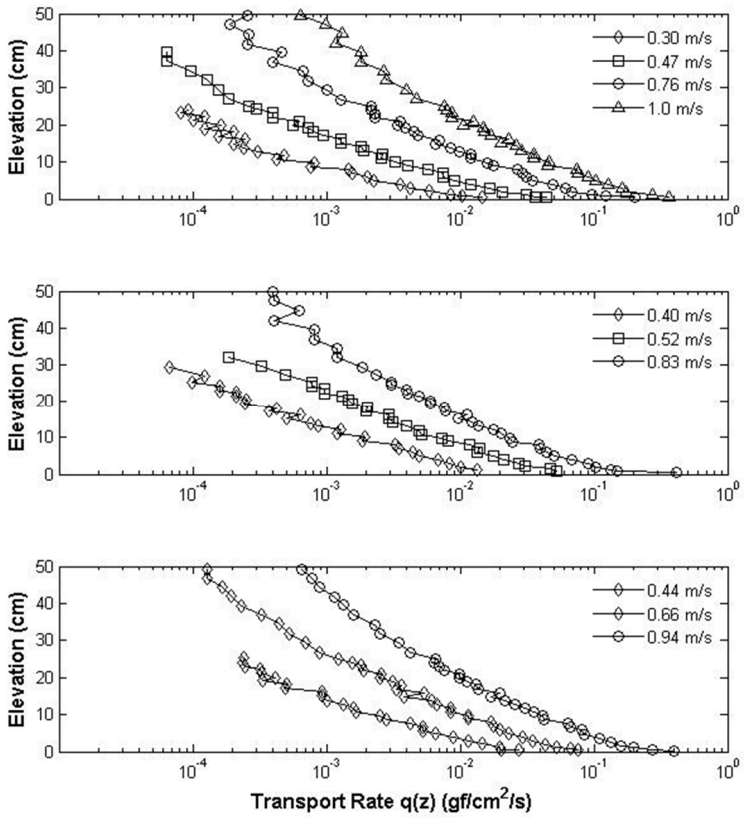

Fig A-7. Vertical mass flux profiles from Hotta and Horikawa (1993).

Hotta et al (2006) conducted a wind tunnel experiment to establish an easier, more reliable predictive formula for the vertical distribution of mass flux than that proposed by Kawamura (1951). The working area of their wind tunnel was 20 m long, with a cross section 1.0 m wide and 1.1 m high. Details of their sand trap are provided schematically in their Figure 1. It is not clear what distances are separating the different trap segments, nor is it possible to establish what the different heights of the openings are. The lowest trap segments, extending up to a height of 200 mm, have much smaller vertical openings than the higher segments. Above these lower segments, the openings are higher, with at least four different segments extending from 200 – 600 mm. All segment openings are 100 mm wide. It appears that the lowest trap segment may be 10

mm above the surface but this is unclear. The digitized heights will be used in these cases. They used natural beach sand sieved into four populations with mean diameters of 0.15, 0.25, 0.48 and 0.68 mm (called D15, D25, D48 and D68). They also worked with a mixed sized sample (obtained from the 0.15 and 0.48 mm populations) that had a mean of 0.28 mm (called MD28). Their Figure 6 (p.2610-2611) has 15 vertical flux profiles with the shear velocities included for each run ranging from 0.40 – 2.33 m/s. The trapping efficiency was constant at 0.55 for the runs with the coarser samples (MD28, D48 and D68). For the two finest samples, D15 and D25, the trapping efficiency increase linearly with increasing shear velocity until it becomes a constant value at 0.45 for shear velocities over 1.20 m/s.

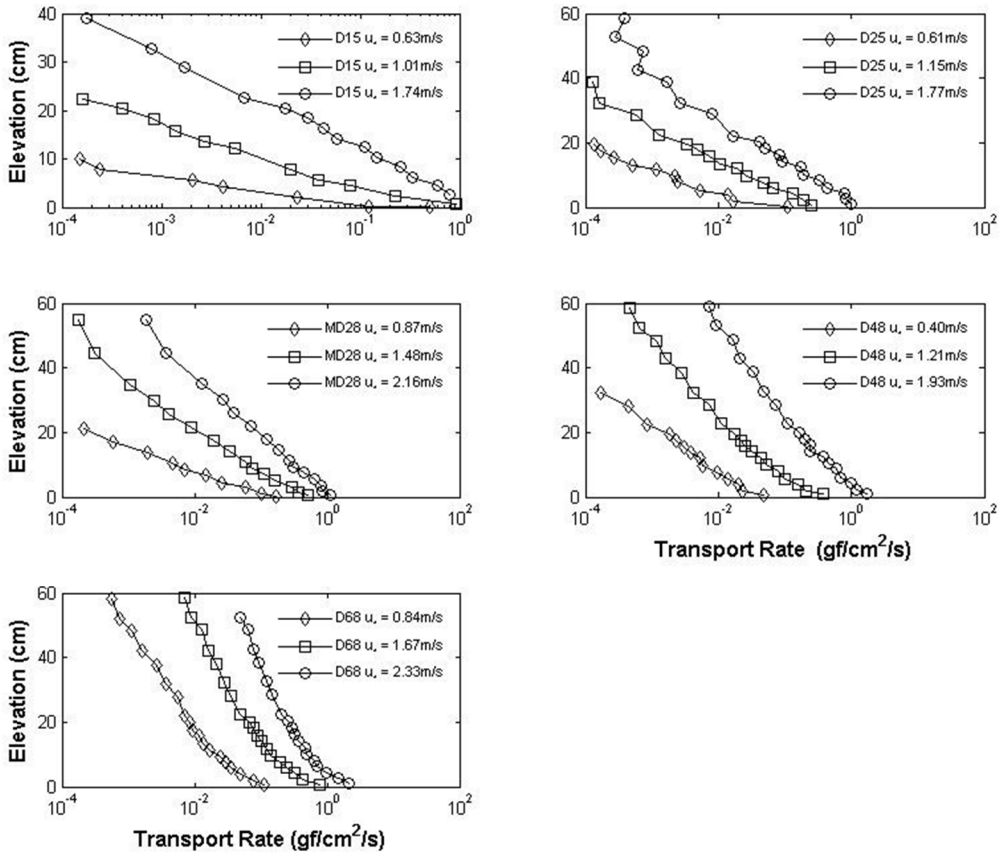

Fig A-8. Vertical mass flux profiles from Hotta et al., (2006).

Kawamura (1951) examined the rates of sand transport with the friction velocity of wind in order to test the relationships for vertical flux and total load. This research was translated from Japanese to English in 1964 by Nagahama and Hiraoka at the Hydraulic Engineering Laboratory, University of California, Berkeley. Ni et al. (2002) also report the two Kawamura wind tunnel vertical flux profiles with shear velocity values 0.488 m/s and 0.732 m/s. The mean grain size used in the wind tunnel runs was 0.248 mm (density 2.48 g/cm^3). These wind tunnel profiles are the same as those reported in Kawamura (1951) Figure 17. The wind tunnel was 1.5 m long with a cross section 0.05 m wide and 0.80 m high. The wind tunnel was only 0.05 m wide. Li and Ni (2003) reported both the wind tunnel and field profiles. The shear velocities for the 2 field profiles are unknown but they reported wind speeds (at 0.30 m above the bed) of 10.5 and 12.6 m/s. Ni et al. (2002) report the shear velocities for the wind tunnel flux profiles: 0.488 and 0.732 m/s. The mean grain size of the field profiles was 0.307 mm; density (2.50 g/cm^3) (Kawamura, Figure 18). The sand was collected in the wind tunnel by moving a single-tube trap with an inlet of 2 x 7 mm. The field experiments were done by deploying an array of nine of these traps within 0.30m of the surface. The mean grain size at the beach was 0.307 mm and a density of 2.50 g/cm^3. The sand was collected using an array of pitot tube type collector whose openings were 7 mm wide and 2 mm high. His wind tunnel profiles were plotted in Ni et al., (2002), figure 14, p.215 with the shear velocity values and were used in this analysis to obtain the Kawamura wind tunnel profiles. The Kawamura field profiles were obtained from Figure 2, Li and Ni (2003) with the wind speeds measured at 0.30m above the ground.

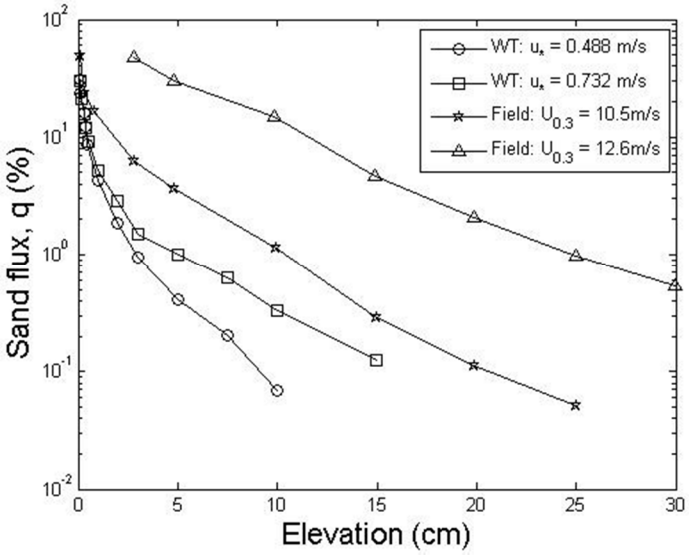

Fig A-9. Vertical mass flux profiles from Kawamura (1951).

Leys and McTainish (1996) collected vertical mass flux profiles to examine sediment fluxes and grain-size characteristics in a field site in SE Australia. They sampled at seven different heights above the bed: 0.07, 0.12, 0.25, 0.50, 1.0, 1.5 and 2.0 m. The sample had an intake with an opening 50 mm by 20 mm with an efficiency of 90 +/- 5%. Their Figure 1 (p.663) shows eight vertical flux profiles they collected and also a vertical profile reported in Zobeck and Fryrear (1986). They found that a power function provides the best fit for the vertical distribution of mass flux with height, $q=\alpha z^{-\beta}$. The regression statistics for these fits are provided in their Table I (p.663). The average durations of each wind transport event are provided in their Table II. The smallest duration is 2.0 hours to a maximum of 42.6 hours. It is unclear if the vertical profiles are an average or aggregate of the transport during these time periods. They found that the exponent β, describing the decrease in flux with height, decreases as flux increased while the coefficient α, characterizing the density of suspended sediment, increased with increasing flux. They reported that the power function can be problematic as it implies that *m* approached infinity as *z* approaches 0 which is physically incorrect.

Liu and Dong (2004) did wind tunnel experiments to examine the concentration profile of a saltation cloud by measuring the mean velocities of the particles using a particle dynamic analyzer technology. The wind tunnel had a working section length of 16.23m and a cross section of 0.8 x 1.0 m. It is unclear which is the height and width but the convention is to list width first. They sieved natural quartz sands into five different size groups: $0.1 < D \leq 0.2$, $0.2 < D \leq 0.3$, $0.3 < D \leq 0.4$, $0.4 < D \leq 0.5$ and $0.5 < D \leq 0.6$. The blowing sand was caught using a conventional vertically segmented trap described in Dong et al. (2002). The trap was 0.60 m high with 60 collection chambers with 10 x 5 mm openings. Their Figure 3 (p.375) shows 25 measured flux profiles for five different grains sizes and five different free stream wind velocities (10, 12, 14, 16 and 18 m/s). The number of point overlapping makes it too difficult to reverse engineer using on screen digitizing. However they also provide the regression parameters and correlation coefficients for the fitted exponential function in their Table 2 (p.376) where $q_h = Ae(-h/B)$. They found that for grains sizes greater than 0.10 mm the flux profile of a sand cloud moving by saltation obeys the law of natural exponential decay with height. The slopes reported here are for $q = ae^{bz}$ with elevation in meters.

Table A-2. Regression parameters and correlation coefficients for the flux profiles in Liu and Dong (2004).

D (mm)	V (m/s)	A	B	r2
$0.1 < D \leq 0.2$	10	0.09286	5.1923	0.99
	12	0.18385	7.5902	0.98
	14	0.40039	7.9755	0.99
	16	0.66460	7.8966	0.99
	18	0.91875	8.1061	0.97
$0.2 < D \leq 0.3$	10	0.05605	11.7546	0.99
	12	0.10497	11.8821	0.99
	14	0.020606	11.1965	0.98
	16	0.30059	12.8098	0.97
	18	0.42348	14.4875	0.96
$0.3 < D \leq 0.4$	10	0.03806	13.2319	0.98
	12	0.06642	15.3707	0.99

	14	0.12278	14.7563	0.97
	16	0.17532	16.8035	0.99
	18	0.25304	18.6908	0.97
$0.4 < D \leq 0.5$	10	0.02787	14.4501	0.98
	12	0.04457	18.3872	0.99
	14	0.07651	18.6904	0.95
	16	0.11539	20.2567	0.98
	18	0.17150	21.8303	0.98
$0.4 < D \leq 0.5$	10	0.02172	21.5894	0.97
	12	0.03139	21.0834	0.98
	14	0.04707	23.0382	0.97
	16	0.08137	23.3432	0.99
	18	0.12522	24.3372	0.99

Liu et al., (2006) examined the empirical fits to experimental data of total transport and the vertical distribution of mass flux for different sized sands. They conducted a series of wind tunnel tests in the same facility described in Dong et al., (2002). The working section of the wind tunnel was 21 m long and had a cross section of 1.2 m x 1.2 m. The same type of trap as used in Dong et al., (2002) was deployed. The vertically segmented trap was 0.60 m high and had 60 segments with openings 10 mm high and 5 mm wide and had a reported efficiency of 0.90. Their Figure 5 (p.665) has five vertical flux profiles for a grain size, d = 0.40 – 0.50 mm (mean 0.45 mm). The five shear velocities are also provided for the runs 0.48, 0.54, 0.64, 0.70 and 0.75 m/s. It is strongly suggested that the symbols in their Figure 4 are incorrect. We associated the lowest to highest shear velocities (0.48 to 0.75 ms-1) with the lowest to highest transport rates. This is opposite to what their Figure 4 has illustrates that the highest transport occurs with the lowest shear velocity and *vice versa*, which cannot be physically correct *ceteris paribus*.

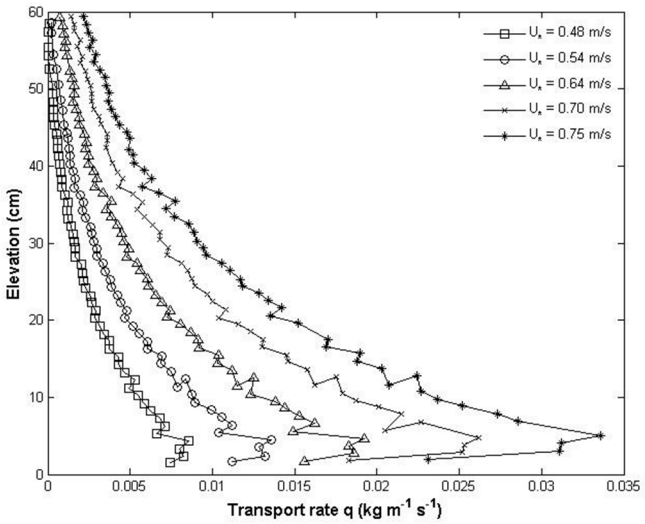

Fig A-10. Vertical mass flux profiles from Liu et al., (2006).

Mikkelsen (1989) reported 6 flux profiles in his Figure 24 (p.45) four of which are reproduced from Rasmussen et al., (1985). The two extra profiles derive from a field experiment in Ferring, Denmark and a wind tunnel experiment in Aarhus. The wind tunnel dimensions are described in Rasmussen and Mikkelsen (1998) as 1.5m long, 0.35 wide and 0.50 m high.There are not many specific details listed for these experiments with regards to friction velocities and grain sizes that we can associate with particular vertical flux profiles. He states (p.21) that he used a mean grain diameter of 0.40 mm was used to estimate the threshold shear velocity at the Ferring site and this number is applied here but with caution. One of their observations was that the same trap used in the field and wind tunnel produced distinctly different shaped vertical flux profiles. They reason that "*a different sand composition could explain the discrepancies, which may, however, also emanate from a real difference between flux profiles in nature and wind tunnel*". Although they state they used the same trap design the chambers heights are slight different in his Figure 24. It is unknown where these differences derive from.

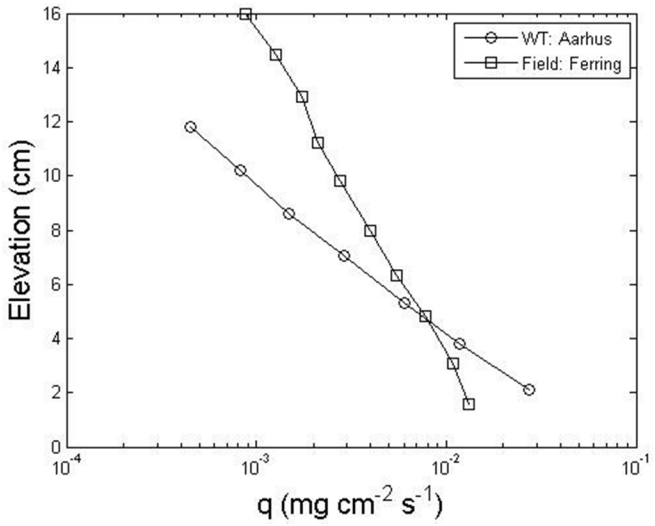

Fig A-10. Vertical mass flux profiles from Mikkelsen (1989).

Mohammed et al., (1996) reported on a wind tunnel and field experiment in the strongly desertified region of Central Sudan in order to test the performance of a new catcher modified from the De Ploey design. The new catcher comprised of eleven stacked coffee cups with a vertical separation of 30 mm between each successive cup. However, in a wind tunnel test they report the catch efficiency to be only 3%. Their Figure 4 shows 6 vertical flux profiles for sampling durations of the order of minutes. They reported that 85% of the sand used in the wind tunnel experiments had a particle diameter 0.1 – 0.3 mm. No tunnel dimensions were forthcoming.

Namikas (2003) examined grain-size distributions from vertical and horizontal mass flux profiles collected in Pismo Beach, CA (USA). He used a vertical trap that comprised of fifteen wedge-shaped sediment collectors (VTRAP) with openings 60 mm wide and varying vertical openings of 10, 20 or 40 mm. The five lowest collectors had vertical openings of 10 mm and extended from the surface to 0.05 m above the bed. The next five collectors had vertical openings of 20 mm and extended from 0.05 m to 0.15 m

above the bed. The top five collectors had 40 mm vertical openings and collected sand from 0.15m to 0.35 m elevations. Mean grain size for the experiments was 0.25 mm. Shear velocity was provided in his Table 1 (p.310) and ranges from 0.27 -0.63 m/s for the 9 runs. Sample duration ranged from 76 s to 2640 s and the mean sand size was 0.25 mm in diameter. Namikas surmises that "*the measured mass flux values cover five orders of magnitude, and the persistence of a trend across such a wide range must be considered indicative of an underlying process* (p.310)". His Figure 6 (p.312) has 9 vertical flux profiles. He found that the logarithmic and exponential functions provided the best fit compared to the power function.

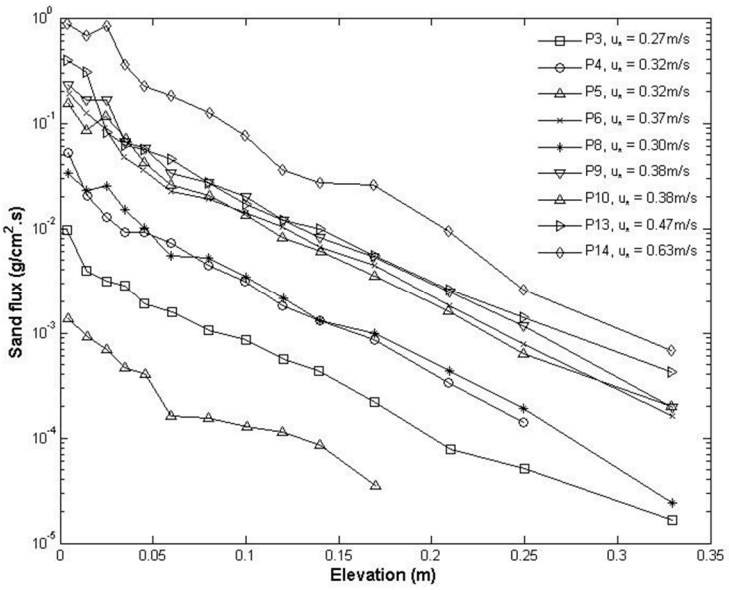

Fig A-11. Vertical mass flux profiles from Namikas (2003).

Namikas et al., (2009) examined the grain-bed collision process on a fine-grained beach by introducing five test beds of different sized sands. Their Figure 6 (p.340) shows 9 different vertical flux profiles measured using three different mean grain sizes (0.11, 0.28 and 0.55 mm) and three different shear velocities (0.42, 0.46, and 0.52 m/s). They only show the lowest 0.10 m of the profiles but argue that the flux collected under this elevation accounts for 90-99% of the total transport. They found that the bed

textures exerts a considerable influence on both the vertical and horizontal distributions of mass flux whereby particles that rebound off increasingly coarser bed material have increasingly higher and longer trajectories which “stretches” the distributions.

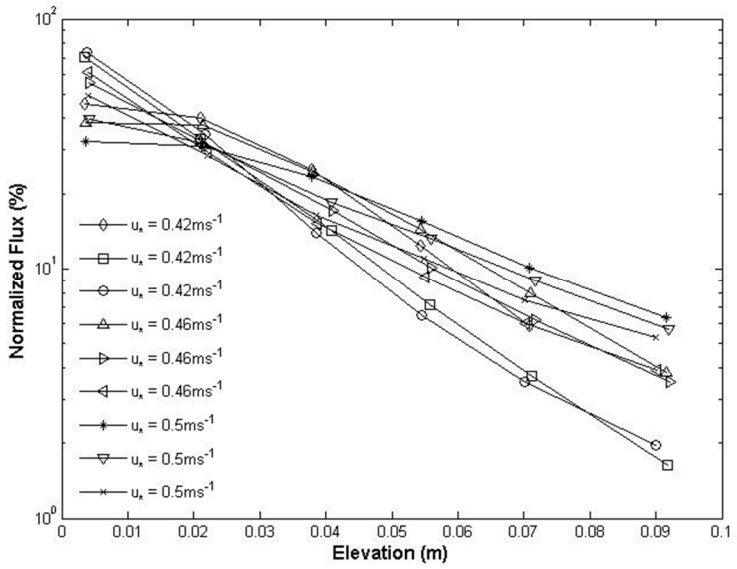

Fig A-12. Vertical mass flux profiles from Namikas (2003).

Ni et al., (2002) conducted a wind tunnel experiment to examine the general characteristics of the vertical and horizontal distributions of mass flux during aeolian sand transport. The wind tunnel had a working section length of 21 m and a cross section 1.2 m high and 1.2 m wide. They used a Liu-type passive vertical trap that was 0.30 m high with thirty collection chambers with openings 0.01 m wide and 0.01 m high. Their Figure 7(p.211) contains 10 vertical flux profiles for two different sized test sands (0.17 and 0.35 mm) and different shear velocities ranging from 0.47 – 2.36 m/s. They found that the exponential decay function was a good fit for their data but with a deviation in the near-bed region from creeping and reptating particles.

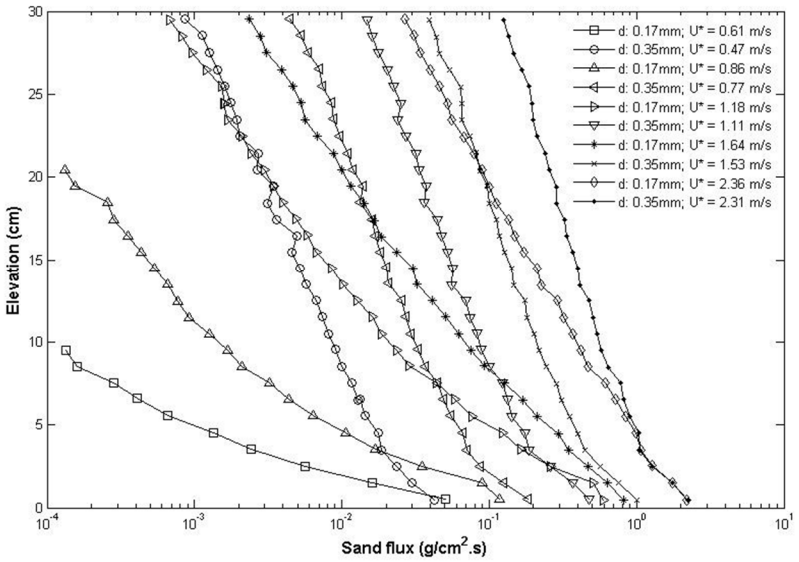

Fig A-13. Vertical mass flux profiles from Ni et al., (2002).

Portugal (2006) was a field experiment carried out in Esposende, northern Portugal. The experiment is described in detail in Li et al., (2009). A vertical stack of hose-style hose traps were used to collect 13 flux profiles. All the traps were 0.10 m wide. The vertical openings of the lowest two traps were 0.025m. Openings of the other traps ranged from 0.025 to 0.01 m, with the size of the opening increasing upward. Total stack height of the traps ranged from 0.40 to 0.50 m above the bed. Each run lasted 10 to 30 minutes depending on wind speed. The mean grain size ranged from 0.27 to 0.35 mm. Shear velocity was measured during nine of the runs and ranged from 0.35 to 0.41 m/s.

Rasmussen and Mikkelsen (1988) focused on carrying out a major wind tunnel experiment to test their ability to confidently measure aeolian transport rates. They did this by comparing transport rates measured by three different field traps (Arhus, Aberdeen, and Ames) and a laboratory designed isokinetic trap. The isokinetic trap consisted of an array of three single-tube isokinetic traps. The Aahus wind tunnel has been described in detail in other reports (Rasmussen and Mikkelsen, 2008). It has a working section 15 m and a cross section 0.60 m wide and 0.90 m high. Similarly the

isokinetic traps have been described in more detail in Rasmussen and Mikkelsen (1998). In this earlier experiment each tube has an openi0.63ng 8 mm wide x 8 mm high. Their Figure 7 (p.29) contain 4 runs (20a, 20b, 20c and 20d) of the isokinetic trap measuring at three different elevations, each time keeping one of the single-tube traps at 0.04 m. The shear velocity for these runs was 0.27 m/s. They used one type of sediment which was a dune sand with a mean grain size was 0.22 mm. They found that trap efficiency can be a serious problem in assessing the confidence in experiment results especially in the near-bed region where the highest transport rates occur.

Rasmussen and Mikkelsen (1998) examined the efficiency of three vertical array sand traps (Aarhus, Aberdeen and Ames) by comparing the results of these traps to that of a single-tube isokinetic trap. The Aarhus wind tunnel had a cross section 0.50 m high and 0.35 m wide and 15 m long. The isokinetic trap comprised of six tubes that had openings 8 mm wide and either 4.5 mm (two lowest tubes) or 9.5 mm high (four highest tubes). Their Figure 5 (p.795) contains 6 vertical flux profiles from a laser Doppler and isokinetic trap of which we are only interested in the latter. Unfortunately we could not reverse engineer these points due to the overlapping of the symbols, especially for the lower elevations. However the single-tube isokinetic trap results were plotted in Li and Ni (2003), Figure 2 (p.246) or Ni et al., (2002), figure 14 (p.215) in a format that allowed us to reproduce the points. The vertical flux profiles form the three field traps are plotted in their Figure 7 (p.796) which again have too many overlapping symbols to allow for reverse engineering of the points. These profiles were subsequently ignored. The authors found the overall efficiency of the field traps ranged from 50-70% with efficiency decreasing to a minimum nearest the bed where the most transport occurs. Using the results they suggest higher trapping efficiency can be obtained using a low wedge-shaped trap in combination with the Aberdeen-type trap in order to improve trapping efficiency nearest the bed.

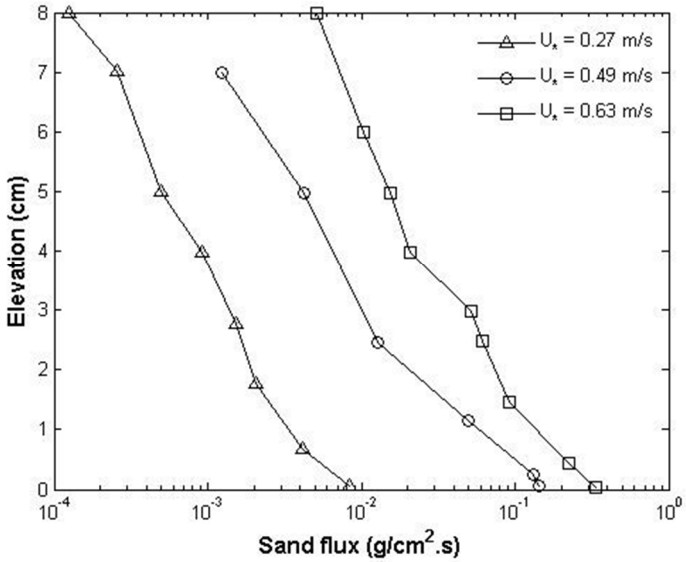

Fig A-14. Vertical mass flux profiles from Rasmussen and Mikkelsen (1998).

Rasmussen and Sorensen (1999) carried out a field experiment to examine aeolian transport near the saltation threshold. They deployed a modified form of the single-tube isokinetic trap described in Rasmussen and Mikkelsen (1998) to measure the vertical distribution of flux. The isokinetic trap comprised of six tubes that had openings 8 mm wide and either 4.5 mm (two lowest tubes) or 9.5 mm high (four highest tubes). The six tubes extended to a height of 45 mm above the bed. Their Figure 4 (p.418) has 3 vertical flux profiles (Runs 4, 5 and 6) with a wide range of transport rates. An averaged shear velocity of these 45 minute runs is provided graphically (Figure 5, p.419). The values of these points can be reproduced using onscreen digitizing tools. We found that the shear velocities for Runs 4, 5 and 6 were 0.177, 0.179 and 0.20 m/s, respectively, although the authors are careful to note that these values are less than the calculated static threshold (u_{*t} = 0.30 m/s). The median grain size for the field site was 0.32 mm.

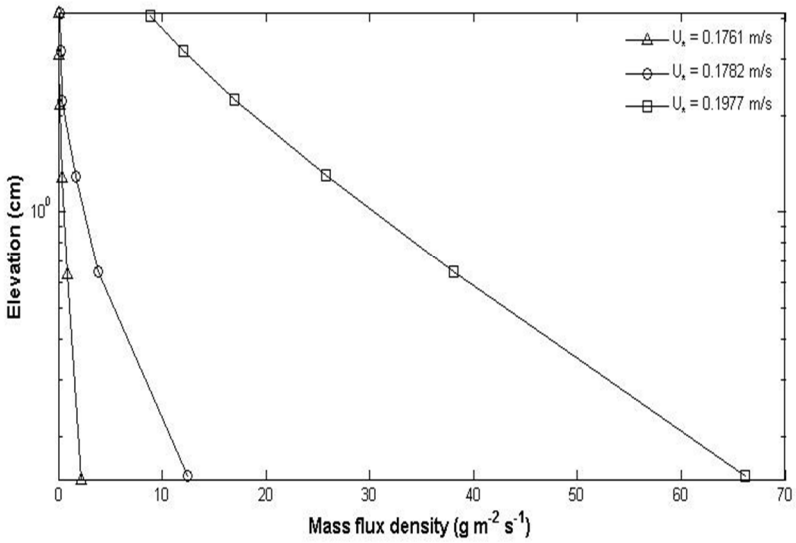

Fig A-14. Vertical mass flux profiles from Rasmussen and Sorensen (1999).

Rasmussen and Sorensen (2008) measured vertical distributions of mass flux using laser-Doppler anemometry in conjunction with a numerical saltation model. The laser-Doppler measures the air and particle speed and the flux density. The quartz sand used in the experiments had mean diameters of 0.254 and 0.320 mm. The Arahus wind tunnel has a working section 15 m and a cross section 0.60 m wide and 0.90 m high. Run durations were between 15 to 60 seconds. Their Figure 7 show 12 profiles of grain rates for two different grain sizes and a range of shear velocities (0.27 – 0.74 m/s). These rates are converted to grain flux densities by dividing the grain rate by the nominal area of the measuring window (*values typically range from about 1-5x10^{6} grains s^{-1} m^{-2} at 80 mm height to 10^{9} grains s^{-1} m^{-2} at 5 mm height*). They found that the decrease in the measured flux densities with height could be approximated by two regions where the mass flux density decays exponentially.

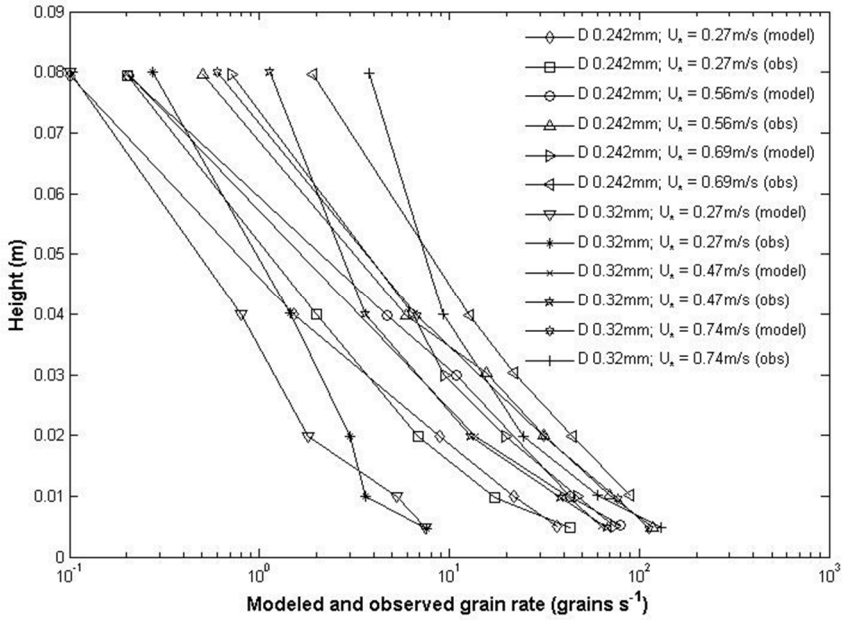

Fig A-15. Vertical mass flux profiles from Rasmussen and Sorensen (2008).

Rasmussen et al., (1985) reported a total of 4 flux profiles from two separate field experiments. The trap used at Hanstholm, Denmark was 0.10 m high and had seven chambers with openings 0.025 m (wide) x 0.025 m (high). The set up was similar during the second field experiment at Foveran (Scotland) with a slightly different trap design. The trap was 0.14 m high and comprised of ten chambers that were 0.015 m wide and 0.014 m high.They report the friction velocities indirectly in Figures 8 and 9 using both cup anemometry and hot-wire anemometry. Their Figure 8 has the values of the shear velocity for Hanstholm measured using the hot-wires (0.63 m/s) and cup anemometers (0.73 m/s) and averaged over 204 seconds. Their Figure 9 has the similar range of values for the hot-wires (0.26 – 0.36 m/s) and cup anemometers (0.20 – 0.24 m/s) for the Foveran field site.They found a constant log-linear relationship between sand flux and elevation above the bed despite a wide range of shear velocities. Grain size data was not provided.

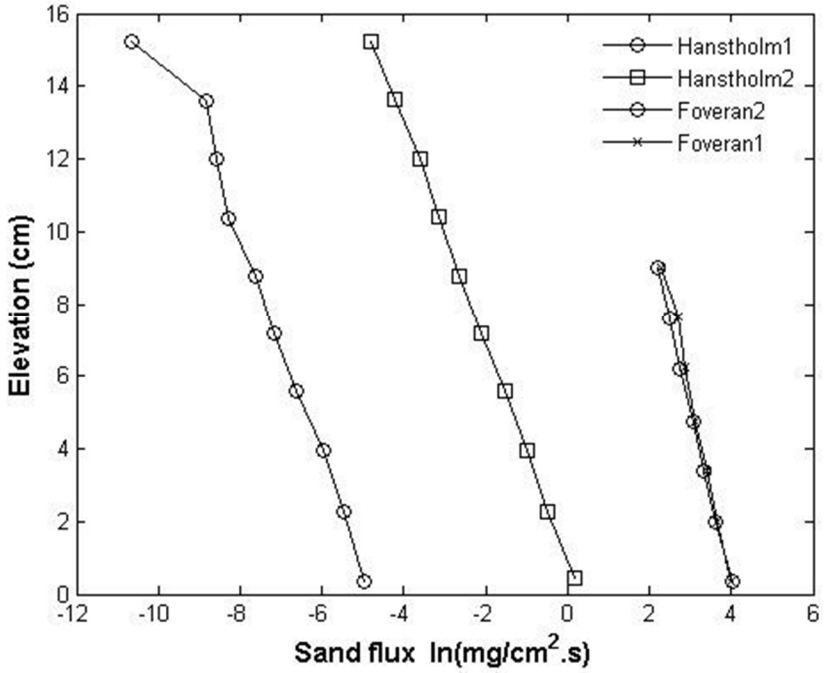

Fig A-16. Vertical mass flux profiles from Rasmussen et al., (1985).

Shao and Raupach (1992) investigated the overshoot phenomenon for saltation approaching equilibrium. The measured vertical flux profiles at different locations along the wind tunnel. Their Figure 3 (p.20,561) shows 12 vertical flux profiles at four different wind speeds (with shear velocities of 0.34, 0.44, 0.50 and 0.60 m/s) at three different locations from the upwind edge of the soil surface (x = 1.0, 6.0 and 14.5 m). The wind tunnel had a working section 1.15 m wide and 0.9 m high with an available length of 10-19 m. The flux profiles were taken for two different wind tunnel lengths: 10 m and 17 m. They used sand with a modal particle size of 0.20 mm. They used Leach traps with openings 10 mm wide and 20 mm high to measure the flux (described in Shao et al., 1993). The efficiency of these traps was determined by calibration against an isokinetic sampler and reported to be 90%. Five of these traps were placed at different elevations above the bed: 10, 50, 110, 220, and 410 mm. Their results confirm that

overshooting occurs and that there is a minimal distance for saltation to reach equilibrium (they suggest approximately 15 m) depending on wind speed.

Sharp (1966) conducted a long term field study (11 years) to examine wind driven sand dynamics. His Figure 2 shows 4 vertical flux profiles. Flux was measured using up to nine different heights above the bed to a maximum elevation of ten feet. The traps were unsophisticated copper tubes with an inner diameter 1.375 inches. He states that the design of the traps did not collect representative grain distributions in their proper proportions as the design was biased towards descending grains versus ascending grains. Also the sample durations were of the order of tens of days. These profiles are subsequently ignored in the analysis.

Sorensen (1985) analyzed field and wind tunnel transport data to investigate a mathematical saltation model. He used the vertical distribution profiles to estimate mean particle jump lengths, mean impact angles, and probability distribution of grain speed during saltation at each height. His Figure 3.1 (p.3.3) shows 2 vertical flux profiles measured in the Aarhus wind tunnel for two different grains size ranges:0.211 – 0.258 mm and 0.106 – 0.129 mm. The trap used was 0.108 m high consisting of twelve different chambers with 0.079 m^2 openings. The bottom chamber was opened at both ends to prevent scour in front of the trap. The shear velocity was 0.46 m/s.

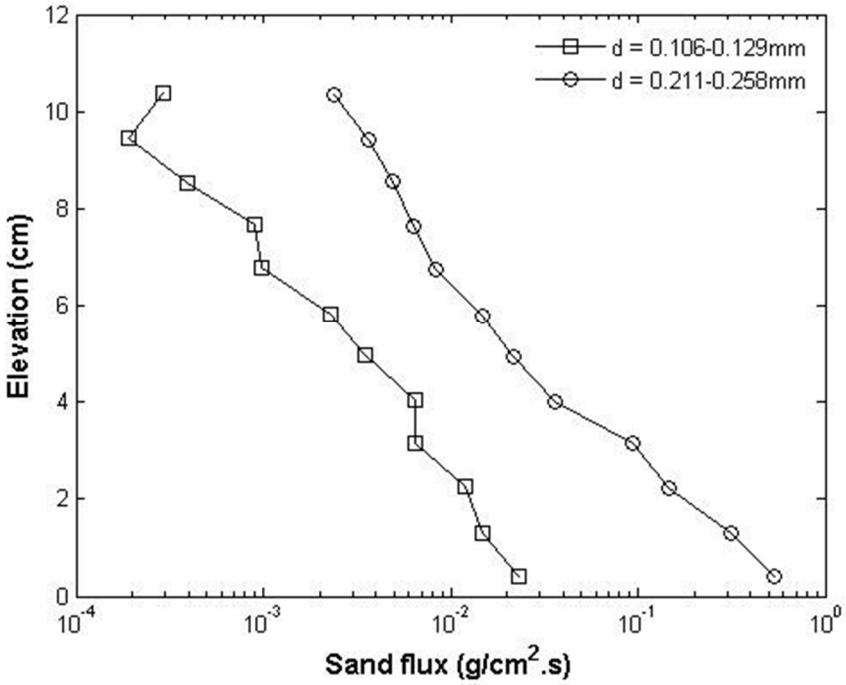

Fig A-17. Vertical mass flux profiles from Sorensen (1985).

Weinan et al., (1996) gathered vertical distributions of mass flux in a series of field and wind tunnel experiments. In the field, the mean particle diameter was 0.09 mm. The flux was measured using step-like passive slit sampler which was 0.20 or 0.40 m high and 0.02 m wide, with 10 or 20 openings with dimensions 0.02 m wide and 0.02 m high. They report the traps to be 95% efficient. The wind tunnel had a test section 16 m long and 0.6 m wide and 1.0 m high. The laboratory test sands had a mean diameter of 0.11 mm. The reported wind speeds were measured at a height of 0.30 m above the bed. Their Figures 4 and 5 had too many points overlapping to reverse engineer for our analyses. Therefore their Figures 10 and 11 were used.

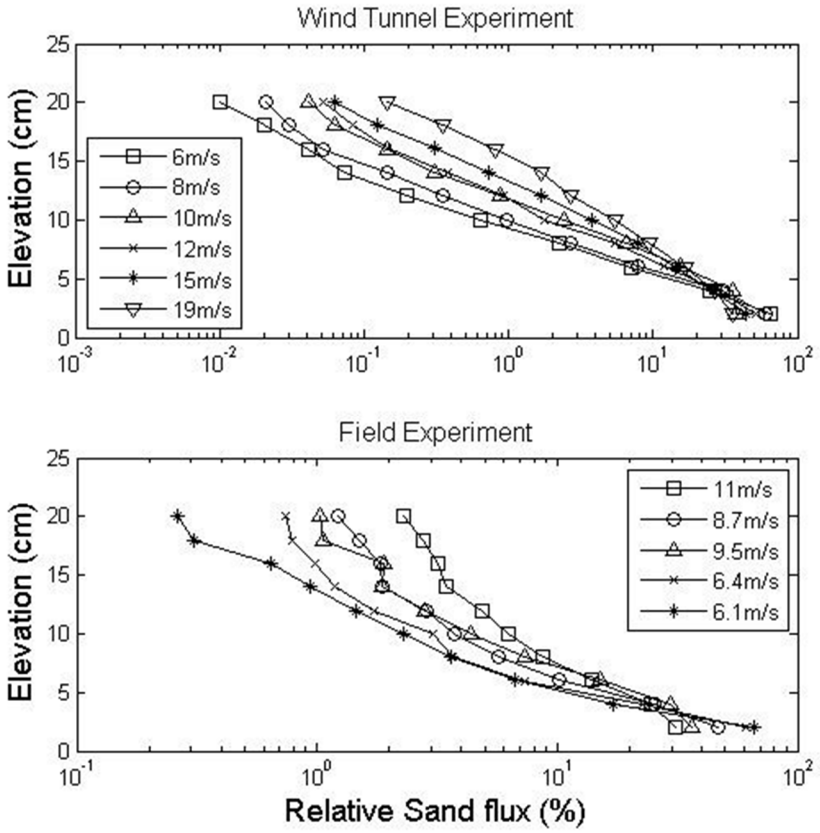

Fig A-18. Vertical mass flux profiles from Weinan et al., (1996).

White and Mounla (1991) Their Figure 7 (p.154), reproduced in White (1996), contains 4 vertical flux profiles at four different wind speeds (6.405, 8.448, 1.072 and 11.94 m/s). The dimensions of the wind tunnel working section are ambiguous in all the descriptions of the UC Davis wind tunnel. White (1996) states that the plexiglass test section was 2.44 m long, 0.47 m high and 0.8 m wide. However the flow development section is 7.32 m long comprised of three different section of which the last one was the designated 'test section'. For our purposes the cross section dimensions are as stated here and the length is taken to be 7.32 m. The test material was ground walnut shell with a density of 1.1 g/cm^3. The mass transport was measured using a stack of twenty five individual 0.02 m high stackable plexiglass collectors as described in White (1982).

Williams (1964) carried out wind tunnel experiment using three different wind speeds with friction velocities 0.57, 0.83 and 1.28 m/s. The wind tunnel had a test section 9.14 m in length and a cross section 0.355 m x 0.355 m. The trap comprised of five collection chambers with openings 0.01 m high and 0.10 m wide. The lowest collection chamber was between 0 and 0.01 m above the bed. The highest was between 0.15-0.16 m above the bed. The midpoints of the trap openings were 0.005, 0.025, 0.055, 0.095, 0.155 m above the bed. Williams used three different particle types to examine the influence of shape on the vertical distribution of mass flux: glass spheres, crushed quartzite particles and quartz sand grains. Three different size distributions of the quartz grains were also used in order to test the influence of initial surface size distribution on the vertical distribution patterns: approximately uniform (equal amounts of the five size classes), approximately symmetrical and truncated or skewed. Li and Ni (2003) reproduced the Williams data for six profiles with mean grain size of 0.40 mm. These profiles were used in this analysis.

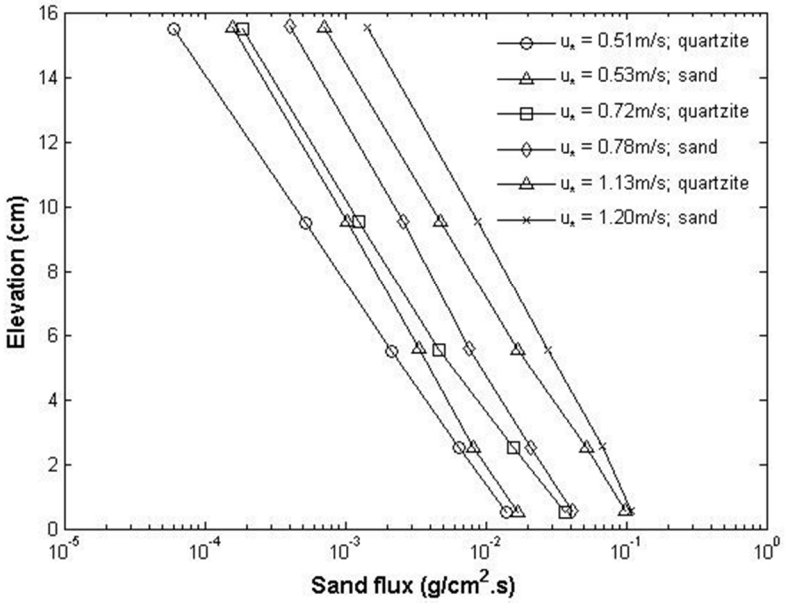

Fig A-19. Vertical mass flux profiles from Williams (1964).

Xing (2007) examined the distribution of grain sizes for flux profiles in wind tunnel experiments with different mixed-bed textures. The wind tunnel had a cross section 0.40 m (wide) x 0.60 (high) m and a length of the order 8 m or more. Wind speeds were reported using a pitot tube placed 0.30 m above the bed. The vertically segmented sand trap was 0.40 m high and contained twenty different segments each with a 0.02 (wide) x 0.10 (high) m opening. He prepared three different mix of different size fractions of quartz dominated sand with a density 2.588g/m^3. A fourth mix was made by mixing two of the mixed samples. The grain size distributions of these test sands are given in his Figure 4 (p.232). The mean sand size of sand 1 was calculated as 0.348 mm using the reverse engineering technique described in the Methods Section. Sands 2,3, and 4 were described in Xing (2011) as 0.525, 0.364, and 0.421 mm. His Figure 5 (p.233) contains 17 vertical flux profiles for four different sand mixtures and for a range of wind speeds from 7.5 m/s to 15.3 m/s. He found a deviation from the exponential decay function for the lowest chamber but in contrast to other reported studies where it underestimates occur, Xing measured less than what was predicted. He explains this by stating that the lowest chamber filled during measurement and subsequently ignores these flux values in his analysis.

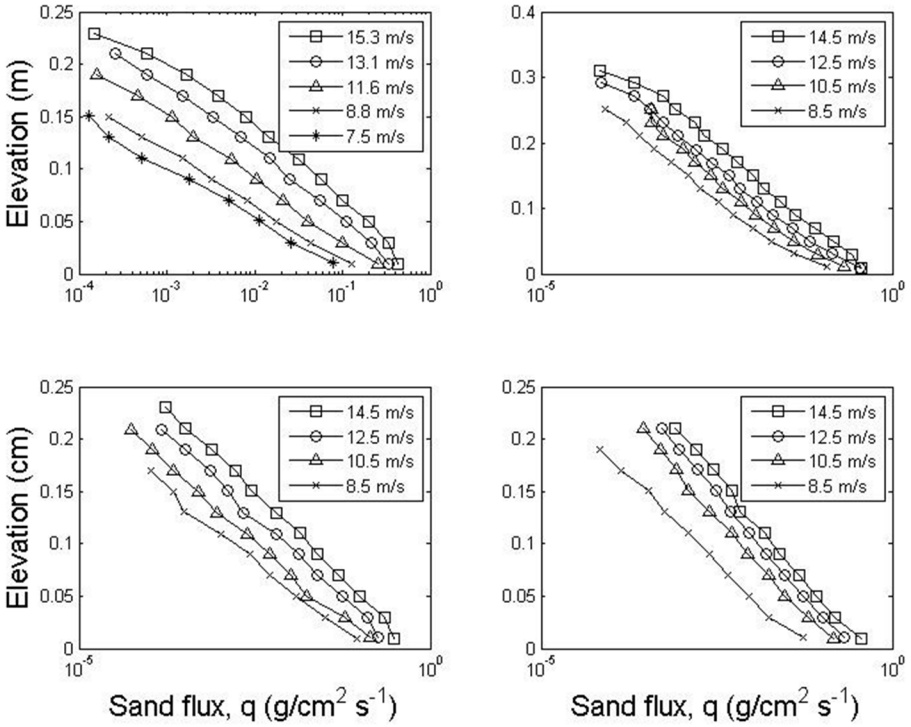

Fig A-20. Vertical mass flux profiles from Xing (2007).

Xing et al. (2011) investigated the effect of mixing particle sizes on aeolian transport dynamics. Their Figure 3 (p.219) contains 12 vertical flux profiles for their test sands No 1, No. 2 and No. 3 at four different wind velocities (8.5, 10.5, 12.5, and 14.5 m/s). The profiles were measured using three different sized test sands (0.525, 0.364, 0.421 mm) that were predominantly quartz with a density of 2588 kg/m^3. They cite Xing (2007) for further details on experimental design. The wind tunnel had a work section 6 m long and a cross section was 0.40 m (width) and 0.60 m (height). The used a "segmented sand trap" – we have to assume the trap is similar to that described in Xing (2007): 0.40 m high, containing twenty different segments each with a 0.02 (wide) x 0.10 (high) m opening.

Zhou et al., (2002) carried out wind tunnel experiments to examine the mass flux patterns for naturally mixed sands. The test section of their wind tunnel was 21 m long

with a cross section 1.2 m x 1.2 m. They used a step-like trap that was 0.30 m high with thirty different collectors, each with an opening 0.01 cm x 0.01 m , and an overall efficiency of about 80%. Interestingly the state that the central height of the lowest opening of their trap was 0.45 m. The distance from the sand surface to the lowest opening of the sand collector was 0.04 m. They do not explain why this is the case. They used different wind speeds (8, 10, 12, 14, 16, and 20 m/s). The test sand had a volume mean diameter of 0.228 mm and a surface area diameter of 0.211. Their Figure 5 shows vertical flux profiles from 14 different experimental runs. They found an exponential decay of flux with elevation above the bed.

Zingg (1953) reports on some exploratory wind tunnel studies that examined the dynamics of wind blown transport using newly developed equipment and experimental techniques. Figure 8 (p.125) shows 23 vertical flux profiles gathered during a series of wind tunnel experiments. The runs times were two minutes in a wind tunnel 56 feet (17 m) long (unknown working section dimensions) and 3 feet (0.9 m) square. The transport was collected using a trap described in Zingg (1951). It consisted of four tubes with 0.92-inch (0.28 m) square openings. The midpoint of the tubes were placed at 0.625 (0.016 m), 2.875 (0.073 m), 5.625 (0.143 m), and 9.625 (0.244 m) inches above the bed. The tests were done using five different mean grains sizes of predominantly quartz sands (d = 0.20, 0.275, 0.36, 0.505, and 0.715 mm). The vertical flux profiles shown in his Figure 8 are for 0.20 mm sand at different pressure levels of the wind tunnel fans. Zingg found that the slope of the decay profiles varied with wind speed (or fan pressure) and surmises that "*as the flow of sand increases a greater proportion of it is carried at given heights above the bed* (p.127)".

Znamensky (1960) used single tube traps with opening 0.01 m x 0.01 m in wind tunnel to examine the vertical distribution of sediment. The wind speed was reported at 0.015 m above the bed ($U_{0.15}$ = 10.61 m/s). The rate of sand feed varied for each profile (reported in g/cm.s). This report was published in Chinese and reproduced in Li and Ni

(2003), Figure 2 (p.246). Grain size is not known.Six of the eight profiles we reuse din this analysis. Two of his profiles had too many overlapping or hidden points to identify.

Zou et al., (2001) used high-speed multiflash photography and vertical traps to analyze flux profiles in wind tunnel experiments.The wind tunnel had an experimental section 16.2 m long and a cross section 1.0 m wide and 0.60 m high. The test sand ranges in size from 0.20 -0.30 mm. Their Figure 8 (p.162) contains 4 vertical flux profiles for four different wind speed friction velocities (u_* = 0.63, 0.64, 0.74 and 0.81 m/s). They obtained the volume concentration of saltating sand by photography and the mass flux was measured using a sand collector (no details provided). The mass flux profiles are plotted in their Figure 8.

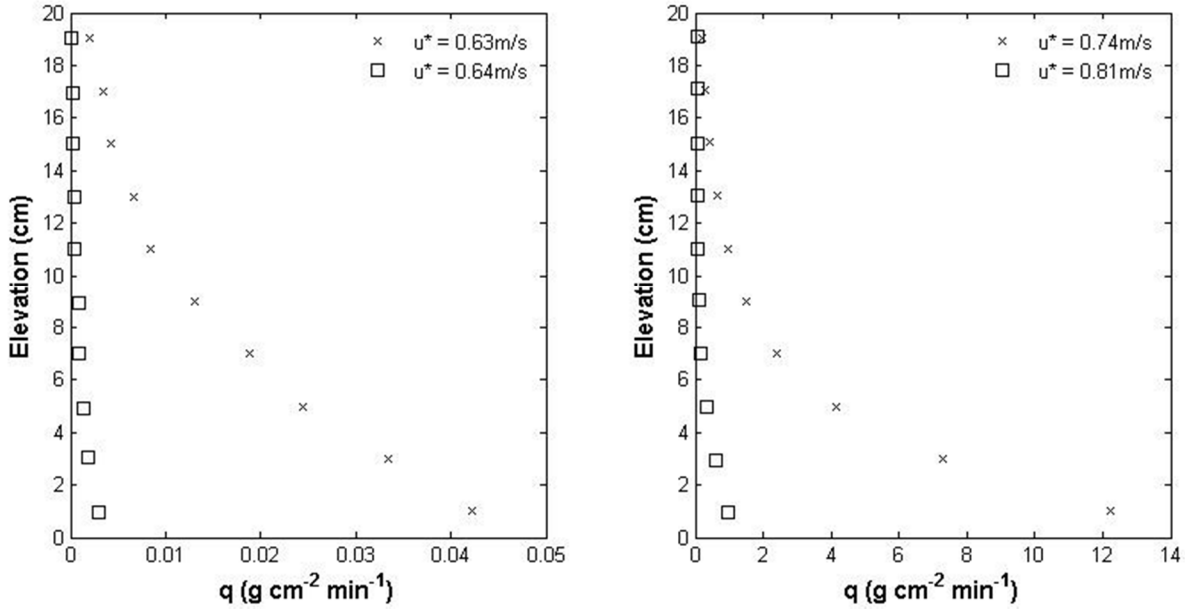

Fig A-21. Vertical mass flux profiles from Zou et al., (2001).

APPENDIX B

This Appendix provides the vertical flux data used to test the Rouse model.

Brazil (2008). This data is provided in Table 4-1.

APPENDIX B

This Appendix provides the vertical flux data used to test the Rouse model.

Brazil (2008). This data is provided in Table 4-1.

Table B-1. Vertical flux data used to test the Rouse model: Butterfield (1999)

Run 1		Run 2		Run 3		Run 4		Run 5	
q ($g/cm^2/s$)	z (cm)	q ($g/cm^2/s$)	z (cm)	q ($g/cm^2/s$)	z (cm)	q ($g/cm^2/s$)	z (cm)	q ($g/cm^2/s$)	z (cm)
0.00001	8.16950	0.00002	10.74080	0.00001	12.02960	0.00000	13.97880	0.00003	10.74110
0.00003	7.50440	0.00003	10.07870	0.00002	11.40170	0.00002	13.34890	0.00010	10.11330
0.00008	6.80640	0.00006	9.41570	0.00004	10.73840	0.00003	12.68710	0.00019	9.46820
0.00024	6.17750	0.00015	8.82220	0.00007	10.07630	0.00005	12.05950	0.00028	8.77070
0.00045	5.51510	0.00023	8.16030	0.00012	9.41410	0.00007	11.32850	0.00040	8.16040
0.00083	4.85270	0.00041	7.49790	0.00022	8.78650	0.00011	10.73600	0.00071	7.44550
0.00137	4.19050	0.00063	6.83600	0.00031	8.12470	0.00019	10.10850	0.00096	6.83520
0.00262	3.56280	0.00098	6.13920	0.00054	7.49720	0.00030	9.44650	0.00158	6.19010
0.00411	2.90080	0.00154	5.51200	0.00081	6.76580	0.00038	8.78510	0.00241	5.54490
0.00743	2.27320	0.00216	4.85020	0.00123	6.10380	0.00051	8.12340	0.00319	4.84740
0.01160	1.61120	0.00329	4.22310	0.00193	5.47660	0.00096	7.49580	0.00493	4.23710
0.02230	0.94870	0.00561	3.52610	0.00255	4.81500	0.00127	6.86900	0.00742	3.57450
0.04630	0.28600	0.00809	2.93390	0.00378	4.15320	0.00204	6.13730	0.01160	2.91190
		0.01170	2.23730	0.00577	3.49120	0.00320	5.51010	0.01630	2.24930
		0.02110	1.57490	0.00905	2.86400	0.00424	4.88330	0.03210	1.58670
		0.03700	0.98220	0.01310	2.20220	0.00647	4.22140	0.05720	0.94160
		0.07070	0.31970	0.02360	1.57470	0.01010	3.52460	0.11090	0.34870
				0.04500	0.91220	0.01500	2.93230		
				0.08610	0.24970	0.02230	2.27040		
						0.04260	1.64270		
						0.07700	0.94560		
						0.14710	0.31790		

Table B-2. Vertical flux data used to test the Rouse model: Dong et al., (2004)

	Run 1	Run 2	Run 3	Run 4	Run 5	Run 6	Run 7	Run 8
z	q	q	q	q	q	q	q	q
(m)	($g/cm^2/s$)	($g/cm^2/s$)	($g/cm^2/s$)	($g/cm^2/s$)	($g/cm^2/s$)	($g/cm^2/s$)	($g/cm^2/s$)	($g/cm^2/s$)
0.60	0.0000005	0.0000089	0.0000395	0.00010192	0.000206958	0.000363641	0.000994437	0.00224344
0.59	0.0000006	0.0000105	0.0000458	0.000117571	0.000237794	0.000415508	0.001120157	0.002501039
0.58	0.0000007	0.0000123	0.0000532	0.000135626	0.000273225	0.000474772	0.001261771	0.002788216
0.57	0.0000009	0.0000145	0.0000618	0.000156453	0.000313934	0.000542489	0.001421289	0.003108367
0.56	0.0000011	0.0000171	0.0000717	0.000180479	0.000360709	0.000619865	0.001600973	0.003465279
0.55	0.0000013	0.0000202	0.0000833	0.000208194	0.000414454	0.000708277	0.001803374	0.003863173
0.54	0.0000016	0.0000237	0.0000967	0.000240165	0.000476206	0.000809299	0.002031363	0.004306754
0.53	0.0000020	0.0000280	0.0001123	0.000277046	0.000547159	0.00092473	0.002288175	0.004801268
0.52	0.0000024	0.0000330	0.0001303	0.000319591	0.000628683	0.001056625	0.002577454	0.005352564
0.51	0.0000030	0.0000388	0.0001513	0.000368669	0.000722355	0.001207332	0.002903305	0.005967162
0.50	0.0000036	0.0000457	0.0001757	0.000425284	0.000829983	0.001379535	0.003270352	0.006652329
0.49	0.0000044	0.0000539	0.0002040	0.000490592	0.000953648	0.001576299	0.003683801	0.00741617
0.48	0.0000054	0.0000635	0.0002368	0.00056593	0.001095738	0.001801128	0.00414952	0.008267717
0.47	0.0000066	0.0000748	0.0002749	0.000652837	0.001258999	0.002058024	0.004674117	0.009217041
0.46	0.0000081	0.0000881	0.0003192	0.00075309	0.001446585	0.002351562	0.005265036	0.010275369
0.45	0.0000100	0.0001038	0.0003705	0.000868739	0.001662121	0.002686967	0.00593066	0.011455218
0.44	0.0000122	0.0001223	0.0004302	0.001002147	0.001909771	0.003070212	0.006680436	0.01277054
0.43	0.0000149	0.0001441	0.0004994	0.001156041	0.00219432	0.003508118	0.007525	0.014236892
0.42	0.0000183	0.0001698	0.0005798	0.001333569	0.002521266	0.004008484	0.008476337	0.015871615
0.41	0.0000224	0.0002000	0.0006731	0.001538358	0.002896926	0.004580218	0.009547946	0.017694042
0.40	0.0000274	0.0002357	0.0007815	0.001774596	0.003328557	0.005233498	0.010755031	0.019725725
0.39	0.0000335	0.0002776	0.0009073	0.002047112	0.0038245	0.005979956	0.012114721	0.021990692
0.38	0.0000411	0.0003271	0.0010533	0.002361477	0.004394337	0.006832882	0.013646307	0.024515729
0.37	0.0000503	0.0003854	0.0012229	0.002724117	0.005049078	0.007807461	0.015371521	0.027330699
0.36	0.0000616	0.0004540	0.0014197	0.003142446	0.005801372	0.008921046	0.017314844	0.030468891
0.35	0.0000754	0.0005349	0.0016482	0.003625015	0.006665756	0.010193462	0.019503848	0.033967421
0.34	0.0000923	0.0006302	0.0019135	0.004181691	0.00765893	0.011647364	0.021969594	0.037867662
0.33	0.0001130	0.0007424	0.0022216	0.004823852	0.008800083	0.013308636	0.024747068	0.042215741
0.32	0.0001384	0.0008747	0.0025792	0.005564627	0.010111264	0.015206858	0.02787568	0.04706308
0.31	0.0001694	0.0010305	0.0029943	0.006419159	0.011617806	0.017375825	0.031399823	0.052467004
0.30	0.0002074	0.0012140	0.0034763	0.007404917	0.013348818	0.019854153	0.0353695	0.058491423

Table B-2 (contd.).

	Run 1	Run 2	Run 3	Run 4	Run 5	Run 6	Run 7	Run 8
z (m)	q (g/cm^2/s)	q (g/cm^2/s)	q (g/cm^2/s)	q (g/cm^2/s)	q (g/cm^2/s)	q (g/cm^2/s)	q (g/cm^2/s)	q (g/cm^2/s)
0.29	0.0002539	0.0014303	0.0040359	0.008542053	0.015337744	0.022685966	0.039841038	0.065207584
0.28	0.0003109	0.0016851	0.0046855	0.009853814	0.017623013	0.025921684	0.044877884	0.072694914
0.27	0.0003807	0.0019853	0.0054398	0.011367015	0.020248779	0.029618915	0.050551505	0.081041963
0.26	0.0004661	0.0023389	0.0063154	0.01311259	0.023265775	0.033843485	0.056942406	0.090347445
0.25	0.0005707	0.0027556	0.0073320	0.015126225	0.026732292	0.038670609	0.064141268	0.10072141
0.24	0.0006987	0.0032464	0.0085122	0.017449084	0.030715308	0.044186229	0.072250235	0.112286544
0.23	0.0008555	0.0038248	0.0098823	0.020128652	0.035291779	0.050488547	0.081384367	0.125179623
0.22	0.0010475	0.0045061	0.0114731	0.023219708	0.040550128	0.057689769	0.091673268	0.139553123
0.21	0.0012825	0.0053088	0.0133199	0.026785443	0.046591953	0.065918108	0.103262928	0.155577032
0.20	0.0015702	0.0062545	0.0154639	0.030898749	0.053533987	0.075320061	0.116317795	0.173440855
0.19	0.0019226	0.0073686	0.0179531	0.035643715	0.06151036	0.086063023	0.131023104	0.193355855
0.18	0.0023539	0.0086813	0.0208430	0.041117342	0.070675184	0.098338261	0.147587511	0.215557555
0.17	0.0028821	0.0102277	0.0241980	0.047431527	0.081205534	0.112364327	0.166246049	0.240308521
0.16	0.0035287	0.0120497	0.0280931	0.054715349	0.093304868	0.128390943	0.187263466	0.267901467
0.15	0.0043205	0.0141962	0.0326152	0.063117711	0.10720696	0.146703447	0.210937979	0.298662719
0.14	0.0052899	0.0167250	0.0378652	0.072810382	0.123180414	0.167627879	0.237605508	0.33295607
0.13	0.0064768	0.0197044	0.0439603	0.083991508	0.141533855	0.191536779	0.267644442	0.371187086
0.12	0.0079301	0.0232144	0.0510365	0.096889664	0.162621894	0.218855826	0.301481004	0.413807903
0.11	0.0097093	0.0273498	0.0592517	0.111768525	0.186851975	0.25007141	0.339595304	0.461322569
0.10	0.0118879	0.0322218	0.0687893	0.128932258	0.214692252	0.285739298	0.382528151	0.514293013
0.09	0.0145552	0.0379617	0.0798621	0.148731739	0.24668063	0.326494526	0.43088872	0.573345682
0.08	0.0178210	0.0447241	0.0927173	0.171571728	0.283435163	0.373062705	0.485363204	0.639178956
0.07	0.0218195	0.0526911	0.1076418	0.197919139	0.325665989	0.426272941	0.546724546	0.712571404
0.06	0.0267153	0.0620774	0.1249686	0.228312591	0.374189058	0.487072597	0.615843408	0.794390994
0.05	0.0327094	0.0731356	0.1450845	0.263373413	0.42994189	0.556544157	0.693700521	0.885605355
0.04	0.0400486	0.0861638	0.1684384	0.30381835	0.494001695	0.635924502	0.781400608	0.987293223
0.03	0.0490344	0.1015128	0.1955515	0.350474213	0.567606183	0.72662693	0.880188052	1.100657197
0.02	0.0600364	0.1195959	0.2270290	0.404294784	0.652177476	0.830266319	0.991464556	1.227037964
0.01	0.0735070	0.1409004	0.2635733	0.46638031	0.749349589	0.948687878	1.116809031	1.36793015

Table B-3. Vertical flux data used to test the Rouse model: Feng et al., (2004)

Run 1		Run 2		Run 3		Run 4		Run 5		Run 6		Run 7		Run 8		Run 9	
q (g/cm2/s)	z (cm)	q (g/cm2/s)	z (cm)	q (g/cm2/s)	z (cm)	q (g/cm2/s)	z (cm)	q (g/cm2/s)	z (cm)	q (g/cm2/s)	z (cm)	q (g/cm2/s)	z (cm)	q (g/cm2/s)	z (cm)	q (g/cm2/s)	z (cm)
0.0006673	29.9563	0.0011737	30.0101	0.0036319	30.0101	0.0084124	30.0101	0.0171	30.0101	0.000494	30.0041	0.00107	29.9459	0.00317	29.9933	0.00619	29.9357
0.0006676	28.9345	0.0015917	28.9345	0.0040212	29.042	0.008539	28.9882	0.0179	28.9882	0.000588	28.9293	0.00123	28.925	0.00346	28.9189	0.00675	28.915
0.0007499	27.9664	0.0018405	27.9664	0.0046501	27.9664	0.0103	27.9664	0.0184	27.9664	0.000579	27.9092	0.00142	27.9577	0.00388	27.8981	0.00768	27.8942
0.0009323	26.9983	0.0020977	26.9445	0.005781	26.9445	0.0113	26.9983	0.0201	26.9445	0.000741	26.9413	0.00167	26.8829	0.00417	26.9313	0.00875	26.927
0.0012642	25.9765	0.0026845	25.9765	0.006494	25.9227	0.0134	26.0303	0.0232	25.9765	0.000907	25.92	0.00193	25.9693	0.00475	25.9104	0.0103	25.9059
0.00134	24.9008	0.0028873	25.0084	0.00719	24.9546	0.0146	25.0084	0.0272	24.9546	0.00099	24.8994	0.00223	24.8946	0.00542	24.9432	0.0104	24.9394
0.0015953	23.9866	0.0036436	22.9109	0.0075128	23.9328	0.0157	23.9866	0.0324	23.9328	0.00116	23.9857	0.00266	23.9272	0.00591	23.9225	0.0117	23.9722
0.0017662	23.0185	0.0039189	21.9966	0.0086873	22.9647	0.0179	23.0185	0.0349	22.9647	0.00142	22.9107	0.00281	22.9604	0.00683	22.9552	0.0137	22.9512
0.0020722	21.9429	0.0050151	20.9748	0.0094802	21.9429	0.0198	21.9966	0.0386	21.9966	0.00151	21.9439	0.00325	21.8857	0.00723	21.9885	0.015	21.9305
0.0023618	20.921	0.0058839	19.9529	0.0106	20.9748	0.0226	20.921	0.046	20.9748	0.00182	20.9227	0.00355	20.9725	0.00789	20.9678	0.0165	21.0172
0.0029361	20.0067	0.0057185	18.9311	0.013	19.9529	0.0265	19.9529	0.0524	19.9529	0.00226	19.955	0.00428	19.9513	0.00952	19.9466	0.0188	19.9963
0.0029803	18.9849	0.0064239	17.9092	0.0127	18.9849	0.0262	19.0387	0.0572	18.9849	0.00246	18.9343	0.00481	18.9304	0.0108	18.9257	0.0215	18.9217
0.0033967	17.963	0.0085857	16.9412	0.0142	17.9092	0.0294	17.963	0.0633	17.963	0.00269	17.9674	0.00488	17.9639	0.0107	17.9593	0.0221	17.9551
0.0047414	16.995	0.0085893	16.0269	0.0193	16.9412	0.0393	16.9412	0.0732	16.995	0.00334	16.946	0.00633	16.9423	0.0131	16.938	0.0271	16.9875
0.0046754	15.9731	0.0097898	14.9513	0.0193	15.9731	0.0393	16.0269	0.0897	15.9731	0.00381	15.9251	0.0068	15.9754	0.0143	15.9711	0.0291	15.9669
0.0054853	14.9513	0.011	13.9832	0.0223	15.005	0.0448	15.005	0.0993	14.9513	0.00427	14.958	0.00775	14.9545	0.0163	15.0039	0.0341	14.9996
0.0059859	13.9832	0.0124	13.0151	0.0244	13.9294	0.0489	13.9832	0.1084	13.9832	0.00523	13.9367	0.00963	13.9868	0.0193	13.9827	0.04	13.9785
0.0081207	11.9933	0.0139	11.9933	0.0274	13.0151	0.0541	13.0151	0.129	12.9613	0.00571	12.9697	0.00991	12.9665	0.0205	12.9623	0.0412	12.9582
0.008991	11.0252	0.0158	10.9714	0.0317	11.9933	0.0617	11.9933	0.1449	11.9933	0.0066	11.9487	0.0123	11.9988	0.0247	11.941	0.049	11.937
0.0102	9.9496	0.018	9.9496	0.0346	10.9176	0.0673	10.9714	0.1605	10.9714	0.00689	10.982	0.0123	10.9787	0.0255	10.9744	0.0519	11.024
0.0115	8.9277	0.02	8.9815	0.0377	10.0034	0.0745	9.9496	0.1701	10.0571	0.00907	9.9603	0.0165	9.9568	0.0326	9.9528	0.0645	9.9489
0.0145	7.9597	0.0252	7.9059	0.0436	8.9277	0.0837	8.9815	0.2084	8.9815	0.00975	8.9934	0.0167	8.9903	0.0355	8.9859	0.0693	8.9283
0.0156	6.9378	0.0271	6.9916	0.0535	7.9597	0.0996	7.9059	0.2275	7.9597	0.0118	7.9722	0.0205	7.969	0.0417	7.9111	0.0813	7.9609
0.0183	5.9697	0.0313	5.9697	0.0592	6.9378	0.1119	6.9378	0.2593	6.9916	0.0138	7.0048	0.0243	7.0552	0.0503	6.9436	0.0996	6.9933
0.0225	4.9479	0.0384	4.9479	0.0675	5.916	0.1276	5.9697	0.3042	5.916	0.0164	5.9837	0.029	5.9267	0.0582	5.9763	0.1151	5.9723
0.0235	4.0336	0.0431	3.9798	0.0827	4.9479	0.1563	4.9479	0.3517	4.9479	0.0196	4.9625	0.036	5.0127	0.0723	4.9549	0.141	4.951
0.0296	2.958	0.0536	2.958	0.0876	3.9261	0.1633	3.9798	0.3838	4.0336	0.0233	3.9414	0.0441	3.9377	0.0873	3.9874	0.1654	3.93
0.0395	1.9899	0.0727	1.9361	0.1121	2.958	0.209	2.958	0.4374	3.0118	0.0302	2.9734	0.0556	3.0236	0.1133	2.9657	0.2085	2.9622
0.0585	1.0218	0.109	0.9681	0.1521	1.9361	0.2524	1.9899	0.6565	1.9361	0.0334	1.9527	0.0701	2.0021	0.145	1.9441	0.2592	1.9408
				0.2315	0.9681	0.4442	0.9681	0.8161	0.9681	0.044	0.9846	0.0924	0.9803	0.1938	0.976	0.4435	0.9712

Table B-4. Vertical flux data used to test the Rouse model: Gerety & Slingerland (1983)

	Run 1	Run 2	Run 3	Run 4
z (cm)	q ($g/cm^2/s$)	q ($g/cm^2/s$)	q ($g/cm^2/s$)	q ($g/cm^2/s$)
7.00				0.0175
5.00	0.0015	0.0068	0.0116	0.0368
3.00	0.0040	0.0124	0.0233	0.0561
2.00	0.0056	0.0164	0.0554	0.0959
1.00	0.0061	0.0368	0.1350	0.5040
0.50	0.0666	0.0927	0.4761	0.9158

Table B-5. Vertical flux data used to test the Rouse model: Greeley et al., (1996)

Run 1		Run 2		Run 3		Run 4		Run 5		Run 6		Run 7		Run 8		Run 9	
q ($g/cm^2/s$)	z (cm)	q ($g/cm^2/s$)	z (cm)	q ($g/cm^2/s$)	z (cm)	q ($g/cm^2/s$)	z (cm)	q ($g/cm^2/s$)	z (cm)	q ($g/cm^2/s$)	z (cm)	q ($g/cm^2/s$)	z (cm)	q ($g/cm^2/s$)	z (cm)	q ($g/cm^2/s$)	z (cm)
0.0000091	17.46	0.0000009	33.87	0.0000005	42.55	0.0000009	42.56	0.0000015	44.14	0.0000027	44.08	0.000003	38.76	0.000003	42.67	0.0000039	44.11
0.0000128	15.49	0.0000018	31.83	0.0000010	40.51	0.0000014	40.52	0.0000021	42.09	0.0000072	40.07	0.000006	36.80	0.000007	40.69	0.0000050	41.99
0.0000179	13.44	0.0000023	29.74	0.0000021	38.67	0.0000036	38.40	0.0000031	40.08	0.0000113	38.02	0.000009	34.67	0.000012	38.73	0.0000041	39.93
0.0000287	11.31	0.0000048	27.74	0.0000021	36.65	0.0000049	36.02	0.0000049	38.04	0.0000142	36.01	0.000013	32.77	0.000014	36.78	0.0000029	37.93
0.0000363	9.30	0.0000077	25.65	0.0000038	34.74	0.0000057	33.88	0.0000130	33.99	0.0000229	33.76	0.000021	30.75	0.000024	34.81	0.0000075	36.07
0.0000459	7.29	0.0000124	23.73	0.0000061	32.73	0.0000118	32.30	0.0000193	31.90	0.0000391	31.88	0.000033	28.90	0.000033	32.85	0.0000092	33.84
0.0000566	5.19	0.0000201	21.60	0.0000107	30.73	0.0000195	29.75	0.0000295	29.73	0.0000568	29.78	0.000050	26.77	0.000055	30.83	0.0000142	31.76
0.0000752	3.22	0.0000303	19.63	0.0000170	28.80	0.0000237	27.78	0.0000462	27.76	0.0000901	27.74	0.000081	24.75	0.000075	28.82	0.0000223	29.63
0.0001286	1.22	0.0000487	17.50	0.0000277	26.68	0.0000454	25.62	0.0000706	25.67	0.0001446	25.69	0.000129	22.79	0.000115	26.80	0.0000322	27.67
		0.0000690	15.54	0.0000462	24.67	0.0000712	23.61	0.0001078	23.66	0.0002181	23.68	0.000190	20.94	0.000175	24.79	0.0000458	25.49
		0.0001122	13.37	0.0000732	22.87	0.0001363	21.61	0.0001605	21.70	0.0003372	21.72	0.000288	18.87	0.000279	22.77	0.0000731	23.58
		0.0001550	11.32	0.0001175	20.87	0.0002107	19.65	0.0002545	19.69	0.0005086	19.63	0.000431	16.96	0.000257	20.93	0.0000971	21.46
		0.0002194	9.39	0.0001910	18.98	0.0003259	17.56	0.0003888	17.52	0.0007295	17.54	0.000544	15.12	0.000593	18.91	0.0001475	19.44
		0.0003031	7.26	0.0002955	16.90	0.0004852	15.63	0.0005575	15.51	0.0011000	15.53	0.000826	13.05	0.001259	16.94	0.0002203	17.32
		0.0004184	5.29	0.0004452	15.09	0.0011185	11.29	0.0008517	13.38	0.0016384	13.44	0.001276	11.09	0.000884	15.05	0.0003181	15.36
		0.0006308	3.28	0.0006548	13.00	0.0015639	9.28	0.0013856	11.25	0.0048337	7.21	0.001781	9.02	0.001878	13.03	0.0004912	13.23
		0.0010390	1.23	0.0009505	11.08	0.0021323	7.27	0.0018646	9.37	0.0067596	5.16	0.002406	7.06	0.002536	11.18	0.0006523	11.10
				0.0013624	9.15	0.0030578	5.22	0.0026740	7.32	0.0086541	3.15	0.003417	5.04	0.003542	9.16	0.0009580	9.09
				0.0018575	7.14	0.0039638	3.25	0.0038845	5.18	0.0186000	1.23	0.004692	3.03	0.003912	6.99	0.0014307	7.02
				0.0026296	5.17	0.0059002	1.32	0.0057813	3.30			0.008148	0.95	0.007513	5.19	0.0021011	5.00
				0.0032829	3.16			0.0097646	1.26					0.010700	3.01	0.0030855	2.93
				0.0054035	1.28									0.021500	0.98	0.0053591	1.08

Table B-6. Vertical flux data used to test the Rouse model: Hotta & Horikawa (1991)

Run 1		Run 2		Run 3		Run 4		Run 5		Run 6		Run 7		Run 8		Run 9		Run 10	
q	z	q	z	q	z	q	z	q	z	q	z	q	z	q	z	q	z	q	z
($g/cm^2/s$)	(cm)	($g/cm^2/s$)	(cm)	($g/cm^2/s$)	(cm)	($g/cm^2/s$)	(cm)	($g/cm^2/s$)	(cm)	($g/cm^2/s$)	(cm)	($g/cm^2/s$)	(cm)	($g/cm^2/s$)	(cm)	($g/cm^2/s$)	(cm)	($g/cm^2/s$)	(cm)
0.000092	24.1289	0.0000637	39.7348	0.000257	49.5637	0.000647	49.446	0.0000662	29.291	0.000186	31.8851	0.000397	49.6673	0.000241	25.4996	0.000129	49.3041	0.00066	49.2618
0.0000809	23.1763	0.0000644	37.1404	0.000191	47.0085	0.000989	47.1653	0.000123	27.0527	0.000329	29.4972	0.000404	47.277	0.000236	24.1289	0.000129	46.8091	0.000778	46.8212
0.000122	22.1924	0.0000961	34.4098	0.000265	44.5248	0.00132	44.6303	0.0000998	25.0598	0.000495	27.0587	0.000623	44.6892	0.000248	23.1032	0.000168	44.5185	0.000888	44.4774
0.000102	21.1882	0.000127	31.9743	0.000258	41.8292	0.00117	42.0813	0.00016	24.016	0.000783	25.2181	0.000406	42.0479	0.000318	22.1822	0.000194	41.9795	0.00114	41.7952
0.000162	20.0067	0.000157	29.3371	0.000459	39.6536	0.00183	39.552	0.00016	22.9204	0.000783	24.2719	0.000819	39.6107	0.000329	21.1559	0.000231	39.4414	0.00135	39.5503
0.000124	18.9995	0.000185	26.8977	0.000395	36.9538	0.00182	36.9071	0.00021	22.2741	0.000976	23.3266	0.000821	36.9215	0.000413	20.0384	0.000325	36.909	0.0016	36.9143
0.000203	18.0685	0.000261	25.0632	0.000671	34.3774	0.00266	34.475	0.00021	21.2781	0.000969	22.2309	0.00121	34.3833	0.000332	19.2483	0.000439	34.3752	0.00229	34.3335
0.000157	16.9119	0.000298	24.1696	0.000724	31.885	0.00282	32.0819	0.000251	20.2331	0.00132	21.3359	0.00121	32.0925	0.000506	18.0884	0.000526	31.9351	0.00251	31.9393
0.000246	16.0292	0.000396	23.2812	0.001	29.4013	0.00398	29.499	0.000249	19.237	0.00146	20.5395	0.00185	29.405	0.000499	17.1583	0.000694	29.3027	0.00348	29.3085
0.000203	14.8249	0.000396	22.0837	0.00129	26.8652	0.00477	27.0601	0.000421	17.9943	0.00156	19.3445	0.00235	27.0654	0.000921	16.1518	0.000887	26.8648	0.00427	26.8693
0.000242	13.883	0.00063	21.0019	0.00218	25.1368	0.00758	25.0802	0.000372	17.1969	0.00202	18.2999	0.00307	25.2738	0.000922	15.1734	0.00123	25.1635	0.00656	25.1226
0.000309	12.8935	0.000567	19.8506	0.00218	23.9392	0.00797	24.1338	0.000638	16.1036	0.00199	17.2042	0.00308	24.3276	0.00101	13.8066	0.00156	23.9976	0.00646	24.0458
0.000488	11.8613	0.00073	19.1108	0.00233	23.0932	0.00865	23.1387	0.0005	15.1066	0.0029	16.16	0.00393	23.233	0.00134	12.8377	0.0018	23.1706	0.00701	23.0701
0.000426	10.7089	0.000799	18.0661	0.00233	22.0454	0.00866	21.8912	0.000764	14.0128	0.00295	15.3134	0.00406	22.2371	0.00159	11.7672	0.00189	21.9003	0.00761	21.8009
0.000821	9.7337	0.000948	17.074	0.00359	21.0124	0.0126	21.0559	0.000871	13.1667	0.0031	14.0686	0.00498	21.242	0.00166	10.7412	0.00255	20.9809	0.00994	21.0272
0.000758	8.7828	0.00128	16.0365	0.0034	19.8129	0.0106	20.052	0.00129	12.0728	0.00399	13.1235	0.00597	20.197	0.0025	9.7279	0.00251	19.953	0.00979	19.8525
0.00146	8.0571	0.00129	15.0888	0.0039	19.0692	0.015	19.1657	0.00121	10.9769	0.0049	11.979	0.00602	19.201	0.00283	8.6557	0.0031	19.0306	0.0113	18.9279
0.00155	6.8615	0.00183	13.9532	0.00448	18.1259	0.0152	18.1683	0.00192	9.9331	0.00519	10.9334	0.00769	18.206	0.0042	7.5928	0.00362	17.9595	0.0132	18.0526
0.00203	5.8728	0.00188	13.0559	0.00487	17.0309	0.0169	17.2238	0.00185	8.9369	0.00726	9.5902	0.00776	17.2599	0.00527	6.7688	0.00334	16.8316	0.0136	16.9771
0.00227	4.9287	0.00261	12.0691	0.00702	15.9458	0.0229	16.0866	0.0033	8.0928	0.00807	8.9931	0.0112	16.1658	0.00524	5.7412	0.00534	15.8691	0.0198	15.9626
0.00355	3.9461	0.00257	11.0706	0.00659	14.8957	0.0203	15.1343	0.00347	7.1468	0.0118	7.9987	0.00961	15.2688	0.00657	4.8683	0.00384	14.8305	0.0172	14.7836
0.00428	3.0045	0.00328	9.9314	0.00841	13.8563	0.0265	14.4949	0.00443	6.1021	0.014	7.0034	0.0123	14.1742	0.00879	3.8019	0.00614	13.8679	0.0214	13.9104
0.00588	2.1672	0.00405	9.0405	0.0099	12.9138	0.0288	13	0.00493	5.1065	0.0133	5.9574	0.0137	13.1786	0.0116	2.8817	0.00671	12.7947	0.0256	12.8401
0.00841	1.2315	0.0057	8.1042	0.0119	11.9223	0.0359	11.9605	0.00678	3.9127	0.0176	5.0124	0.0177	12.134	0.0145	2.0577	0.00856	11.7755	0.0303	11.6718
0.0103	0.8394	0.00739	7.0155	0.012	11.0242	0.0357	11.062	0.00838	2.8678	0.0212	4.0172	0.0201	11.0389	0.0197	1.2853	0.0085	10.6501	0.0354	10.6496
0.0147	0.4525	0.00746	6.0178	0.016	9.7868	0.0463	10.0731	0.0102	1.9722	0.0277	2.9725	0.0236	9.8942	0.0202	0.6502	0.0114	9.8283	0.0416	9.6767
		0.00915	4.9271	0.0178	8.8923	0.0452	8.9745	0.0135	1.326	0.0306	2.0766	0.0246	8.8983	0.0275	0.3671	0.0116	8.8504	0.0424	8.6988
		0.0119	3.9381	0.027	7.8588	0.0742	8.0435			0.0475	1.431	0.0392	7.9541			0.0172	7.9343	0.0635	7.6362
		0.0167	3.0018	0.029	6.9631	0.0755	6.8465			0.0524	0.8339	0.0399	6.8586			0.0178	7.1037	0.0662	6.6102
		0.0208	1.8617	0.0315	5.8183	0.0903	5.9047					0.0444	5.9128			0.0199	5.8356	0.0817	5.8346
		0.031	1.2268	0.0345	4.9232	0.103	4.8114					0.0506	5.017			0.0231	4.8621	0.0858	4.7111
		0.0361	0.5336	0.049	3.8874	0.1273	3.8706					0.0679	3.9724			0.0294	3.794	0.1112	3.6925
		0.0443	0.3909	0.0615	2.8973	0.1638	2.8315					0.0903	2.878			0.0349	2.8703	0.1351	2.6717
				0.0684	1.8531	0.175	1.8358					0.103	2.032			0.0438	1.9484	0.159	1.6009
				0.097	1.3163	0.2756	1.1529					0.1337	1.1865			0.0532	1.319	0.1977	1.1191
				0.1237	0.8756	0.3662	0.5141					0.1487	0.689			0.0667	0.7396	0.2731	0.494
				0.2028	0.4437							0.4183	0.3946			0.0759	0.5483	0.3958	0.311

Table B-7. Vertical flux data used to test the Rouse model: Hotta et al., (2006)

D15 Run1		D15 Run2		D15 Run3		D25 Run1		D25 Run2		D25 Run3		MD28 Run1		MD28 Run2	
q ($g/cm^2/s$)	z (cm)	q ($g/cm^2/s$)	z (cm)	q ($g/cm^2/s$)	z (cm)	q ($g/cm^2/s$)	z (cm)	q ($g/cm^2/s$)	z (cm)	q ($g/cm^2/s$)	z (cm)	q ($g/cm^2/s$)	z (cm)	q ($g/cm^2/s$)	z (cm)
0.000153	9.9919	0.000162	22.3593	0.000175	39.1324	0.000134	19.606	0.00013	38.6864	0.000384	58.5121	0.000218	21.2304	0.000175	54.8113
0.000241	7.7195	0.0004	20.3519	0.000789	32.6828	0.000173	17.4846	0.000162	32.0615	0.000278	52.7839	0.000596	16.8496	0.000302	44.6428
0.00204	5.6354	0.000846	18.1421	0.00173	28.7887	0.000271	15.5626	0.000591	28.5007	0.000723	48.4684	0.00191	13.659	0.00108	34.9021
0.00415	4.264	0.00136	15.8733	0.0069	22.6517	0.000516	13.031	0.00129	22.364	0.000621	42.5966	0.00459	10.6292	0.00249	29.9973
0.0236	1.9259	0.00268	13.6487	0.0174	20.4787	0.00118	11.7427	0.00332	19.6683	0.0017	38.967	0.00724	8.5578	0.00415	25.8129
0.1224	0.2461	0.00546	12.2774	0.0293	18.3901	0.00217	9.7946	0.00486	17.8731	0.0027	32.4185	0.0149	6.6618	0.0088	21.4761
0.4971	0.0372	0.0202	7.8172	0.0424	16.2684	0.0024	7.9286	0.00736	15.7256	0.00791	28.7776	0.0255	4.4652	0.0194	17.4649
		0.0379	5.7508	0.0592	14.1393	0.00539	5.2553	0.0106	13.47	0.017	22.0649	0.0585	2.8823	0.0339	14.0468
		0.08	4.3868	0.1127	12.584	0.014	3.9465	0.0194	12.1016	0.041	20.305	0.1004	1.0177	0.0588	10.7415
		0.223	2.4051	0.1469	10.271	0.0165	1.7226	0.0265	9.8553	0.051	18.3048	0.1728	0.3703	0.0736	8.8205
		0.9252	0.6774	0.2568	8.359	0.1073	0.3817	0.0477	7.6797	0.0818	16.1479			0.1134	7.196
				0.3348	6.046			0.0673	5.8901	0.0904	14.0509			0.1642	5.0286
				0.6049	4.6488			0.1302	4.1657	0.1729	12.5594			0.2921	3.1577
				0.7882	2.505			0.1882	2.2568	0.1867	10.2349			0.3798	1.5624
								0.2452	0.7114	0.3289	8.2943			0.5065	0.5163
										0.4278	5.9399				
										0.7806	4.2248				
										0.8342	2.48				
										1.0138	1.0614				

Table B-7 (contd.)

MD28 Run3		D48 Run1		D48 Run2		D48 Run3		D68 Run1		D68 Run2		D68 Run3	
q ($g/cm^2/s$)	z (cm)	q ($g/cm^2/s$)	z (cm)	q ($g/cm^2/s$)	z (cm)	q ($g/cm^2/s$)	z (cm)	q ($g/cm^2/s$)	z (cm)	q ($g/cm^2/s$)	z (cm)	q ($g/cm^2/s$)	z (cm)
0.00182	54.9591	0.000167	32.0929	0.000465	58.5237	0.00738	58.9469	0.000562	57.976	0.00692	58.3575	0.0493	52.4935
0.00373	44.7613	0.000443	28.0518	0.000637	52.5798	0.0091	53.0237	0.000744	51.785	0.00894	52.2829	0.0639	48.6486
0.0127	35.029	0.000835	22.4736	0.00116	48.3983	0.0164	48.5237	0.00112	48.2448	0.0127	48.6436	0.0769	42.5889
0.0275	30.024	0.00185	19.4313	0.00158	42.8843	0.0212	42.8051	0.00165	42.0315	0.016	42.2396	0.0916	38.4269
0.0383	26.0923	0.0023	17.5704	0.00275	38.605	0.0336	38.8649	0.00267	37.8075	0.021	38.1692	0.1228	32.5678
0.0703	21.8912	0.00303	15.4842	0.00418	32.3198	0.0477	32.5935	0.00376	32.05	0.0281	32.3102	0.1501	28.7353
0.1231	17.9198	0.00391	13.8302	0.00729	28.3612	0.0722	28.6624	0.00558	27.8434	0.036	28.1333	0.2011	22.4303
0.1821	14.5309	0.00529	11.9532	0.0108	22.6151	0.1075	22.8094	0.00705	21.8853	0.0495	22.2693	0.2619	20.2576
0.2663	11.2548	0.00585	9.6876	0.0177	19.6324	0.1689	19.7267	0.00864	19.8365	0.0669	20.0892	0.2947	18.1147
0.3104	9.3464	0.00954	7.774	0.0222	17.5554	0.203	17.9795	0.00937	17.5895	0.0762	18.1667	0.3198	16.2022
0.4442	7.4024	0.0138	5.4556	0.0258	15.8152	0.244	16.2324	0.0118	15.6472	0.0901	16.0139	0.3778	14.0493
0.6435	5.4564	0.0198	3.781	0.0317	14.1704	0.2428	14.2013	0.0132	13.3928	0.1014	14.0939	0.4631	12.112
0.8162	3.5333	0.0235	1.8224	0.0434	11.9704	0.3736	12.406	0.0172	11.3316	0.1227	11.8246	0.4964	10.0904
0.8639	1.7523	0.0469	0.5111	0.0521	10.1163	0.4488	10.3381	0.025	9.1366	0.1432	9.7857	0.6546	8.1382
1.1377	0.4869			0.0802	8.1073	0.6069	8.675	0.03	7.4272	0.1981	7.4892	0.7192	6.3347
				0.1021	5.7072	0.7029	6.0795	0.0355	5.9433	0.246	5.9953	0.9838	4.3751
				0.1607	3.8005	0.9844	4.3025	0.0491	3.8697	0.3245	4.1546	1.4656	2.5096
				0.2073	2.0396	1.2108	2.337	0.0767	1.7713	0.428	2.3139	2.1583	0.981
				0.3767	0.8536	1.758	0.8739	0.1118	0.8027	0.7943	0.6268		

Table B-8. Vertical flux data used to test the Rouse model: Kawamura (1951)

Run 1		Run 2	
q ($g/cm^2/s$)	z (cm)	q ($g/cm^2/s$)	z (cm)
0.0017604	9.9859	0.0083226	14.9929
0.0051538	7.4682	0.022	10.0141
0.0106	4.9788	0.0421	7.4682
0.0242	2.9986	0.0665	4.9788
0.0483	1.9802	0.1005	2.9986
0.1099	0.9901	0.192	1.9519
0.2226	0.4809	0.3457	0.9901
0.3167	0.396	0.6044	0.5092
0.4187	0.2829	0.7991	0.396
0.6135	0.1132	1.0564	0.2829
0.7993	0.0849	1.4173	0.198
		1.9871	0.0849

Table B-9. Vertical flux data used to test the Rouse model: Namikas (2003)

Run P5		Run P4		Run P3		Run P8		Run P14		Run P6		Run P9		Run P10		Run P13	
z (m)	q (g/cm^2/s)	z (m)	q (g/cm^2/s)	z (m)	q (g/cm^2/s)	z (m)	q (g/cm^2/s)	z (m)	q (g/cm^2/s)	z (m)	q (g/cm^2/s)	z (m)	q (g/cm^2/s)	z (m)	q (g/cm^2/s)	z (m)	q (g/cm^2/s)
0.004254	0.001368	0.004105	0.0528	0.00394	0.009558	0.004124	0.0335	0.003991	0.8785	0.004756	0.1916	0.004514	0.2284	0.004061	0.1552	0.004023	0.3962
0.0146	0.000917	0.0147	0.0204	0.0143	0.003918	0.014	0.0232	0.0141	0.6778	0.0144	0.124	0.0139	0.1662	0.0144	0.0853	0.0141	0.3021
0.0251	0.000699	0.0248	0.0129	0.0251	0.003131	0.025	0.0255	0.0249	0.8452	0.024	0.0892	0.0249	0.1659	0.0247	0.1168	0.025	0.0812
0.0348	0.000469	0.0347	0.009289	0.0349	0.002813	0.0346	0.015	0.035	0.3631	0.0344	0.0479	0.035	0.0664	0.0353	0.0705	0.0348	0.0612
0.0456	0.000402	0.0454	0.009165	0.0453	0.00193	0.045	0.0102	0.0453	0.2242	0.0449	0.0361	0.0456	0.0576	0.0454	0.0425	0.0451	0.0556
0.0599	0.000163	0.0597	0.007233	0.06	0.001597	0.0598	0.0055252	0.0596	0.1833	0.0595	0.0225	0.0597	0.0332	0.0597	0.0256	0.0594	0.046
0.0796	0.000153	0.0799	0.004408	0.0797	0.001056	0.0799	0.0051934	0.0805	0.1256	0.0799	0.0191	0.0801	0.0274	0.0806	0.0204	0.0801	0.0274
0.1005	0.000129	0.0996	0.003092	0.1002	0.000862	0.1001	0.0033953	0.0993	0.0765	0.1	0.0142	0.0998	0.0199	0.1003	0.0135	0.0998	0.0171
0.1195	0.000115	0.1196	0.001819	0.1201	0.000557	0.1203	0.0021431	0.1199	0.036	0.1197	0.0103	0.1202	0.012	0.1198	0.008146	0.1202	0.012
0.1396	0.00009	0.14	0.001306	0.1393	0.000434	0.14	0.0013061	0.1399	0.0271	0.1397	0.006576	0.1399	0.008118	0.1404	0.005987	0.1399	0.01
0.1697	0.00004	0.1693	0.000863	0.1691	0.000222	0.1695	0.00099274	0.1689	0.0261	0.169	0.004446	0.1688	0.005362	0.169	0.003476	0.169	0.005554
		0.209	0.000332	0.21	0.00008	0.2094	0.00042934	0.2093	0.009454	0.2094	0.001835	0.2098	0.002458	0.2089	0.001613	0.2094	0.002607
		0.2496	0.00014	0.2501	0.00005	0.2495	0.00019231	0.2492	0.00262	0.2493	0.000784	0.2492	0.001154	0.2493	0.000628	0.2495	0.001392
				0.3294	0.00002	0.3296	0.000024153	0.3292	0.000672	0.3297	0.000161	0.3295	0.000197	0.3292	0.000201	0.3292	0.000426

Table B-10. Vertical flux data used to test the Rouse model: Ni et al., (2002)

Run 1		Run 2		Run 3		Run 4		Run 5		Run 6		Run 7		Run 8		Run 9		Run 10	
q ($g/cm^2/s$)	z (cm)	q ($g/cm^2/s$)	z (cm)	q ($g/cm^2/s$)	z (cm)	q ($g/cm^2/s$)	z (cm)	q ($g/cm^2/s$)	z (cm)	q ($g/cm^2/s$)	z (cm)	q ($g/cm^2/s$)	z (cm)	q ($g/cm^2/s$)	z (cm)	q ($g/cm^2/s$)	z (cm)	q ($g/cm^2/s$)	z (cm)
0.00013353	9.5269	0.00085981	29.5278	0.00013244	20.4359	0.0044676	29.539	0.0006752	29.4946	0.0148	29.5025	0.0023345	29.5168	0.0391	29.47	0.0267	29.5132	0.1255	29.4897
0.0001604	8.5428	0.0011305	28.5443	0.00015555	19.4282	0.0052473	28.5313	0.00082695	28.5098	0.0162	28.4704	0.0028079	28.5095	0.0439	28.4627	0.0307	28.5279	0.1347	28.5044
0.00028283	7.5613	0.0012693	27.4894	0.00025631	18.4463	0.0058914	27.4998	0.0009571	27.5014	0.0177	27.5088	0.0030839	27.5022	0.0461	27.4553	0.0341	27.5191	0.147	27.4721
0.00040699	6.5784	0.0014251	26.4579	0.00028133	17.4381	0.0070771	26.5157	0.0012062	26.4697	0.0205	26.4769	0.003882	26.4714	0.0542	26.448	0.0399	26.4633	0.1661	26.4399
0.00065574	5.5494	0.0015998	25.4734	0.00035356	16.4543	0.0074261	25.4603	0.0015197	25.4849	0.0224	25.4683	0.0046692	25.4641	0.0637	25.4173	0.0458	25.478	0.1876	25.4545
0.0013542	4.5456	0.0017559	24.4887	0.00043444	15.4469	0.0085263	24.4994	0.0016157	24.4528	0.0252	24.4364	0.0052457	24.4802	0.0654	24.4334	0.0518	24.4457	0.1945	24.4457
0.0024426	3.5173	0.0019274	23.457	0.00053376	14.4864	0.0087452	23.5142	0.0015707	24.4293	0.024	23.4509	0.0056322	23.4495	0.0655	23.4261	0.0556	23.437	0.1982	23.437
0.005647	2.5142	0.0020219	22.4955	0.00065587	13.4791	0.0096002	22.4592	0.0016694	23.4676	0.027	22.4424	0.0067744	22.4422	0.0736	22.4656	0.0672	22.4282	0.2126	22.4751
0.016	1.5125	0.0027198	21.4183	0.00077033	12.4713	0.011	21.4278	0.0021036	22.4594	0.0321	21.4341	0.008723	21.4348	0.0809	21.4583	0.0786	21.4194	0.2402	21.3959
0.0507	0.5115	0.0026665	20.4329	0.00092537	11.4873	0.0118	20.443	0.0024347	21.4509	0.0332	20.4488	0.01	20.4275	0.0868	20.4041	0.0903	20.434	0.2577	20.434
		0.0034276	19.4492	0.0012728	10.5041	0.0139	19.4587	0.0029825	20.4192	0.0373	19.4638	0.0115	19.4436	0.0975	19.4436	0.1003	19.4252	0.2861	19.4252
		0.0031406	18.4398	0.0016736	9.4971	0.0133	18.4731	0.0034512	19.4577	0.0364	18.4549	0.0142	18.4129	0.1001	18.3895	0.1114	18.4399	0.2866	18.4399
		0.0036064	17.432	0.0021032	8.5368	0.016	17.4186	0.0039939	18.4727	0.0446	17.4466	0.0167	17.3821	0.1124	17.4524	0.1348	17.4311	0.3237	17.4311
		0.0049605	16.4488	0.0032388	7.531	0.0168	16.4571	0.0048921	17.4645	0.0474	16.438	0.0187	16.3982	0.118	16.4217	0.1496	16.4457	0.3356	16.4457
		0.0045452	15.4394	0.0043555	6.5476	0.0184	15.4489	0.0058241	16.4796	0.0519	15.4529	0.0236	15.4378	0.1267	15.4612	0.172	15.437	0.3663	15.437
		0.0052186	14.4785	0.0064111	5.5415	0.0202	14.5111	0.0067408	15.4711	0.0567	14.4912	0.0303	14.4773	0.1423	14.4773	0.2117	14.4751	0.3998	14.4516
		0.005728	13.4703	0.0106	4.5126	0.0207	13.526	0.008494	14.4629	0.0554	13.4589	0.0326	13.47	0.146	13.4231	0.2271	13.4428	0.4144	13.4428
		0.0067272	12.4861	0.017	3.507	0.0255	12.4951	0.0101	13.478	0.0698	12.4976	0.041	12.5095	0.1756	12.4861	0.2893	12.4809	0.4763	12.4809
		0.0073834	11.5014	0.0352	2.5032	0.0273	11.5103	0.0127	12.4933	0.0742	11.489	0.0505	11.5256	0.1801	11.4788	0.3213	11.4721	0.5109	11.4956
		0.0081042	10.4932	0.0889	1.5241	0.0293	10.5019	0.0161	11.5085	0.0834	10.5274	0.0621	10.4949	0.2024	10.4714	0.3692	10.4633	0.5388	10.5103
		0.0090972	9.5321	0.117	0.4937	0.0329	9.5408	0.0186	10.5001	0.0887	9.5657	0.0747	9.511	0.2173	9.4876	0.4171	9.5015	0.5781	9.5015
		0.0099852	8.5239			0.037	8.5328	0.0234	9.5154	0.0998	8.5103	0.0919	8.5505	0.2441	8.5037	0.4712	8.4927	0.642	8.4692
		0.0117	7.5397			0.0444	7.5253	0.0287	8.554	0.1222	7.5254	0.1266	7.5198	0.287	7.4729	0.6106	7.5308	0.7767	7.5308
		0.0129	6.5081			0.0488	6.5406	0.0441	7.5228	0.1336	6.5638	0.1706	6.5124	0.3081	6.5124	0.7139	6.522	0.8191	6.5455
		0.0132	6.5317			0.0547	5.556	0.0587	6.5617	0.142	5.5317	0.21	5.4817	0.3541	5.4817	0.8491	5.5132	0.8941	5.4897
		0.0145	5.547			0.0658	4.525	0.0762	5.5066	0.174	4.5234	0.2961	4.451	0.3979	4.451	0.9928	4.5044	1.0453	4.5044
		0.0178	4.5161			0.0706	3.4932	0.1238	4.4991	0.185	3.4913	0.3482	3.4436	0.4471	3.4436	1.0651	3.4956	1.0471	3.4487
		0.0186	3.4842			0.0867	2.5093	0.1651	3.5145	0.186	3.49	0.4691	2.4597	0.5626	2.5066	1.2667	2.5572	1.2669	2.4868
		0.0234	2.5004			0.1248	1.5264	0.2611	2.4599	0.261	2.5068	0.6321	1.4758	0.7581	1.4993	1.7588	1.5015	1.7588	1.5015
		0.0301	1.5168			0.1837	0.4968	0.5032	1.4997	0.3684	1.5224	0.814	0.4685	0.9987	0.4685	2.2027	0.4692	2.241	0.4457
		0.0424	0.4634					0.5991	0.4914	0.4775	0.5142								

Table B-11. Vertical flux data used to test the Rouse model: Rasmussen & Mikkelsen (1998)

Run 1		Run 2		Run 3	
q ($g/cm^2/s$)	z (cm)	q ($g/cm^2/s$)	z (cm)	q ($g/cm^2/s$)	z (cm)
0.00012578	7.9937	0.0012328	6.9924	0.005112	7.9803
0.00025613	7.0146	0.0042549	4.9851	0.0104	5.9916
0.00049818	4.9928	0.0128	2.4653	0.0156	4.9805
0.00091494	3.981	0.0495	1.1529	0.0207	3.9863
0.001533	2.7709	0.1313	0.2556	0.0513	2.9734
0.0020657	1.7767	0.1423	0.0567	0.0609	2.4763
0.004111	0.6653			0.092	1.4651
0.0083712	0.0668			0.2251	0.4357
				0.3325	0.0371

Table B-12. Vertical flux data used to test the Rouse model: Sorensen (1985)

Run 1		Run 2	
q ($g/cm^2/s$)	z (cm)	q ($g/cm^2/s$)	z (cm)
0.00028976	10.385	0.0023907	10.3546
0.00019302	9.4429	0.0036461	9.4305
0.0003913	8.5439	0.0049471	8.5609
0.00089111	7.6665	0.0063766	7.6331
0.00098306	6.7734	0.0083235	6.7436
0.0022985	5.8395	0.0148	5.8038
0.0035045	4.9534	0.0217	4.9359
0.0064065	4.0332	0.0363	4.0137
0.0064544	3.1572	0.0941	3.1392
0.012	2.2563	0.1473	2.2346
0.0148	1.3085	0.3145	1.2987
0.0229	0.4227	0.5319	0.4149

Table B-13. Vertical flux data used to test the Rouse model: Williams (1964)

Run 1		Run 2		Run 3		Run 4		Run 5		Run 6	
q ($g/cm^2/s$)	z (cm)	q ($g/cm^2/s$)	z (cm)	q ($g/cm^2/s$)	z (cm)	q ($g/cm^2/s$)	z (cm)	q ($g/cm^2/s$)	z (cm)	q ($g/cm^2/s$)	z (cm)
0.00006	15.504	0.0001569	15.5457	0.0001863	15.4957	0.0004094	15.5589	0.0007034	15.525	0.0014405	15.5276
0.0005271	9.5088	0.0010359	9.5383	0.0012419	9.5175	0.0026087	9.5212	0.0048242	9.5193	0.0086966	9.5163
0.0021472	5.4912	0.0033352	5.5679	0.0046136	5.5246	0.0075632	5.5749	0.017	5.5527	0.028	5.5459
0.0064921	2.5233	0.0081902	2.5047	0.0157	2.5045	0.0208	2.5168	0.0523	2.5283	0.0682	2.5685
0.014	0.5173	0.017	0.497	0.0365	0.5018	0.0419	0.5365	0.0997	0.5744	0.1077	0.5777

Table B-14. Vertical flux data used to test the Rouse model: Zou et al., (2001)

Run 1		Run 2		Run 3		Run 4	
q ($g/cm^2/min$)	z (cm)	q ($g/cm^2/min$)	z (cm)	q ($g/cm^2/min$)	z (cm)	q ($g/cm^2/min$)	z (cm)
0.0422	1.0341	0.0029563	0.9856	0.2003	19.0422	0.0684	19.0729
0.0334	3.0231	0.001778	3.0369	0.3005	17.0438	0.0727	17.1047
0.0245	4.9835	0.001413	4.9414	0.4128	15.0741	0.0767	15.0496
0.0189	6.9913	0.00095343	6.9905	0.6689	13.0447	0.0689	13.0526
0.013	8.9712	0.00087639	8.9518	0.9611	11.0437	0.073	11.0265
0.0083709	11.0044	0.00032105	11.0011	1.4811	9.0107	0.1132	9.0289
0.0066648	12.9709	0.00038803	12.9908	2.3854	7.0306	0.1773	7.002
0.0041929	15.0264	0.00031155	15.0098	4.1294	4.9814	0.3254	4.974
0.0033971	16.9899	0.00023451	16.9711	7.3017	3.0000	0.6055	2.9442
0.002027	19.013	0.0001583	19.019	12.238	1.0243	0.9817	0.9421

APPENDIX C

APPENDIX

The results of the Rouse analysis for each experiment are provided here. Each experiment has:

1. Rouse profiles using $\beta = 1$, Adjusted β and Modeled β.
2. Comparison of aeolian vertical mass flux profiles and re-constructed vertical flux profiles using the Rouse model.
3. Table and bar graphs showing the performance of each β value in predicting the observed transport rate.

Butterfield (1999)

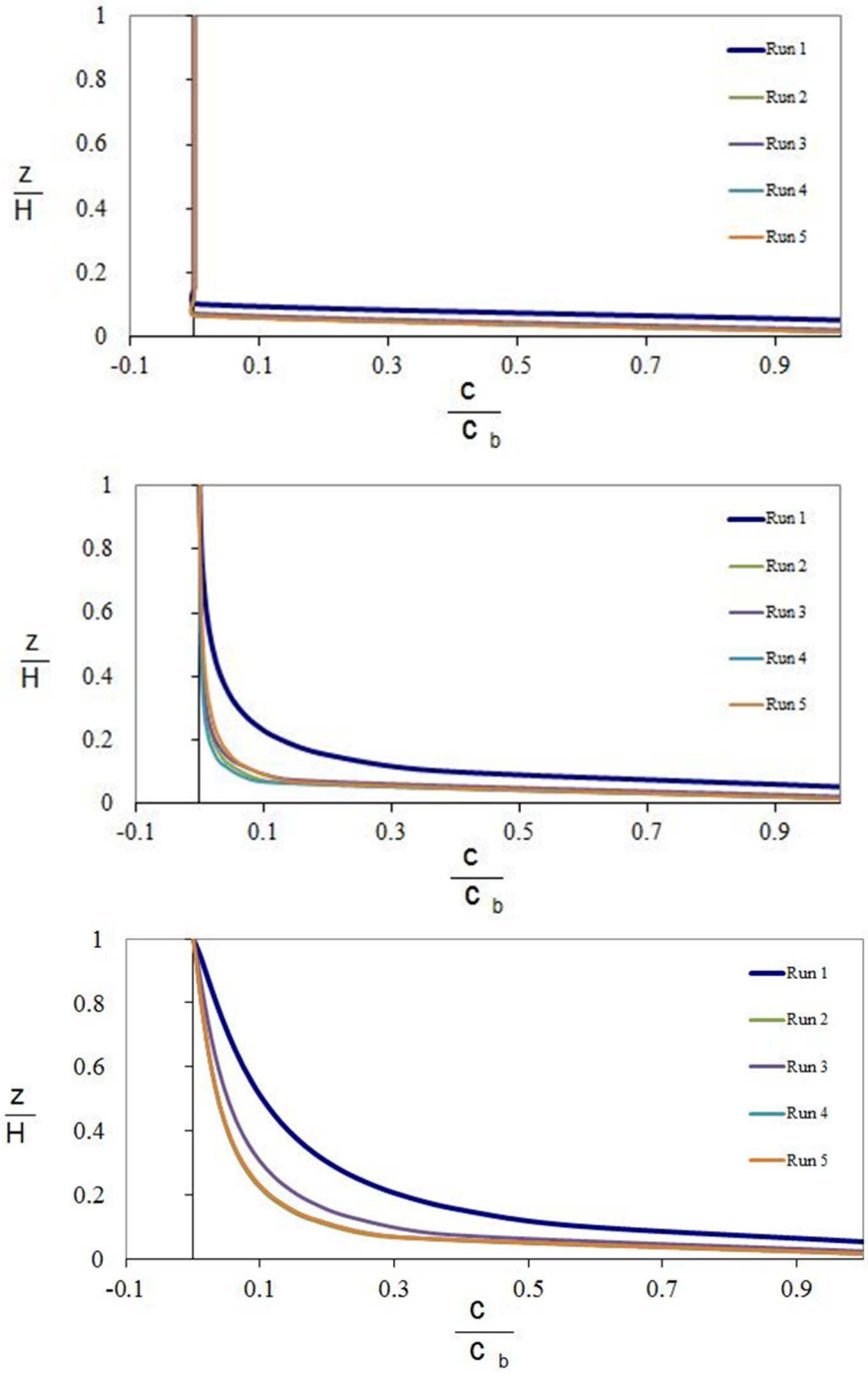

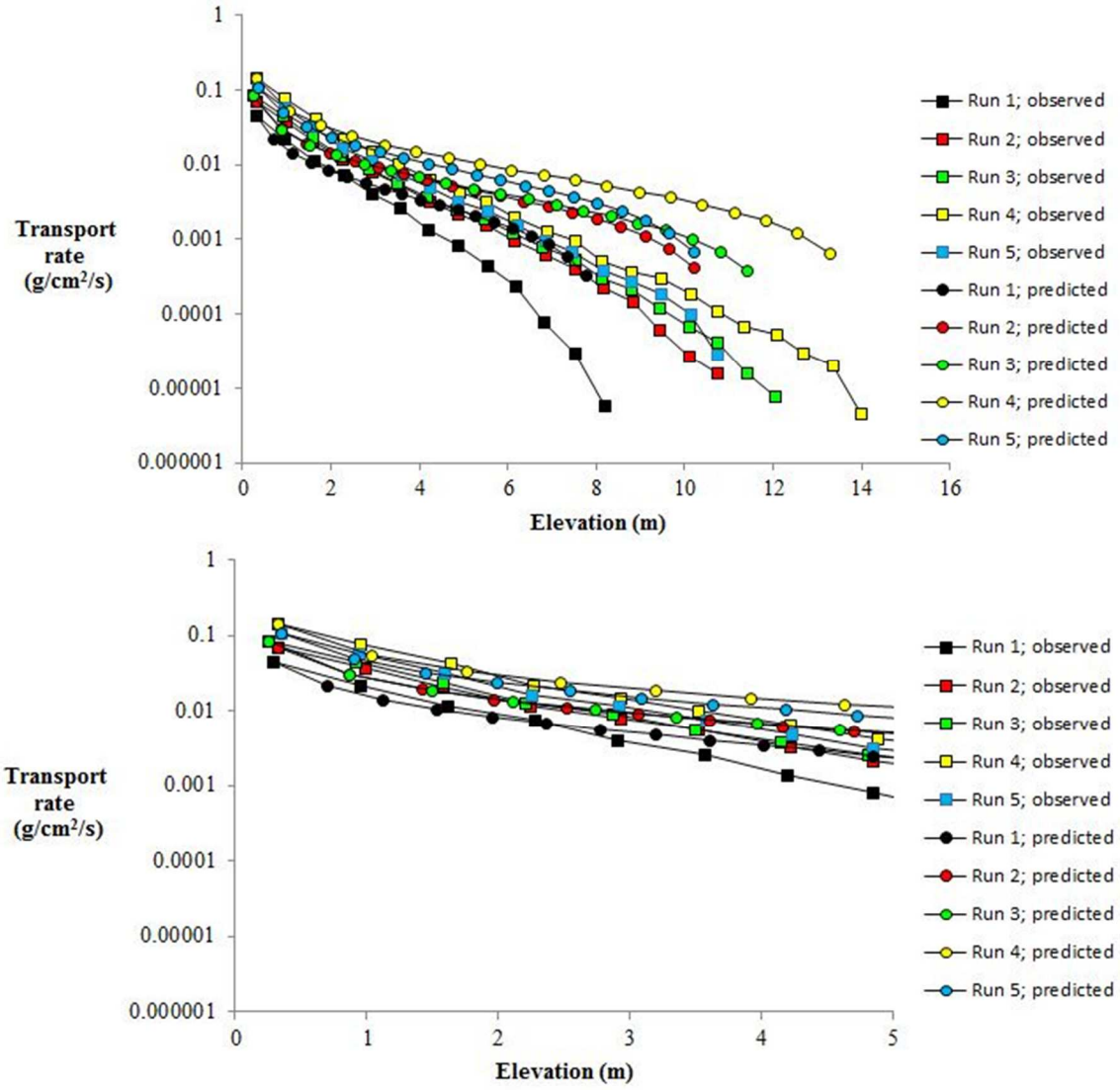

	Run 1	Run 2	Run 3	Run 4	Run 5	
Observed transport rate ($g/cm^2/s$)	0.097355	0.16369	0.19423777	0.33395	0.25029	
Predicted transport rate ($Q_{pre.}/Q_{obs.}$)						*Average*
β= 1	0.48	0.43	0.44	0.44	0.44	***0.45***
β adjusted	0.96	0.54	0.62	0.53	0.60	***0.65***
β modeled	1.74	0.93	1.13	0.96	0.96	***1.14***

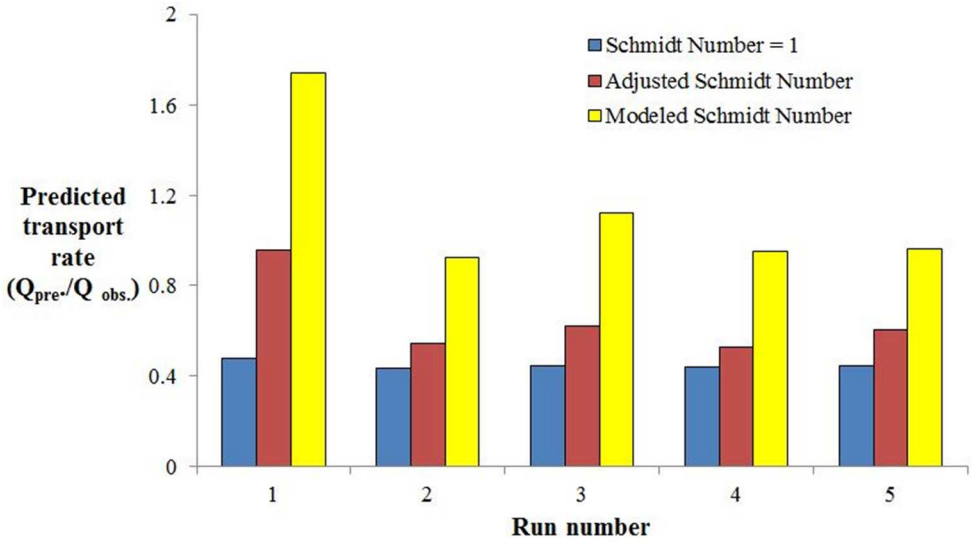
Schmidt Number = 1
Adjusted Schmidt Number
Modeled Schmidt Number
Predicted transport rate ($Q_{pre.}/Q_{obs.}$)
2
1.6
1.2
0.8
0.4
0
1
2
3
4
5
Run number

Dong et al. (2004)

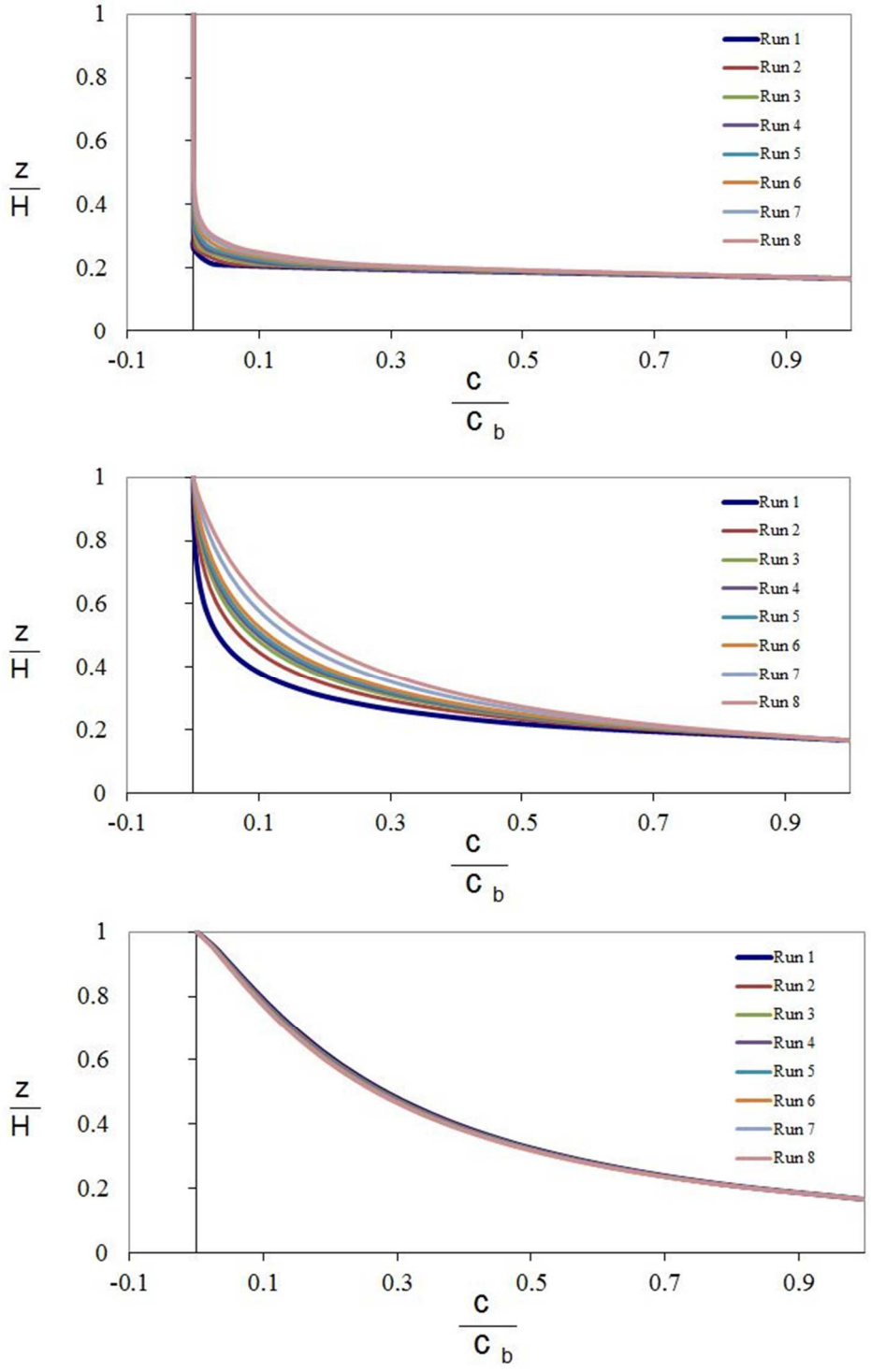

	Run 1	Run 2	Run 3	Run 4	Run 5	Run 6	Run 7	Run 8	
Observed transport rate ($g/cm^2/s$)	0.04011	0.09318	0.19008	0.35027	0.57773	0.75975	0.99428	1.32618	
Predicted transport rate ($Q_{pre.}/Q_{obs.}$)									***Average***
β= 1	0.19	0.16	0.16	0.16	0.16	0.16	0.15	0.15	***0.16***
β adjusted	0.47	0.46	0.45	0.45	0.45	0.45	0.45	0.45	***0.46***
β modeled	1.10	0.91	0.83	0.79	0.77	0.73	0.66	0.60	***0.80***

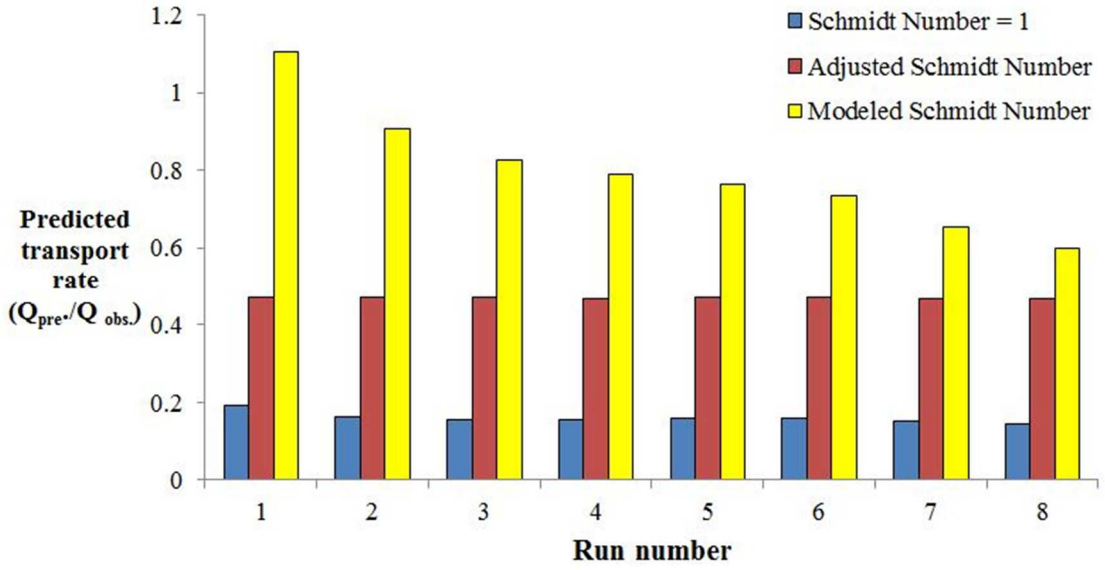

Namikas (2003)

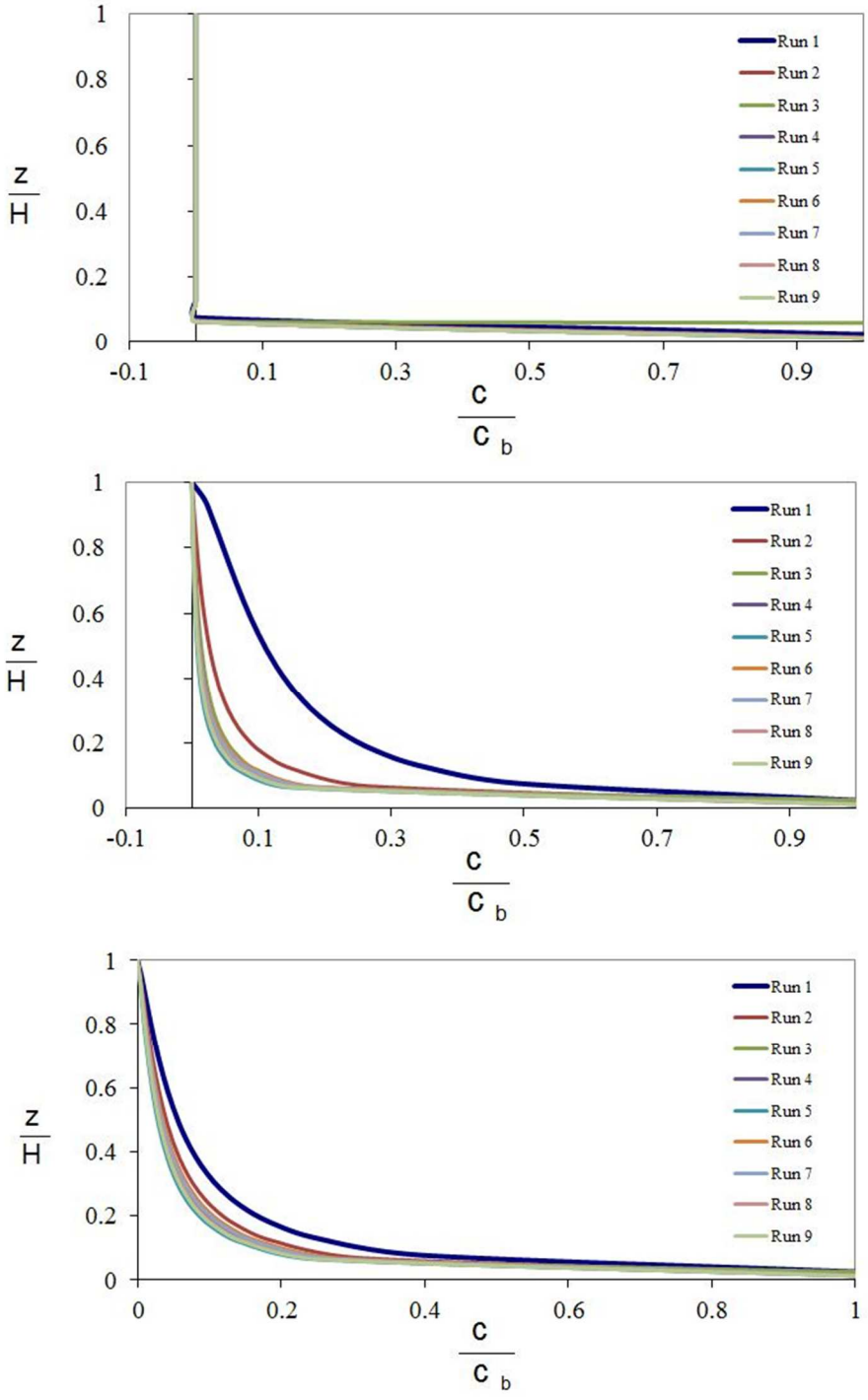

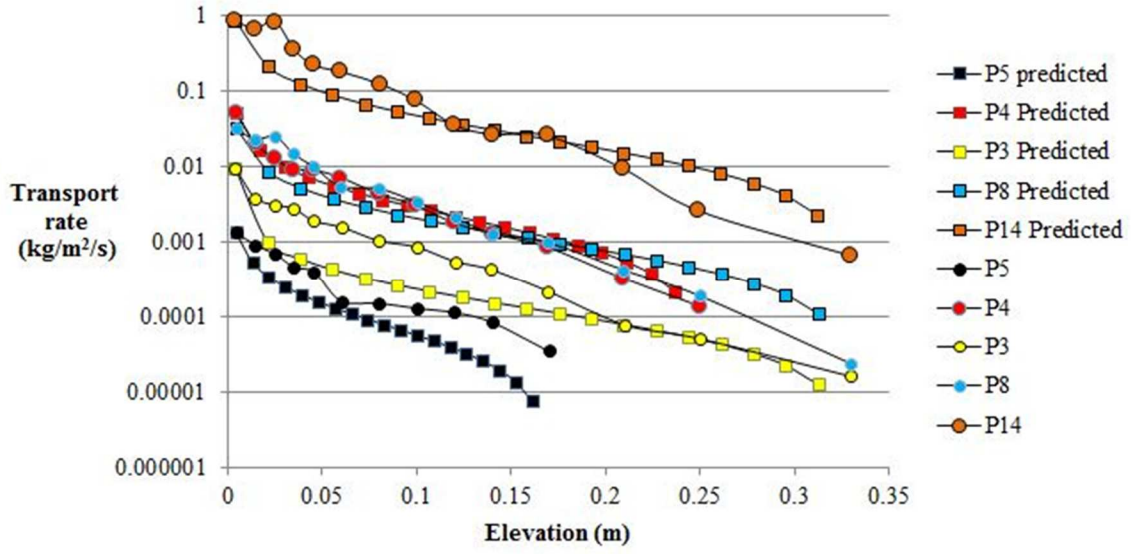
Transport rate (kg/m²/s)
1
0.1
0.01
0.001
0.0001
0.00001
0.000001
0
0.05
0.1
0.15
0.2
0.25
0.3
0.35
Elevation (m)
P5 predicted
P4 Predicted
P3 Predicted
P8 Predicted
P14 Predicted
P5
P4
P3
P8
P14

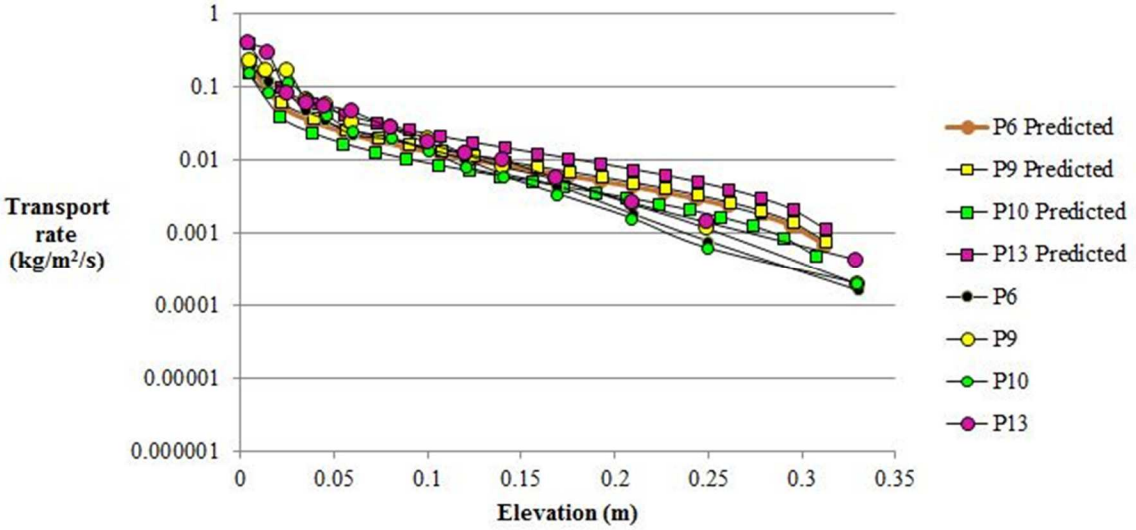
Transport rate (kg/m²/s)
1
0.1
0.01
0.001
0.0001
0.00001
0.000001
0
0.05
0.1
0.15
0.2
0.25
0.3
0.35
Elevation (m)
P6 Predicted
P9 Predicted
P10 Predicted
P13 Predicted
P6
P9
P10
P13

	Run 1	Run 2	Run 3	Run 4	Run 5	Run 6	Run 7	Run 8	Run 9	
Observed transport rate ($g/cm^2/s$)	0.0045	0.1237	0.0262	0.1266	3.4761	0.5687	0.7943	0.5499	1.0188	
Predicted transport rate ($Q_{pre.}/Q_{obs.}$)										***Average***
β= 1	0.64	0.43	0.36	0.26	0.25	0.34	0.29	0.28	0.39	**0.36**
β adjusted	1.08	0.82	0.45	0.40	0.35	0.52	0.43	0.41	0.55	**0.56**
β modeled	0.79	0.95	0.51	0.53	0.48	0.71	0.59	0.56	0.76	**0.65**

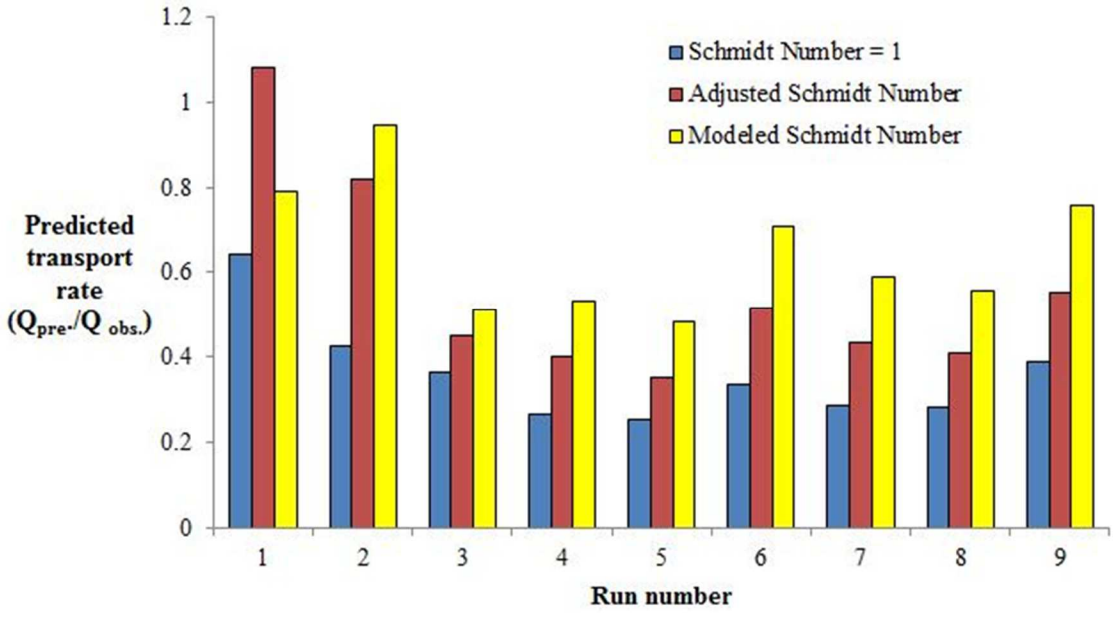

Greeley et al. (1996)

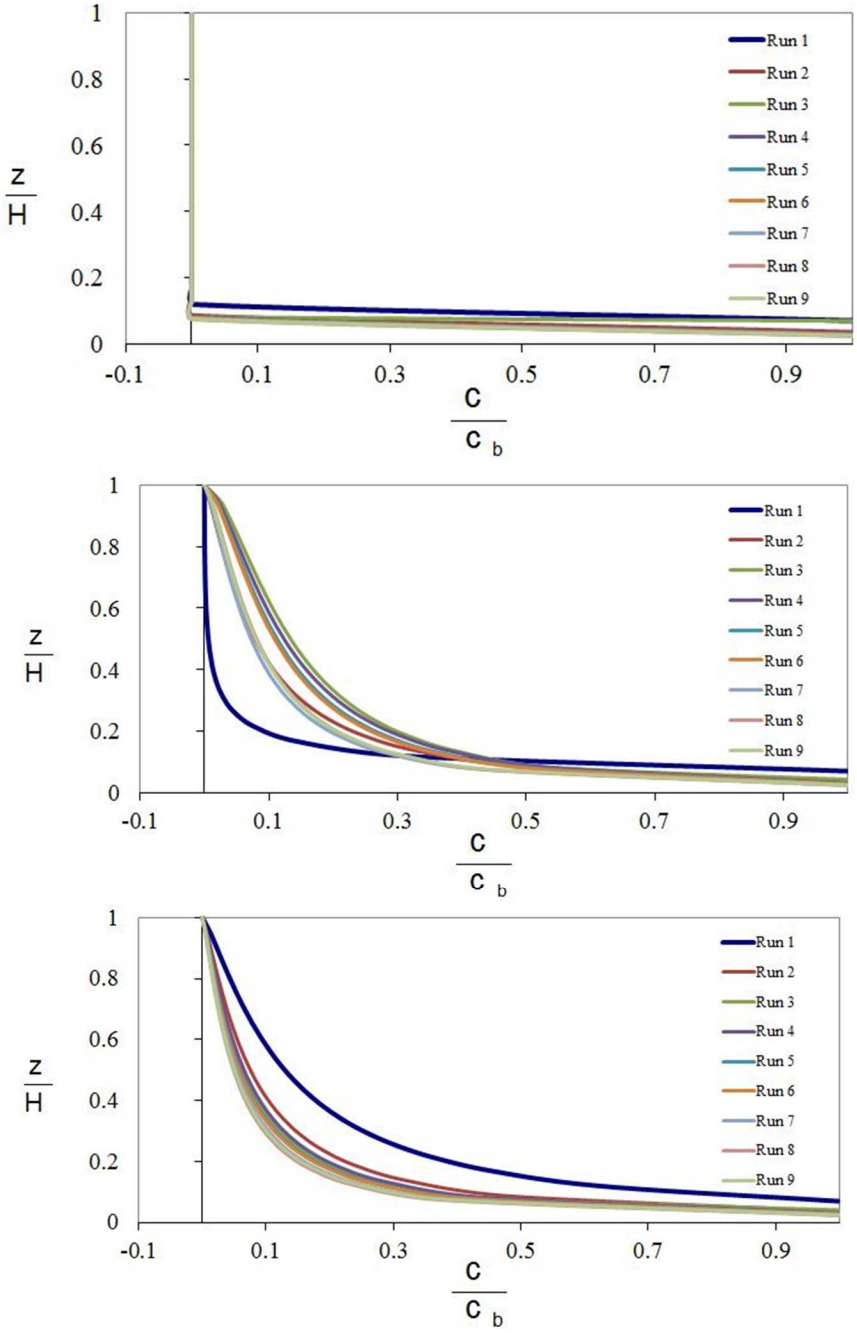

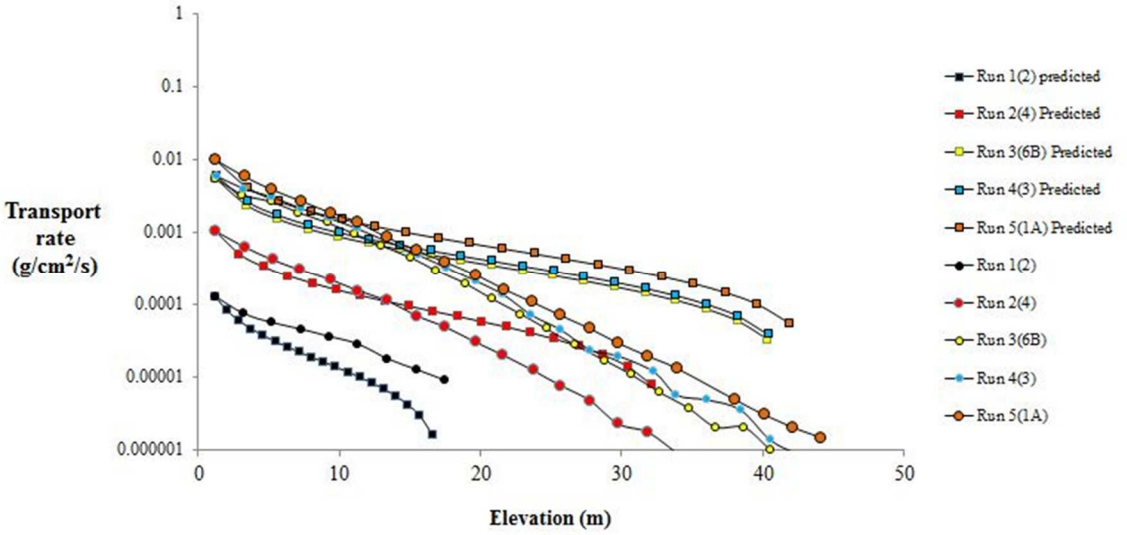
Transport rate (g/cm²/s)
1
0.1
0.01
0.001
0.0001
0.00001
0.000001
0
10
20
30
40
50
Elevation (m)
Run 1(2) predicted
Run 2(4) Predicted
Run 3(6B) Predicted
Run 4(3) Predicted
Run 5(1A) Predicted
Run 1(2)
Run 2(4)
Run 3(6B)
Run 4(3)
Run 5(1A)

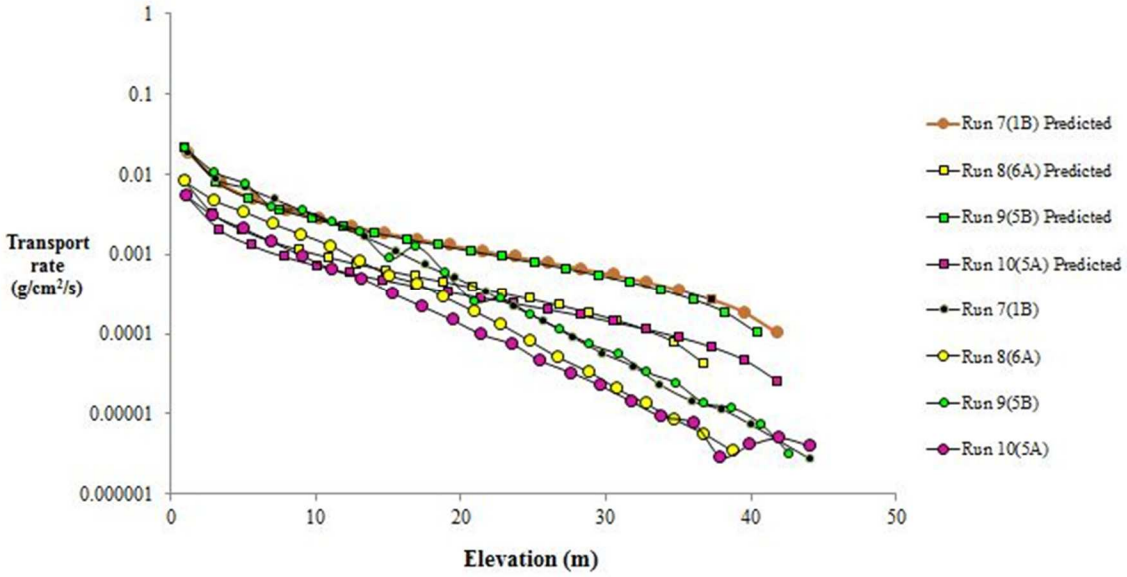
Transport rate (g/cm²/s)
1
0.1
0.01
0.001
0.0001
0.00001
0.000001
0
10
20
30
40
50
Elevation (m)
Run 7(1B) Predicted
Run 8(6A) Predicted
Run 9(5B) Predicted
Run 10(5A) Predicted
Run 7(1B)
Run 8(6A)
Run 9(5B)
Run 10(5A)

	Run 1	Run 2	Run 3	Run 4	Run 5	Run 6	Run 7	Run 8	Run 9	
Observed transport rate ($g/cm^2/s$)	0.0004	0.0031	0.0174	0.0191	0.0279	0.0438	0.0243	0.0554	0.0151	
Predicted transport rate ($Q_{pre.}/Q_{obs.}$)										*Average*
β= 1	0.31	0.34	0.31	0.31	0.35	0.43	0.33	0.39	0.36	**0.35**
β adjusted	0.52	1.06	1.26	1.21	1.30	1.54	0.98	1.20	1.09	**1.13**
β modeled	1.29	1.04	0.87	0.89	0.95	1.14	0.86	0.96	0.90	**0.99**

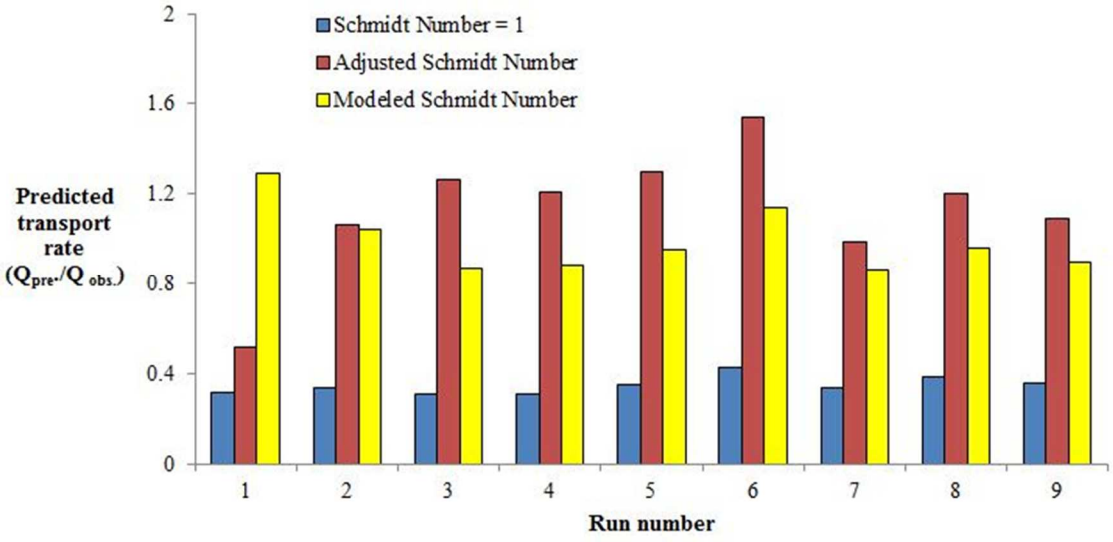

Hotta & Horikawa (1991)

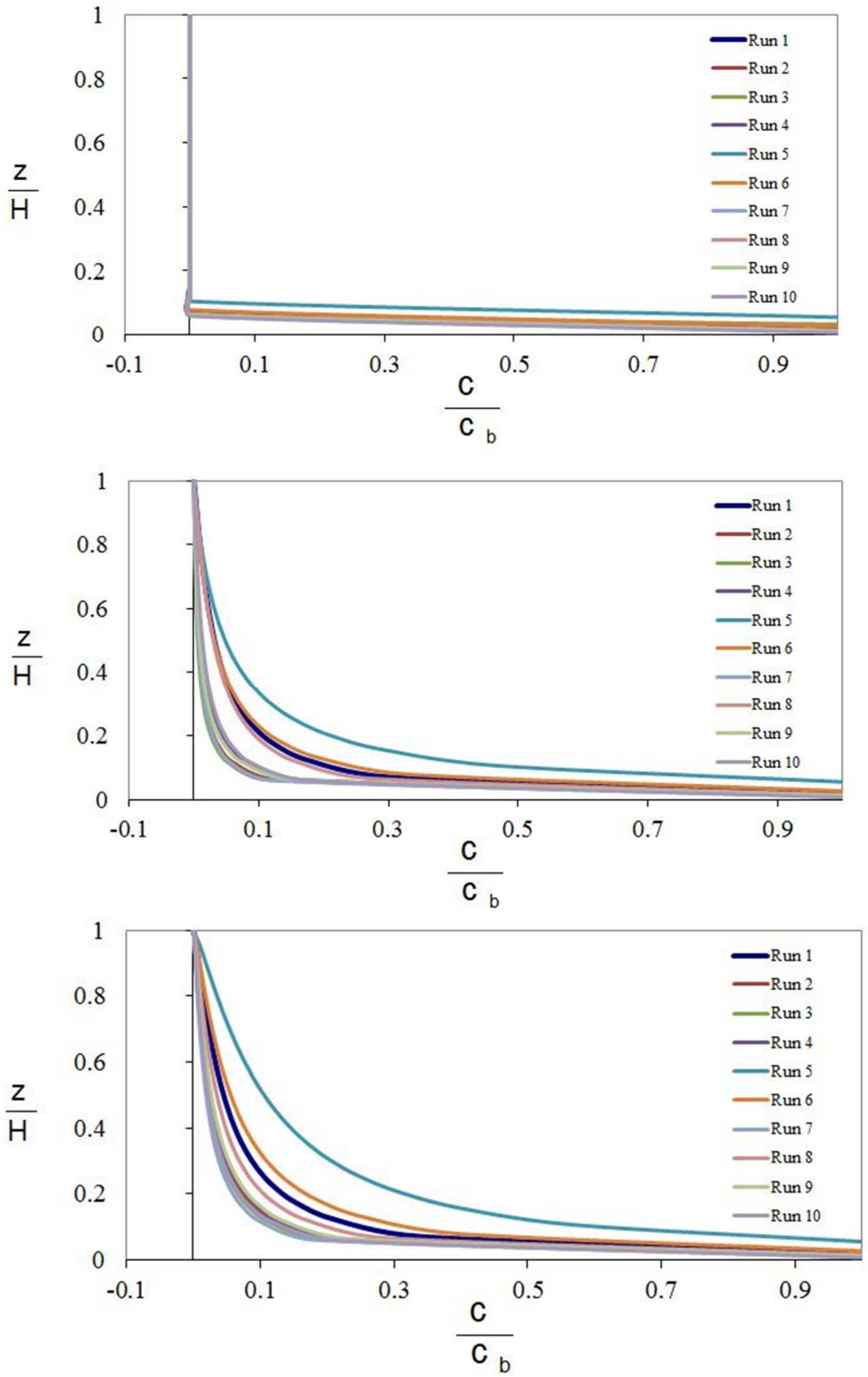

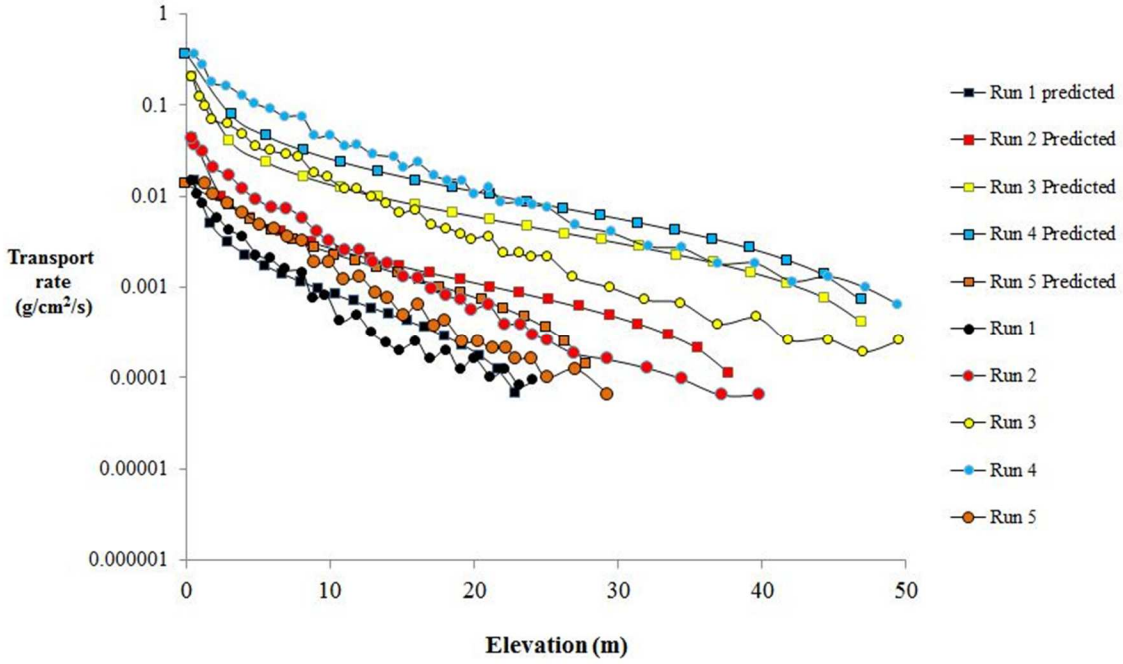

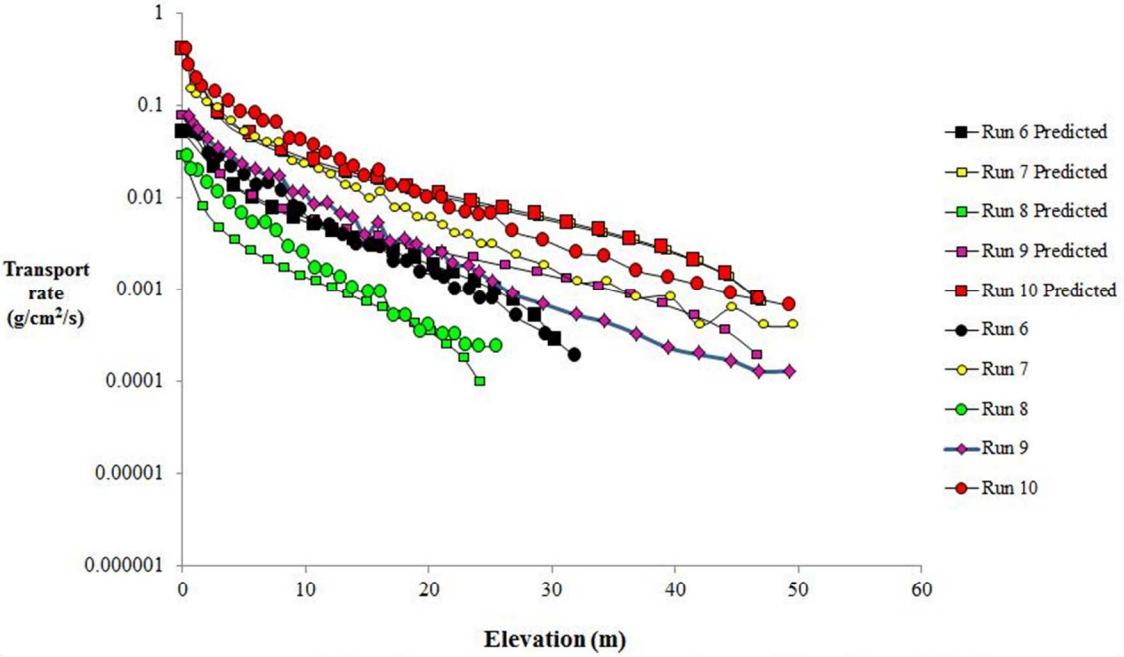

	Run 1	Run 2	Run 3	Run 4	Run 5	Run 6	Run 7	Run 8	Run 9	Run 10	
Observed transport rate ($g/cm^2/s$)	0.0590	0.2150	0.8488	1.8377	0.0664	0.2873	1.3255	0.1395	0.4693	1.9072	
Predicted transport rate ($Q_{pre.}/Q_{obs.}$)											***Average***
β= 1	0.25	0.21	0.24	0.20	0.20	0.18	0.32	0.20	0.16	0.21	***0.22***
β adjusted	0.52	0.28	0.31	0.30	0.54	0.39	0.42	0.39	0.23	0.32	***0.37***
β modeled	0.59	0.38	0.41	0.35	0.75	0.48	0.52	0.41	0.30	0.36	***0.45***

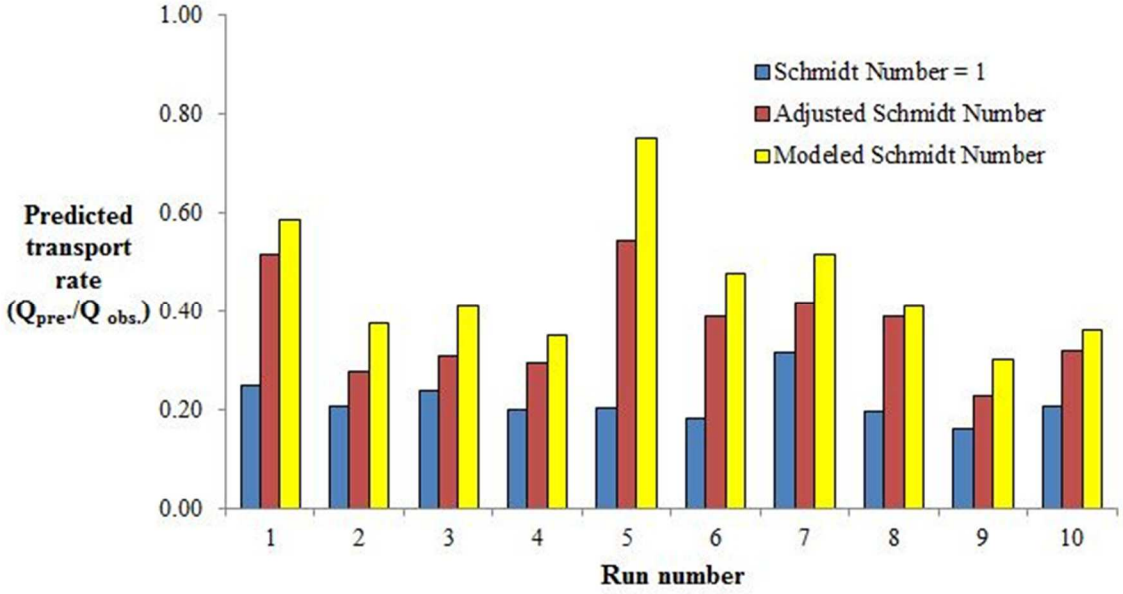
1.00
0.80
0.60
0.40
0.20
0.00
Predicted transport rate ($Q_{pre.}/Q_{obs.}$)
Schmidt Number = 1
Adjusted Schmidt Number
Modeled Schmidt Number
1
2
3
4
5
6
7
8
9
10
Run number

Hotta et al. (2006)

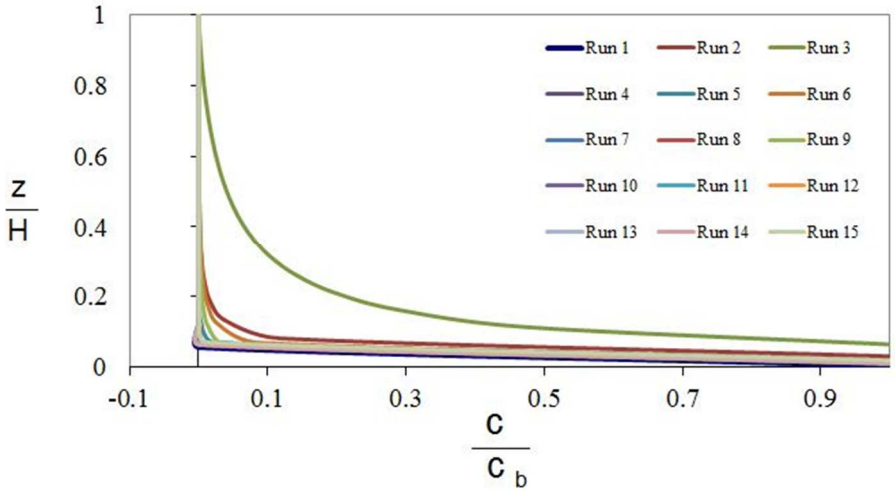

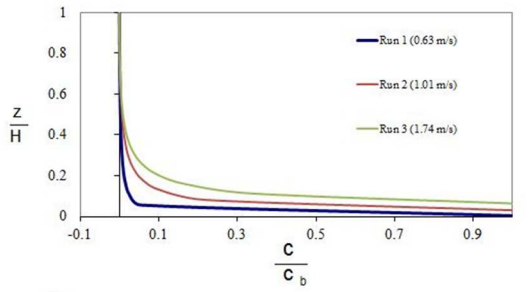

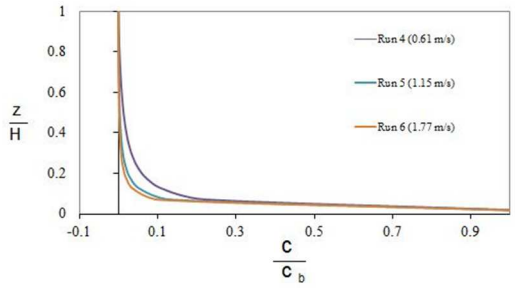

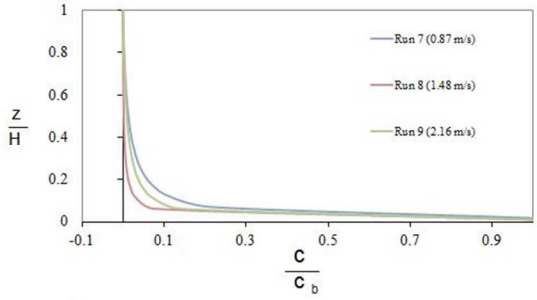

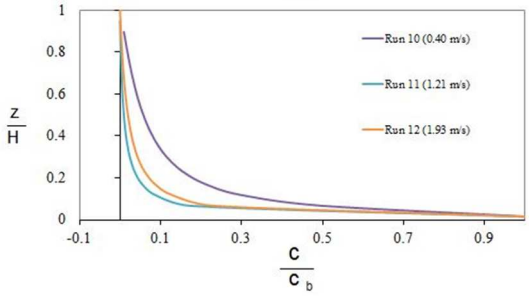

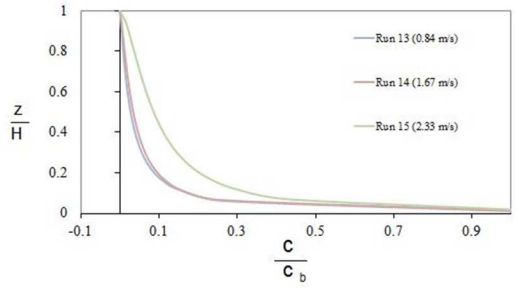

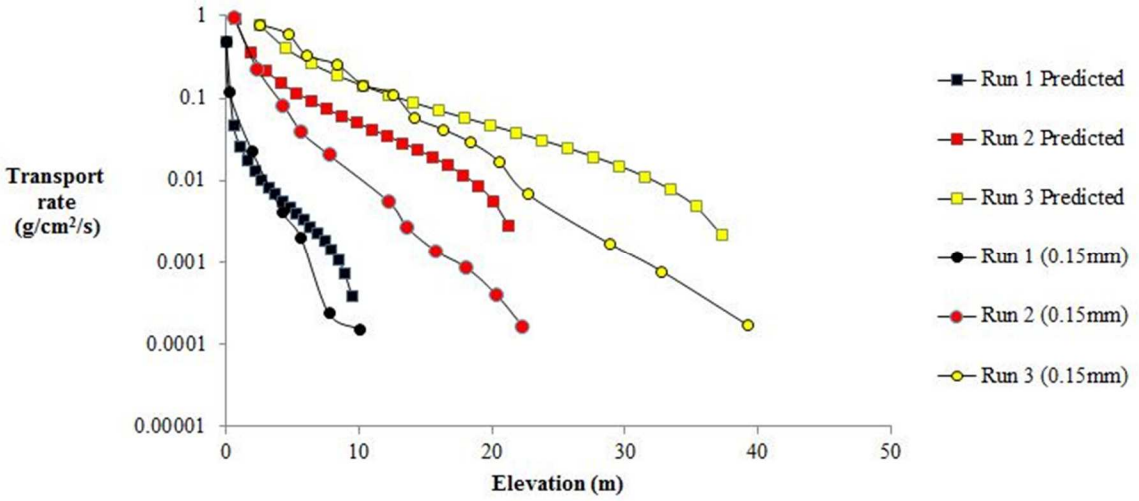
Transport rate (g/cm²/s)
1
0.1
0.01
0.001
0.0001
0.00001
0
10
20
30
40
50
Elevation (m)
Run 1 Predicted
Run 2 Predicted
Run 3 Predicted
Run 1 (0.15mm)
Run 2 (0.15mm)
Run 3 (0.15mm)

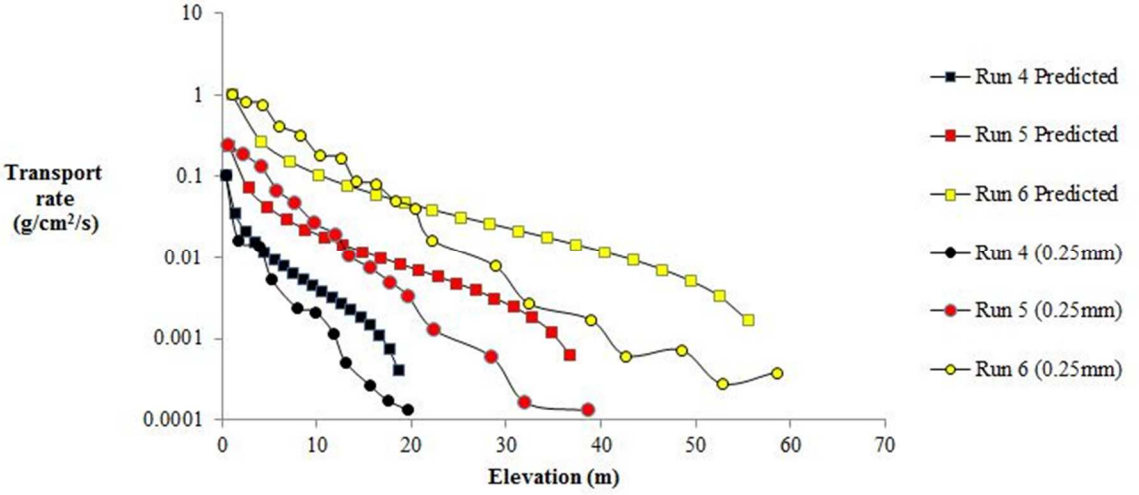
Transport rate (g/cm²/s)
10
1
0.1
0.01
0.001
0.0001
0
10
20
30
40
50
60
70
Elevation (m)
Run 4 Predicted
Run 5 Predicted
Run 6 Predicted
Run 4 (0.25mm)
Run 5 (0.25mm)
Run 6 (0.25mm)

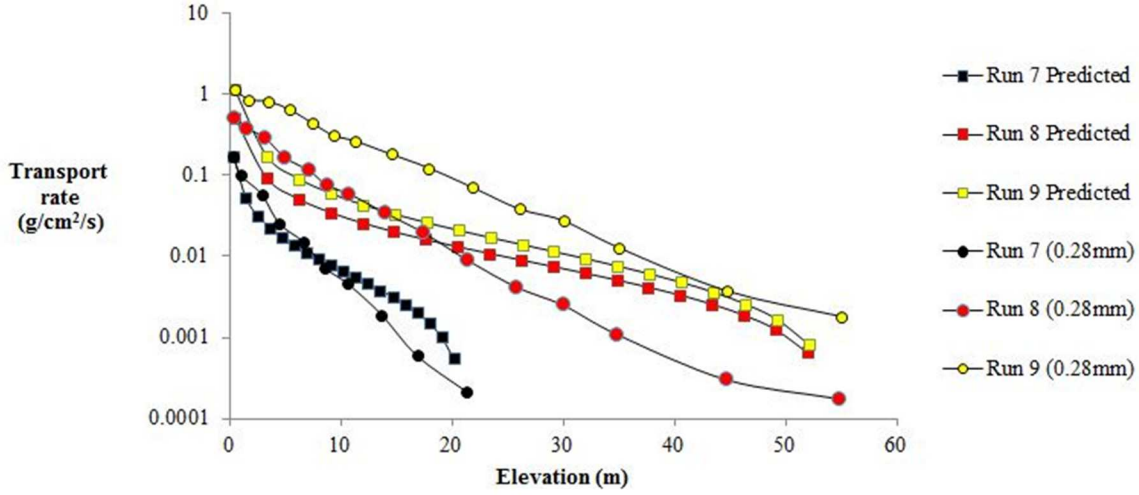
Transport rate (g/cm²/s)
10
1
0.1
0.01
0.001
0.0001
0
10
20
30
40
50
60
Elevation (m)
Run 7 Predicted
Run 8 Predicted
Run 9 Predicted
Run 7 (0.28mm)
Run 8 (0.28mm)
Run 9 (0.28mm)

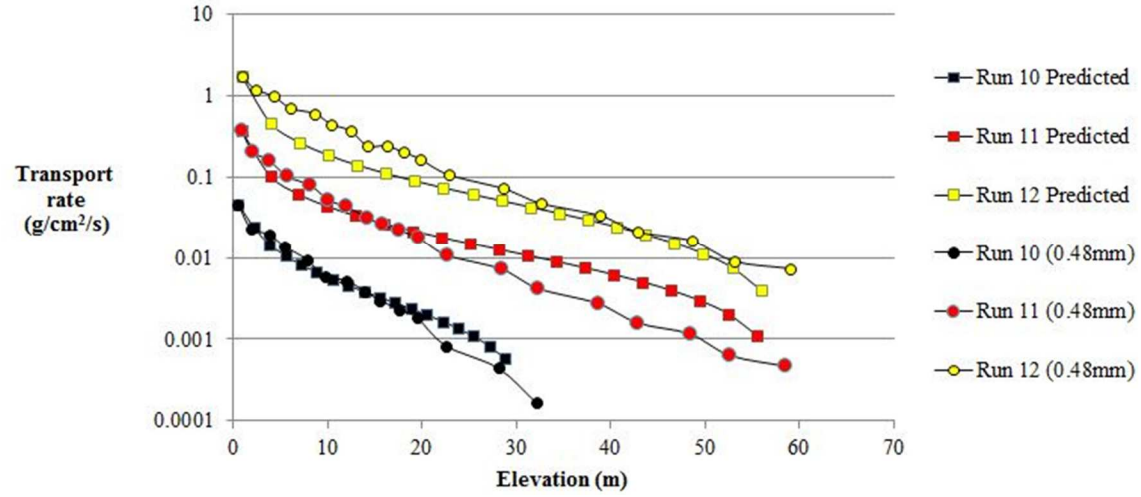
Transport rate (g/cm²/s)
10
1
0.1
0.01
0.001
0.0001
0
10
20
30
40
50
60
70
Elevation (m)
Run 10 Predicted
Run 11 Predicted
Run 12 Predicted
Run 10 (0.48mm)
Run 11 (0.48mm)
Run 12 (0.48mm)

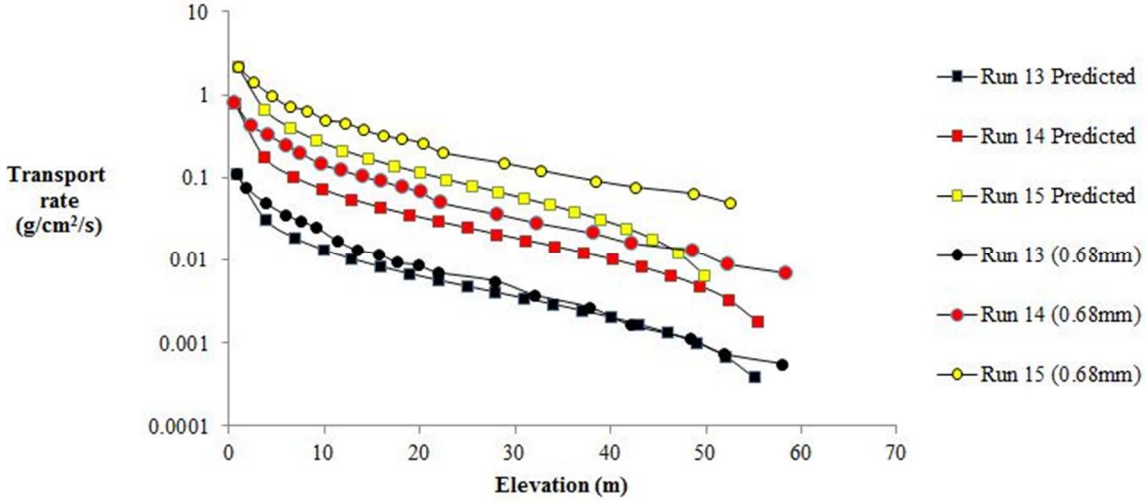
Transport rate (g/cm²/s)
10
1
0.1
0.01
0.001
0.0001
0
10
20
30
40
50
60
70
Elevation (m)
Run 13 Predicted
Run 14 Predicted
Run 15 Predicted
Run 13 (0.68mm)
Run 14 (0.68mm)
Run 15 (0.68mm)

	Run 1	Run 2	Run 3	Run 4	Run 5	Run 6	Run 7	Run 8
Observed transport rate ($g/cm^2/s$)	0.650	1.297	2.402	0.150	0.753	4.040	0.387	1.659
Predicted transport rate ($Q_{pre.}/Q_{obs.}$)								
β= 1	0.77	0.85	0.84	0.72	0.34	0.29	0.45	0.31
β adjusted	0.87	1.07	0.58	1.16	0.42	0.30	0.72	0.36
β modeled	1.01	1.74	0.97	1.64	0.68	0.48	0.96	0.49

	Run 9	Run 10	Run 11	Run 12	Run 13	Run 14	Run 15	
Observed transport rate ($g/cm^2/s$)	4.942	0.137	1.149	7.259	0.411	2.771	8.951	
Predicted transport rate ($Q_{pre.}/Q_{obs.}$)								***Average***
β= 1	0.77	0.85	0.84	0.72	0.34	0.29	0.45	***0.43***
β adjusted	0.87	1.07	0.58	1.16	0.42	0.30	0.72	***0.64***
β modeled	1.01	1.74	0.97	1.64	0.68	0.48	0.96	***0.80***

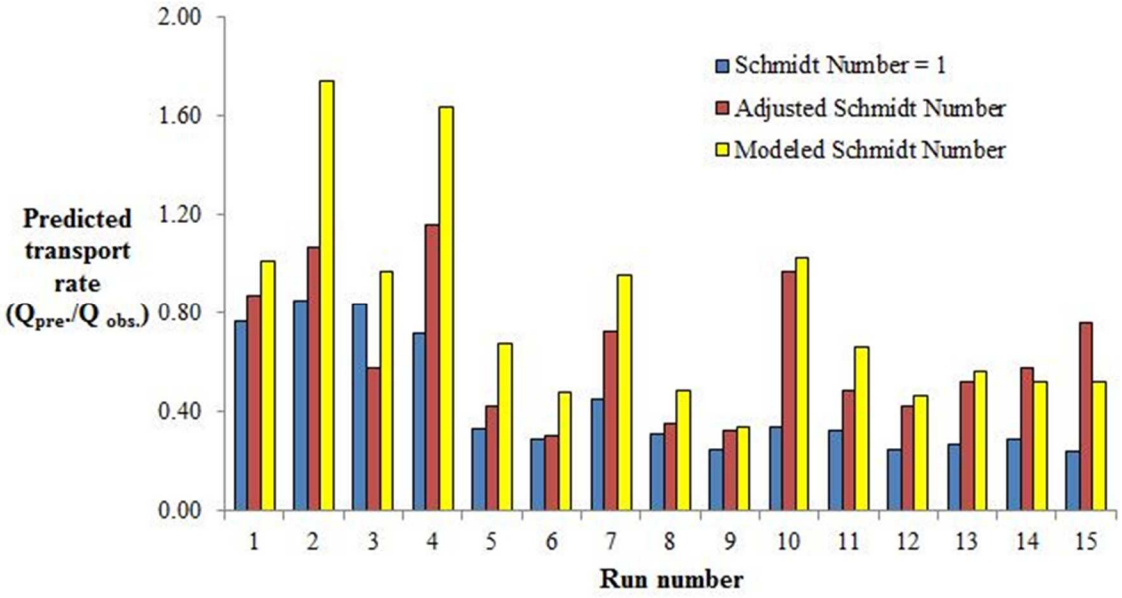

Ni et al. (2002)

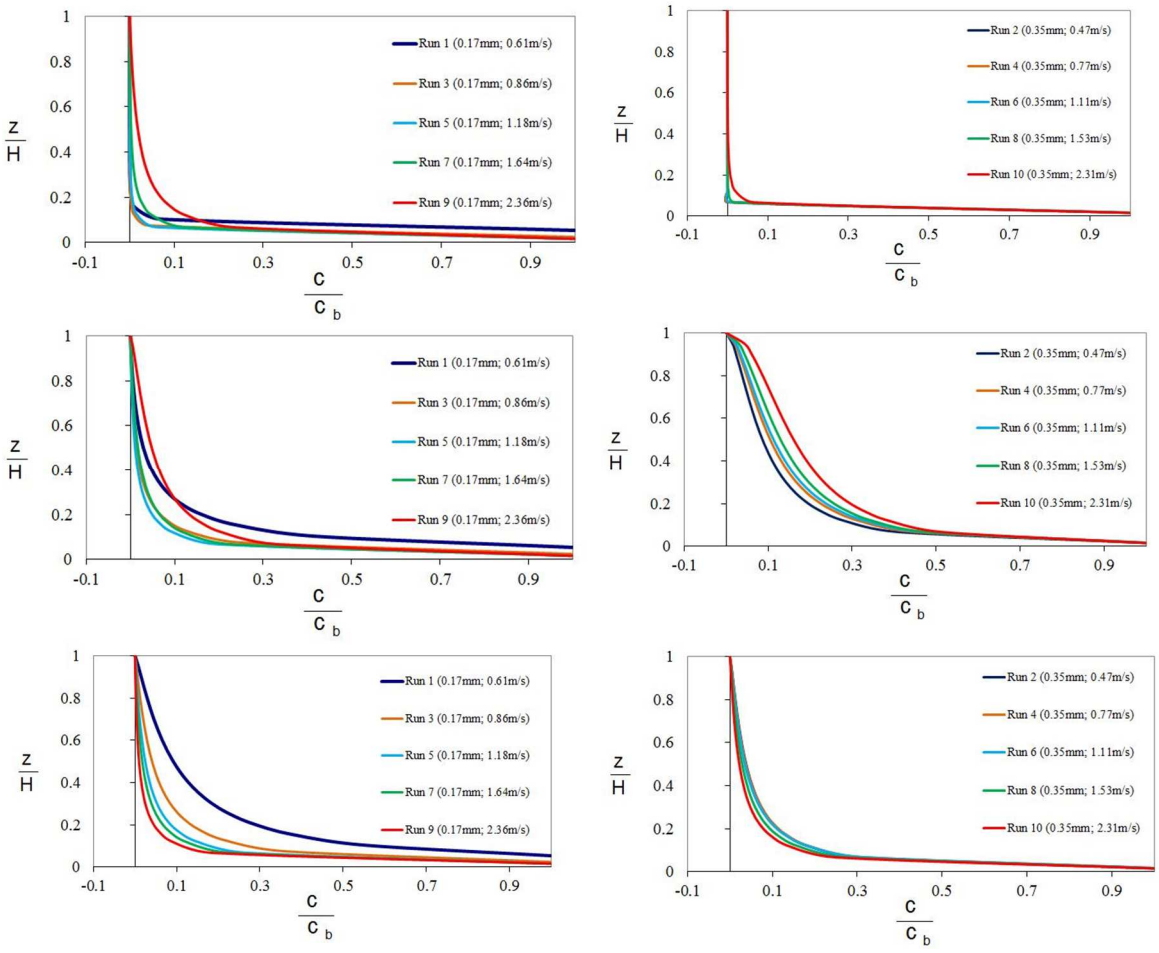
z/H
c/c b
Run 1 (0.17mm; 0.61m/s)
Run 3 (0.17mm; 0.86m/s)
Run 5 (0.17mm; 1.18m/s)
Run 7 (0.17mm; 1.64m/s)
Run 9 (0.17mm; 2.36m/s)
Run 2 (0.35mm; 0.47m/s)
Run 4 (0.35mm; 0.77m/s)
Run 6 (0.35mm; 1.11m/s)
Run 8 (0.35mm; 1.53m/s)
Run 10 (0.35mm; 2.31m/s)

	Run 1	Run 2	Run 3	Run 4	Run 5
Observed transport rate ($g/cm^2/s$)	0.07778	0.2739	0.29225	1.03058	1.99186
Predicted transport rate ($Q_{pre.}/Q_{obs.}$)					
β= 1	0.71	0.15	0.42	0.18	0.33
β adjusted	1.48	0.48	0.67	0.62	0.46
β modeled	2.25	0.34	0.93	0.39	0.57

	Run 6	Run 7	Run 8	Run 9	Run 10	
Observed transport rate ($g/cm^2/s$)	3.0284	3.58765	6.5953	12.9554	16.8717	
Predicted transport rate ($Q_{pre.}/Q_{obs.}$)						***Average***
β= 1	0.16	0.29	0.15	0.29	0.15	***0.36***
β adjusted	0.57	0.38	0.59	0.41	0.59	***1.09***
β modeled	0.34	0.39	0.30	0.25	0.24	***0.90***

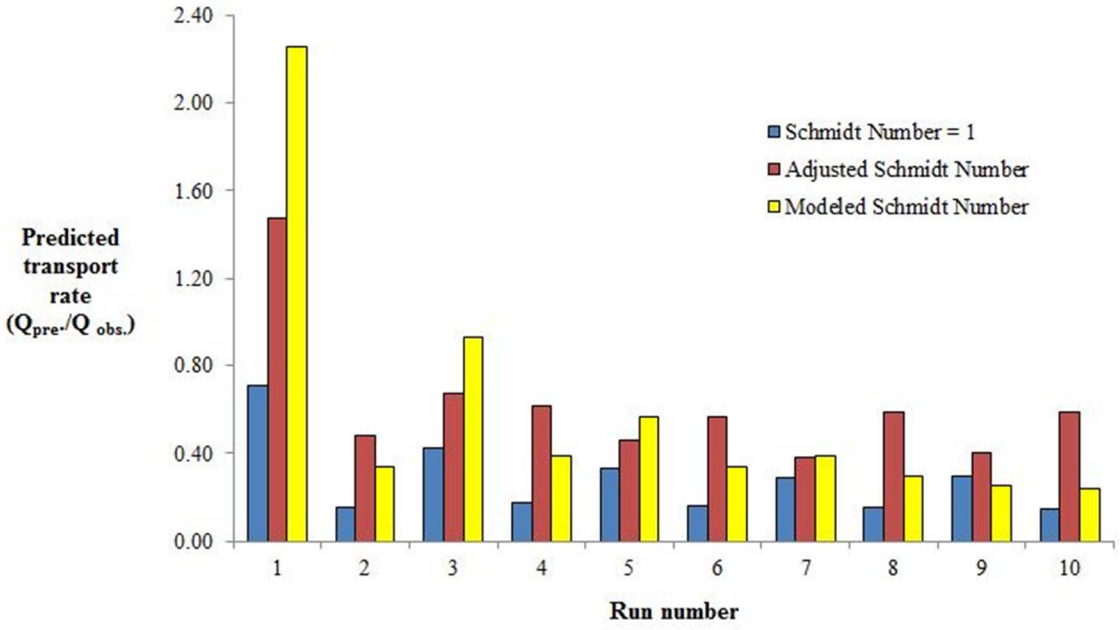

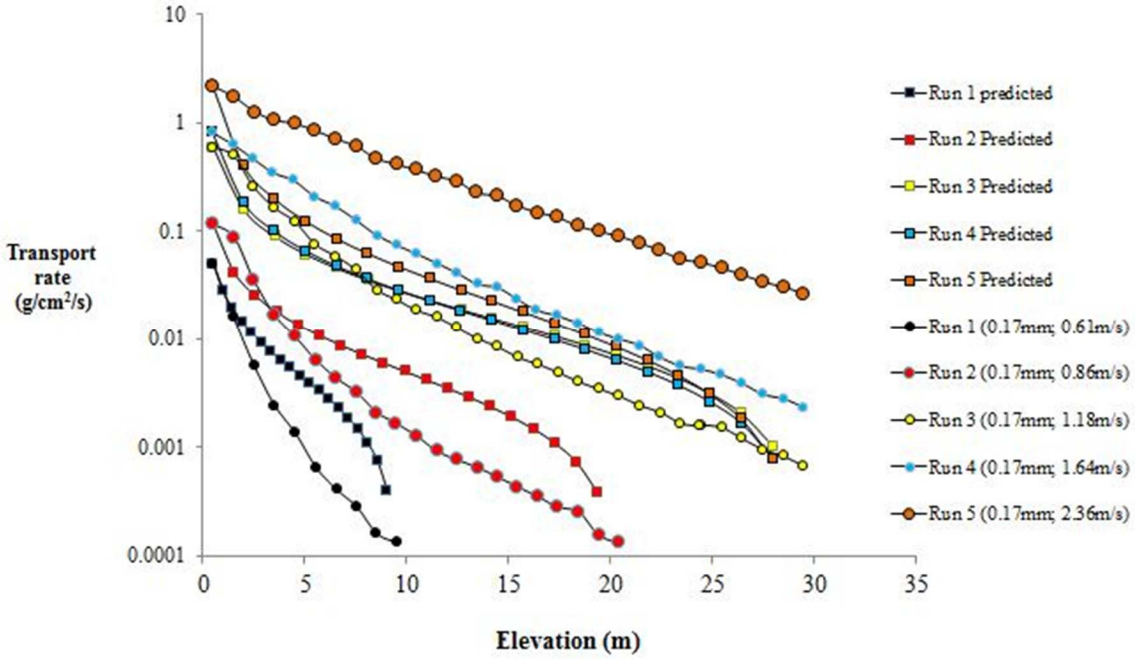
Transport rate (g/cm²/s)
10
1
0.1
0.01
0.001
0.0001
0
5
10
15
20
25
30
35
Elevation (m)
Run 1 predicted
Run 2 Predicted
Run 3 Predicted
Run 4 Predicted
Run 5 Predicted
Run 1 (0.17mm; 0.61m/s)
Run 2 (0.17mm; 0.86m/s)
Run 3 (0.17mm; 1.18m/s)
Run 4 (0.17mm; 1.64m/s)
Run 5 (0.17mm; 2.36m/s)

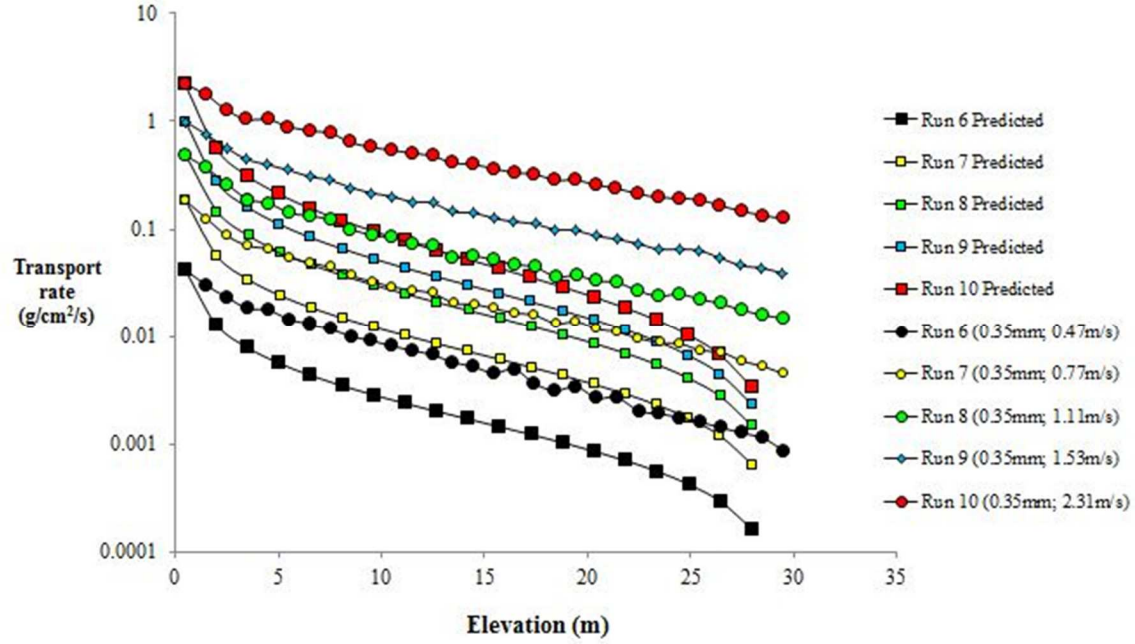
Transport rate (g/cm²/s)
10
1
0.1
0.01
0.001
0.0001
0
5
10
15
20
25
30
35
Elevation (m)
Run 6 Predicted
Run 7 Predicted
Run 8 Predicted
Run 9 Predicted
Run 10 Predicted
Run 6 (0.35mm; 0.47m/s)
Run 7 (0.35mm; 0.77m/s)
Run 8 (0.35mm; 1.11m/s)
Run 9 (0.35mm; 1.53m/s)
Run 10 (0.35mm; 2.31m/s)

Zou et al. (2001)

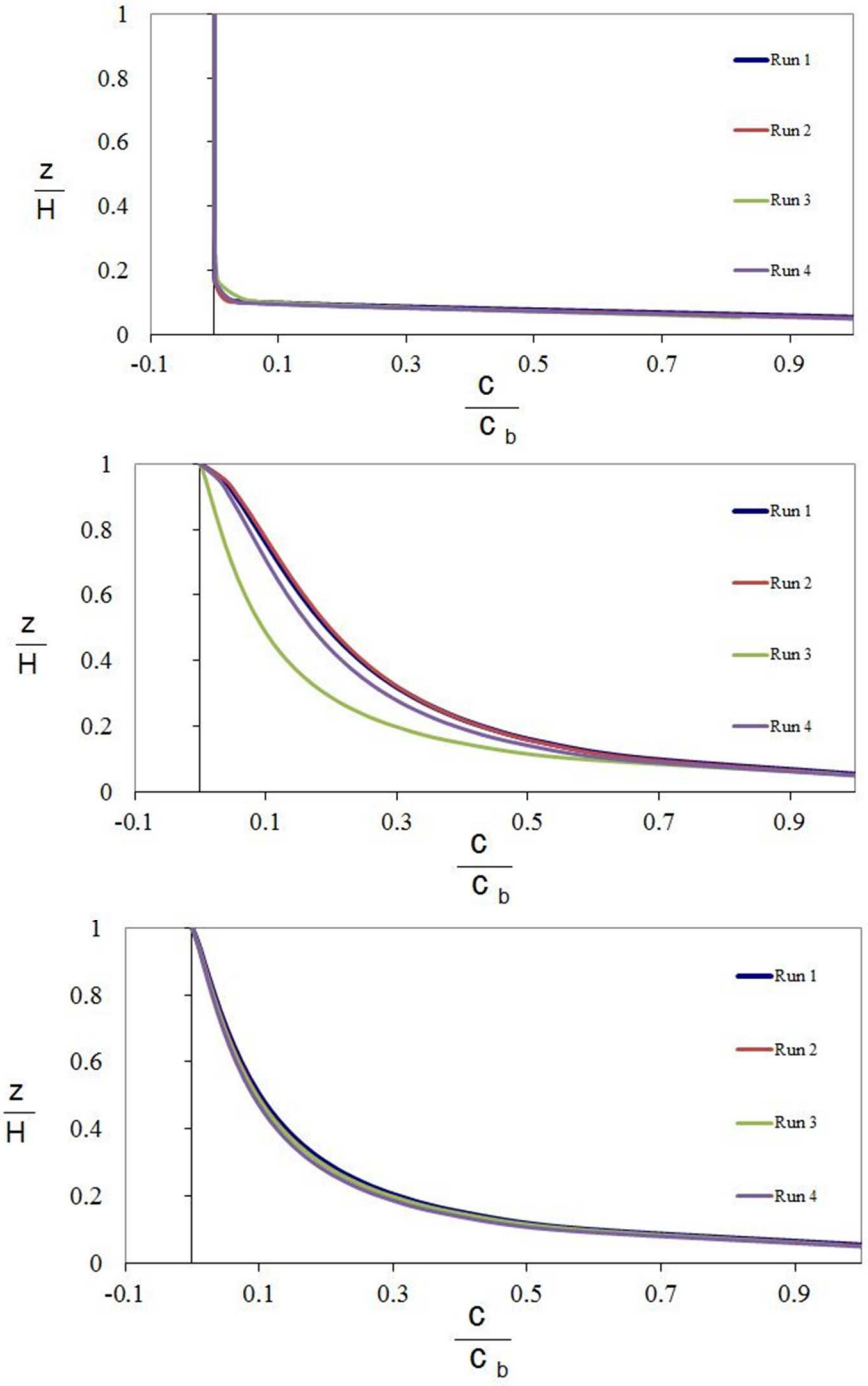

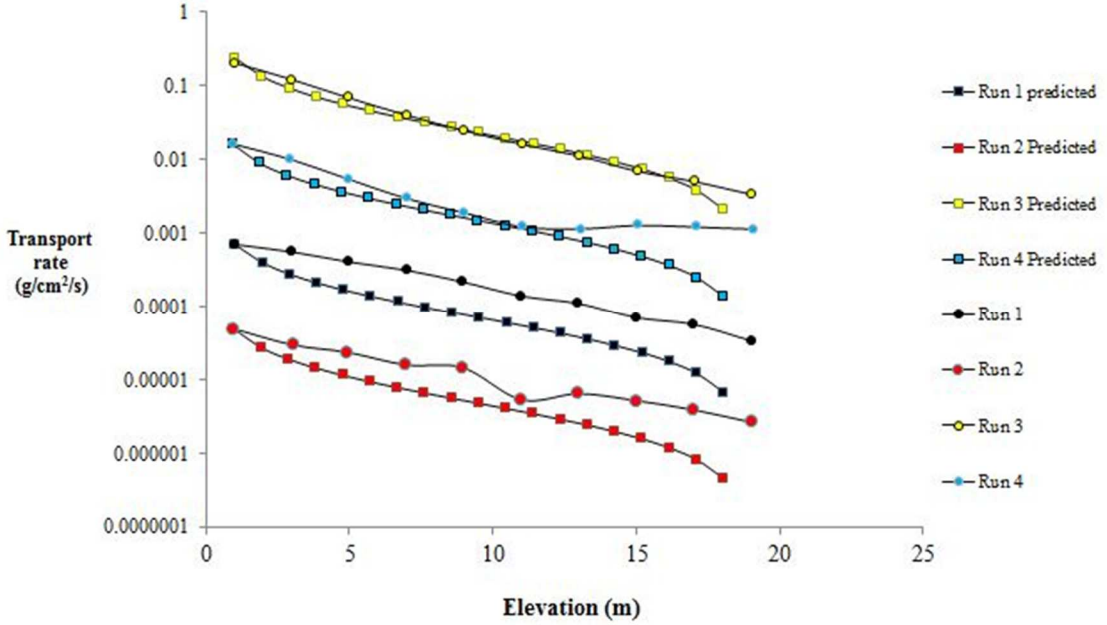

	Run 1	Run 2	Run 3	Run 4	
Observed transport rate (g/cm²/s)	0.0026	0.0002	0.5013	0.0427	
Predicted transport rate ($Q_{pre.}/Q_{obs.}$)					*Average*
β= 1	0.28	0.32	0.52	0.40	***0.38***
β adjusted	1.38	1.63	1.68	1.82	***1.63***
β modeled	0.97	1.11	1.69	1.31	***1.27***

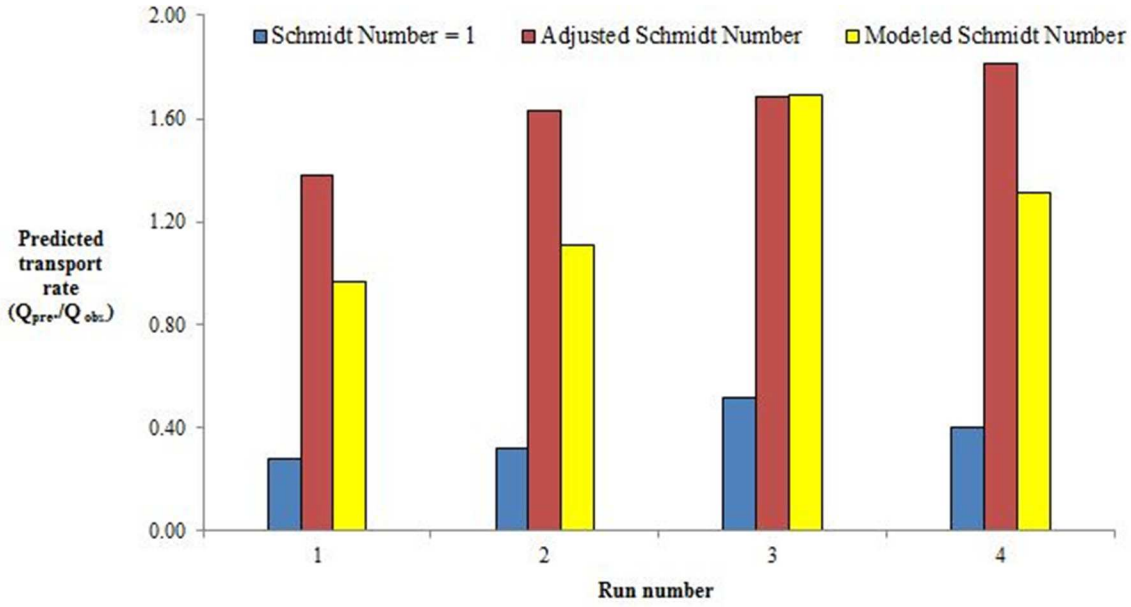
Schmidt Number = 1
Adjusted Schmidt Number
Modeled Schmidt Number
2.00
1.60
1.20
0.80
0.40
0.00
Predicted transport rate ($Q_{pre.}/Q_{obs.}$)
1
2
3
4
Run number

Sorensen (1985)

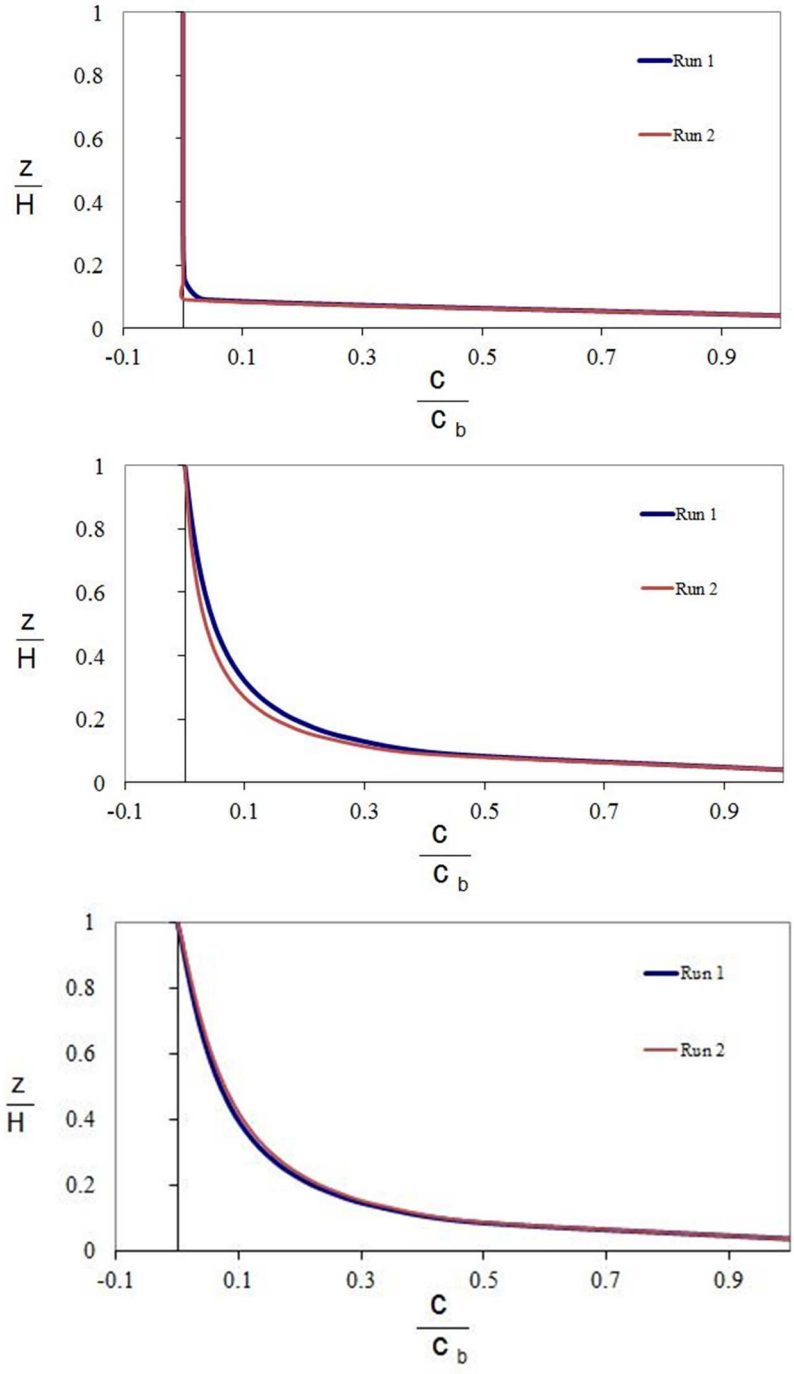

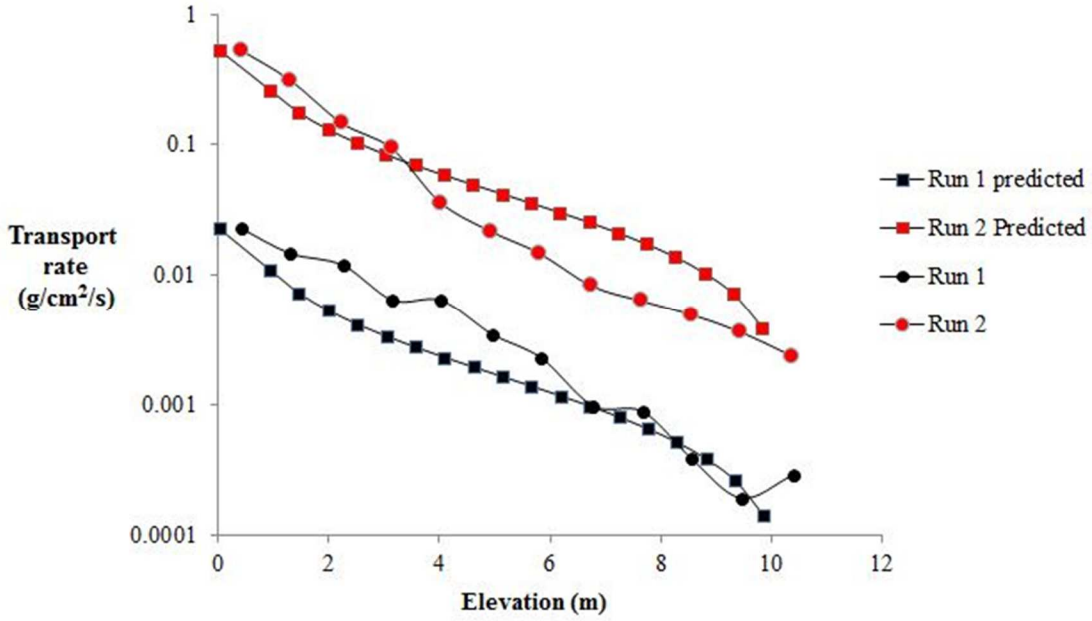
Transport rate (g/cm²/s)
1
0.1
0.01
0.001
0.0001
0
2
4
6
8
10
12
Elevation (m)
Run 1 predicted
Run 2 Predicted
Run 1
Run 2

	Run 1	Run 2	
Observed transport rate ($g/cm^2/s$)	0.0710	1.1860	
Predicted transport rate ($Q_{pre.}/Q_{obs.}$)			*Average*
β= 1	0.34	0.45	***0.40***
β adjusted	0.84	1.03	***0.94***
β modeled	0.98	1.41	***1.20***

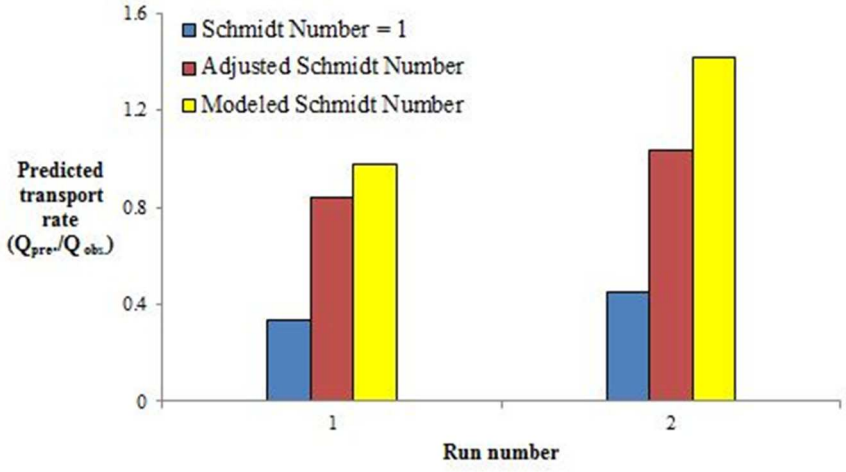

Rasmussen & Mikkelsen (1998)

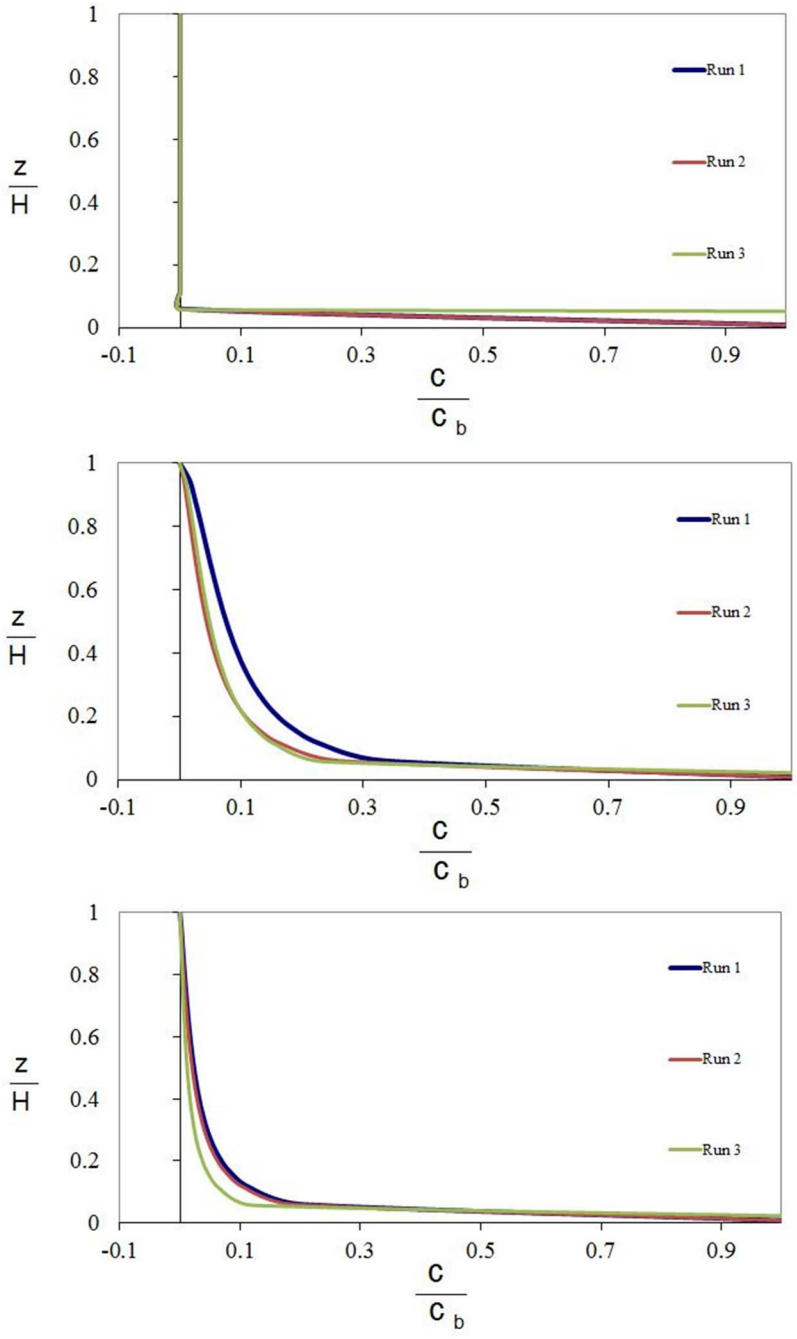

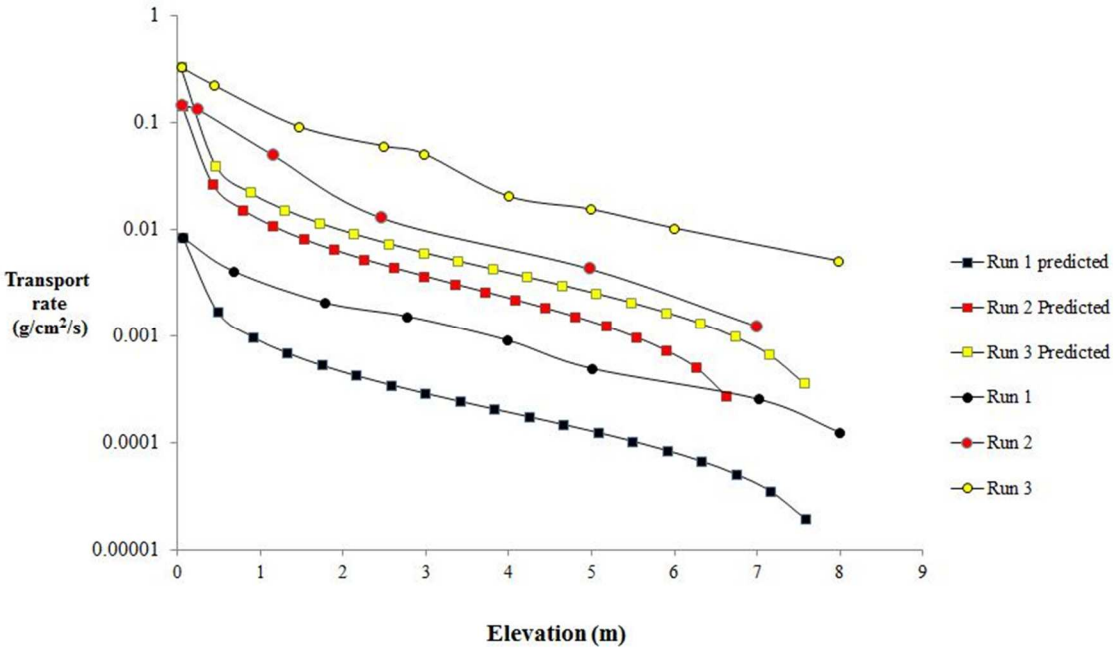

	Run 1	Run 2	Run 3	
Observed transport rate (g/cm²/s)	0.1787	0.3410	0.8140	
Predicted transport rate ($Q_{pre.}/Q_{obs.}$)				***Average***
β= 1	0.05	0.42	0.41	***0.29***
β adjusted	0.13	0.91	0.90	***0.65***
β modeled	0.08	0.70	0.58	***0.45***

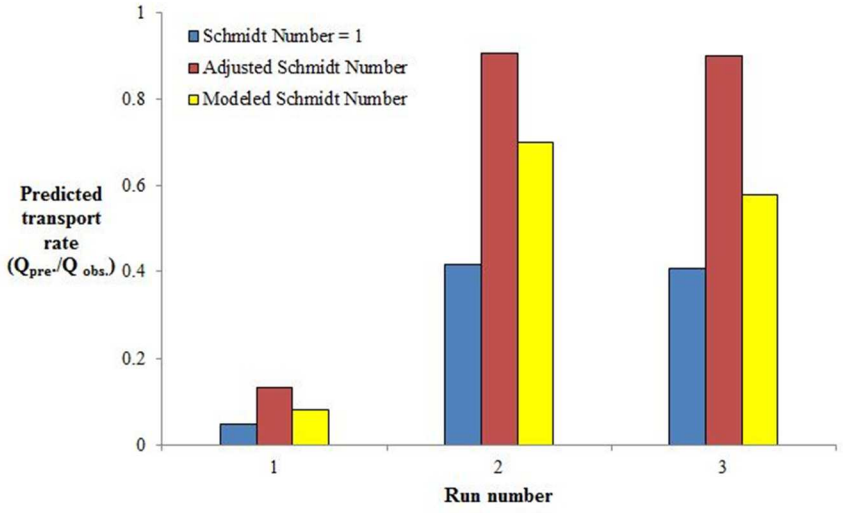
Schmidt Number = 1
Adjusted Schmidt Number
Modeled Schmidt Number
Predicted transport rate ($Q_{pre.}/Q_{obs.}$)
1
0.8
0.6
0.4
0.2
0
1
2
3
Run number

Kawamura (1951)

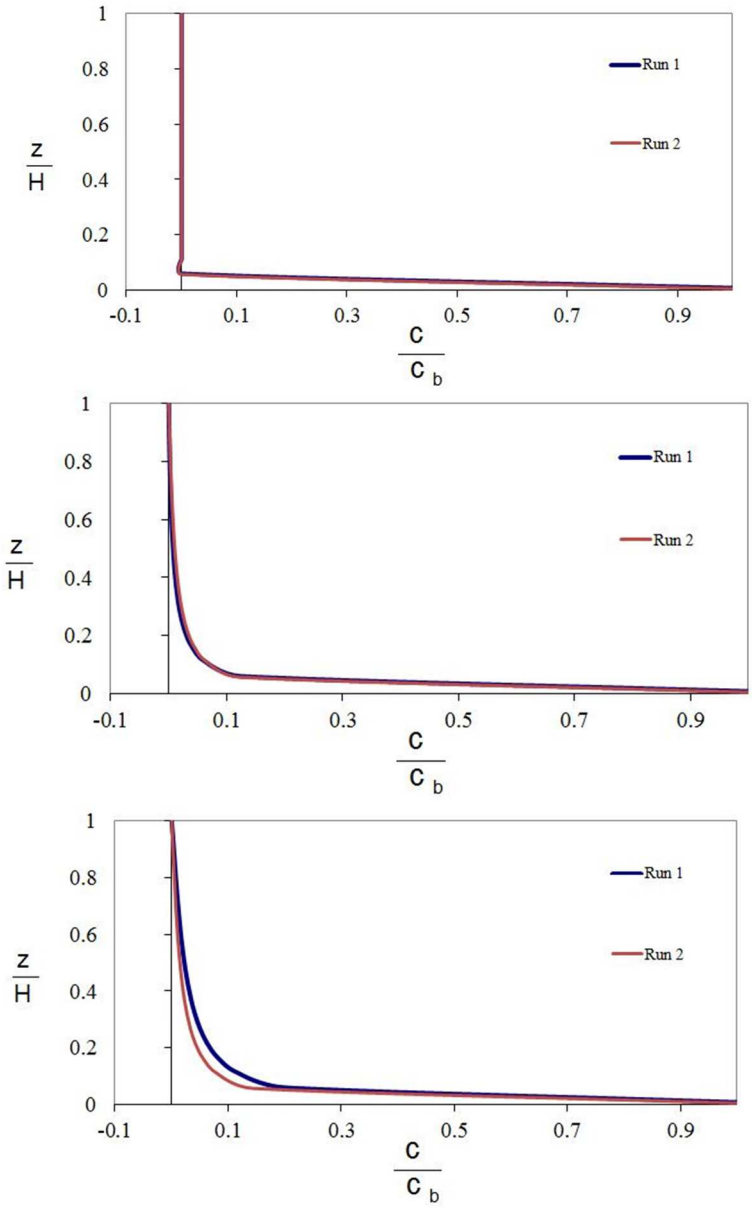

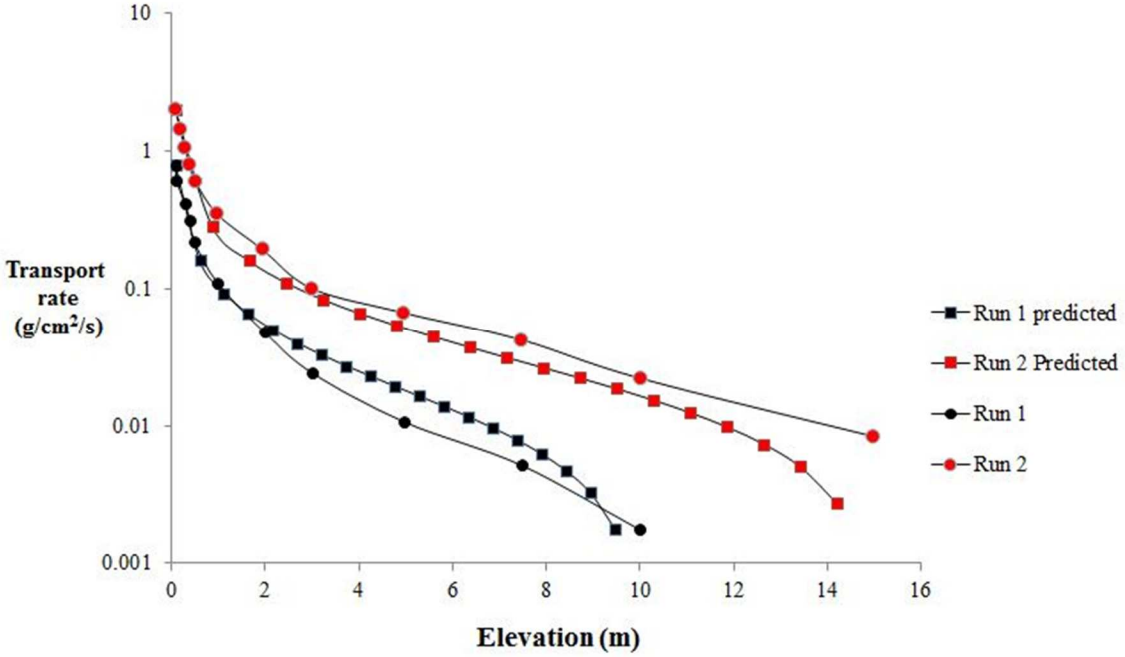
10
1
0.1
0.01
0.001
Transport rate (g/cm²/s)
0
2
4
6
8
10
12
14
16
Elevation (m)
Run 1 predicted
Run 2 Predicted
Run 1
Run 2

	Run 1	Run 2	
Observed transport rate ($g/cm^2/s$)	2.57	6.64	
Predicted transport rate ($Q_{pre.}/Q_{obs.}$)			*Average*
β= 1	0.31	0.30	***0.31***
β adjusted	0.42	0.42	***0.42***
β modeled	0.54	0.45	***0.50***

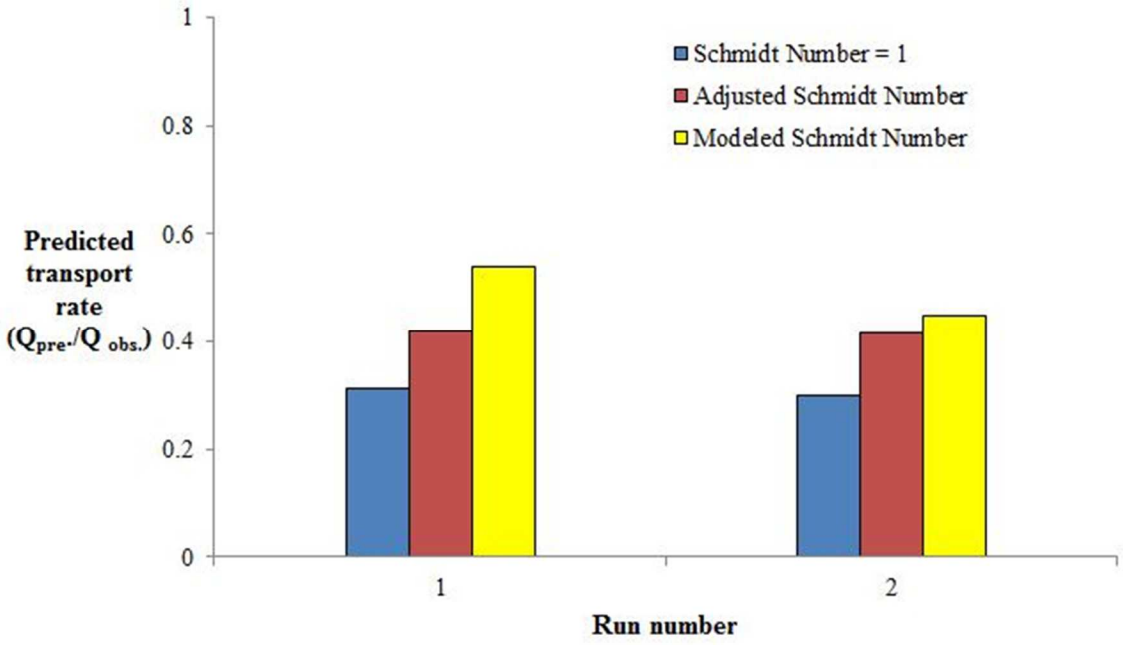

Gerety & Slingerland (1983)

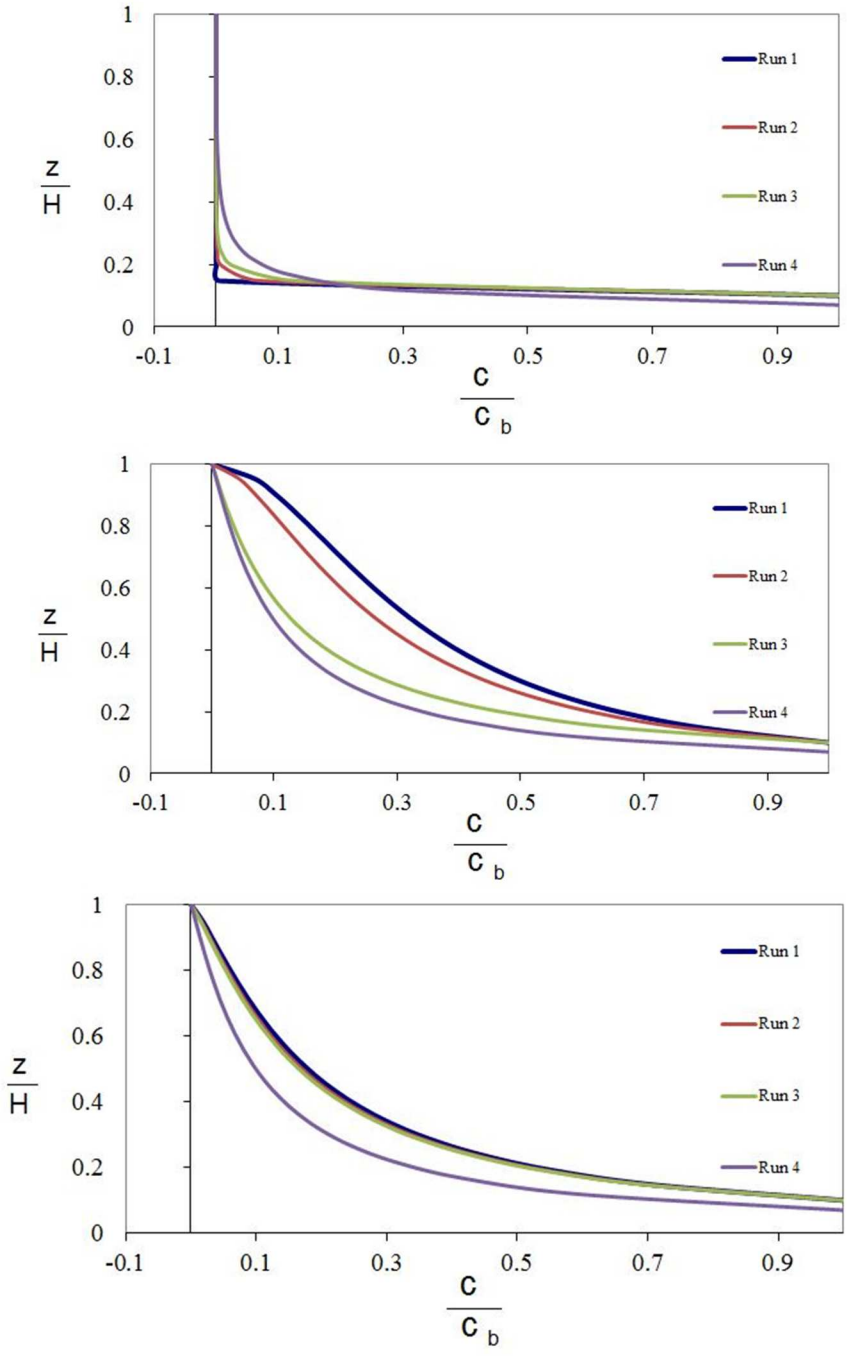

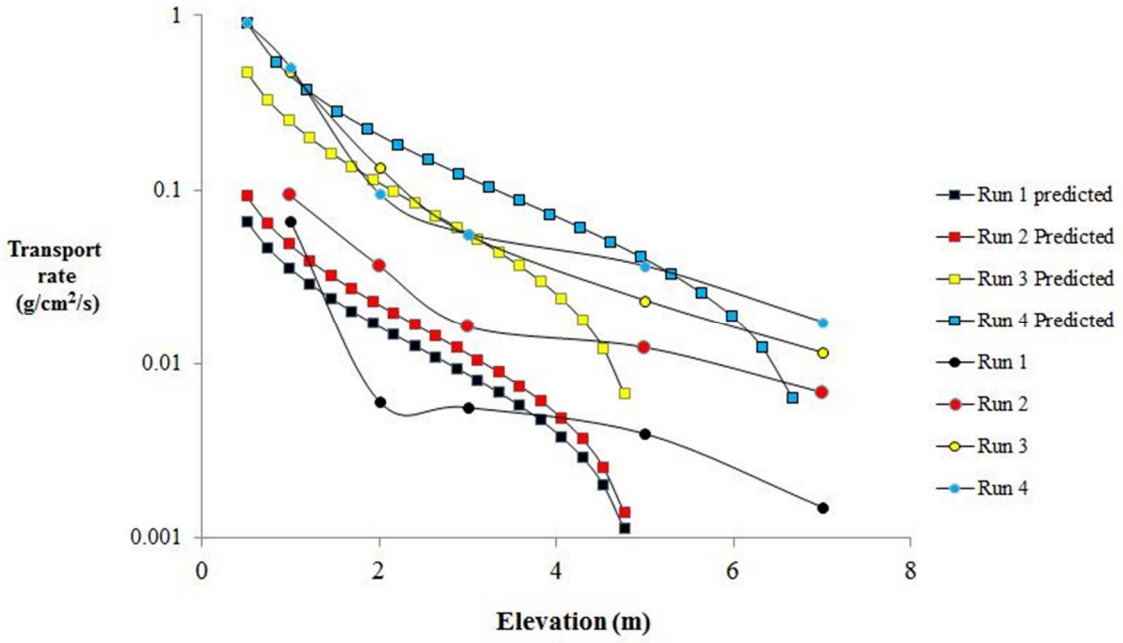
Transport rate (g/cm²/s)
1
0.1
0.01
0.001
0
2
4
6
8
Elevation (m)
Run 1 predicted
Run 2 Predicted
Run 3 Predicted
Run 4 Predicted
Run 1
Run 2
Run 3
Run 4

	Run 1	Run 2	Run 3	Run 4	
Observed transport rate ($g/cm^2/s$)	0.08	0.17	0.70	1.63	
Predicted transport rate ($Q_{pre.}/Q_{obs.}$)					*Average*
β= 1	0.80	0.61	0.79	0.87	*0.77*
β adjusted	5.59	3.46	2.78	2.04	*3.47*
β modeled	3.87	2.66	3.16	2.05	*2.93*

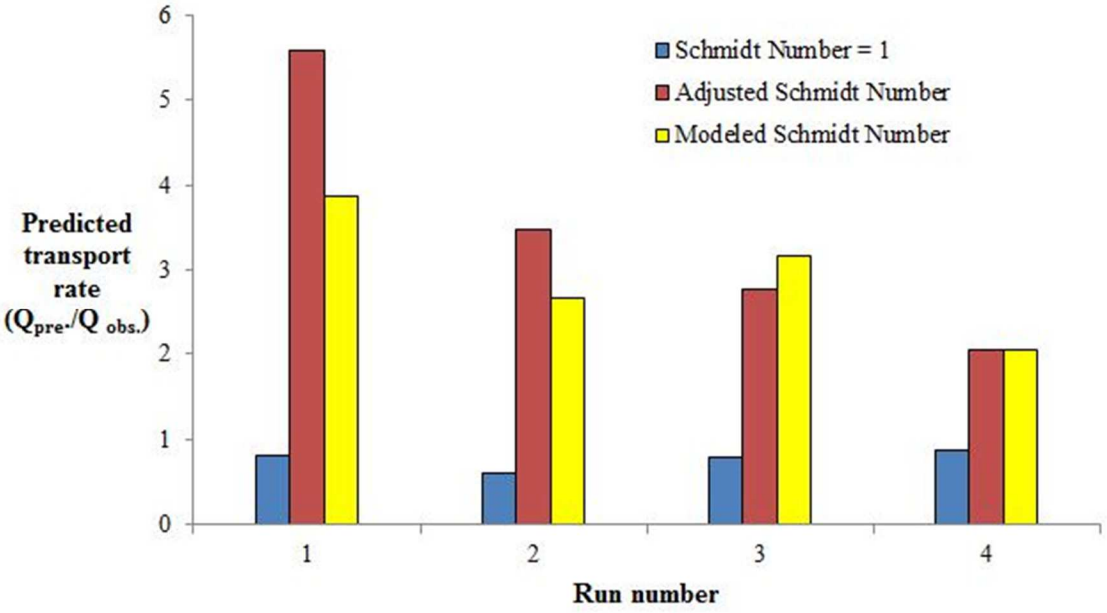

Williams (1964)

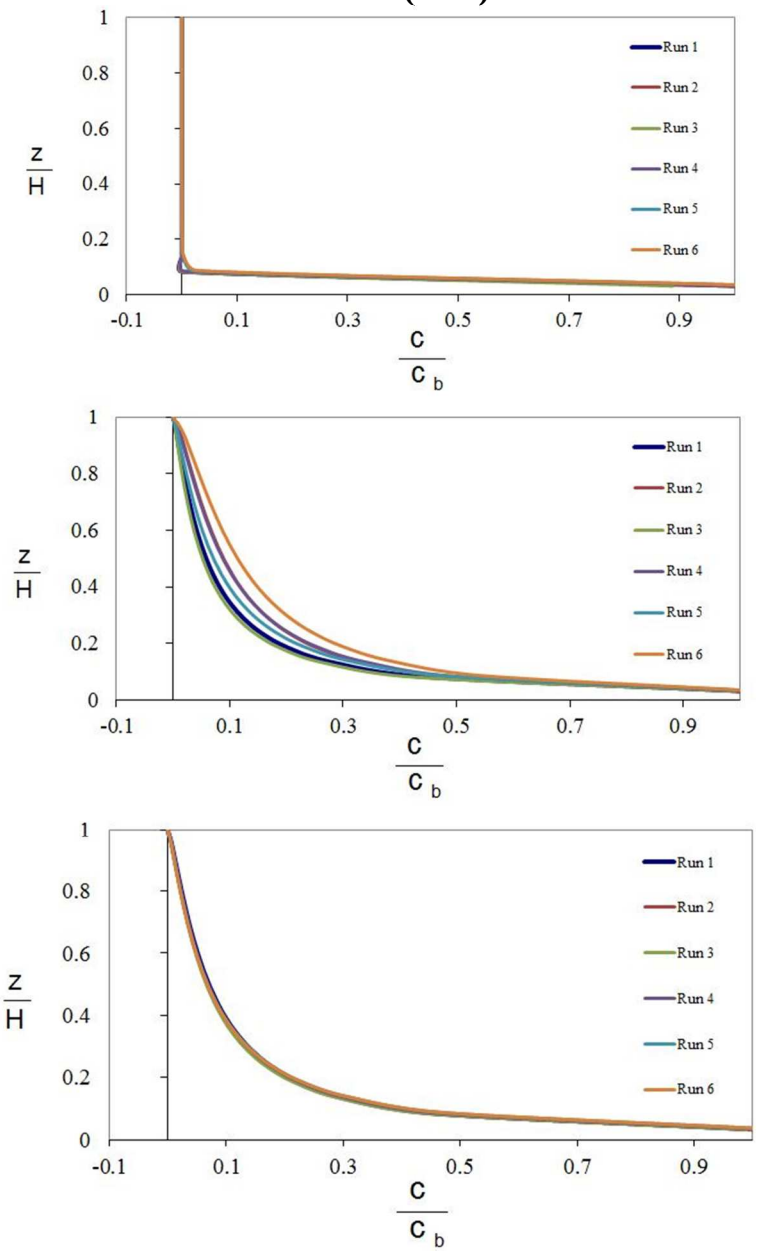

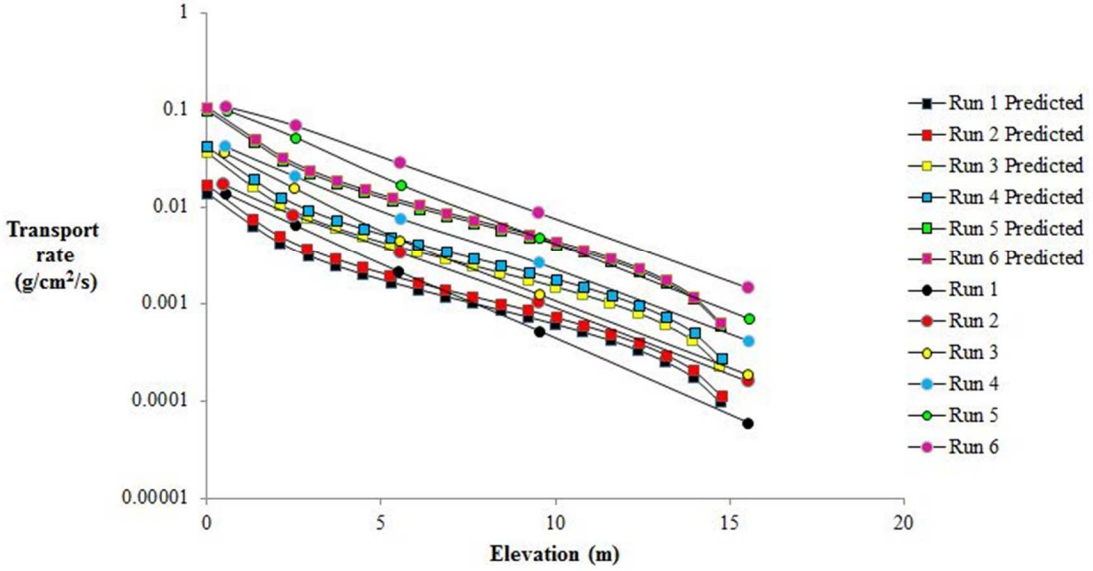
1
0.1
0.01
0.001
0.0001
0.00001
Transport rate (g/cm²/s)
0
5
10
15
20
Elevation (m)
Run 1 Predicted
Run 2 Predicted
Run 3 Predicted
Run 4 Predicted
Run 5 Predicted
Run 6 Predicted
Run 1
Run 2
Run 3
Run 4
Run 5
Run 6

	Run 1	Run 2	Run 3	Run 4	Run 5	Run 6	
Observed transport rate ($g/cm^2/s$)	0.0232	0.0355	0.0582	0.0733	0.1745	0.2140	
Predicted transport rate ($Q_{pre.}/Q_{obs.}$)							*Average*
β= 1	0.60	0.48	0.63	0.57	0.59	0.52	***0.56***
β adjusted	1.65	1.58	1.64	1.88	1.72	1.89	***1.73***
β modeled	1.79	1.39	1.81	1.69	1.69	1.48	***1.64***

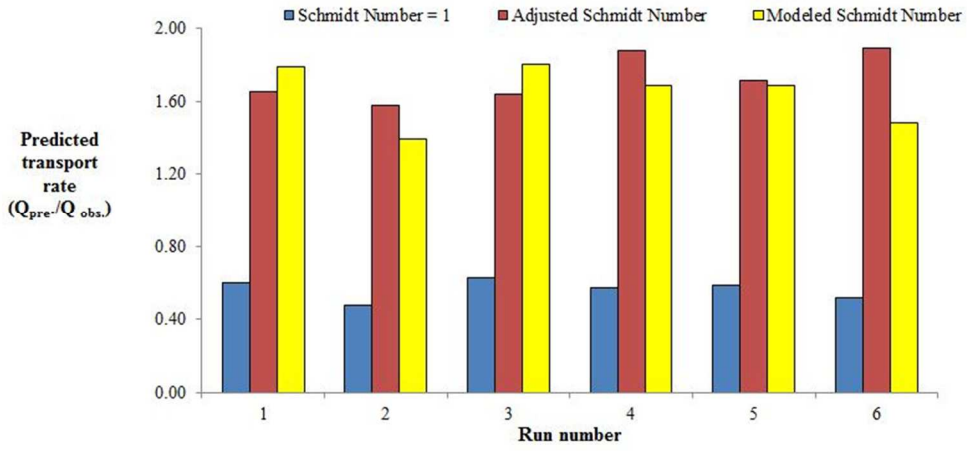

VITA

Name:	Eugene John Farrell
Address:	Department of Geography, Texas A&M University, TX 77843-3147
Email Address:	ejfarrell@tamu.edu
Education:	B.S., Earth Science, University College Cork, 1995
	M.S., Geography, University of Southern California, 2001
	Ph.D., Geography, Texas A&M University, 2012